ANALYSIS AND APPLICATIONS OF PERIODIC OPTICAL WAVEGUIDES

Sujata Leilani Arambepola

A thesis submitted for the degree of
Doctor of Philosophy in the University of London

October 1986

Department of Electrical Engineering
Imperial College of Science and Technology
Exhibition Road
London SW7 2BT

To

Thathi and Ammi and Arambe

ABSTRACT

This thesis is mainly a theoretical investigation of the effects of some periodic refractive index variations on the wave propagation in optical waveguides, and possible applications of these structures.

Wave propagation in cylindrical periodic structures, in particular the large-cored Bragg fibre, is considered. It is shown that the infinite Bragg fibre supports Bloch-type modes and may be lossless at certain wavelengths of operation, and that the attenuation of all the modes in a real finite fibre decrease with increasing number of cladding layers. The application to guiding of long wavelength laser radiation is discussed.

The Bragg fibre is also considered for multimode transmission of broad band radiation. It is found that increasing the number of claddings does not cause the wavelength dependence of the loss to become unacceptably large, and that it improves the tolerance to bending when the fibre is used for multimode transmission.

Some characteristics of a slab dielectric waveguide with a periodic index perturbation in the direction of propagation are considered. Approximate formulae for the fields resulting from the propagation of a pulse signal in a periodic medium are derived, which describe the fields as a sum of components with similar signal velocities and dispersions but different path lengths. Hence it is shown that a periodically perturbed guide may be designed which has a minimum dispersion at a chosen wavelength.

A waveguide with two periodic perturbations of similar pitch but different amplitude is considered. Monochromatic wave propagation in such a guide, in which the harmonics of the perturbation are interacting, is analysed. The use of this "doubly" periodic design is shown to result in a limited narrowing of the reflection band.

A second part of this thesis contains an analysis of the effect of short-range correlations on the permittivity of Nematic Liquid Crystals

ACKNOWLEDGEMENTS

It is with pleasure that I record my appreciation to the following :

Dr. J.R. Cozens, under whose supervision the main part of the work described in this dissertation was carried out. I am most grateful to him for suggesting the topics of research in Optical Waveguides and for helping me throughout the period of study.

Dr. K.D. Leaver, to whom I express my sincere thanks for introducing me to, and advising me on, the research into Liquid Crystals.

Professor M. Green, head of the Optical Devices group, who has been a source of unfailing encouragement and support.

The U.K. Science and Engineering Research Council for the generous award of a studentship.

Dr. T.J. Tate, whose practical assistance and entertaining conversation made my final year much easier.

Mrs. S.T. Nimalasuriya, for the great help in bringing the figures to their final form.

My husband, for his unfailing support, invaluable help and advice in all matters.

CONTENTS

PART I

1. INTRODUCTION

1.1 Background

The use of periodic structures [1] in classical (or "bulk") optics is well established and has a broad range of applications. One important device is the diffraction grating [2]. This may be a physical grating structure, for example cut into the surface of a device, or it may be a refractive index variation of a permanent or transient nature. Its applications include acousto-optic spectrum analysis [3], beam deflection [4], beam splitting, optical spectrum analysis [5], pulse shaping [6] and compression [7]. A closely related component is the hologram, which is used for wavefront reconstruction, displays [8], spatial filtering [9], signal processing [2] and data storage [10]. Another commonly used periodic structure is the multilayer coating, which is used essentially for impedance matching [11], both for high-reflectance, as in Bragg reflectors, and for anti-reflection coatings [12]. In these applications the optical wave propagates in what is, in effect, an unbounded medium.

The past two decades have seen a rapid increase in the use of optical frequency radiation in a variety of engineering systems, where previously predominantly electrical techniques were employed [13]. Perhaps one of the best known examples is that of optical fibre communication [14], [15]. Other examples include optical sensing [16], laser welding in medical and industrial applications and optical computing [17]. The potential of dielectric optical waveguides for communications was first noted in 1966 [18]. Since about this time the possibility of the use of

optical frequencies attracted considerable interest and this has continued with the development of continuous-wave room temperature operation semi-conductor lasers in 1970 [14], efficient semi-conductor detectors and the development of low loss materials [19], [20]. Together with these advances there has been improvement in the fabrication capabilities and technology, allowing manufacture of reliable high-quality optical scale components.

As well as utilising the bulk optic components, this new generation of optical systems and devices has relied heavily on waveguided optical radiation, particularly in integrated optics and, of course, optical transmission. These devices have included many with periodic features [21], such as distributed feedback lasers, [22], reflection and transmission filters [23], [24], surface acoustic-wave cells [25], input/output grating waveguide couplers [26], grating multiplexers [27] and phase matching in parametric interaction [28]. Other examples are distributed Bragg reflection lasers [29] and Bragg reflection waveguides [30], [31].

The characteristics of a dielectric waveguide depend primarily on the materials of which it is composed and on its structure, in particular its refractive index profile. The extent to which a guide can be designed to possess a desired set of characteristics is limited by the availability of materials of suitable refractive index, absorption and dispersion and by fabrication properties. One method by which the range of possible structures can be increased is by the creation of periodic structures from the available materials. For example, we have mentioned the use of multilayers for impedence matching to minimise reflection

(in general of an unguided wave), when use of a single layer of appropriate refractive index is impossible or impractical [11]. Pulse compression by grating pairs relies on the additional (angular) dispersion provided by the gratings [7]. The topics considered in this thesis may be regarded as examples of waveguiding structures in which periodic refractive index variations are used to create characteristics which are not easily achievable with available uniform materials.

1.2 Outline of contents

The effect of a discontinuity in the refractive index of a dielectric on a propagating electromagnetic optical wave is to cause part of the wave to be reflected and part of it to be refracted and transmitted. When there is a periodic series of these discontinuities, interference of the successive reflections and refractions gives rise to resonance phenomena. In particular, for certain frequency bands the interference is such that very little power is transmitted and the wave is strongly reflected (the reflection bands) or scattered. These phenomena can be described using the dispersion curve (the variation of the propagation constant with frequency), and in these terms the periodic perturbation causes the dispersion curve to be distorted. The dispersion curve can be regarded as characterising, to a large extent, the features of propagation for a particular material or structure (or in general the combination of both of these). Thus the introduction of a periodic perturbation may in some

circumstances be utilised to produce desired properties in a device.

The following two chapters of this thesis are concerned with effects which occur (at frequencies inside or near the reflection bands) when a multilayer Bragg reflector is used as the cladding for a hollow cylindrical guide, the Bragg fibre [32]. The multilayer reflector will, of course, reflect a wave incident in air. Therefore if we compare an infinite multilayer cladding with the cladding of a step-index fibre, which must have an index less than that of the core if it is to be lossless, we can consider the former to have an effective refractive index of less than unity. Thus in some senses the cladding is analagous to a metal with zero absorption. However for any finite number of claddings the loss from the less than total reflection must be considered and so the wave is still attenuated, though by a different mechanism. There are features of the multilayer which differ significantly from that of a metal, in particular the strong wavelength and angular dependence of the reflectivity [31] and the polarisation dependence [28].

The first chapter investigates the dispersion relation of the large-cored Bragg fibre and considers how to optimise the layer thicknesses for low loss. The attenuation of a low loss mode at wavelengths of high material absorption is calculated. In the second chapter the analysis is altered slightly in order to consider much less well confined modes and wavelengths of operation at which the cladding is less than maximally reflecting. The suitablity of the Bragg fibre for use as a component of a high-temperature sensor is considered.

In chapters four and five some phenomena which take place in a

slab dielectric waveguide with a longitudinal periodic index variation, and which occur at frequencies outside the reflection band, are considered.

Even at frequencies well away from the resonance frequency, there is a small but non-zero distortion of the dispersion curve. Therefore the variation of the propagation constant with frequency has been altered and this will effect the manner in which a pulse of finite spectral width is transmitted. This is analysed in chapter four. This effect may be regarded as an additional waveguide or material dispersion, which may be varied to a relatively large extent by varying the pitch and amplitude of the perturbation. As an example of this, the possibilty of introducing a zero velocity dispersion point at a chosen wavelength in a single mode, doped silica guide is considered.

As the frequency of operation approaches a band edge, the group velocity of propagation is reduced. Chapter five is concerned with the manner in which this reduction affects the bandwidth of a further periodic perturbation with resonance frequency in this area. In order to determine this, propagation in a multiply periodic waveguide is considered.

1.3 Analysis of Electromagnetic Wave propagation in Periodic media

Wave propagation in a medium may be described in terms of a complete set of normal modes. Any possible wave motion can be expressed as a linear combination of these modes [33]. When a periodic variation is introduced into a uniform medium, the effect

on the propagation is commonly regarded in one of two ways. The resulting medium can be considered to have an altered set of characteristic modes, the form of which is given by Floquet's/Bloch's theorem [34], [31]. Alternatively the periodic perturbation can be viewed as causing two of the normal modes of the uniform structure to become degenerate, leading to transfer of power between them. This is the Coupled Mode theory [35], [31].(Both these methods are used in the analysis of a very wide range of wave phenomena and are not limited to optical or general electromagnetic waves [34]). In this section we will summarise the main features of these two approaches (these are described in more detail in the references).

(a) Bloch modes

It can be shown that wave propagation governed by a one dimensional periodic equation of motion may be described by a complete set of normal modes, or Bloch waves, of the form

$$F(z) = \exp(iQz)\, U(z)$$

where F is a component of the electric or magnetic field, z is the direction of the periodicity, Λ is the periodicity, m is an integer, U is a periodic function of period Λ and Q is the "Bloch wavenumber" characterising the particular mode. Thus the effect of propagation through one period of the medium is only to change the wave by a scalar multiple $\exp(iQ\Lambda)$. This is clearly closely related to the idea of an eigenfunction of the medium. Since U is periodic it can be expanded in a Fourier series. These Fourier coefficients, $\{ A(Q-m2\pi/\Lambda) \}$ say, are obtained by requiring that the Bloch mode satisfies the wave equation. The Bloch wavenumber Q has that value which leads to a non-trivial solution . That is, Q is such that the matrix of coefficients of $\{ A \}$, known as

Hill's determinant [36], is zero. As long as the Fourier series of the periodic variation is absolutely convergent the solution is [36]

$$\sin^2(Q\Lambda/2) = \det(0)\, \sin^2(\beta\Lambda/2)$$

where the determinant of the coefficients is $\det(Q\Lambda/2)$ and β is the propagation constant in the direction of the periodicity at which the wave is incident into the medium. At frequencies for which Q is real the wave propagates and these are the pass or allowed bands. Between these lie frequency ranges for which Q is complex. Here the wave is strongly reflected and these are the stop or forbidden bands. When propagation in a two-dimensional medium (with one dimensional periodicity) is considered, there are in general frequency bands, at which Q is strongly perturbed from its value in an uniform medium but remains real, for which the incident wave may be scattered into another forward direction. These are the general results. There are some special cases of interest.

When the perturbation is small (this is the case for most gratings) the only directions of propagation which are significantly coupled are those with propagation constants in the direction of the periodicity β_1, β_2 such that

$$\beta_1 - \beta_2 = 2n\pi/\Lambda \text{ for integer } n.$$

This is the Bragg condition and holds for both forward and backward scattering. For the case of a one dimensional medium, if $Q - 2m\pi/\Lambda = \beta$ then $Q - 2(m+n)\pi/\Lambda = -\beta$ and so as long as the nth harmonic of the index perturbation is non-zero, either of these two terms (and only these two) may be large. Light incident at one of these angles can be strongly scattered into the other as it propagates. The dispersion relation is (setting m= 0) [31]

$$(Q^2 - \beta^2)[(Q - \frac{2n\pi}{\Lambda})^2 - \beta^2] - (w^2\mu|\epsilon_n|)^2 = 0$$

where ϵ_n is the amplitude of the nth harmonic of the permittivity. When the medium is bounded the above equation determines the set of possible transverse propagation constants in terms of Q. Q must then be obtained from the boundary conditions [37].

For a purely cosinusoidal variation the wave equation is known as Mathieu's equation and the solutions for the fields are the periodic Mathieu functions [34].

An important structure for which the Fourier series of the variation is not absolutely convergent is that of a stratified periodic medium [34]. However in this case an exact solution can be obtained, since the boundary conditions at the interfaces can be easily expressed. The requirement that after translation through one whole period the wave vector changes by $\exp(iQ\Lambda)$ only means that the Bloch wave is an eigenvector of the translation matrix [38], [39]. The eigenvalues are of course $\exp(iQ\Lambda)$ and the frequency regions of real and complex Q lead again to the characteristic stop and pass bands.

(b) Coupled mode theory

At any point z in the direction of propagation, the field may be expressed as a superposition of the normal modes of the unperturbed guide. Therefore the field in the periodic medium may be expressed as a z-dependent superposition of the unperturbed modes [31], [33]. The requirement that the field satisfies the perturbed wave equation and the use of the orthogonalitiy of the normal modes leads to a set of coupled differential equations. Assuming the effect of the perturbation to be slowly varying with z and assuming that the terms with non-zero arguments in the exponential make no contribution over moderate distances, because

of cancellation, leads again to the Bragg condition for non-negligible coupling. For the case of backward coupling by a small perturbation in an infinite medium, this yields the same dispersion equation as is obtained from considering Bloch modes. For a bounded medium and for co-directional coupling, the equations in the coupled mode theory are of essentially the same form as for backward coupling in an infinite medium and are thus simpler than the Bloch wave approach in these cases.

1.4 The Dispersion diagram and the Reflectivity

The diagram showing the variation of the propagation constant with frequency for a periodic medium contains most of the characteristics of the propagation. This diagram is shown in figure 1.1(a) for the case in which the perturbation causes strong reflection, or equivalently, coupling to the backward mode [31].

The frequencies at which Q is first complex are the band edges. At these frequencies it can be assumed that the waves with forward and backward phase velocities have equal amplitudes and so form a standing wave.

For any possible Bloch wavenumber Q, $2n\pi/\Lambda - Q$ is also a solution near the nth resonance frequency and so these two modes can be interpreted as the two normal Bloch waves of the structure in this case. The successive curves in the dispersion diagram of positive slope can be interpreted as representing the fundamental and harmonic components of a Bloch wave with positive group velocity. The curves with negative slope similarly represent

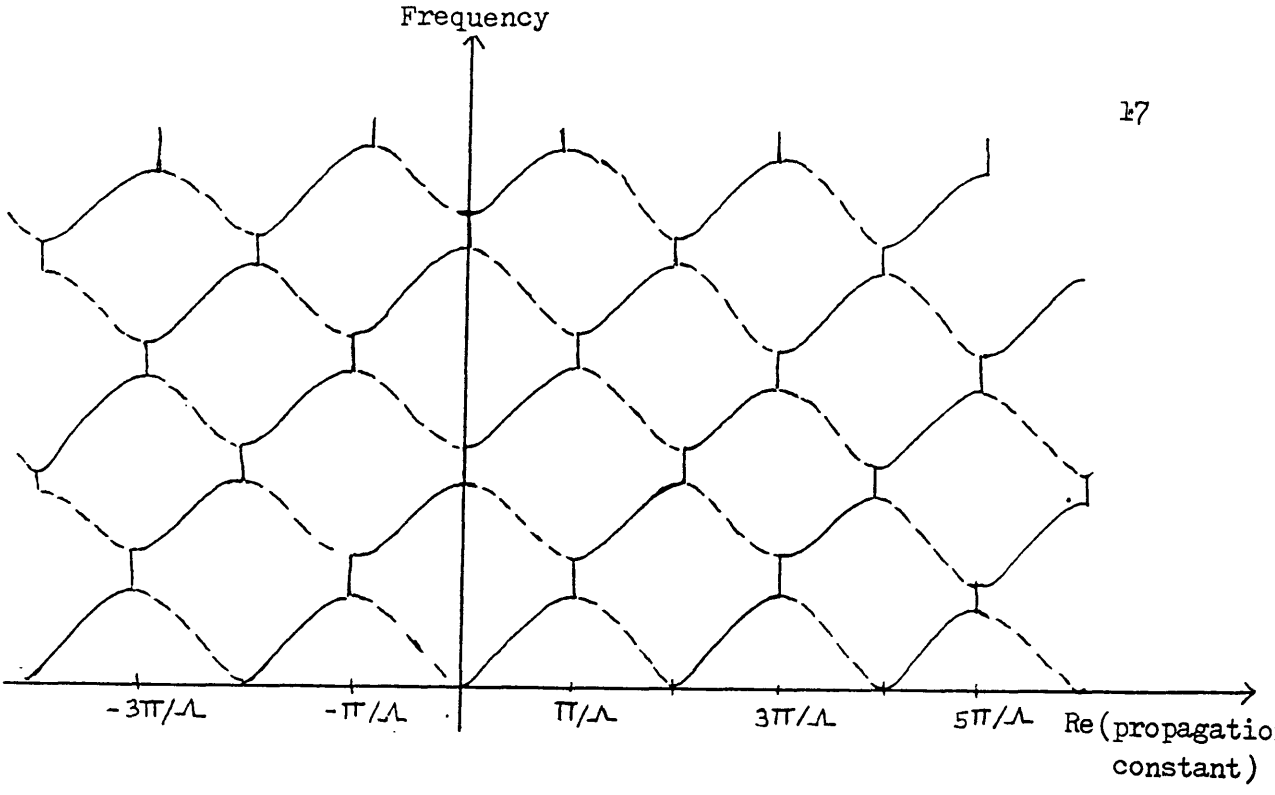

Figure 1.1(a) Schematic dispersion diagram for backward coupling

—— components of Bloch wave with forward group velocity
---components of Bloch wave with backward group velocity

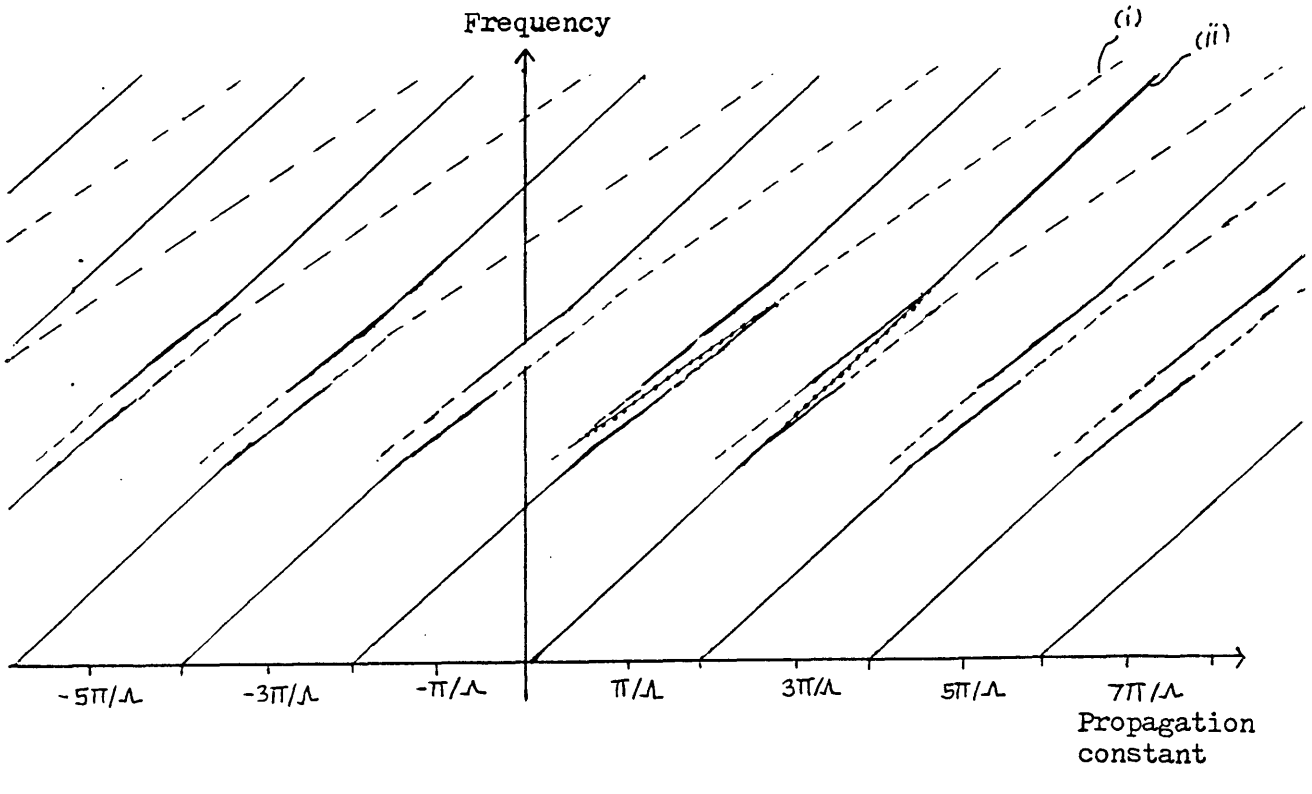

Figure 1.1(b) Schematic dispersion diagram for forward coupling between modes (i) and (ii). The dotted sections indicate the unperturbed dispersion when it differs significantly from the perturbed values [118].

the other Bloch mode. The reflection or forbidden bands occur where the curves of the two Bloch modes intersect. Thus the forbidden bands can be interpreted as the frequencies at and near which the modes would become degenerate if they could propagate. Since the normal modes must be independent, they cannot propagate. The dispersion curves may also be interpreted in terms of coupling between modes. The two curves through the origin represent the forward and backward propagating modes of the uniform structure. The reflection bands are the frequencies for which the perturbation causes power to be transferred between these two modes. The other dispersion curves are described by the coupled mode formulae, which can be made arbitrarily accurate by retaining enough terms, as in the Bloch wave formalism, but they do not have a simple interpretation in terms of the normal modes of the original unperturbed structure.

Figure 1.1(b) shows the (schematic) dispersion curve for the case of coupling between two forward waveguide modes by a periodic perturbation. Now the propagation constant remains real always. Similar remarks to those above apply regarding the Bloch wave and coupled mode interpretations.

Figure 1.2 shows the reflectivity for backward coupling in a periodic medium as a function of frequency. The width of the central reflection band is a function of the effective amplitude of the pericdic index variation. It is independent of the length of the periodic medium in the long length approximation. The value of the maximum reflectivity inside this band depends on the length of the device, as does the position of the first zero crossing outside the reflection band. The envelope of the reflectivity is similarly independent of the length outside the

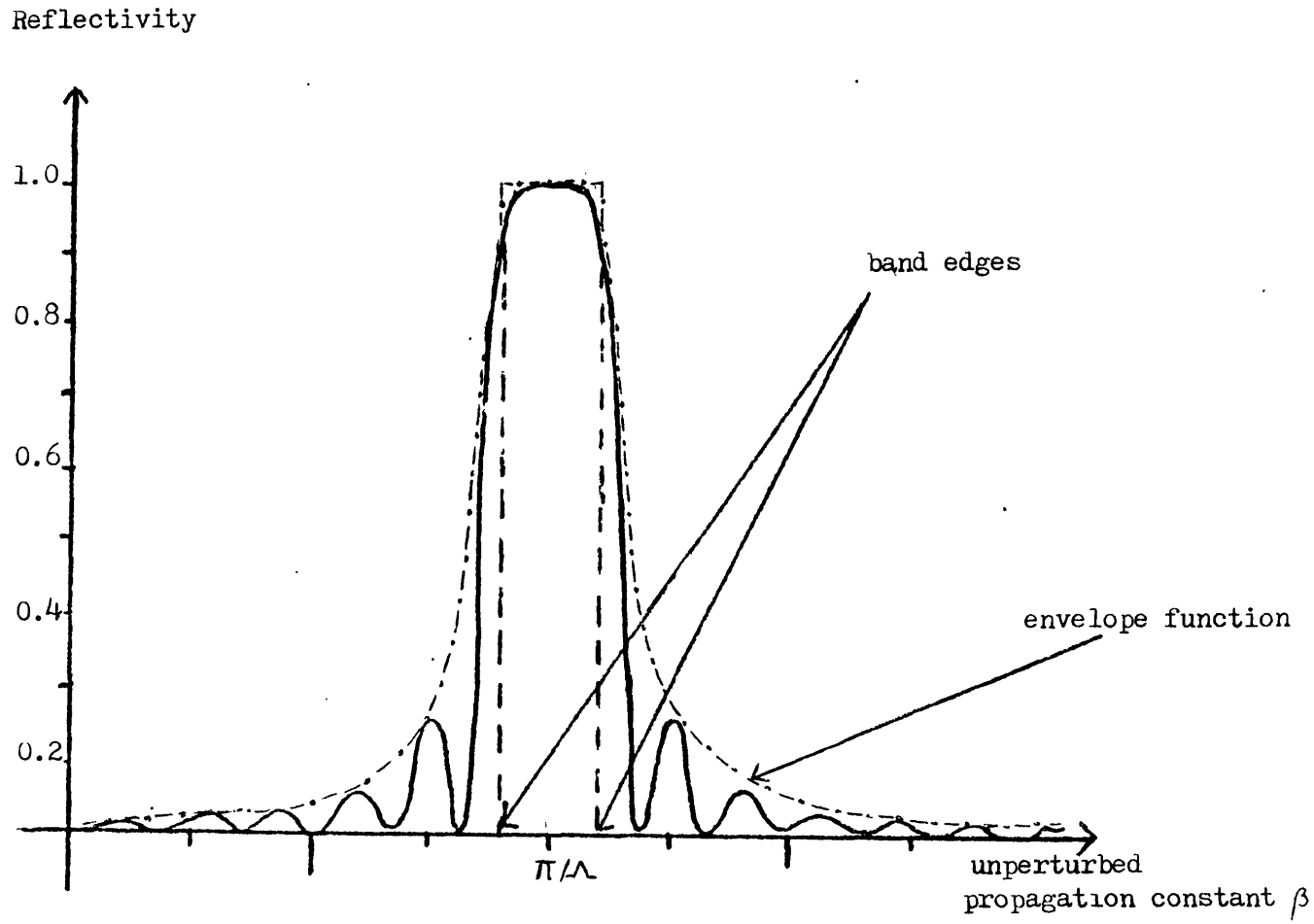

Figure 1.2 Reflectivity in a periodic medium. The envelope function $\propto |\epsilon_n|^2/(\beta - \pi/\Lambda)^2$ outside the stop band

reflection band. However as the length increases the oscillations inside this envelope become larger and more rapid. The positions of the first zeros tend to the band edges. Therefore although the region for which the propagation constant is complex is essentially independent of length, the width of the central reflection lobe can be considered to decrease with increasing length. However the maxima of the side lobes also increase and move towards the band edge. In the limit of an infinite structure the reflectivity is described by the envelope function.

For forward coupling the amount of power transferred into the coupled mode does nct increase monotonically with length. The power is exchanged periodically between the two modes as the length is increased [31]. This may also be interpreted as the interference between the fundamental and harmonic components of the two Bloch modes of the structure.

2. THE INFINITE BRAGG FIBRE

2.1 Introduction

The Bragg fibre [32] is a cylindrical waveguide in which the cladding is composed of periodic layers of alternately high and low refractive index (figure 2.1). The power is confined to the core by reflection at the successive layer interfaces of the cladding, which acts as a cylindrical analogue of a dielectric mirror. The core is generally assumed to be of a lower index than the cladding layers, since otherwise guiding could be obtained more simply and efficiently in the conventional manner, that is, by total internal reflection.

The Bragg fibre structure was proposed by Yeh, Yariv and Marom in 1978 [32] and the TE mode of the guide was analysed. This analysis showed that, when the wavelength is small enough compared to the core radius, the optimum thicknesses of the cladding layers (that is, for greatest reflectivity) are such that the layer interfaces occur at the successive zeros and maxima of the electric field. This result is the same as that for a planar periodic medium. These optimium thicknesses were obtained for both geometries by minimising the "outflowing" power of a radiation mode of the structure [43]. In the cylindrical case TM and hybrid modes were not considered.

In contrast to the case of cylindrical geometries, optical wave propagation in a planar stratified periodic medium has been considered widely [28], [38], [44], [45]. It has been shown that determining the optimum thicknesses by minimising the outflowing power is equivalent to maximising the reflectivity of a Bloch wave

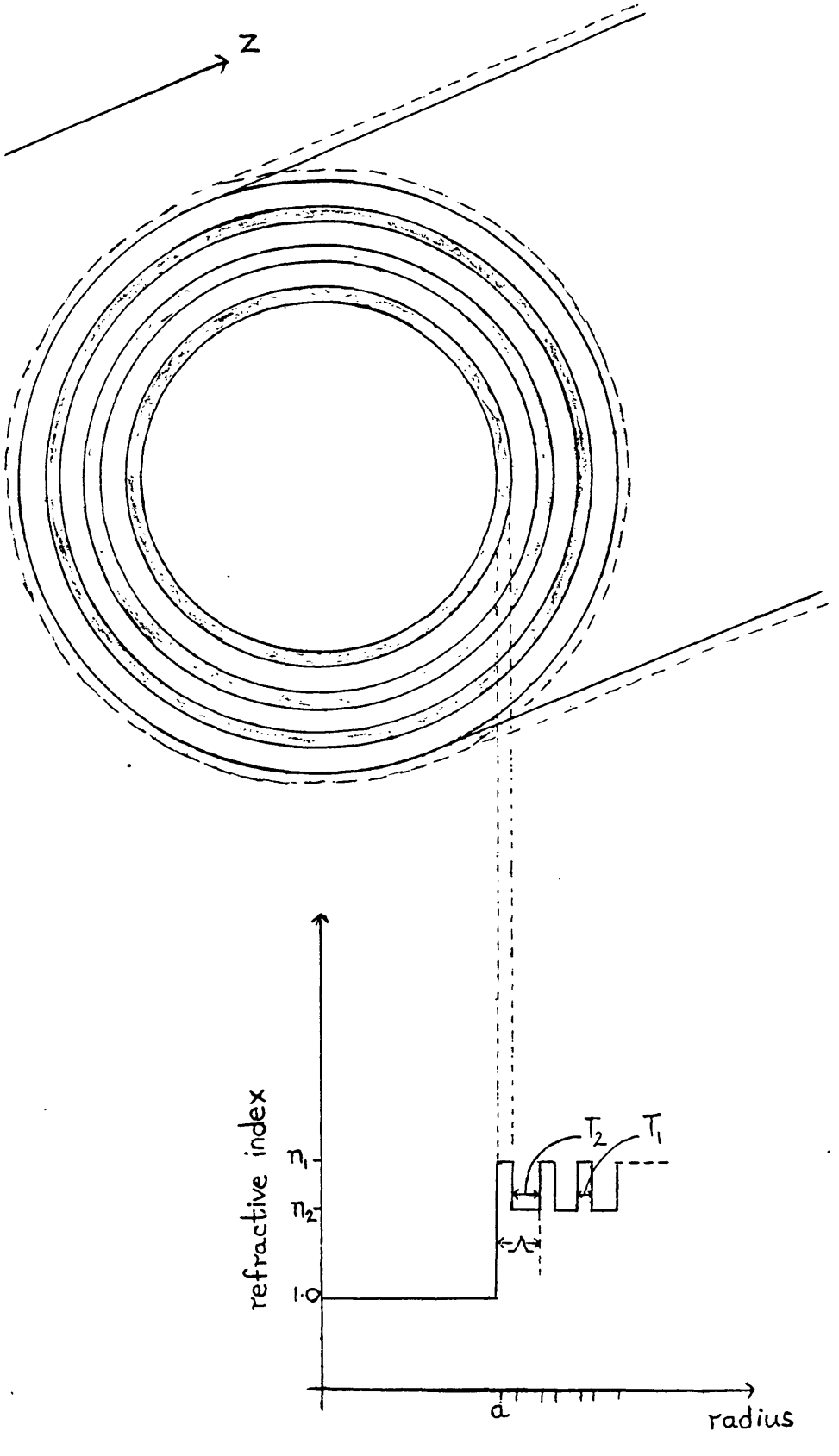

Figure 2.1 Cross-section and refractive index profile of the Bragg fibre

in the cladding and hence that these thicknesses are one quarter of the effective wavelength in the material in the direction of the periodicity [43]. The dispersion relation for a planar Bragg waveguide has been obtained by matching the fields at the core boundary to those of a Bloch wave in the cladding [38], and guiding by a Bragg layer has been observed experimentally [46].

Although the planar Bragg waveguide is better understood, the cylindrical fibre seems to represent a potentially more useful structure. We will consider in particular the hollow-cored Bragg fibre. Hollow-cored waveguides have a possible application in the guiding of high power long wavelength radiation, for which material absorption is in general very large . A hollow guide with a oxide glass functioning as a cladding of refractive index less than one (and hence with a non-zero absorption), has been proposed for this purpose [47]. Several hollow metal guides, with both planar [48] and cylindrical [49], [50] geometries have also been considered. In general the cylindrical guide suffers from the disadvantage that the lowest loss mode is the TE_{01}, the field distribution of which has a null at the centre of the core [50]. This differs greatly from the Gaussian field profile of the output from a typical laser.

Metal guides with inner single or periodic multilayer dielectric coatings to provide an increased reflectivity have been suggested, in particular for use in transmission of long wavelength CO_2 laser radiation. The planar [51], (singly coated) rectangular [52] and the cylindrical [53], [54], [55] cases have been considered. The multilayer structures have been analysed by considering an effective wave impedance and admittance of a finite number of dielectric layers surrounded by an infinitely thick metal

cladding. This analysis is a generalisation of that for a hollow cylindrical guide with a single cladding [50]. Expressions for the attenuation constants of the low loss leaky modes have been obtained.

In this chapter we will consider propagation in the infinite Bragg fibre. We will show that modes analogous to the Bloch modes in planar periodic media can be supported by cylindrical periodic structures as long as the radius of curvature is large enough. By using these modes we obtain the dispersion relation for the Bragg fibre. This expression holds for any periodic cladding, and not only for one with optimised layer thicknesses, (for which the equations reduce to simple forms) as has been the case for previous results concerning cylindrical periodic guides [54], [55].

The previous analysis of the Bragg fibre [32] has used a power minimisation to determine the optimum cladding layer thicknesses of the TE mode only. We will extend this method to include the TM and hybrid modes and show that the results so obtained are equivalent to those obtained from the use of Bloch waves. The values for the attenuation constants of low loss modes of the Bragg fibre are obtained. The field patterns and designations of these modes are considered and the suitability of this fibre for transmission of CO_2 laser light with a wavelength of 10.6 μm is discussed.

2.2 Bloch waves in a weakly curved, radially periodic meduim

We will consider electromagnetic wave propagation in a cylindrically symmetric medium consisting of an infinite number of concentric dielectric layers of alternating refractive indices n_1, n_2 (dielectric permittivities ϵ_1, ϵ_2) and thicknesses T_1, T_2 (figure 2.1). The radii of curvature, r,are assumed to be large, that is

$$\lambda/r << 1$$

It will be shown that this medium has a set of modes which are analogous to the Bloch modes of a linearly periodic medium.

Using cylindrical polar co-ordinates r,θ,z (figure 2.1) eigensolutions to Maxwell's equations may be written [40]

$$E = E(r) \cos(l\theta) \exp(i\beta z - iwt)$$

$$H = H(r) \sin(l\theta) \exp(i\beta z - iwt)$$

where E, H are the electric and magnetic fields respectively

l is an integer

(all results follow similarly for the orthogonal polarization, for which the θ dependences of the electric and magnetic field are interchanged). Then for a region of uniform dielectric perimittivity ϵ and magnetic permeability μ, the longitudinal field components are given by

$$\left(\frac{d^2}{dr^2} + \frac{1}{r}\frac{d}{dr} - \frac{l^2}{r^2} + w^2\mu\epsilon - \beta^2\right) E_z = 0 \qquad (2.1a)$$

$$\left(\frac{d^2}{dr^2} + \frac{1}{r}\frac{d}{dr} - \frac{l^2}{r^2} + w^2\mu\epsilon - \beta^2\right) H_z = 0 \qquad (2.1b)$$

The tangential components are

$$E_\theta = \frac{i}{k^2}\left(-\frac{\beta l E_z}{r} - w\mu\frac{dH_z}{dr}\right)\sin(l\theta)\exp(i\beta z - iwt) \qquad (2.2a)$$

$$H_\theta = \frac{i}{k^2}\left(\frac{\beta l H_z}{r} + w\epsilon\frac{dE_z}{dr}\right)\cos(l\theta)\exp(i\beta z - iwt) \qquad (2.2b)$$

where $k^2 = w^2\mu\epsilon - \beta^2$

The exact solutions to (2.1) are Bessel functions [40]. However, in order to obtain a Bloch wave solution, it is convenient to transform the equations by multiplying them by $r^{1/2}$ to yield

$$\left(\frac{d^2}{dr^2} + k^2\left(1 + \frac{0.25 - l^2}{k^2 r^2}\right)\right)\left(r^{1/2} E_z\right) = 0 \qquad (2.3a)$$

$$\left(\frac{d^2}{dr^2} + k^2\left(1 + \frac{0.25 - l^2}{k^2 r^2}\right)\right)\left(r^{1/2} H_z\right) = 0 \qquad (2.3b)$$

If we define a periodic function

$$k(r) = k_1 = w^2\mu\epsilon_1 - \beta^2 \qquad 2m\Lambda < r < (2m+1)\Lambda$$

$$k_2 = w^2\mu\epsilon_2 - \beta^2 \qquad (2m+1)\Lambda < r < (2m+2)\Lambda$$

then equations (2.3) determine the fields in the periodic medium. Neglecting terms of order $(1/kr)^2$ (strictly we neglect terms of order $(1/kr)^2$), the solution in the mth cladding layer of refractive index n_j may be written

$$E_z = \frac{1}{r^{1/2}}\left(A_{2m-j}\cos(k_j x) + B_{2m-j}\sin(k_j x)\right) \qquad (2.4a)$$

$$H_z = \frac{1}{r^{1/2}} \left(C_{2m-j} \cos(k_j x) + D_{2m-j} \sin(k_j x) \right) \qquad (2.4b)$$

where Λ is the radial period

$x = r - a - (m-1)\Lambda - \Lambda_j$

a is the radius of curvature of the first cladding layer

$$\Lambda_j = \begin{cases} 0 & \text{if } j=2 \\ T_1 & \text{if } j=1 \end{cases}$$

To the same order of accuracy, equations (2.3) are invariant under translation by Λ. However, since they are derived from the reduced Maxwell equations for a region of uniform permittivity, it is necessary to consider the boundary conditions.

At each of the cladding layer interfaces, E_z, H_θ, H_z, E_θ must be continuous. Using (2.2), (2.4)

$$\begin{bmatrix} r^{1/2}E_z \\ r^{1/2}H_\theta/i \\ r^{1/2}H_z \\ r^{1/2}E_\theta/i \end{bmatrix} = \begin{bmatrix} \cos(k_j x) & \sin(k_j x) & 0 & 0 \\ \epsilon_j g_1 & \epsilon_j g_2 & \dfrac{\beta_1 \cos(k_j x)}{k_j^2 r} & \dfrac{\beta_1 \sin(k_j x)}{k_j^2 r} \\ 0 & 0 & \cos(k_j x) & \sin(k_j x) \\ \dfrac{\beta_1 \cos(k_j x)}{k_j^2 r} & \dfrac{\beta_1 \sin(k_j x)}{k_j^2 r} & \mu g_1 & \mu g_2 \end{bmatrix} \begin{bmatrix} A_{2m-j} \\ B_{2m-j} \\ C_{2m-j} \\ D_{2m-j} \end{bmatrix}$$

$$= M_j(x,r)\, V_{2m-j} \qquad (2.5)$$

where $g_1 = \dfrac{\cos(k_j x)}{2rk_j^2} + \dfrac{\sin(k_j x)}{k_j}$

$g_2 = \dfrac{\sin(k_j x)}{2rk_j^2} - \dfrac{\cos(k_j x)}{k_j}$

Then at an interface with a layer of thickness T_1, index n_1 on

the left, the boundary conditions may be written

$$M_1(T_1,r)\ V_{2m-1} = M_2(0,r)\ V_{2m} \qquad (2.6a)$$

and at an interface with index n_2 on the left

$$M_2(T_2,r)\ V_{2m-2} = M_1(0,r)\ V_{2m-1} \qquad (2.6b)$$

From equations (2.5) it is clear that equations (2.6) are not periodic because of the presence of terms of O(1/kr). These same terms also couple together (A_m,B_m) and (C_m,D_m),so that,if a Bloch type solution did exist, E_z and H_z would have to have the same Bloch wave number.When terms of O(1/kr) are negligible, these effects may be ignored and then both the defining equations and the boundary conditions are periodic.

Neglecting terms of O(1/kr),(2.6) becomes

$$V_{2m} = \tilde{M}_1\ V_{2m-1} \qquad (2.7a)$$

$$V_{2m-1} = \tilde{M}_2\ V_{2m-2} \qquad (2.7b)$$

where, for i = 3 - j,

$$\tilde{M}_j = \begin{bmatrix} \cos(k_jT_j) & \sin(k_jT_j) & 0 & 0 \\ -\dfrac{k_i\epsilon_j}{k_j\epsilon_i}\sin(k_jT_j) & \dfrac{k_i\epsilon_j}{k_j\epsilon_i}\cos(k_jT_j) & 0 & 0 \\ 0 & 0 & \cos(k_jT_j) & \sin(k_jT_j) \\ 0 & 0 & -\dfrac{k_i}{k_j}\sin(k_jT_j) & \dfrac{k_i}{k_j}\cos(k_jT_j) \end{bmatrix}$$

Therefore $r^{1/2}E_z$ and $r^{1/2}H_z$ are uncoupled and are defined exactly as field components in a linearly periodic two-dimensional medium. Thus results which are analagous (in fact nearly identical) to those for linear periodicity hold in the radially periodic case. The main equations [43], for fields in the layers of index n_2, are listed here for later convenience. The

corresponding expressions for the fields in the layers of refractive index n_1 follow from (2.7b).

The matrices for translation by one whole period are

$$\begin{bmatrix} A_{2m} \\ B_{2m} \end{bmatrix} = \begin{bmatrix} c_1c_2 - g_M s_1 s_2 & c_1 s_2 + g_M s_1 c_2 \\ -c_1 s_2 - s_1 c_2 / g_M & c_1 c_2 - s_1 s_2 / g_M \end{bmatrix} \begin{bmatrix} A_{2m-2} \\ B_{2m-2} \end{bmatrix} \qquad (2.8)$$

$$\begin{bmatrix} C_{2m} \\ D_{2m} \end{bmatrix} = \begin{bmatrix} c_1c_2 - g_E s_1 s_2 & c_1 s_2 + g_E s_1 c_2 \\ -c_1 s_2 - s_1 c_2 / g_E & c_1 c_2 - s_1 s_2 / g_E \end{bmatrix} \begin{bmatrix} C_{2m-2} \\ D_{2m-2} \end{bmatrix} \qquad (2.9)$$

where $c_j = \cos(k_j T_j)$, $s_j = \sin(k_j T_j)$

$g_M = k_1 \epsilon_2 / k_2 \epsilon_1$

$g_E = k_1 / k_2$

The corresponding Bloch waves are:

$$E_z = \frac{1}{r^{1/2}} \exp(iQ_M(r-a)) \exp(-iQ_M x) \left(A_o \cos(k_2 x) + B_o \sin(k_2 x) \right)$$

$$H_z = \frac{1}{r^{1/2}} \exp(iQ_E(r-a)) \exp(-iQ_E x) \left(C_o \cos(k_2 x) + D_o \sin(k_2 x) \right)$$

where $\exp(iQ_M)$, $\exp(iQ_E)$ are the eigenvalues of the matrices in (2.8), (2.9) and (A_o, B_o), (C_o, D_o) are the corresponding eigenvectors. That is

$$\cos(Q_M \Lambda) = c_1 c_2 - 0.5\left(g_M + 1/g_M \right) s_1 s_2$$
$$\exp(iQ_M \Lambda) = \cos(Q_M \Lambda) \pm \sqrt{\cos^2(Q_M \Lambda) - 1}$$
(so Q_M, $-Q_M$ are both solutions)

(2.10)

$$\cos(Q_E \Lambda) = c_1 c_2 - 0.5\left(g_E + 1/g_E \right) s_1 s_2$$
$$\exp(iQ_E \Lambda) = \cos(Q_E \Lambda) \pm \sqrt{\cos^2(Q_E \Lambda) - 1}$$

(so Q_E, $-Q_E$ are both solutions)

$$(A_o, B_o)^T = (c_1 s_2 + g_M s_1 c_2 , \exp(iQ_M \Lambda) - c_1 c_2 + g_M s_1 s_2)$$
$$(C_o, D_o)^T = (c_1 s_2 + g_E s_1 c_2 , \exp(iQ_E \Lambda) - c_1 c_2 + g_E s_1 s_2) \qquad (2.11)$$

As in the case of linear periodicity, the frequency dependence of the propagation may be described in terms of pass and stop frequency bands. We are primarily interested in the reflective properties of the medium. The reflection bands for E_z,H_z occur for [43]

$$| \cos(Q\Lambda) | > 1$$

and then

$$Q = n\pi/\Lambda + iQ_i \qquad \text{for integer } n \qquad (2.12)$$

for $Q = Q_M$, Q_E

Inside the reflection band the physically possible solution is that for which the wave amplitude is decaying radially. For E_z, E_r, H_θ, this requires $|\exp(iQ_M\Lambda)| < 1$, so the sign chosen in (2.10) must be opposite to the sign of $\cos(Q_M)$, that is, the trace of the translation matrix. The analagous condition in terms of Q_E holds for the H_z, E_r, E_θ fields. The most rapid decay occurs (considering E_z and H_z separately) for [43]

$$k_1 T_1 = k_2 T_2 = \pi/2$$

This condition is the same for the E_z and H_z fields and so clearly here at least the respective reflection bands overlap. We will see in more detail later the relative variation of the stop and pass bands.

Thus in summary, for weak curvature, that is as long as terms of O(1/kr) are negligible, a radially periodic structure is fully

analagous to a linearly periodic one. It will support modes which have the form of Bloch waves, but which decay in amplitude radially as $r^{-1/2}$, as is expected from the cylindrical geometry. These Bloch type modes are not supported for smaller radii of curvature. Therefore, for example, if we require our solutions to be accurate to within 2% and the wavelength of the radiation is 1μm, then we must consider only structures with minimum radius of curvature of at least 8.3μm. In practice, the structures of interest are likely have much larger radii.

2.3 Dispersion relation for large-cored infinite Bragg fibre

Having determined the characteristics of propagation in the cladding of the Bragg fibre, we may now obtain the dispersion relation of the guide. For a waveguide, the periodic cladding is assumed to be preceeded by a single cladding layer of index n_1. This ensures that the boundary conditions are correct for the first interface of the periodic cladding.The notation is changed appropriately, the coefficients in the core being denoted A_o, B_o, C_o, D_o and those in the first layer of the periodic cladding being A_2, B_2, C_2, D_2. A confined mode will exist if evanescent Bloch waves can be excited in this cladding. That is, if the mode propagation constant at some frequency is such that the field is non-decaying in the core but the Bloch wave numbers Q_M, Q_E both lie in the forbidden gap. As long as the core refractive index is lower than both those of the cladding layers, the fields must be non-decaying in each cladding

layer (but will have decreasing amplitudes in successive layers). Another possible use of the structure is as a multichannel tube waveguide, in which the fields are evanescent in the core and low index cladding layers. If one of the cladding indices is lower than that of the core then it is conceivable that modes for which the field is evanescent in the low index cladding layers, but not in the core, may propagate. The dispersion relation which will be derived may be applied to these cases by allowing the appropriate wavenumbers to be imaginary. However the specific case of interest here is that in which the structure is used as a hollow waveguide, with the bulk of the power confined to the core.

The radially dependent parts of the fields in the core ($r < a$) may be written

$$E_z = A_o J_1(k_o r)$$

$$H_z = C_o J_1(k_o r)$$

where $k_o^2 = w^2 \mu \epsilon_o - \beta^2$

ϵ_o = permittivity of the core

n_o = refractive index of core

J_1 = 1th order Bessel function of the first kind.

and those in the first cladding layer

$$E_z = \frac{1}{r^{1/2}} \left(A_1 \cos(k_1(r-a)) + B_1 \sin(k_1(r-a)) \right)$$

$$H_z = \frac{1}{r^{1/2}} \left(C_1 \cos(k_1(r-a)) + D_1 \sin(k_1(r-a)) \right)$$

The boundary conditions at the core/cladding interface, r=a, are

$$\begin{bmatrix} A_1 \\ B_1 \\ \\ \\ C_1 \\ D_1 \end{bmatrix} = a^{1/2} A_o \begin{bmatrix} J_1 \\ \dfrac{J_1}{2k_1 a} + \dfrac{k_1 \epsilon_o}{k_o \epsilon_1} J_1' + \dfrac{\beta 1 k_1}{w \epsilon_1 a} J_1 \left(\dfrac{1}{k_o^2} - \dfrac{1}{k_1^2} \right) R_o \\ \\ \\ R_o J_1 \\ \dfrac{\beta 1 k_1}{w \mu a} J_1 \left(\dfrac{1}{k_o^2} - \dfrac{1}{k_1^2} \right) + \left(\dfrac{J_1}{2k_1 a} + \dfrac{k_1}{k_o} J_1' \right) R_o \end{bmatrix} \tag{2.13}$$

where $J_1 = J_1(k_o a)$

$R_o = C_o / A_o$

$J_1' = \dfrac{1}{k_o} \dfrac{dJ_1(k_o a)}{dr}$

and at the first interface between cladding layers, $r=a+t_1$, are

$$\begin{bmatrix} A_2 \\ B_2 \\ \\ C_2 \\ D_2 \\ \\ \end{bmatrix} = \begin{bmatrix} A_1 \cos(k_1 t_1) + B_1 \sin(k_1 t_1) \\ \dfrac{k_2 \epsilon_1}{k_1 \epsilon_2} \left(- A_1 \sin(k_1 t_1) + B_1 \cos(k_1 t_1) \right) \\ C_1 \cos(k_1 t_1) + D_1 \sin(k_1 t_1) \\ \dfrac{k_2}{k_1} \left(- C_1 \sin(k_1 t_1) + D_1 \cos(k_1 t_1) \right) \\ \\ \end{bmatrix} \tag{2.14}$$

In order to excite a Bloch wave , from (2.11), it is necessary for

$$\frac{A_2}{B_2} = \frac{c_1 s_2 + g_M s_1 c_2}{\exp(iQ_M \Lambda) - c_1 c_2 + g_M s_1 s_2} \tag{2.15}$$

$$\frac{C_2}{D_2} = \frac{c_1 s_2 + g_E s_1 c_2}{\exp(iQ_E \Lambda) - c_1 c_2 + g_E s_1 s_2}$$

From (2.13), (2.14), (2.15), setting

$$\frac{B_1}{A_1} = N_M = \frac{g_M A_2 \tan(k_1 t_1) + B_2}{g_M A_2 - B_2 \tan(k_1 t_1)}, \quad \frac{D_1}{C_1} = N_E = \frac{g_E C_2 \tan(k_1 t_1) + D_2}{g_E C_2 - D_2 \tan(k_1 t_1)}$$

and eliminating the unknown parameter R_o,

$$\left(\frac{\beta 1 k_1 J_1}{w\sqrt{\epsilon_1 \mu}\, a}\left(\frac{1}{k_o} - \frac{1}{k_1}\right)\right)^2 = \left(N_E J_1 - \frac{J_1}{2k_1 a} + \frac{k_1 J_1'}{k_o}\right)\left(N_M J_1 - \frac{J_1}{2k_1 a} + \frac{k_1 \epsilon_o J_1'}{k_o \epsilon_1}\right)$$

Neglecting terms of order $1/ka$ (but retaining terms containing N_E, N_M as these may not be of order unity) this is

$$\left(\frac{n_e}{n_o}\frac{1}{k_o^2 a^2}\right)^2 \approx \left(\frac{J_1'}{k_o a J_1} - \frac{N_E}{k_1 a}\right)\left(\frac{J_1'}{k_o a J_1} - \frac{\epsilon_1 N_M}{\epsilon_o k_1 a}\right) \tag{2.16}$$

where n_e = effective index = $\beta\lambda/2\pi$

This is the dispersion equation for the infinite Bragg fibre for the unknown β in terms of a, t, T_1, T_2, that is any given structure. It holds for any periodic cladding, and not only for optimum layer thicknesses. It is convenient at this point to define (analogously to the case of a finite cladding [50], [54])

$$N = \begin{cases} N_E & \text{for TE modes} \\ N_M & \text{for TM modes} \\ N_H/2 = (N_E + (\epsilon_1/\epsilon_o)N_M)/2 & \text{for hybrid modes} \end{cases}$$

As long as N is real (using the approximation $n_e \approx 1$), the solution for β is real. Therefore the frequencies for which

this quantity is real can be taken as the effective reflection bands for the corresponding mode. The regions for which N_M, N_E and N_H are real and complex as functions of w,β (for real β) are shown in figure 2.2.

Equation (2.16) is clearly similar in form to the dispersion equation for a hollow guide with a single dielectric cladding [50], and may be solved in the same way as long as N_M, N_E are not too large. For TE and TM modes the equation is linear in J_1'/J_1. For hybrid modes, regarding the equation as a quadratic in J_1'/J_1, if we can neglect terms of order

$$\left(\frac{N_H}{2k_1a}\right)^2$$

then (2.28) becomes

$$\frac{J_1'}{J_1\, k_o a} \approx \frac{N_H}{2k_1a} \pm \frac{n_e\, 1}{n_o (k_o a)^2}$$

If also $n_e \approx n_o$ then the equation for hybrid modes takes the same form as that for TE and TM modes giving

$$J_{l\mp1} \approx \pm \frac{k_o a}{k_1 a} N J_l' \qquad (2.17)$$

where N takes the value appropriate for the particular mode. If u_o is such that $J_{l\mp1}(u_o) = 0$, then since the right hand side of (2.17) is small,

$$k_o a \approx u_o \left(1 - \frac{N}{k_1 a} \right)$$

Setting $\beta = \beta_r + i\beta_i$ and assuming β_i is small, this implies that

$$(n_o^2 4\pi^2/\lambda^2 - \beta_r^2)^{1/2} a \approx u_o \left(1 + \mathrm{Re}(N)/k_1 a \right) \qquad (2.18)$$

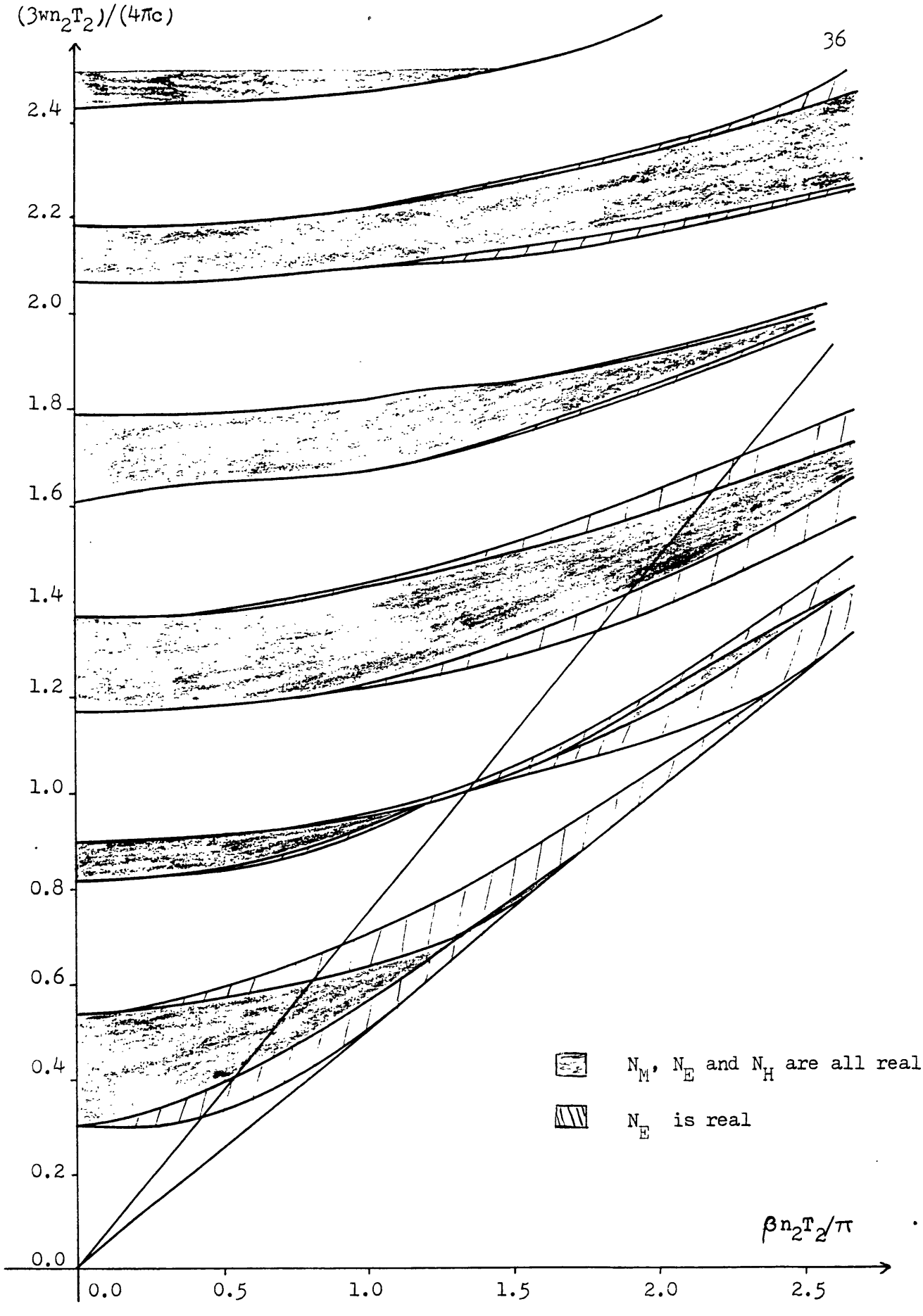

Figure 2.2 Reflection and transmission bands in a periodic medium
The shaded areas are the reflection bands
$n_1 = 4.0$ and $n_2 = 1.5$

$$\alpha_1 = \beta_i = \pm \frac{u_o^2 \lambda \, \mathrm{Im}(N)}{n_o 2\pi a^2 k_1 a}$$

and from (2.13)

$$R_o = \sqrt{\epsilon_o/\mu} \; (\; 1 + O(1/k_1 a) \;)$$

Equation (2.18) is identical to that for a hollow singly clad guide [50]. Thus if the mode considered has low loss and N_E, N_H are not too large, the change in the real part of the propagation constant as a result of the multiple claddings is small. Figure 2.3 shows how N_E, N_M, N_H vary with w for the first hybrid (HE_{11}) mode.

When β is real, the propagation is theoretically lossless. Therefore the modes for which the field amplitudes are exponentially decaying may be taken to correspond to guided modes of the fibre. The modes for which the amplitudes are increasing correspond to the conventional unphysical modes with the same β which increase exponentially with increasing radial distance from the core. Thus the infinite Bragg fibre can be considered to posses a set of guided modes similar to those resulting from total internal reflection in a conventional high index core fibre.

The solutions obtained at frequencies for which N is complex correspond to leaky modes of the fibre. The mode corresponding to an outgoing wave is obtained by choosing the Bloch eigenvalue with positive imaginary part (the plus sign in equation (2.10)), which ensures that α_1 is positive.

However, the Bloch wave numbers Q_E, Q_M, which describe the shape of the envelopes of the fields, cannot be related directly to the propagation constants in the radial direction for a singly

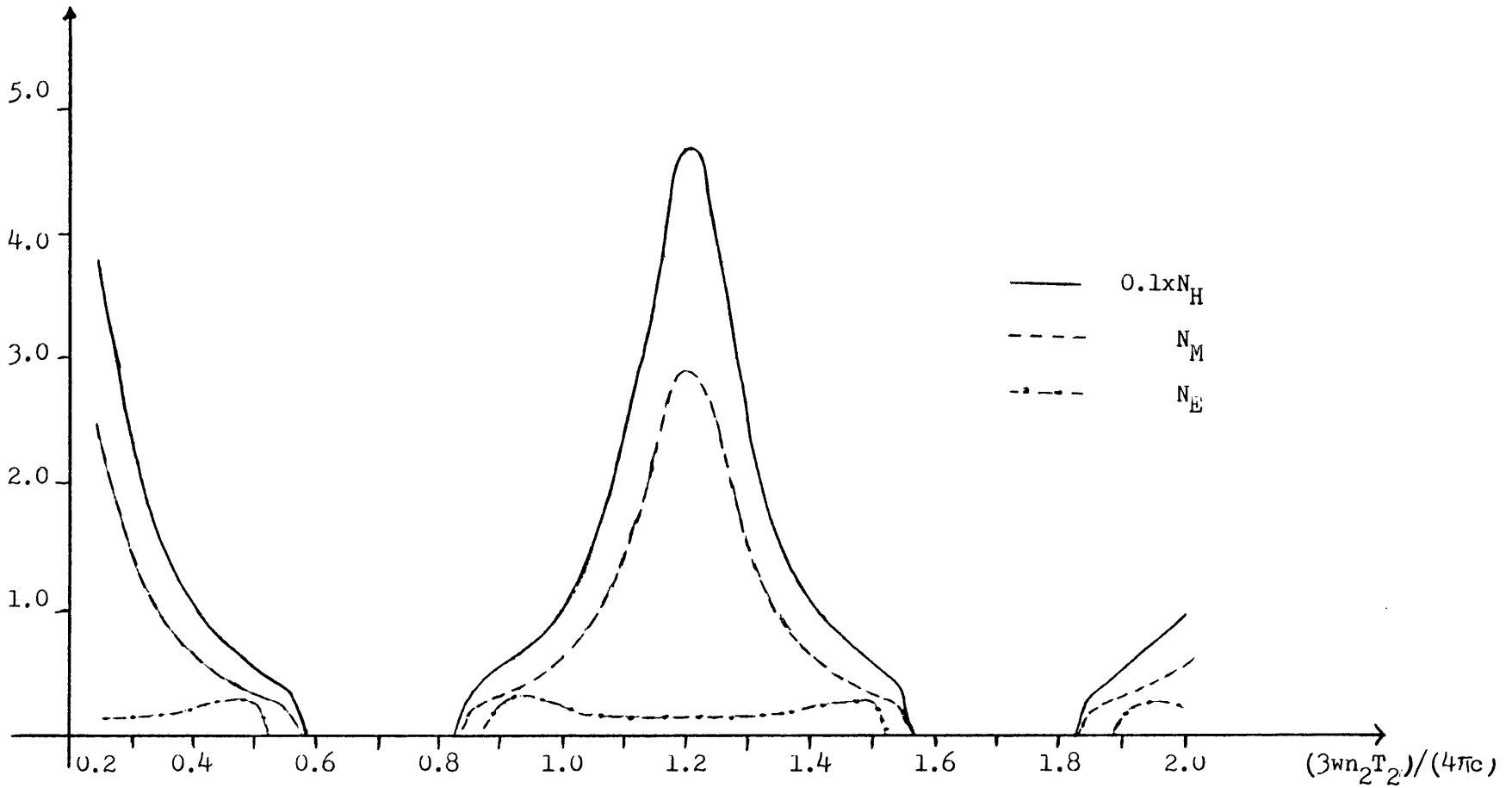

Figure 2.3 N_E, N_M and $0.1N_H$ as a function of frequency for the HE_{11} mode ($n_1 = 4.0$, $n_2 = 1.5$)

cladded hollow or high index cored guide. In particular, in the latter cases, these constants are equal for the field components in all directions, while $Q_E \neq Q_M$.

The solutions analogous to the conventional radiation modes may be obtained either by removing the constraint of exciting a Bloch-type mode in the cladding or by taking the field in the cladding to be a sum of both the incoming and outgoing Bloch waves which may exist for any given vaue of β (that is assuming Bloch wavenumbers $|Q_E|$, $|Q_M|$ for one wave and $-|Q_E|$, $-|Q_M|$ for the other). In both these cases the number of unknown coefficients increases by two, which results in an inhomogeneous set of equations (and one undetermined coefficient) and so removes the constraint on β. The fields are only meaningful when Q_E, Q_M are real and so the range of values of β is that for which N is complex, that is the range of values for which "lossless" modes cannot be excited. These properties are of course those of radiation modes of conventional cylindrical fibres also.

In the following section we will consider the cladding layer thicknesses which will minimise the loss in the Bragg fibre.

2.4 Optimal Bragg fibre

For a Bloch mode of a planar periodic stratified medium it has been shown that the decay rates of the field amplitudes in the claddings $|Q_{iE}|$, $|Q_{iM}|$ (defined in (2.12)) are each maximised when the cladding layers are "quarter-wave" thicknesses [43]. That is

$$k_1 T_1 = k_2 T_2 = \pi/2 \qquad (2.19)$$

In this case, if the mode is a TE (TM) mode, the electric (magnetic) field and its derivative (in the direction of the periodicity) are zero at alternate interfaces between cladding layers. It has been shown also that this field pattern (and so the same layer thicknesses (2.19)) is a sufficient condition for the outflowing power at each successive cladding interface to have a minimum value.

For the cylindrical Bragg fibre the optimum structure for the TE and TM modes has been obtained by minimising the outflowing power. It has been shown that, if terms of order (1/kr) may be neglected, then similarly to the planar case, the TE (TM) mode field has zeros of the H_z (E_z) field and its radial derivative at alternate cladding interfaces.

We have seen in sections 2.2, 2.3 that in fact TE, TM and hybrid Bloch type modes exist in weakly curved cylindrical periodic media. Therefore the maximum decay of E_z, H_z (at least when these fields are considered separately) is acheived for each of these modes when the layers are of the corresponding "quarter-wave" thicknesses given by (2.19). In this case the Bloch eigenvalues and eigenvectors (for a decaying wave) and the dispersion relations are as follows (considering in particular hybrid modes).

Since in our notation $k_2 < k_1$,

$$\exp(iQ_E \Lambda) = -k_2/k_1$$

$$C_2/D_2 = 0 \qquad (2.20)$$

$$N_E = -1/\tan(k_1 t_1)$$

There are two cases to consider:

(i) $k_2 \epsilon_1 / k_1 \epsilon_2 = 1/g_M < 1$

$$\exp(iQ_M\Lambda) = -k_2\epsilon_1/k_2\epsilon_1$$

$$A_2/B_2 = 0 \qquad (2.21)$$

So

$$A_1/B_1 = -\tan(k_1t_1) = C_1/D_1$$

This leads directly to a condition on R_o independently of t

$$\left(\frac{R_o^2}{\epsilon_1} - \frac{1}{\mu}\right)\frac{\beta 1 k_1 J_1}{wa}\left(\frac{1}{k_o^2} - \frac{1}{k_1^2}\right) + R_o\frac{k_1 J_1'}{k_o}\left(\frac{\epsilon_o}{\epsilon_1} - 1\right) = 0 \qquad (2.30)$$

(2.22)

Also $N_M = -1/\tan(k_1t_1)$

Therefore if $k_1t_1 = \pi/2$

then $N_H = 0$

so $k_oa = u_o$, $R_o = \sqrt{\epsilon_o/\mu}$

This is of course a possible low loss solution and so the first cladding is also part of the periodic reflector (that is, an initial layer to satisfy the boundary conditions to excite a Bloch wave is unnecessary). It seems likely that this thickness of the first cladding layer will give maximum power confinement and it will be shown simply in the following chapter that this is indeed the case.

(ii) $k_2\epsilon_1/k_1\epsilon_2 = 1/g_M > 1$

Now

$$\exp(iQ_M\Lambda) = -k_1\epsilon_2/k_2\epsilon_1$$

$$B_2/A_2 = 0 \qquad (2.23)$$

So

$$B_1/A_1 = \tan(k_1t_1) = -C_1/D_1$$

and the equation for R_o is

$$\left[\frac{\beta 1}{wk_o a}\left(\frac{\epsilon_o}{\mu} + R_o^2\right)J_1 J_1' + R_o\epsilon_o(J_1'^2 + \frac{\beta^2 1^2 J_1^2}{w^2\mu\epsilon_o k_o^2 a^2})\right](1 + O\left(\frac{1}{k_1 a}\right)) = 0 \qquad (2.24)$$

Also $N_M = \tan(k_1 t_1)$

so $N_H = \tan(k_1 t_1) - (\epsilon_1/\epsilon_o \tan(k_1 t_1))$

Now it is not clear that $k_1 t_1 = \pi/2$ leads to a possible low loss solution since this makes N_H large. Therefore in this case an intermediate layer between the core and periodic reflector is required. The optimum value in this case is considered in chapter 3.

From the form of the eigenvectors ((2.20), (2.21), (2.23)) and translation matrix (2.7b) evaluated for the case of quarter-wave thicknesses it is clear that the E_z, H_z fields and their radial derivatives have zeros at the alternate layer interfaces in the optimum case.

We have seen that the propagating mode in a Bragg fibre may have different properties depending on whether g_M is greater or less than one. The condition $g_M = 1$ represents the case when the refractive indices and propagation constant are such that the TM-like part of the field is incident on the periodic cladding at the Brewster angle and so the power corresponding to this part of the field is totally lost. Here N_M becomes large and it should be remembered that approximate solution for the attenuation is valid only for small loss.

For a real Bragg fibre with a finite number of layers, the power loss is not zero even for frequencies inside the reflection band, as the reflectivity is always less than one. We may estimate this loss if we know the power lost radially per unit length. Therefore we will extend the result obtained for TE and TM modes [32] to

obtain an expression for the outflowing power of a general hybrid mode.

In order to retain some generality, we will write the fields in the cladding layers as follows:

$$E_z = (A_j J_1(kr) + B_j Y_1(kr)) \cos(1\theta) \exp(i\beta z - iwt)$$

$$H_z = (C_j J_1(kr) + D_j Y_1(kr)) \sin(1\theta) \exp(i\beta z - iwt)$$

Re-writing these expressions in terms of Hankel functions

$$2E_z = (A_j + B_j/i) H_1^{(1)}(kr) + (A_j - B_j/i) H_1^{(2)}(kr)$$

$$2H_z = (C_j + D_j/i) H_1^{(1)}(kr) + (C_j - D_j/i) H_1^{(2)}(kr)$$

For our choice of exponential factor, $H_1^{(1)}(kr)$ is associated with a wave travelling in the positive r direction, i.e., an outgoing wave, and $H_1^{(2)}(kr)$ represents an incoming wave. Considering the outgoing z-fields and the corresponding radial and tangential components only, the time-averaged Poynting vector of the outgoing wave in the jth cladding layer is

$$\begin{aligned} S_r &= \mathrm{Re} (E_{\theta out} H^*_{Zout} - E_{zout} H^*_{\theta out})/2 \\ &= \frac{w}{8k} (\epsilon(A_j^2 + B_j^2) + \mu(C_j^2 + D_j^2))(J_1 Y_1' - J_1' Y_1) \end{aligned}$$

Using the Wronskian of the Bessel functions [36] and integrating over a unit length cylindrical surface gives the radially outward power flow per unit length in the jth cladding as

$$P_{rj} = \frac{w}{2k^2} (\epsilon(A_j^2 + B_j^2) + \mu(C_j^2 + D_j^2)) \qquad (2.25)$$

From the well known asymptotic expressions for the Bessel functions in terms of circular functions [36], when A_m, B_m, C_m, D_m are the coefficients for the fields expressed in circular functions (defined by (2.4)) the right-hand side of equation (2.25) must be multiplied by $\pi k_2/2$ to give,

$$P_{rm} = w\pi(\epsilon(A_m^2 + B_m^2) + \mu(C_m^2 + D_m^2))(1 + O(1/kr))/4k \quad (2.26)$$

It should be noted that P_{rm} gives an estimate of the loss given that the last cladding is the (m+1)th and does not represent the net power flow out of the (m+1)th cladding for each m. Also, we have satisfied the boundary conditions for a radiation mode, which has both incoming and outgoing components, but we have only taken the contribution to the power flow of the outgoing part. In the last cladding layer the amplitudes of a mode with only an outgoing component must be twice those of the radiation mode. Therefore the actual value of the outflowing power must be taken as $4P_{rm}$. This then gives agreement with the leaky mode result [50] for the case of a singly cladded guide.

From (2.10), (2.26) in a layer of index n_2, for a Bloch wave (for given values of β, A_1, B_1, C_1, D_1)

$$P_{r2m} = w\pi(\epsilon_2 \exp(iQ_E(2m-2)\Lambda)B_2^2(1 + A_2^2/B_2^2) + \mu \exp(iQ_H(2m-2)\Lambda)D_2^2(1+C_2^2/D_2^2))/4k \quad (2.27)$$

For an "optimum" Bragg fibre with 2m+1 cladding layers we get from (2.20), (2.21), (2.23)

(i) $g_M > 1$

$$P_{r2m} = w\pi A_o^2 (\epsilon_2 (1/g_M)^{2m} + \epsilon_o (1/g_E)^{2m})/4k$$

(ii) $g_M < 1$

$$P_{r2m} = w\pi A_o^2 (\epsilon_2 g_M^{2m} A_2^2 + \mu (1/g_E)^{2m} C_2^2)/4k$$

Clearly the power is reduced for a fixed number of cladding layers if g_E is increased and g_M is increased in the first case and decreased in the second. Figure 2.4 shows the contours of constant g_E, g_M as the refractive indices n_1, n_2 are varied. From this it can be seen that, for most likely refractive indices for which g_E is large, g_M is less than one.

Now that we have an expression for the outward radial power flow per unit length $4P_r$, the attenuation constant α_1 (that is the imaginary part of the propagation constant) can be determined since these quantities are simply related by [50]

$$2\alpha_1 = 4P_r / \text{(longitudinal power flow)}$$

Therefore it is useful to consider

radially outward power flow per unit length in the (m+1)th clad

---

longitudinal power flow in the core and first m claddings

$$= 4P_{rm} / (P_{zcore} + \sum_{s=1}^{m} P_{zcladds})$$

P_{zcore} and $P_{zcladds}$ are obtained by integrating the z-component of the time averaged Poynting vector

$$S_z = \text{Re}(E_r H_\theta^* - E_\theta H_r^*)/2$$

over the relevant cross-section to yield

$$P_{zcore} = (\pi\beta^2/2k_o^4) A_o^2 [2lR_o (1 + (w^2\mu\epsilon_o/\beta^2) J_1^2) +$$

$$w(\epsilon+\mu R_o^2)((k_o^2a^2-l^2)J_1^2 + k_o^2a^2J_1'^2 + 2k_oal^2J_1J_1')/\beta]$$

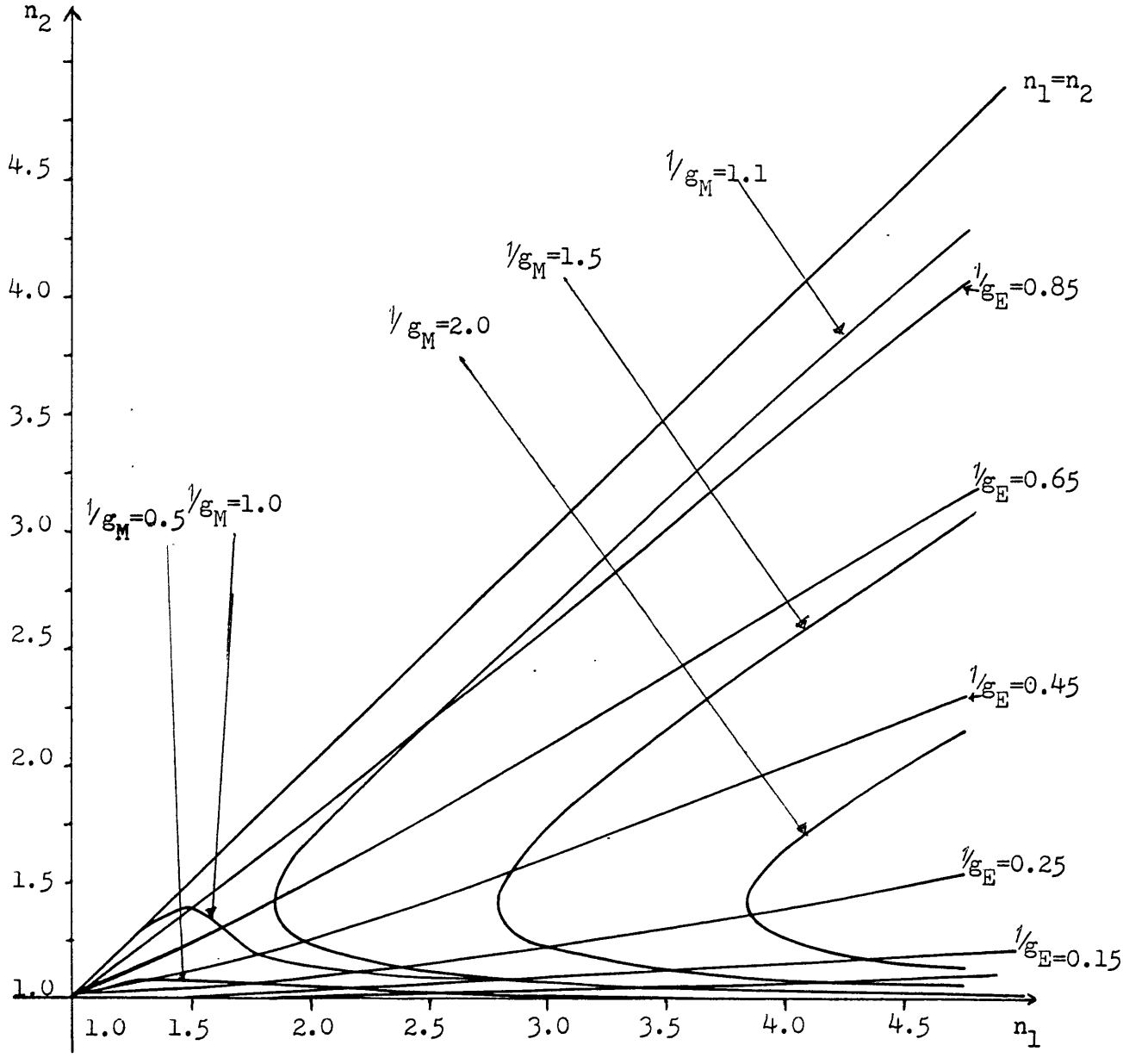

Figure 2.4 Contours of constant g_E and g_M

$$P_{zcladds} = \pi\beta w(kr((\epsilon A_s^2 + \mu C_s^2)(J_1 J_1' + 0.5kr(J_1'^2 + J_1^2)) + (\epsilon B_s^2 + \mu D_s^2)(Y_1 Y_1' + 0.5kr(Y_1'^2 + Y_1^2)) + 0.5(\epsilon A_s B_s + \mu C_s D_s)(J_1^2 - Y_1^2)(1 + O(1/kr)))/k^4$$

$$= \pi^2 \beta w T (\epsilon A_s^2 + \epsilon B_s^2 + \mu C_s^2 + \mu D_s^2)(1 + O(1/kr))/4k$$

where $J_1 = J_1(k_o a)$ and similarly for J_1'

and if the cladding layer s has index n_j (j = 1,2) then

$$k = k_j, \ \epsilon = \epsilon_j, \ T = T_j$$

In fact for low loss cases,

$$P_{zcore} >> \sum_{s=1}^{m} P_{zcladds} \qquad (2.28)$$

and also if $R_o \simeq \sqrt{\epsilon_o/\mu}$, $k_o a \simeq u_o$ (2.18) then

$$P_{zcore} = \pi A_o^2 (\sqrt{\epsilon_o/\mu}) a^2 J_1^2$$

and so we can write for a structure with m+1 claddings

$$2\alpha_{1m} = 4P_{rm}/(\pi A_o^2 (\sqrt{\epsilon_o/\mu}) a^2 J_1^2) \qquad (2.29)$$

Thus from (2.27), (2.29) we have obtained an expression for the attenuation constant of a low loss Bragg fibre with a finite number of cladding layers.

2.5 Alternative derivation of optimal Bragg fibre

In this section we will show that we can obtain a low loss Bragg fibre structure for a general hybrid mode by minimising the outflowing power in each successive cladding layer. It should be noted that neither this procedure, or the equivalent one of maximising $|Q_i|$, i.e. setting T_1, T_2 to satisfy (2.19), gives an exactly optimum structure for any finite number of cladding layers. However it will be assumed that for a low loss mode for

which the field amplitudes are small at the last cladding layer, the infinite structure is a good approximation to the finite one.

We now consider an arbitrary radiation mode of the Bragg fibre. Therefore there is no dispersion equation and β can take any chosen value less than $n_o 2\pi/\lambda$. We then construct a structure which will propagate a mode with this value of β with low loss.

For a cladding boundary at r_j (figure 2.5) with cladding refractive indices n_1, n_2 on the left-hand side and right-hand side of the interface respectively, the fields in the two claddings at the interface can be written as shown below (since A_j, B_j, C_j, D_j and hence E_{z1}, H_{z1} are real for all j)

n_1	r_j	n_2
$E_z(k_1 r_j) = E_{z1} \cos(l\theta)$		$E_z(k_2 r) = (AJ_{12} + BY_{12}) \cos(l\theta)$
$H_z(k_1 r_j) = H_{z1} \sin(l\theta)$		$H_z(k_2 r) = (CJ_{12} + DY_{12}) \sin(l\theta)$

where $J_{12} = J_l(k_2 r_j)$, $Y_{12} = Y_l(k_2 r_j)$

From continuity of E_z, H_z, E_θ, H_θ at the interface

$$A = \frac{\pi k_2 r_j}{2}\left(E_{z1}Y_{12}' - \frac{k_2 \epsilon_1}{k_1 \epsilon_2} E_{z1}'Y_{12} - \frac{\beta l}{k_2 r_j}\frac{1}{we_2}\left(\frac{k_2^2}{k_1^2} - 1\right)H_{z1}Y_{12}\right)$$

$$B = \frac{\pi k_2 r_j}{2}\left(-E_{z1}J_{12}' + \frac{k_2 \epsilon_1}{k_1 \epsilon_2} E_{z1}'J_{12} + \frac{\beta l}{k_2 r_j}\frac{1}{we_2}\left(\frac{k_2^2}{k_1^2} - 1\right)H_{z1}J_{12}\right)$$

$$C = \frac{\pi k_2 r_j}{2}\left(H_{z1}Y_{12}' - \frac{k_2}{k_1} H_{z1}'Y_{12} - \frac{\beta l}{k_2 r_j}\frac{1}{w\mu}\left(\frac{k_2^2}{k_1^2} - 1\right)E_{z1}Y_{12}\right)$$

$$D = \frac{\pi k_2 r_j}{2}\left(-H_{z1}J_{12}' + \frac{k_2}{k_1} H_{z1}'J_{12} + \frac{\beta l}{k_2 r_j}\frac{1}{w\mu}\left(\frac{k_2^2}{k_1^2} - 1\right)E_{z1}J_{12}\right) \qquad (2.30)$$

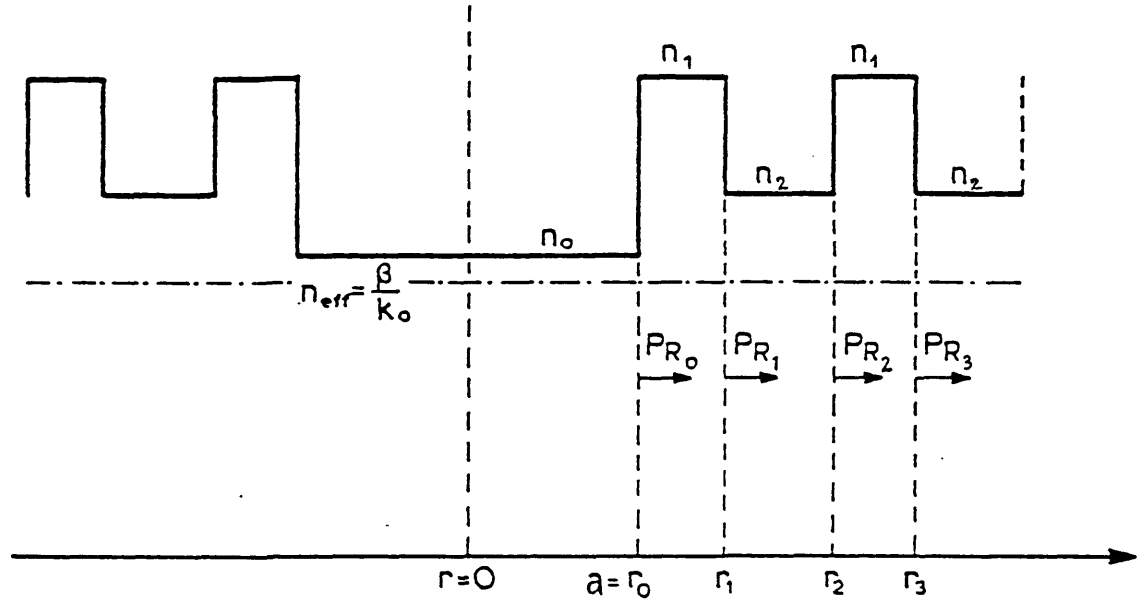

Figure 2.5 Notation used in section 2.5

Therefore substituting from (2.30) into equation (2.25) gives, to O(1/kr),

$$P_{rj} = \frac{w}{2k_2^2}\left(\frac{\pi k_2 r_j}{2}\right)^2 (J_1^2 + Y_1^2) (\epsilon_2 E_{z1}^2 + \mu H_{z1}^2 + \epsilon_2 \frac{k_2^2}{k_1^2} E_{z1}'^2 + \mu \frac{k_2^2}{k_1^2} H_{z1}'^2)(1 + O(\frac{1}{k_1 r_j}))$$

So

$$\frac{dP_{rj}}{dr_j} = \left(\frac{\pi k_2 r_j}{2}\right)^2 (J_1^2 + Y_1^2) w k_1 [\epsilon_2 E_{z1} E_{z1}' (1 - \frac{k_2^2 \epsilon_1^2}{k_1^2 \epsilon_2^2}) + \mu H_{z1} H_{z1}' (1 - \frac{k_2^2}{k_1^2})](1 + O(\frac{1}{k_1 r_j}))$$

and

$$\frac{d^2 P_{rj}}{dr_j^2} = \left(\frac{\pi k_2 r_j}{2}\right)^2 (J_1^2 + Y_1^2) w\mu \frac{(k_1^2 - k_2^2)}{k_2^2} \times (\gamma (E_{z1}'^2 - E_{z1}^2) + (H_{z1}'^2 - H_{z1}^2))(1+O(\frac{1}{k_1 r_j})) \quad (2.32)$$

where $\gamma = (k_1^2 \epsilon_2^2 - k_2^2 \epsilon_1^2)/(\mu \epsilon_2 (k_1^2 - k_2^2))$

From equation (2.32) it can be seen that, unlike in the case of TE modes [32], having placed a cladding boundary at r_{j-1} to minimise P_{rj-1}, the first zero of dP_{rj}/dr_j is not necessarily a minimum point of P_{rj}. However, if $\gamma > 0$ and it is possible to put cladding boundaries at

$$E_{z1} = H_{z1} = 0 \qquad \text{if } k_1 > k_2 \quad (2.33)$$
$$E_{z1}' = H_{z1}' = 0 \qquad \text{if } k_1 < k_2$$

then dP_{rj}/dr_j has its first zero and $d^2P_{rj}/dr_j^2 > 0$ at each boundary. Similarly this is true when $\gamma < 0$ if it is possible to put cladding boundaries at

$$E_{z1}' = H_{z1} = 0 \qquad \text{if } k_1 > k_2 \tag{2.34}$$
$$E_{z1} = H_{z1}' = 0 \qquad \text{if } k_1 < k_2$$

The condition $\gamma > 0$ is equivalent to requiring $k_2\epsilon_1/k_1\epsilon_2$ to be greater than one if k_2/k_1 is, that is, the two cases here correspond to those encountered in the Bloch wave approach and $\gamma = 0$ when $g_M = 1$.

The form of the fields assumed in the core and cladding layers are those of a radiation mode of the structure. As in the case of the conventional step-index cylindrical guide, in these radiation mode solutions, one coefficient, without loss of generality the ratio of the amplitudes of E_z and H_z in the core, remains undefined by the field equations and the boundary conditions (including the axial power flow) [56]. This degree of freedom can be used to obtain modes which satisfy equations (2.33), (2.34). We consider the usual two cases.

(i) $\gamma < 0$

Neglecting terms of $0(1/kr)$,

$$J_1'(kr) = -Y_1(kr)$$
$$Y_1'(kr) = J_1(kr)$$

so $E_{z1} = H_{z1}' = 0$ at r_j if

$$A_{j-1}/B_{j-1} = -D_{j-1}/C_{j-1} \tag{2.35}$$

Requiring $E_{z1}' = H_{z1} = 0$ at r_j also yields equation (2.35).

Now from the expressions for the coefficients in terms of the fields on the left hand side of the interface with the previous layer, equation (2.30), if $E_{z1}' = H_{z1} = 0$ then

$$A_j/B_j = -Y_{12}/J_{12}' = J_{12}/Y_{12}\,(1 + 0(1/k_1r_j))$$
$$D_j/C_j = -J_{12}/Y_{12}\,(1 + 0(1/k_1r_j))$$

so

$$A_j/B_j = -D_j/C_j\,(1 + 0(1/k_1r_j)) \tag{2.36}$$

Similarly if $E_{z1} = H_{z1}' = 0$ then again equation (2.36) is satisfied. Therefore by induction, the condition on the fields, equation (2.34), will be satisfied at each interface when

$$A_1/B_1 = - D_1/C_1 \qquad (2.37)$$

(ii) $\gamma > 0$

Similarly and more simply, equation (2.33) is satisfied if

$$A_1/B_1 = C_1/D_1 \qquad (2.38)$$

Equations (2.37), (2.38) are exactly the conditions required to excite an optimum Bloch mode and they are satisfied when equations (2.22), (2.24) hold. Thus although conditions (2.33), (2.34) were imposed rather arbitrarily, the results of the previous sections show that they are indeed the conditions for a minimum loss mode, at least for an infinite structure. Also it is clear that (2.22), (2.24) are the conditions that the relative "phases" radially of E_z, H_z are such that the layer boundaries occur at the correct postions for both the field amplitudes to be reduced by the layer structure, as is clearly necessary for a low loss solution. This is illustrated in figure 2.6, which shows the E_θ field in the cladding layers for various values of R_o for the optimum structure in each case.

In order to calculate β it is necessary to minimise α_{1o}, rather than just P_{ro}, since the longitudinal power flow is a function of β also. Terms of order $k_o a$ cannot be neglected and so

$$P_{ro} = \frac{w}{2k_o^2}\frac{(\pi k_1 r)^2}{2}(J_{11}^2+Y_{11}^2)(\epsilon_1 E_{z1}^2 + \mu H_{z1}^2 + \frac{\epsilon_1 k_1^2}{\epsilon_o k_o^2} E_{z1}'^2 + \frac{\mu k_1^2}{k_o^2} H_{z1}'^2 + \frac{b^2}{k_o^2 a^2 w^2}\frac{k_1^2}{k_o^2}(\frac{H_{z1}^2}{\mu} + \frac{E_{z1}^2}{\epsilon_1}).$$

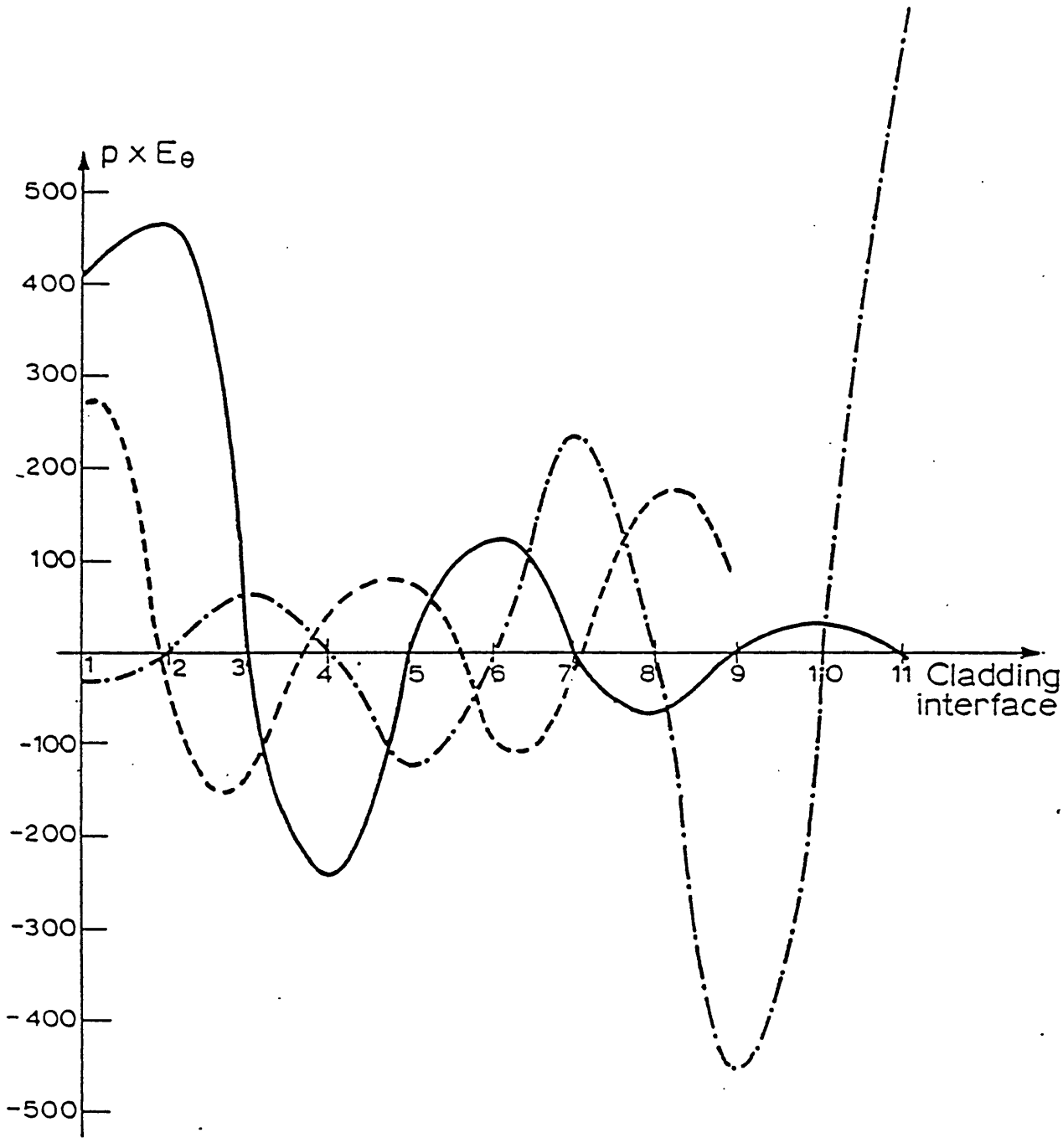

Fig. 2.6 : Scaled values of E_0 field in cladding layers, for $\theta = \pi/2$; $\lambda = 10.6\mu m$; a = 1.0 mm ; n = 1.5 ; $n_1 = 2.38$; $\beta = \beta_{optimal}$.

In the core $|E_\theta|$ has a maximum at r = 0 (not shown) of order 10^5

$$+ \frac{2\beta}{k_o a w k_o^2} \frac{k_1^2}{\epsilon_1} \left(\epsilon_o E_{z1}' H_{z1} + H_{z1}' E_{z1} \right))$$

The results of a minimisation of α_{1o} are shown in figure 2.7 and figure 2.8. Table 2.1 gives the optimium values for $k_o a$ and R_o for various values of refractive index and core radius.

The field pattern in the core of the minimum loss Bragg fibre is essentially determined by R_o. Since the optimum value of R_o can be regarded as one of an infinite number of possible values for a radiation mode with the same value of β, it is likely that the particular field pattern contributes to minimising the loss.

It is well known that, for example, if $l = 1$ and $R_o = \sqrt{\epsilon/\mu}$ then the fields in a large cored step-index fibre (both for high and low index cores) are linearly polarised. For a hollow core, this corresponds to $R_o = 2.653791 \times 10^{-3}$.

From table 2.1 it is clear that this condition is satisfied at least approximately for the minimum loss mode. The field patterns for a minimum loss mode and non-low loss modes are shown in figures 2.9 and 2.10. Clearly the minimum loss mode corresponds closely to the most linearly polarised mode. Also, from table 2.1, the first minimum of α_{1o} occurs at $k_o a = 2.4$ and here $R_o \sim 2.6 \times 10^{-3}$, the exact value depending on a, β, n_1, n_2. Thus in general the minimum loss mode has transverse electric and magnetic fields which have a radial dependence $J_o(k_o r)$. Therefore this mode corresponds very closely to the HE_{11} mode of the conventional step-index fibre, both for $\gamma > 0$ and $\gamma < 0$, the similarity being greater for $\gamma > 0$ and also large a/λ, as suggested by the results of section 2.4.

The next minimum of α_{1o} occurs for $k_o a = 5.13$ and here

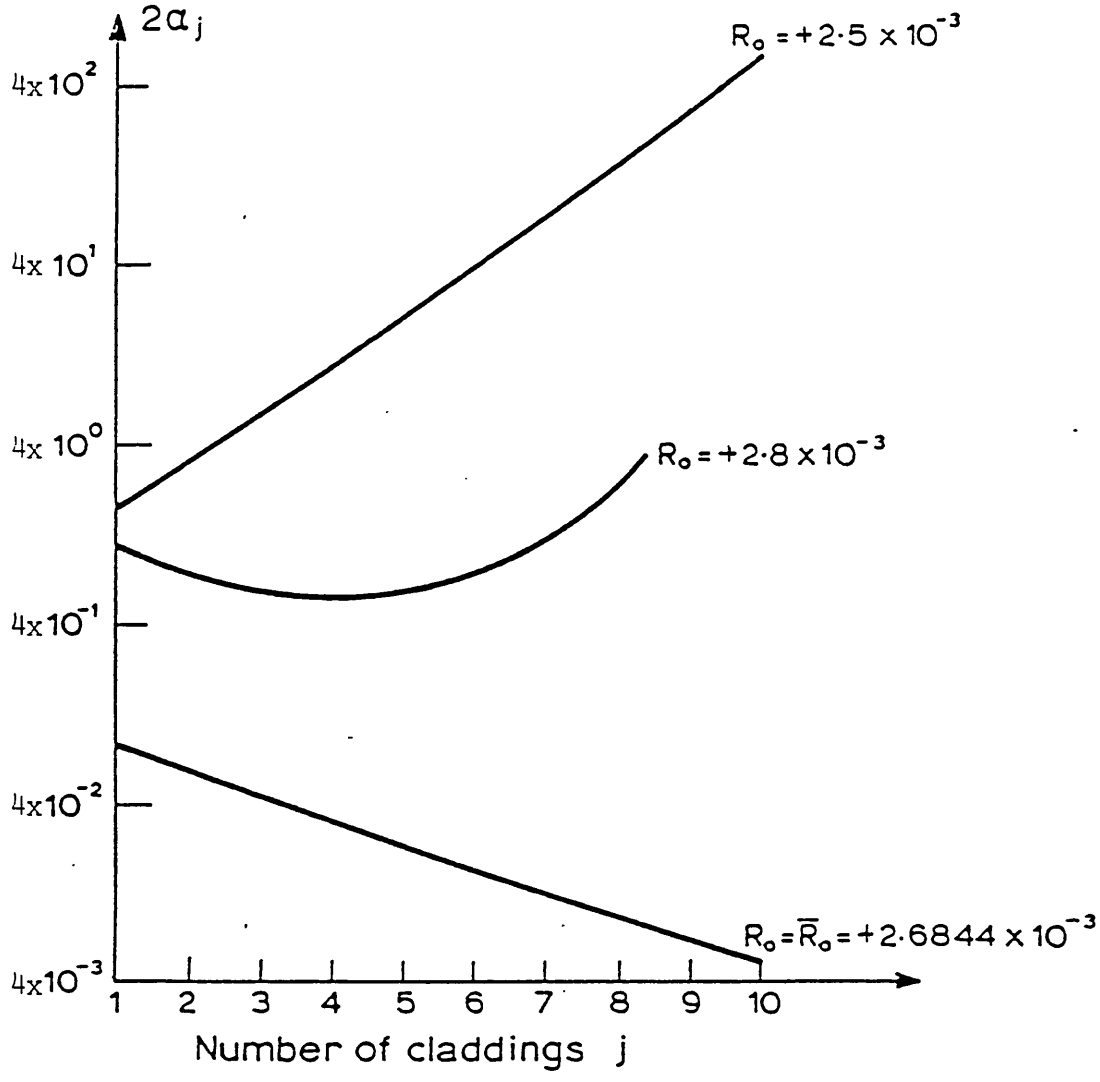

Fig. 2.7 : Power attenuation constant vs number of cladding layers. for different values of R_o

λ= 10.6 μm. a = 1.0 mm, n_2= 1.5. n_1= 2.38, u_o= 2.403

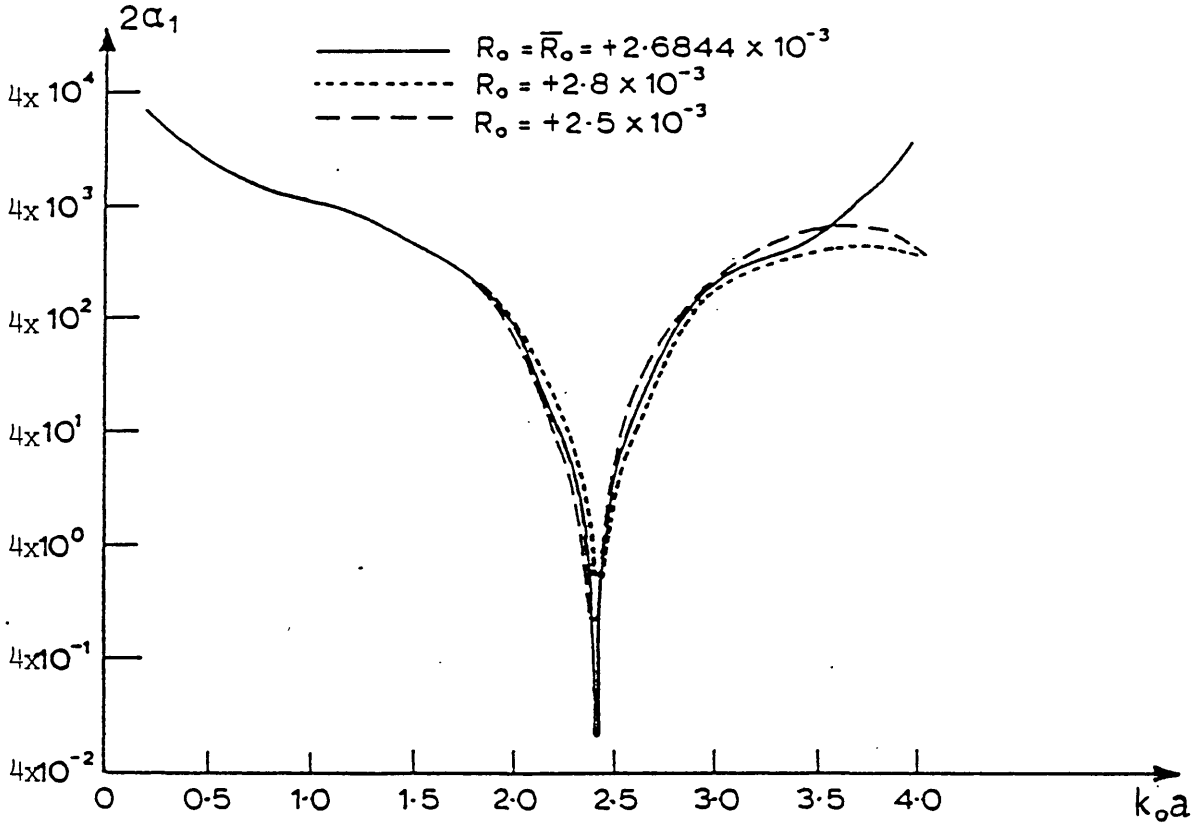

Fig. 2.8 : Power attenuation constant vs $k_o a$

λ = 10.6 μm, n_2= 1.5. n_1= 2.38.

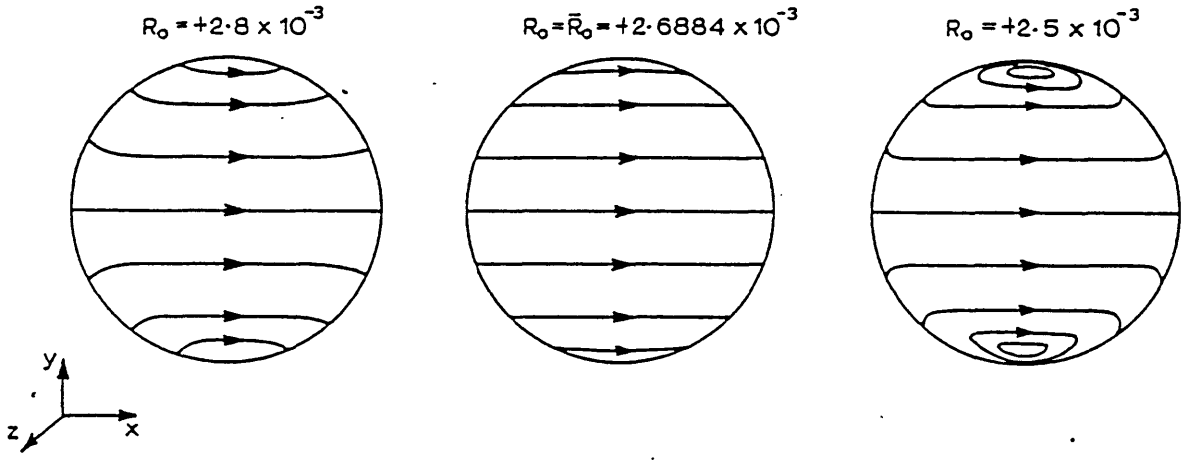

Figure 2.9 : Field lines of transverse electric field (for fixed α, β)

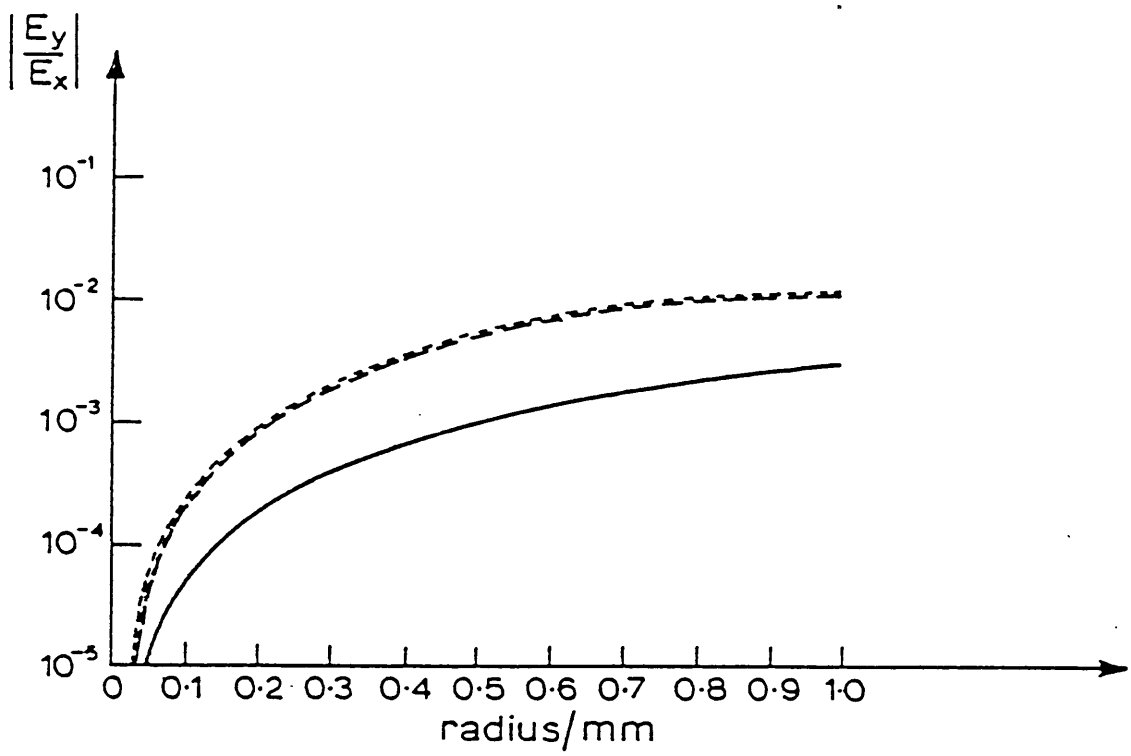

Fig. 2.10 : Ratio of magnitudes of transverse electric fields E_x . E_y in the core ($\theta = \pi/4$).

λ = 10.6 μm. n_2 = 1.5. n_1 = 2.38. a = 1.0 mm. $k_o a$ = 2.463

——— $R_o = \bar{R}_o$ = 2.6844 x 10^{-3}

------- R_o = 2.5 x 10^{-3}

– – – – R_o = 2.8 x 10^{-3}

					1st minimum		2nd minimum	
λ /μm	a /mm	n_2	n_1	γ	$k_o a$	$\bar{R}_o$	$k_o a$	$\bar{R}_o$
10.6	0.5	1.5	2.38	negative	2.401	2.7162×10^{-3}	5.127	-2.3886×10^{-3}
10.6	1.0	1.5	2.38	negative	2.403	2.6844×10^{-3}	5.136	-2.6552×10^{-3}
10.6	1.0	1.3	1.5	positive	2.405	2.6529×10^{-3}	5.131	-2.5143×10^{-3}
1.0	1.0	1.3	1.5	positive	2.405	2.6529×10^{-3}	5.136	-2.6553×10^{-3}
10.6	1.0	1.5	4.003	negative	2.401	2.6895×10^{-3}	5.129	-2.5082×10^{-3}

Table 2.1

$R_o = -2.65 \times 10^{-3}$. This gives a mode with fields with transverse parts which have a radial dependence $J_2(k_o r)$. This mode has a similar field pattern to the EH_{11} mode of the conventional step-index fibre.

In general, we find that the (2m-1)th and the 2mth minima of α_t have field patterns similar to those of the conventional HE_{1m} and EH_{1m} modes respectively. However, for increasing m, the transverse fields deviate more from the field patterns of the conventional modes, as seen from Table 2.2.

2.6 Application to guiding of long wavelength radiation

Numerical values of the leakage loss of the TE mode of the Bragg fibre that would result from a realistic finite number of claddings have been calculated previously for a guide with indices and dimensions reprsentative of the wavelength range of interest in optical communications [57]. These calculations suggest that the Bragg fibre is unlikely to compete effectively with existing solid-core, conventional fibres where the loss in available materials at the relevant optical wavelengths is extremely small, of the order of 0.2 dB/km for silica at its minimum loss wavelength of 1.55μm [20]. However the balance of the argument may well change at substantially longer wavelengths, for example 10.6μm and above, where material losses are high [58], required propagation distances small and allowable losses relatively large by the standards of modern optical communication [59].

We will determine the likely power loss owing to the less than

λ = 10.6 μm n_2 = 1.5 n_1 = 2.38 a = 1.0 mm $\gamma < 0$						
n^{th} minimum of $\bar{\alpha}_1$	n=1	2	3	4	5	6
$k_o a$	2.403	5.136	5.515	8.410	8.646	11.611
$\bar{R}_o \times 10^3$	2.6844	-2.6552	2.8285	-2.3050	3.1118	-2.0511
'Similar' conventional mode	HE_{11}	EH_{11}	HE_{12}	EH_{12}	HE_{13}	EH_{13}
$k_o a$ of conventional mode	2.405	5.136	5.52	8.417	8.654	11.620

Table 2.2 Mode characteristics

unity reflectivity at the core/cladding interface for light with a wavelength of 10.6μm by using the results of the previous sections. The mode considered is the lowest loss mode with angular dependence l = 1. We have already seen that this mode is similar to the conventional HE_{11} mode. Its transverse electric field profile has a maximum at the centre of the core and is similar in shape to a Gaussian beam profile. Therefore this mode is likely to have a relatively high launching efficiency and to be of most general interest. First we consider briefly the power distribution of this mode between the core and the cladding and hence estimate the reduction in the effective absorption coefficient which results from using a guide in which the bulk of the power propagates in a hollow core.

Let the core absorption coefficient be α_{co}/m and cladding absorption coefficient be α_{cl}/m (taken to be approximately equal for all the cladding materials). A power attenuation coefficient may be defined as

$$\alpha_{abs}(z) = -\,(1/P(z))\; dP(z)/dz$$

where P(z) is the power flow through a cross section of the guide at fixed z and dP(z) is the change in power in propagation through a distance dz.

Assuming the power outside the guide to be negligible,

$$dP(z) = -\alpha_{co}\, dz\, P_{zcore} - \alpha_{cl}\, dz \sum_j P_{zcladdj}$$

and

$$\alpha_{abs} = \frac{\alpha_{co}\, P_{zcore} + \alpha_{cl} \sum_j P_{zcladdj}}{P_{zcore} + \sum_j P_{zcladdj}}$$

For a hollow waveguide, $\alpha_{co} = 0$, so

$$\alpha_a = \frac{\alpha_{abs}}{\alpha_{cl}} = \frac{\sum_j P_{zcladdj}}{P_{zcore} + \sum_j P_{zcladdj}}$$

From calculation it is found that this is typically of the order of 10^{-6} or less for an optimal structure with 16 claddings. We will find that this loss is negligible when compared with the leakage loss (Table 2.3).

Figure 2.11 and 2.12 show calculated values of the attenuation coefficient, for leakage loss only, for optimal Bragg fibre structures for the HE_{11} mode for various core radii and refractive indices. As expected $\log(\alpha_1)$ decreases approximately linearly with increasing number of claddings.From the figures it can be seen that for a hollow-cored guide with eight claddings, of alternately, say, KBr and KRS-5, whose indices are 1.50 and 2.38 respectively at 10.6μm, we can expect losses of 34 x 10^{-2} dB/m for a core radius of 0.5mm and 4.8 x 10^{-2} dB/m for a core radius of 1.0mm. For a structure with 16 cladding the losses are 5.2 x 10^{-2} dB/m and 6.4 x 10^{-3} dB/m respectively. If take the absorption coefficient to be that of KRS-5, 2dB/m [58], the absorption loss in the latter case is 4 x 10^{-6}dB/m. This is insignificant when compared with the leakage loss and may be neglected. Thus the total loss can be taken to be given by the leakage loss. This may be compared with, for example, a measured overall loss in a KRS-5 fibre of 1dB/m. Clearly the Bragg fibre structure has a considerably lower loss.

In general the loss of a Bragg fibre is reduced if

(i) In general, the difference between the indices n_1 and n_2 is increased.

From figure 2.4, for a fixed value of n_1, $1/g_M$ is small for n_2 = 1(so the loss is low) and then tends to one as n_2 increases. For n_2 larger than the value at which g_M = 1, we are interested in increasing $1/g_M$ and $1/g_M$ increases as n_2

λ	n_2	n_1	a /mm	α_{abs}/a_{Cl}
10.6 µm	1.5	2.38	0.5	1.3×10^{-6}
10.6 µm	1.5	2.38	1.0	1.7×10^{-7}
10.6 µm	1.3	1.5	1.0	8.0×10^{-7}
1.0 µm	1.3	1.5	1.0	1.0×10^{-9}

Table 2.3 Effective relative absorption coefficient

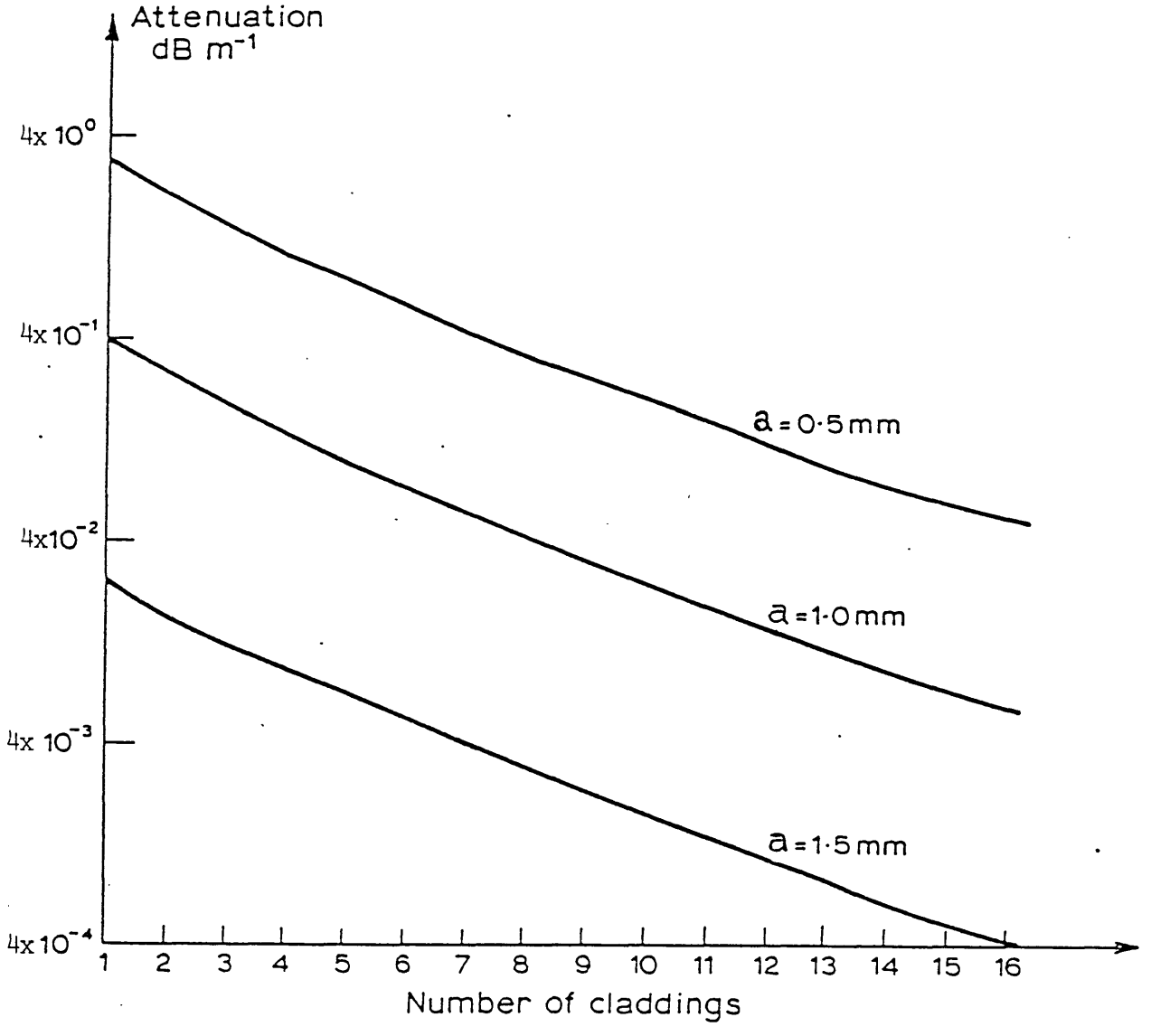

Fig. 2.11 : Attenuation of the optimal structure vs number of cladding layers for different core radii.

$\lambda = 10.6\ \mu m.\quad n_2 = 1.5.\quad n_1 = 2.38.$

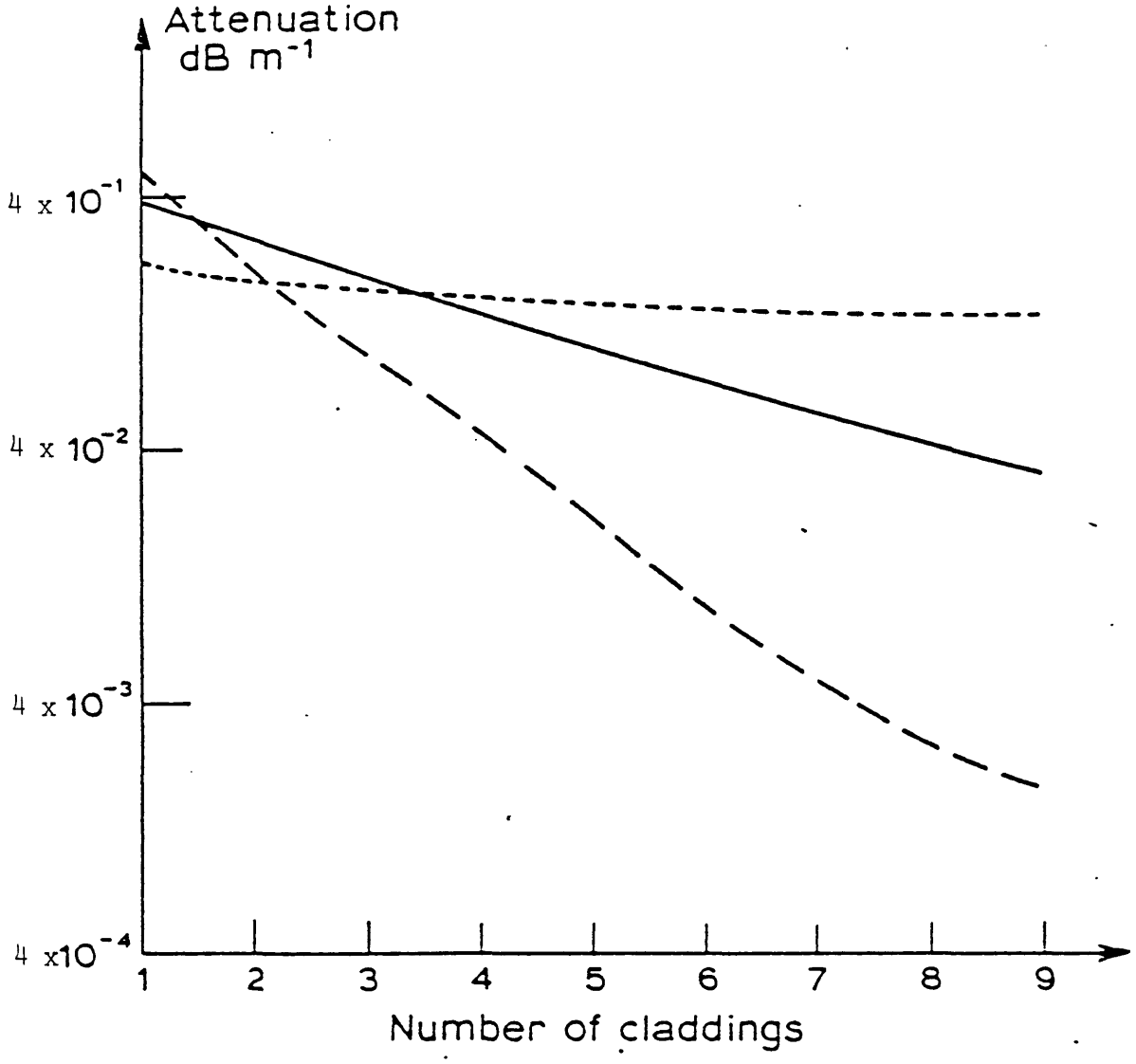

Fig. 2.12 : Attenuation of the optimal structure vs number of cladding layers for different values of index difference. n_1-n_2 . = 10.6 μm. a = 1.0 mm.

--------- $n_2 = 1.3$. $n_1 = 1.5$ ($\gamma > 0$)

———— $n_2 = 1.5$. $n_1 = 2.38$ ($\gamma < 0$)

— — — — $n_2 = 1.5$. $n_1 = 4.003$ ($\gamma < 0$)

does. Therefore now the loss decreases as n_1-n_2 is reduced. $1/g_M$ reaches its local maximum at a value of n_2 which increases with increasing n_1. Suitable available materials are likely to have indices greater than = 1.3 and so in practise in it is desirable to increase n_1. Beyond this value of n_2, $1/g_M$ decreases again as n_2 tends to n_1. Therefore in general it is best to maximise $n_1- n_2$, but there is a small range of n_2 for which the loss does not decrease with increasing $n_1 - n_2$. The achievable difference for any specific application is of course governed by material limitations, both availability and ease of fabrication.

(ii) The ratio a/λ, that is the relative size of the core, is increased. This is true for low index cored guides in general [50] (physically we can imagine that the light is reflected and transmitted at the core boundary fewer times per unit length). Thus increasing the core size appears to offer a much simpler alternative to increasing the number of claddings. However as the core size is increased for a fixed number of claddings the susceptibility of the guide to bending losses increases. We shall discuss this further in chapter 3.

(iii) The number of claddings is increased. At least in theory this offers the possibility of designing an arbitrarily low loss guide. In practise the attenuation of lowest loss mode is likely to deviate from that predicted as the number of layers is increased, because of the difference of the cladding layer thicknesses from the optimal value. This difference may result from inaccuracy in fabrication or possibly from the approximate nature of the analysis, although this latter effect seems likely to be small.

As we have seen, there are an infinite number of first-order hybrid-mode solutions with the same propagation constant. These modes are not, in general, orthogonal to the preferred low-loss HE_{11} mode. However they can all be represented as linear combinations of the low-loss HE_{11} mode and an orthogonal mode. Since the low-loss HE_{11} mode is most nearly plane polarised, it may be expected that the orthogonal mode is much less plane polarised and hence coupling from our preferred mode must require a z-dependent perturbation that is not isotropic. Thus undesirable mode conversion may not be too severe over reasonable distances.

It is perhaps worth discussing briefly also the launching efficiency of the Bragg fibre. It seems likely that a low loss mode will have a very different field pattern from the orthogonal mode with the same propagation constant. If the latter has a high loss its fields are likely to be small inside the core. Therefore coupling to high loss modes from, for example, a Gaussian shaped input field,(the degree which is determined primarily by the "overlap integral" of the transverse fields [33]) is likely to be small and most of the power is likely to be coupled into low loss modes with propagation constants in a small interval about the minimum loss mode. Thus the launching efficiency of the Bragg fibre is likely to be adequate, and very probably better than that of a singly cladded hollow guide.

3. THE BRAGG FIBRE FOR MULTIMODE AND BROAD BAND TRANSMISSION

3.1 Introduction

One of the main advantages of the Bragg fibre over a conventional step index waveguide is that it allows the confined power to propagate in an air core. It is primarily when this feature outweighs the disadvantage of the relatively large leakage loss that the Bragg fibre is likely to compare favourably with other guides. One such application, that of transmission of light at wavelengths of high material absorbtion, has been considered in chapter 2. For this application, the guide was ideally single mode at the single wavelength of operation. Another possible application of the Bragg fibre will be considered in this chapter which involves its use as a multimode guide for broadband transmission.

The temperature of a hot object can be determined from the spectrum of the emitted radiation. Therefore remote temperature sensing can be achieved by analysing the radiation transmitted by a waveguide from a hot or hostile environment. At very high temperatures, conventional solid-cored fibres cannot be used for this purpose. For example the glass transition temperature of silica is approximately 1500 °C. Materials of sufficiently high melting point for use at, say, 2000-2500 °C, such as magnesium oxide, zirconia, alumina and high temperature metals (for example molybdemum, tungsten) are likely to be difficult to draw into fibres or to be highly absorbing, or both.

It is possible that, for very high temperature sensing, a Bragg fibre structure may provide a design which is relatively easy to

fabricate and which has low absorption loss. The multilayers may conceivably be made by vapour deposition on the inner surface of a metal tube, followed by high temperature heat treatment, the remaining inner hollow forming the core. This may be a cheap alternative to fabricating a high temperature waveguide fibre by, for example, growing a single crystal of alumina of the required dimensions [60], [61].

In order to obtain an accurate estimate of the temperature it is desirable to transmit as much of the radiated power as possible and with minimum spectral distortion. Therefore it is now necessary to consider the suitability of the Bragg fibre for multimode transmission of a broad range of wavelengths. It has already been noted that the leakage loss increases with mode number as for any low index core (leaky) guide. In addition the multilayer reflector of the Bragg fibre is likely to be significantly wavelength sensitive.

The modes of a Bragg fibre which are not necessarily low loss, either because of high mode order or because the layer thicknesses are not optimised at this particular wavelength, may be obtained by solving the general dispersion equation (for a large cored guide), equation (2.16) of chapter 2. However this equation is based on the assumption of Bloch type modes, which hold strictly for an infinte structure. For finite structures for which the loss is large, this may be an unacceptable assumption, since the field is non-negligible at the last cladding layer. Therefore it is useful to model the Bragg fibre as a finite structure. We will use exactly the same boundary condition approach as in chapter 2 and substitute explicit expressions appropriate to a finite structure for N_E and N_M into equation (2.16). This allows the

dependence of the propagation charateristics of the Bragg fibre on wavelength and number of cladding layers to be easily calculated. As mentioned in chapter 2, a calculation for a hollow guide with a finite number of dielectric periodic cladding layers surrounded by a metal has been carried out [54], using the leaky mode approach. The general form of the solution for a low impedence and admittance cladding has been given.The explicit analytical expressions obtained were specifically for the case of "quarter-wave" layers (surrounded by a metal), and do not apply for a general wavelength.

3.2 Dispersion relation for the finite Bragg fibre

The dispersion relation for the finite Bragg fibre may be derived in a manner similar to that for the infinite case. The interest here is in the higher order mode and wavelength dependent characteristics of the guide and so the losses to be determined will be much larger than for the previously considered minimum loss case. Therefore it is necessary to bear in mind the limits of the validity of the solution which will be obtained. As before the total loss of the guide is ideally as small as possible and so we assume a large core radius relative to the centre wavelength (and so in fact.all wavelengths) considered.

The form of the dispersion equation is exactly as in the previous chapter, equation (2.16) (and we will use essentially the same notation here), since, in our approximation of large radius, the E_z and H_z fields are not coupled in the cladding layers.

However the expressions for A_2/B_2 and C_2/D_2 are now those for a finite structure. Equations (2.8), (2.9) give the transformation of the vectors of the field coefficients by one period, that is, a pair of claddings. It is convenient to invert these relations to yield

$$\begin{bmatrix} A_{2m} \\ B_{2m} \end{bmatrix} = \begin{bmatrix} c_1c_2 - s_1s_2/g_M & -c_1s_2 - g_Ms_1c_2 \\ c_1s_2 + s_1c_2/g_M & c_1c_2 - g_Ms_1s_2 \end{bmatrix} \begin{bmatrix} A_{2m+2} \\ B_{2m+2} \end{bmatrix}$$

$$= \begin{bmatrix} I & J \\ K & L \end{bmatrix} \begin{bmatrix} A_{2m+2} \\ B_{2m+2} \end{bmatrix} \quad \text{say}$$

$$\begin{bmatrix} C_{2m} \\ D_{2m} \end{bmatrix} = \begin{bmatrix} c_1c_2 - s_1s_2/g_E & -c_1s_2 - g_Es_1c_2 \\ c_1s_2 + s_1c_2/g_E & c_1c_2 - g_Es_1s_2 \end{bmatrix} \begin{bmatrix} C_{2m+2} \\ D_{2m+2} \end{bmatrix}$$

$$= \begin{bmatrix} I' & J' \\ K' & L' \end{bmatrix} \begin{bmatrix} C_{2m+2} \\ D_{2m+2} \end{bmatrix} \quad \text{say}$$

The mth power of a unimodular matrix may be obtained by diagonalisation (the Chebychev identity) [38] and so for a cladding composed of m pairs of layers,

$$\begin{bmatrix} A_2 \\ B_2 \end{bmatrix} = \begin{bmatrix} I & J \\ K & L \end{bmatrix}^m = \begin{bmatrix} IU_{m-1} - U_{m-2} & JU_{m-1} \\ KU_{m-1} & LU_{m-1} - U_{m-2} \end{bmatrix} \begin{bmatrix} A_{2m+2} \\ B_{2m+2} \end{bmatrix} \tag{3.1}$$

where $U_m = \dfrac{\sin((m+1)Q_M\Lambda)}{\sin(Q_M\Lambda)}$

and $\exp(iQ_M\Lambda)$ is the eigenvalue of the single period translation matrix, and similarly

$$\begin{bmatrix} C_2 \\ D_2 \end{bmatrix} = \begin{bmatrix} I' & J' \\ K' & L' \end{bmatrix}^m = \begin{bmatrix} I'U'_{m-1} - U'_{m-2} & J'U'_{m-1} \\ K'U'_{m-1} & L'U'_{m-1} - U'_{m-2} \end{bmatrix} \begin{bmatrix} C_{2m+2} \\ D_{2m+2} \end{bmatrix} \tag{3.2}$$

For a leaky mode of the structure there is no incoming wave into the guide in the last cladding layer. Therefore since A_{2m+2}, B_{2m+2} are the coefficients of the sine and cosine functions (equation (2.4)), and $\exp(-ik_2 r)$ corresponds to an incoming wave,

$$B_{2m+2} = iA_{2m+2}$$

and similarly

$$C_{2m+2} = iD_{2m+2}$$

Therefore from equations (3.1), (3.2)

$$\frac{A_2}{B_2} = \frac{I - U + iJ}{K + i(L - U)}$$

$$\frac{C_2}{D_2} = \frac{I' - U' + iJ'}{K' + i(L' - U')}$$

where $U = U_{m-2}/U_{m-1} = \sin((m-1)Q_M\Lambda)/\sin(mQ_M\Lambda)$

$$U' = \sin((m-1)Q_E\Lambda)/\sin(mQ_E\Lambda)$$

U, U' are always real and it is convenient to write the above equations as a sum of real and imaginary parts. Using the definitions of U, U' and the expressions for Q_M, Q_E we obtain

$$\frac{A_2}{B_2} = \frac{IK + JL - U(J + K) + i(U(I + L) - 1 - U^2)}{K^2 + (L - U)^2}$$

$$= \frac{\frac{1}{2}(I-L)(K-J)+(J+K)\frac{\sin(Q_M\Lambda)}{\tan(mQ_M\Lambda)} - i\frac{\sin^2(Q_M\Lambda)}{\sin^2(mQ_M\Lambda)}}{K^2 + \left(\frac{1}{2}(L-I) + \frac{\sin(Q_M\Lambda)}{\tan(mQ_M\Lambda)}\right)^2}$$

and similarly

$$\frac{C_2}{D_2} = \frac{\frac{1}{2}(I'-L')(K'-J')+(J'+K')\frac{\sin(Q_E\Lambda)}{\tan(mQ_E\Lambda)} - i\frac{\sin^2(Q_E\Lambda)}{\sin^2(mQ_E\Lambda)}}{K'^2 + \left(\frac{1}{2}(L'-I') + \frac{\sin(Q_E\Lambda)}{\tan(mQ_E\Lambda)}\right)^2}$$

Since

$$N_M = \frac{g_M(A_2/B_2)\tan(k_1t_1) + 1}{g_M(A_2/B_2) - \tan(k_1t_1)} \quad ,$$

taking k_1, k_2 real to O(1/kr) as before, the imaginary part of N_M is

$$\mathrm{Im}(N_M) = \frac{-g_M \sec^2(k_1t_1)\,\mathrm{Im}(A_2/B_2)}{(g_M\mathrm{Re}(A_2/B_2) - \tan(k_1t_1))^2 + g_M^2\mathrm{Im}(A_2/B_2)^2}$$

$$= \frac{g_M \sec^2(k_1t_1)\sin^2(Q_M\Lambda)/\sin^2(mQ_M\Lambda)}{g_M^2(J^2+T_{m1}^2) - 2g_M\tan(k_1t_1)T_{m2} + \tan^2(k_1t_1)(K^2+T_{m3}^2)}$$

where $T_{m1}^2 = \left(\frac{(I-L)}{2} + \frac{\sin(Q_M\Lambda)}{\tan(mQ_M\Lambda)}\right)^2$.

$$T_{m2} = \frac{(I - L)(K - J)}{2} + (J + K)\frac{\sin(Q_M \Lambda)}{\tan(mQ_M \Lambda)}$$

$$T_{m3}^2 = \left(\frac{(L - I)}{2} + \frac{\sin(Q_M \Lambda)}{\tan(mQ_M \Lambda)} \right)^2$$

and a corresponding expression of course holds for $Im(N_E)$

From these expressions, $Im(N_M)$, $Im(N_E)$ and $Im(N_H)$ are non-zero and so now α_1 is in general non-zero, as is necessary for a finite structure. However it is small when Q_M, Q_E are complex and very much larger when either or both Q_M, Q_E is real. Therefore we will continue to refer to the frequency regions for which both Q_M, Q_E are complex as the reflection bands and the remaining regions as pass bands. For large values of m, $Im(N_M)$ and $Im(N_E)$ decrease as $\exp(-mQ_{Mi}\Lambda)$, $\exp(-mQ_{Ei}'\Lambda)$ respectively inside the reflection band.

Since we wish to consider high order mode and non-low loss wavelength solutions, it is useful to consider the range of values for which the above expression is valid. The approximations used in its derivation are as follows.

(i) $1/kr \ll 1$

This is necessary to justify the simple planar form of the translation matrices and hence the use of the Chebychev identity and (in the last chapter) Bloch-type modes. It was also used to simplify the form of the dispersion equation. If we take a = 1mm, λ = 1μm, then this constraint requires $1 \lesssim 100$.

Assumptions (ii) and (iii) are similarly used to simplify the dispersion equation.

(ii) $| 2N/k_1 a |^2 << 1$

If a = 1mm, λ = 1μm then this requires

$$| 2N | << 4 \times 10^7$$

For a single cladding, $N_M = N_E = 1$. Therefore this inequality seems unlikely to be a limiting condition, and we will see in the following section that this is indeed the case for a wide range of wavelengths and numbers of cladding pairs.

(iii) $n_e = n_o$

Since $$n_e^2 = n_o^2 - k_o^2 a^2/(4\pi^2 a^2/\lambda^2) ,$$

this is true if $$|k_o^2 a^2/(4\pi^2 a^2/\lambda^2)| << 1$$

If we assume $a/\lambda = 1000$ then this requires

$$k_o^2 a^2 << 4 \times 10^7$$

If we are considering a high order mode so $|k_o a| = 1000$ then it is necessary that

$$\lambda^2/a^2 << 4 \times 10^{-5}$$

$$(iv)\quad \left(n_o^2 \frac{4\pi^2}{\lambda^2} - \frac{u_o^2}{a^2}\left(\frac{1-Re(N)}{2k_1 a}\right) \right)^2 >> 4\left(\frac{u_o^2 Im(N)}{a^2\, 2k_1 a}\right)^2$$

This is satisfied if

$$u_o^2 << \frac{2\pi^2 a^2}{\lambda^2} \quad \frac{1}{(1 + 2(Im(N)-Re(N))/k_1 a))}$$

where u_o is the nth zero of J_l, J_{l-1}, J_{l+1} for TE and TM, HE_{ln},

EH_{1n} modes respectively. This is assumed in obtaining an expression for β from the first order perturbation solution (about u_o) for $k_o a$. The expression for the real part of $k_o a$ is then

$$k_o a = \frac{u_o}{a}\left(1 - \frac{Re(N)}{k_1 a}\right)$$

If this expression is approximated further to $k_o a = u_o$ then it is being assumed additionally that

$$Re(N) \ll k_1 a$$

Thus considering all the constaints, if the core radius is 1mm and the wavelengths considered are less than $\approx 1.5\mu m$, the results are accurate for $u_o < 1000$ as long as $1 < 100$.

3.3 Optimal thickness of first cladding layer

In this section we will obtain the expression for the loss of the mode for which the periodic cladding thicknesses are optimised, that is, such that

$$k_1 T_1 = k_2 T_2 = \pi/2 \qquad (3.3)$$

and hence obtain the thickness of the first cladding layer which minimises the attenuation for this mode.

When (3.3) holds,

$$J = K = J' = K' = 0$$

$$I = -1/g_M, \quad L = -g_M$$

$$I' = -1/g_E, \quad L' = -g_E$$

Therefore

$$\frac{A_2}{B_2} = \frac{-i}{g_M^{2m}}, \qquad U = -g_M\frac{(1 - g_M^{2m-2})}{(1 - g_M^{2m})}$$

So

$$Im(N_M) = \frac{1}{(1/G_M - G_M)\cos^2(k_1 t_1) + G_M}$$

and similarly

$$Im(N_E) = \frac{1}{(1/G_E - G_E)\cos^2(k_1 t_1) + G_E}$$

where $G_M = g_M^{2m-1}$, $G_E = g_E^{2m-1}$

Therefore in order to obtain the optimal value of t_1 for hybrid modes we consider

$$\frac{dIm(N_H)}{dt_1} = k_1 \sin(2k_1 t_1)\left(\frac{\epsilon_1}{\epsilon_o}\left(1 - G_M\right)Im(N_M)^2 + \left(1 - G_E\right)Im(N_E)^2 \right) \frac{1}{G_M} \frac{1}{G_E} \tag{3.4}$$

$$\frac{d^2Im(N_H)}{dt_1^2} = 2k_1\Big[\left(\frac{\epsilon_1}{\epsilon_o}\left(1-G_M\right)Im(N_M)^2 + \left(1-G_E\right)Im(N_E)^2 \right) \frac{1}{G_M} \frac{1}{G_E} k_1 \cos(2k_1 t_1)$$

$$+ \left(\frac{\epsilon_1}{\epsilon_o}\left(1-G_M\right)Im(N_M)\frac{dIm(N_M)}{dt_1} + \left(1-G_E\right)Im(N_E)\frac{dIm(N_E)}{dt_1} \right)\sin(2k_1 t_1) \Big] \frac{1}{G_M} \frac{1}{G_E} \tag{3.5}$$

For TE modes the derivatives of Im(N) follow from those above by setting $Im(N_M) = 0$ and for TM modes by setting $Im(N_E) = 0$.

It is convenient to treat separately the usual two cases.

(i) $g_M > 1$

Then $G_M > 1$ and since $G_E > 1$ always it follows that the first derivative (3.4) is zero if and only if

$$k_1 t_1 = n\pi/2 \qquad \text{for integer } n$$

If n is odd then the second derivative is positive and if n is even the second derivative is negative. Therefore the first minimum occurs at

$$k_1 t_1 = \pi/2$$

This result is independent of the number of cladding layers and agrees with the result assumed in the previous chapter. It holds for TE, TM and hybrid modes.

(ii) $g_M < 1$

Clearly the minimum point for TE modes remains unchanged and is as for case (i). However for TM modes the second derivative now has opposite sign and so the minimum occurs for

$$k_1 t_1 = 0 \quad \text{or} \quad k_1 t_1 = \pi$$

For hybrid modes, both $\sin(2k_1 t_1)$ and the term multiplying it in the expression for the first derivative (3.4) may be zero. Therefore there are now three possible values of t_1 for which the first derivative vanishes.

(a) $k_1 t_1 = \pi/2$

(b)
$$\cos^2(k_1 t_1) = \frac{n_1 G_E \left(\frac{1}{G_M} - G_M\right)^{1/2} - n_o G_M \left(G_E - \frac{1}{G_E}\right)^{1/2}}{n_1 \left(G_E - \frac{1}{G_E}\right)\left(\frac{1}{G_M} - G_M\right)^{1/2} + n_o \left(\frac{1}{G_M} - G_M\right)\left(G_E - \frac{1}{G_E}\right)^{1/2}} \qquad (3.6)$$

(c) $k_1 t_1 = 0$ or π

Setting

$$X = \frac{\epsilon_1}{\epsilon_o} \frac{1}{G_M^2} \left(1/G_M - G_M \right) + \frac{1}{G_E^2} \left(1/G_E - G_E \right)$$

$$Y = \frac{\epsilon_1}{\epsilon_o} G_M^2 \left(1/G_M - G_M \right) + G_E^2 \left(1/G_E - G_E \right)$$

it follows from equation (3.5) that:

If $X < 0$ then $Y < 0$ and so (a) is a minimum and (c) is a maximum. (b) has no solution since the right hand side is negative.

If $X > 0$ and $Y < 0$ then (a) and (c) are both maxima. Also (b) has a solution and is a minimum.

If $Y > 0$ then $X > 0$ and so (c) is a minimum and (a) is a maxium. The right hand side of (b) is greater than one and so (b) has no real solution.

Therefore for small values of m the optimum thickness for the first layer is again a quarter "wavelength". Beyond some threshhold value (depending on n_1, n_2), as m increases, the optimum thickness tends towards zero (or half a wavelength). This is illustrated in figure (3.1). It should be noted that for finite values of m, the perturbation solution of the dispersion equation (2.18) remains valid even for $k_1 t_1 = \pi/2$. It is only when m is infinite that A_2/B_2 is exactly zero and so N_M becomes large for this value of t_1.

When the thickness of the first layer is an integer multiple of $\pi/2k_1$ at the optimum wavelength, simple expressions may be obtained for Im(N) at a general wavelength, since now the whole cladding is a periodic structure.

If $k_1 t_1 = 0$ then for a structure with exactly 2m cladding layers (so assuming the index surrounding the fibre is n_2)

$$\mathrm{Im}(N_M) = \frac{\sin^2(Q_M \Lambda)}{g_M \left(\tilde{J}^2 + \left(\frac{I-L}{2} + \frac{\sin(Q_M \Lambda)}{\tan(mQ_M \Lambda)} \right)^2 \right) \sin^2(mQ_M \Lambda)}$$

$$= G_M \text{ at the optimum wavelength}$$

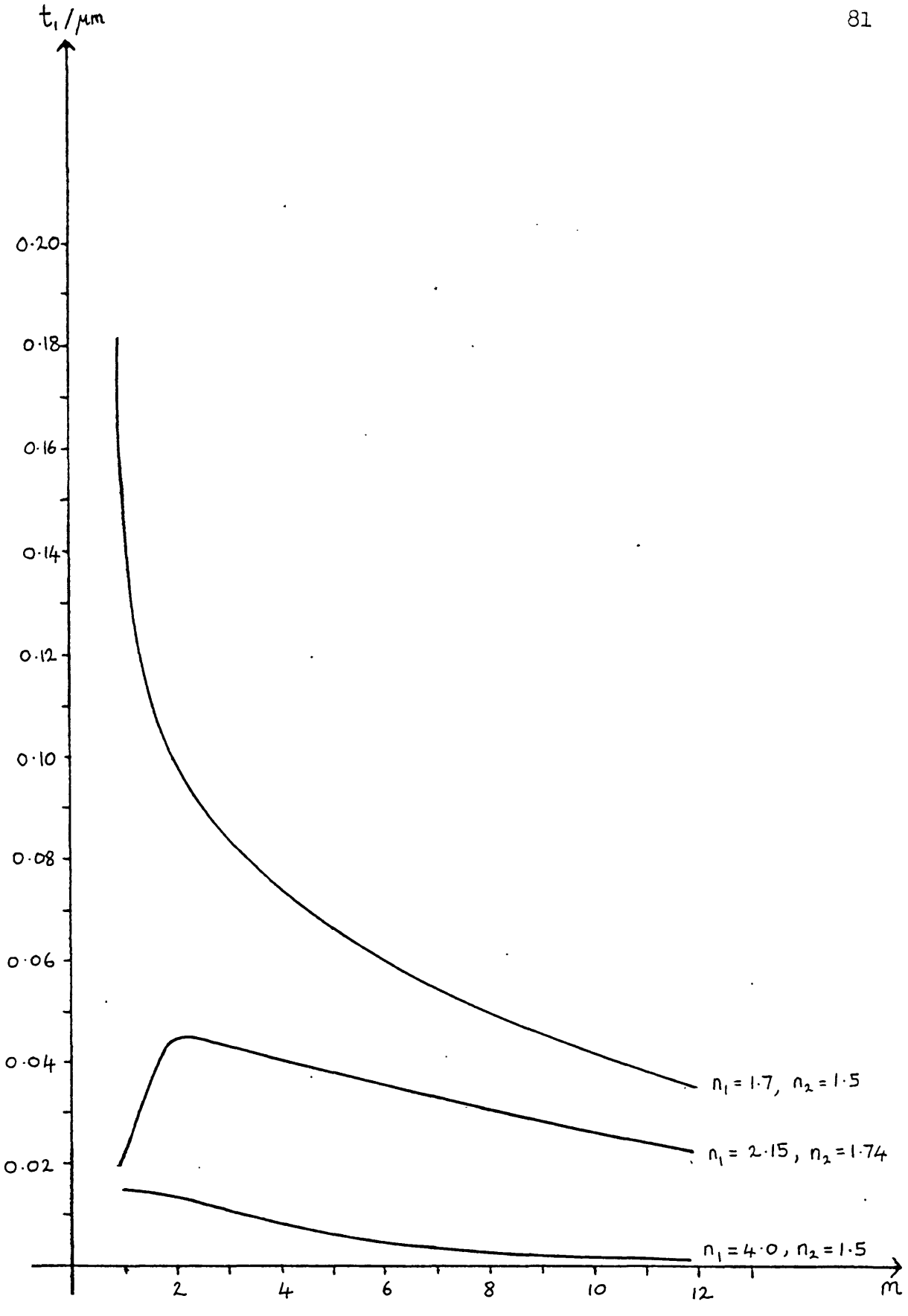

Figure 3.1 Thickness of the first cladding layer, t_1, as a function of the total number of cladding pairs, m, with refractive indices n_1, n_2.

$$\mathrm{Im}(N_E) = \frac{\sin^2(Q_E\Lambda)}{g_E\left(\tilde{J}'^2 + \left(\frac{I'-L'}{2} + \frac{\sin(Q_E\Lambda)}{\tan(mQ_E\Lambda)}\right)^2\right)\sin^2(mQ_E\Lambda)}$$

$= G_E$ at the optimum wavelength

where $\tilde{J} = -s_1c_2 - g_Mc_1s_2$

$\tilde{J}' = -s_1c_2 - g_Ec_1s_2$

If $k_1t_1 = \pi/2$ then for a structure with exactly 2m cladding layers (so assuming the index surrounding the fibre is n_1)

$$\mathrm{Im}(N_M) = \frac{\sin^2(Q_M\Lambda)}{\left(J^2 + \left(\frac{I-L}{2} + \frac{\sin(Q_M\Lambda)}{\tan(mQ_M\Lambda)}\right)^2\right)\sin^2(mQ_M\Lambda)}$$

$= 1/G_M$ at the optimum wavelength

$$\mathrm{Im}(N_E) = \frac{\sin^2(Q_E\Lambda)}{\left(J'^2 + \left(\frac{I'-L'}{2} + \frac{\sin(Q_E\Lambda)}{\tan(mQ_E\Lambda)}\right)^2\right)\sin^2(mQ_E\Lambda)}$$

$= 1/G_E$ at the optimum wavelength

When (b) is satisfied the expressions do not have such a simple form in general. At the optimum wavelength we have

$$\mathrm{Im}(N_E) = (1/G_M - G_M)^{1/2}\,\hat{G}$$

$$\mathrm{Im}(N_M) = (G_E - 1/G_E)^{1/2}\,\hat{G}$$

$$\mathrm{Im}(N_H) = \hat{G}^2\,(G_E/G_M - 2G_EG_M + G_M/G_E)$$

where $\hat{G} = \dfrac{(1/G_M - G_M)^{1/2} + (G_E - 1/G_E)^{1/2}}{(1/G_M - G_M)G_E - (G_E - 1/G_E)G_M}$

If $G_M^2 << 1$ and $1/G_E^2 << 1$ then

$$\text{Im}(N_H) = \left(\frac{1}{G_E^{1/2}} + \frac{(\epsilon_1 G_M)^{1/2}}{\epsilon_o} \right)^2$$

Since the periodic cladding of the Bragg fibre behaves in some respects analogously to a metal, it is interesting to consider which mode has the lowest attenuation, in particular at the optimum wavelength. If the first layer has thickness $\pi/2k_1$ then the HE_{11} mode has the lowest attenuation if

$$1.539/n_1 > G_E/G_M$$

Otherwise the TE_{01} mode has the lowest loss. If the first layer has thickness given by (3.6) then similarly the HE_{11} mode has the lowest loss if

$$1.539/n_1 > (G_E - 1/G_E)/(1/G_M - G_M)$$

and otherwise again the TE_{01} mode has the lowest loss (even though the thickness of the first cladding layer is optimal for the HE_{11} mode).

The right-hand sides of these conditions become large in general for large m. Therefore as the number of cladding layers is increased the behaviour of the Bragg fibre varies from that of a dielectric hollow guide to a structure resembling a hollow metal guide.

3.4 Variation of the attenuation with wavelength and mode number

Now that we have determined the optimal thickness for the first caldding layer we can return to the case of operation at a general wavelength (near enough to the optimum wavelength for the conditions described in section 3.2 to remain satisfied).

The form of the expression for the attenuation constant of the Bragg fibre, that is

$$\alpha_1 = \frac{u_o^2}{\beta_r k_1 a^3} \mathrm{Im}(N)$$

allows the dependence on the mode number, which is contained essentially only in u_o, to be separated from the wavelength and cladding number dependence. All the wavelength dependence of the multilayer cladding (as distinct from that of the resonance condition required in the core) is contained in Im(N). The variation of the loss with number of cladding layers is also contained only in this term, which thus may be considered to characterise the cladding. This decoupling of the terms in the attenuation describing the effects of the core and cladding is a consequence of the approximation

$$n_e \approx n_o$$

That is, all modes are treated as entering the multilayer cladding at grazing incidence. Therefore the size of the component of the wavevector in the radial direction is a function of the wavelength only. The interference effects of the cladding layers, which effect the detailed shape of the attenuation function, are strongly dependent on this magnitude. In contrast

the order of magnitude of the loss of a particular mode is determined primarily by the transverse resonance condition in the core (that is, that phase shift of a wavefront resulting from one round trip inside the core must be such as to interfere constructively with a following wavefront) and so depends strongly on the exact mode angle. We have seen already that the effect of this condition dominates that of the periodic cladding on the real part of the wavevector in the direction of propagation, β_r.

Thus it is possible to investigate first the wavelength and cladding number dependence of the Bragg fibre independently of the particular mode and then consider the effect of the mode number.

(i) Variation with wavelength and number of claddings

We consider first the case of hybrid modes of a structure such that $k_1 t_1 = \pi/2$ at the optimal wavelength. Very similar remarks of course hold for the simpler cases of TE and TM modes of this structure and also for the (less useful) case $k_1 t_1 = 0$

$$\mathrm{Im}(N_H) = \frac{n_1^2 \sin^2(Q_M \Lambda)}{\left(J^2 + \left(\frac{I - L}{2} + \frac{\sin(Q_M \Lambda)}{\tan(m Q_M \Lambda)} \right)^2 \right) \sin^2(m Q_M \Lambda)}$$

$$+ \frac{\sin^2(Q_E \Lambda)}{\left(J'^2 + \left(\frac{I' - L'}{2} + \frac{\sin(Q_E \Lambda)}{\tan(m Q_E \Lambda)} \right)^2 \right) \sin^2(m Q_E \Lambda)}$$

Each of the two terms in this expression consists of two parts. One is the ratio of squared sine terms. This alone would lead to a

function with m-2 minima and m-1 maxima between the dominant minima which occur at the band edges $Q\Lambda = n\pi$ and have the value $1/m^2$ there. However this term is divided by another term which also contains a similarly oscillating component added to a slowly varying one. This term has a similar "periodic" behaviour and removes the singularities. Therefore the resulting function varies rapidly with "period" $2\pi/m\Lambda$ but with a slower modulation of period $2\pi/\Lambda$.

Since the reflection band of the first term is contained inside the second, the total function will vary similarly as long as Q_E, Q_M are not very different. The width of the reflection band of the sum is determined in effect by the minimum of the two individual bandwidths, that is the range for which Q_M is complex, since outside its forbidden band each term increases rapidly. This in turn is increasing for increasing g_M. Figure 3.2 shows $Im(N_H)$ as a function of frequency for various numbers of cladding layers for indices such that g_M is greater than one. Clearly the loss is symmetric about the optimum wavelength.

When g_M is less than one the expressions for Im(N) are more complicated, but in general the wavelength dependence is likely to be broadly similar. Figures 3.3, 3.4, 3.5 show $Im(N_E)$, $Im(N_M)$, $Im(N_H)$ respectively in this case. Now t_1 (optimised for hybrid modes, as in equation (3.6)) is less than $\pi/2$ and the functions are no longer symmetric.

Clearly in both cases the wavelength sensitivity increases with increasing number of cladding layers, as may be expected from the formulae and by analogy with the linear case. The width of the central minimum about the optimum wavelength decreases to a fixed value as the number of cladding layers is increased. The

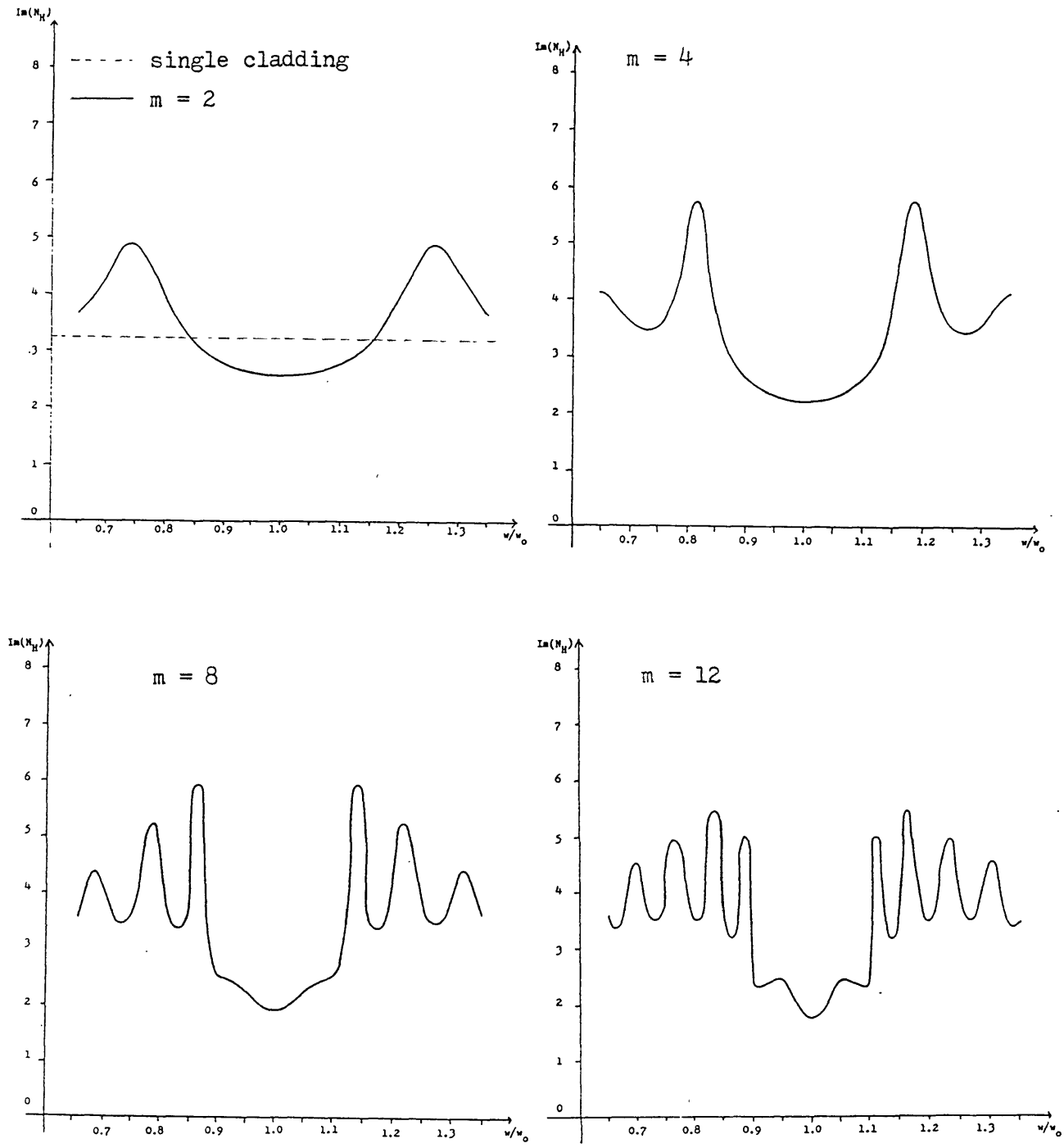

Figure 3.2 Attenuation factor for hybrid modes, $Im(N_H)$ as a function of normalised frequency w/w_o, where w_o is the frequency at the optimum wavelength λ_o, for various numbers of cladding pairs m
$n_1 = 1.5$, $n_2 = 1.3$, a = 1mm, $\lambda_o = 1\mu m$

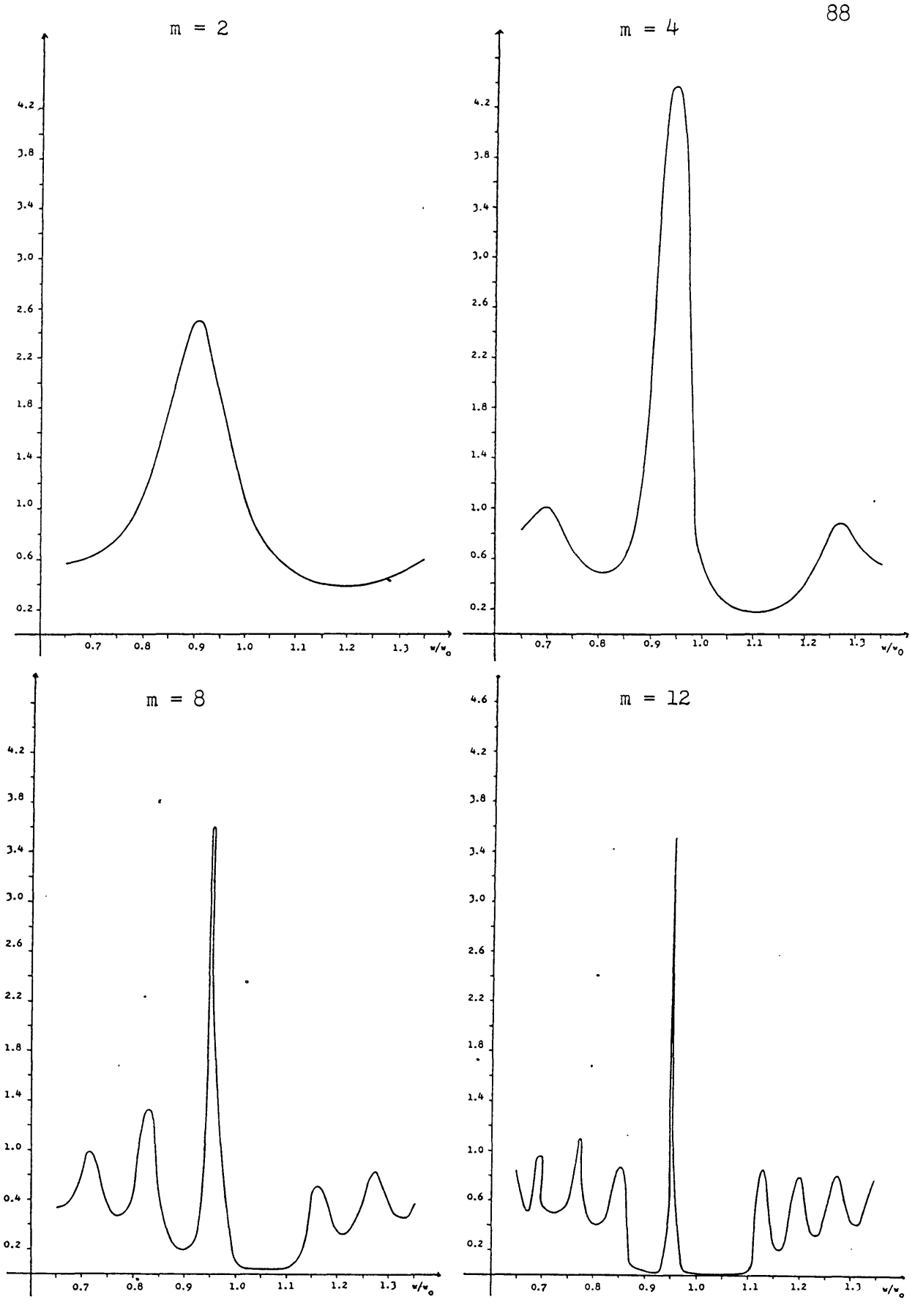

Figure 3.3 Attenuation factor for TE modes, $Im(N_E)$, as a function of normalised frequency w/w_o, for various number of cladding pairs m.

$n_1 = 2.15$, $n_2 = 1.74$, a = 1mm, λ_o = 1μm

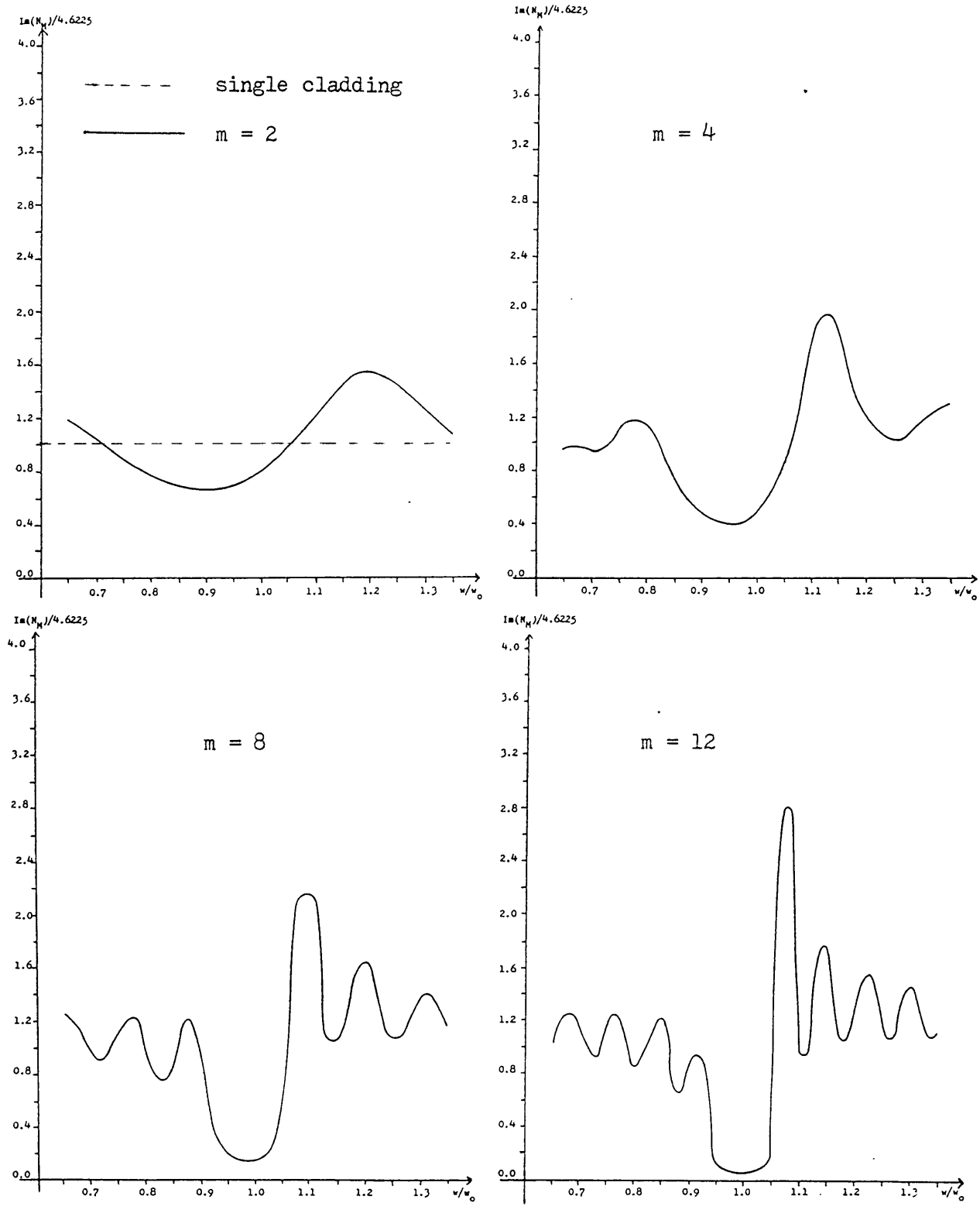

Figure 3. 4 Attenuation factor for TM modes, $Im(N_M)$, as a function of normalised frequency w/w_o, for various number of cladding pairs m.

$n_1 = 2.15$, $n_2 = 1.74$, $a = 1$ mm, $\lambda_o = 1$ μm

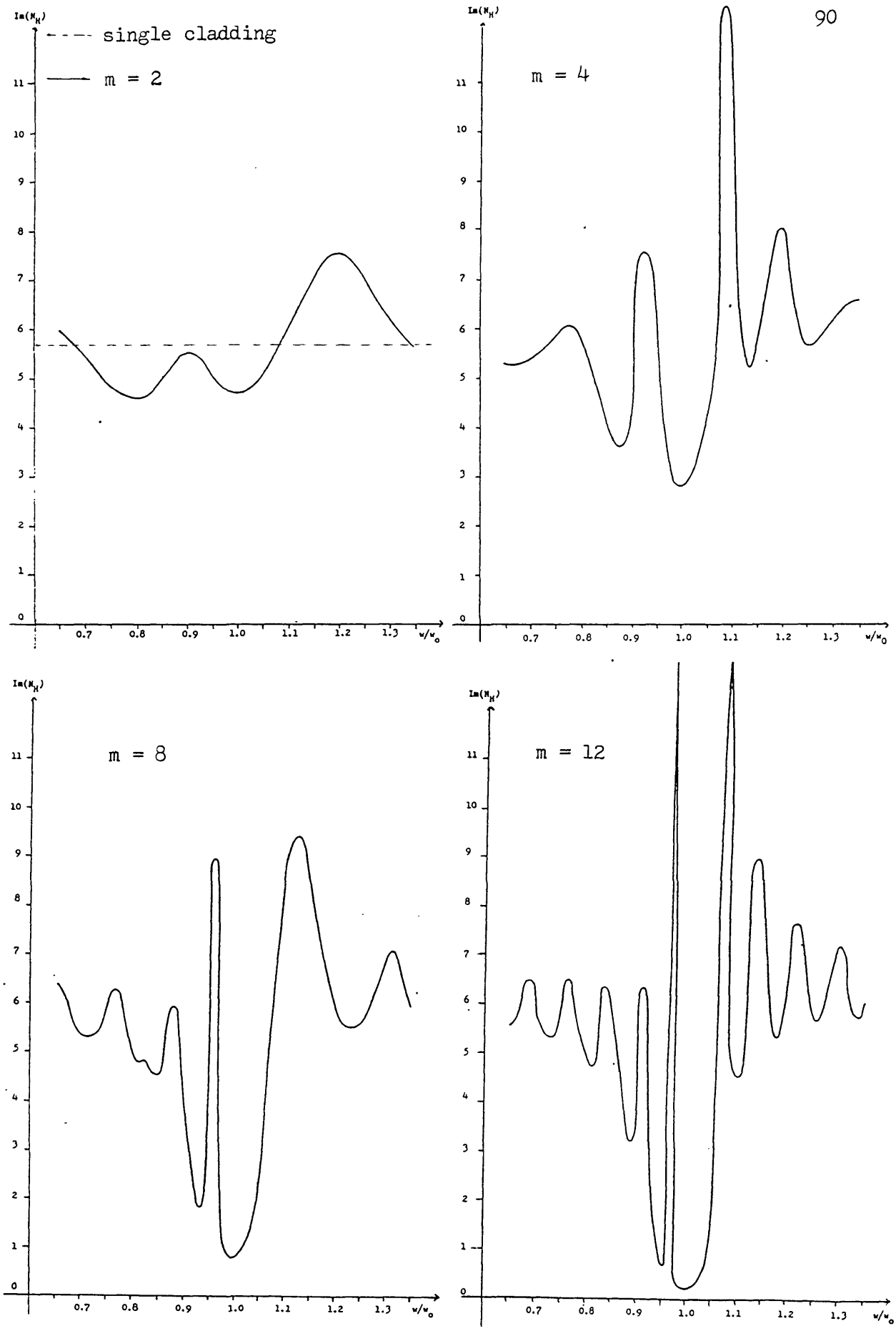

Figure 3.5 Attenuation factor for hybrid modes, $Im(N_H)$, as a function of normalised frequency w/w_o
$n_1 = 2.15$, $n_2 = 1.74$, a = 1mm, $\lambda_o = 1\mu m$

positions of the intermediate maxima and minima are determined by the number of cladding pairs m.

The asymmetry of the wavelength dependence of figure 3.5 may be transformed to a function approximating its reflection about the optimum wavelength by setting $t_1 = \pi - t_1$. It should be noted that when t_1 is not an integer multiple of $\pi/2$, N_E and N_M may become large for a particular wavelength and number of claddings. For example, this occurs for 18 cladding pairs as shown in figure 3.6. For such large values of N_E (or N_M) the approximate solution of the dispersion equation is no longer valid and the value of the attenuation at this point may not be as calculated here.

Figures 3.7, 3.8 show how the loss varies with the number of cladding layers at various wavelengths of operation. Clearly the loss is monotonic only close to the optimum wavelength. At other wavelengths the effect of increasing the number of cladding layers is in general oscillatory. When $k_1 t_1 \neq \pi/2$ it may be very erractic. This is partly because in this case the precise positions,as well as the widths, of the minima and maxima are functions of the number of claddings. Therefore the exact curve is very strongly dependent on the precise wavelength considered.

(ii) Higher order modes

We now consider the effect of the cladding layers on the higher order modes of the structure. Because the dependence of the loss on mode number is purely through u_o, all mode polarisations and field patterns,that is, all TE, TM, HE, EH modes, affect the wavelength and cladding dependence only insofar as they have different losses in a hollow guide. As the value of u_o becomes larger any variation of the attenuation with wavelength is

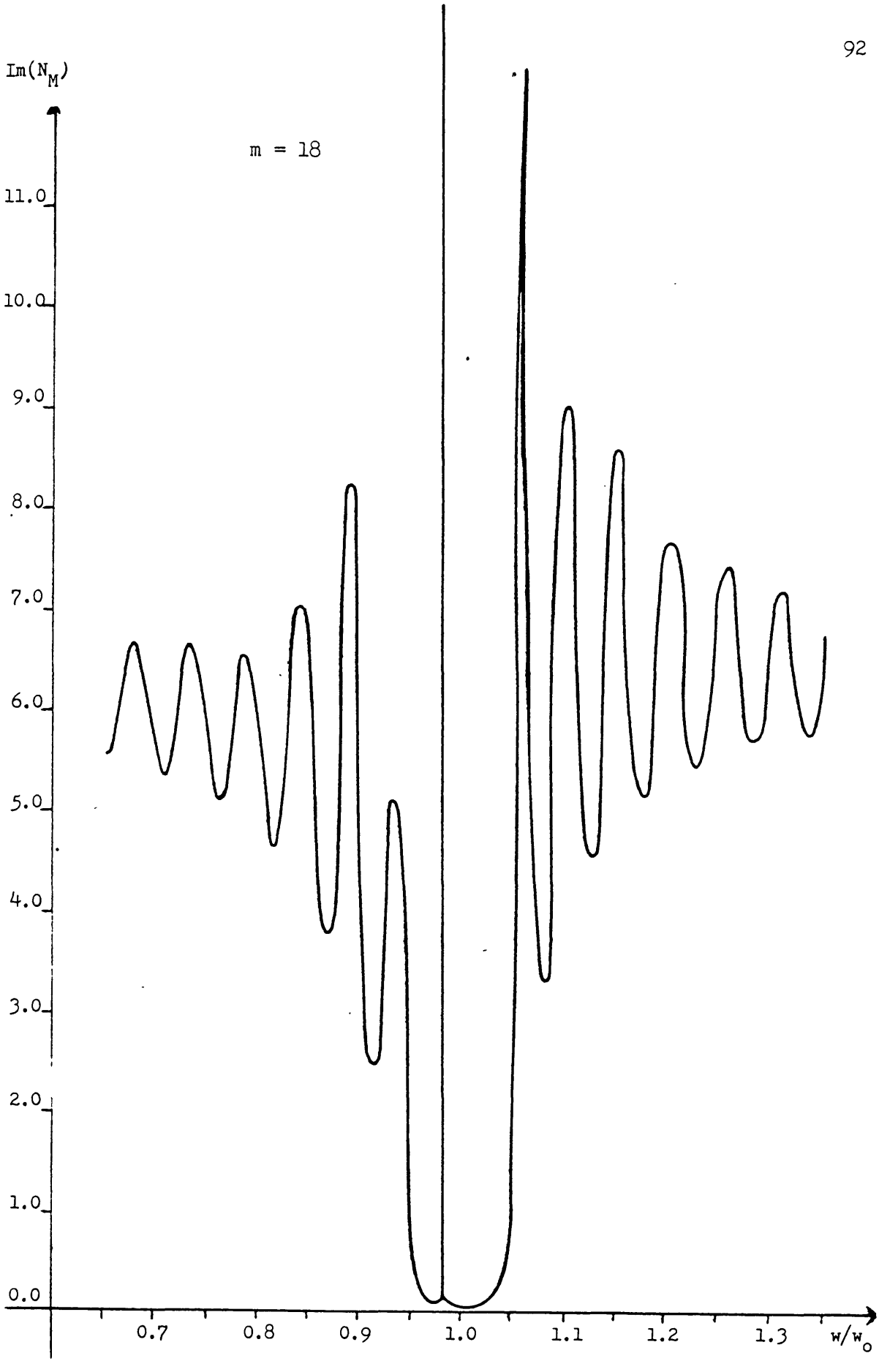

Figure 3.6 Attenuation factor for hybrid modes, Im(N_H), as a fraction of normalised frequency w/w_o for 18 cladding pairs.
n_1 = 2.15, n_2 = 1.74, a = 1mm, λ_o = 1μm

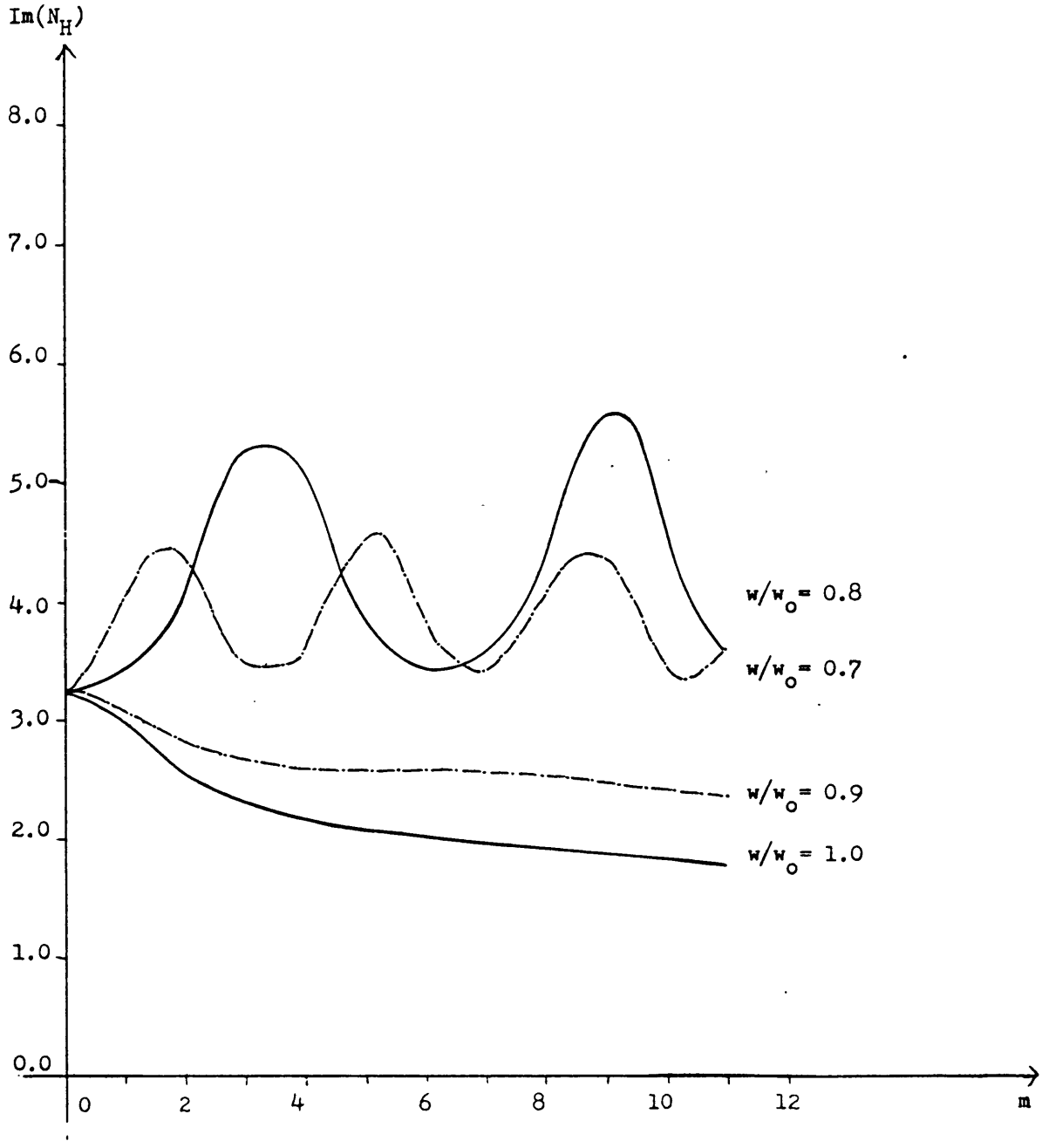

Figure 3.7 Attenuation factor for hybrid modes, $Im(N_H)$, as a function of the number of claddings pairs m, for operation at various frequencies.

$n_1 = 1.5$, $n_2 = 1.3$, $a = 1mm$, $\lambda_o = 1\mu m$

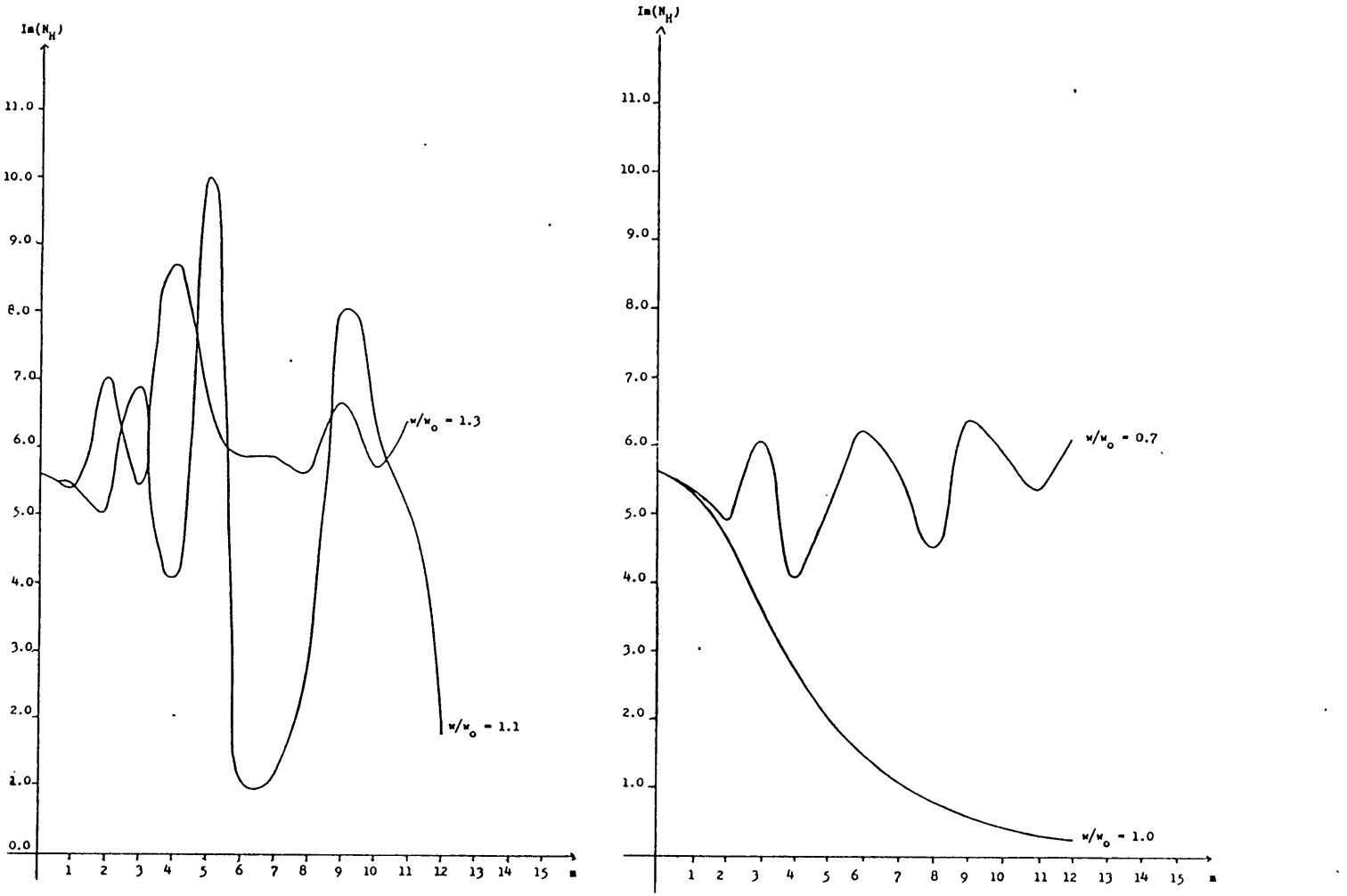

Figure 3.8 Attenuation factor for hybrid modes, $Im(N_H)$, as a function of number of cladding pairs, m, for operation at various frequencies.

$n_1 = 2.15$, $n_2 = 1.74$, $a = 1$ mm, $\lambda_o = 1\ \mu m$

exaggerated. This is illustrated in figure 3.9. Similarly the effect on the loss of increasing the number of claddings is increased. Figure 3.10 shows the variation of $\log(\alpha_1)$ with number of cladding pairs for operation at the optimum wavelength and for operation at a slightly longer wavelength which also lies inside the reflection band. As before, the variation with number of cladding pairs is very nearly linear at the optimum wavelength, even for hybrid modes.

Physically the increased effects of the cladding on higher order modes is reasonable. The higher order modes have a larger component of the field parallel to the periodic cladding layers and are incident on the cladding at smaller angles to the normal and so are more greatly effected by changes in the claddings. This is a well known charateristic of multilayer reflectors. Also, as was seen in the previous chapter, in the limit of an infinite number of claddings the attenuations of all the modes are equal and zero. Therefore the absolute reduction of the loss must be greater for higher order modes as the number of cladding layers is increased.

We may write u_o in terms of the mode angle θ to yield the attenuation as

$$\alpha_1 = 4\,\frac{\mathrm{Im}(N)(\,1 - \cos(\theta))}{a\sqrt{n_1^{\,2} - 1}} \qquad (3.7)$$

and so if we consider the attenuation as a function of θ then the effect of additional cladding layers is to vary the slope of the linear dependence with $\cos(\theta)$. For example, from figure 3.10, a structure with 9 cladding pairs and the indices considered results in a reduction of the attenuation from that of a structure with a single cladding by approximately one order of magnitude.

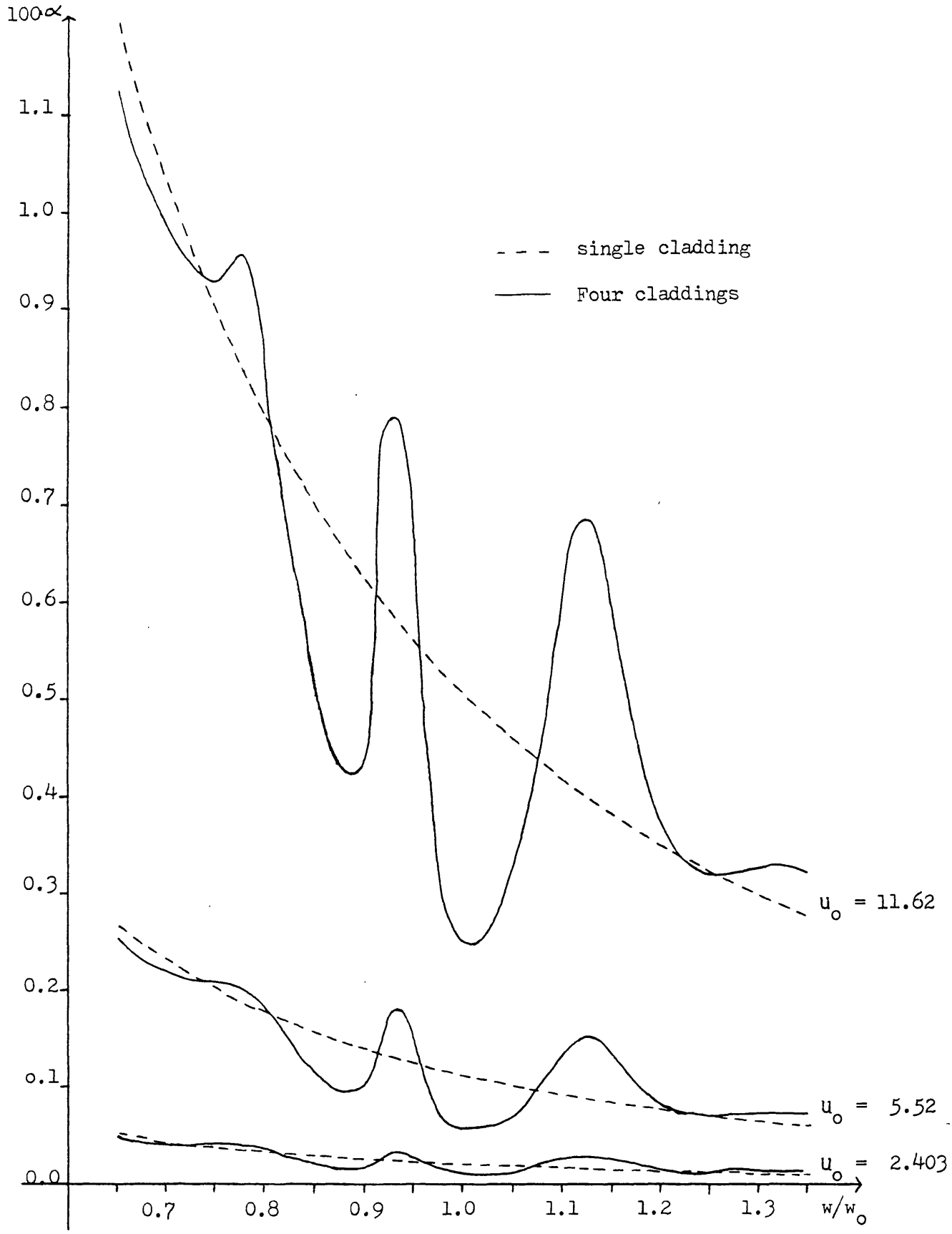

Figure 3.9 Attenuation α as a function of normalised frequency w/w_o for various modes

$n_1 = 2.15$, $n_2 = 1.74$, a = 1mm , $\lambda_o = 1\ \mu m$

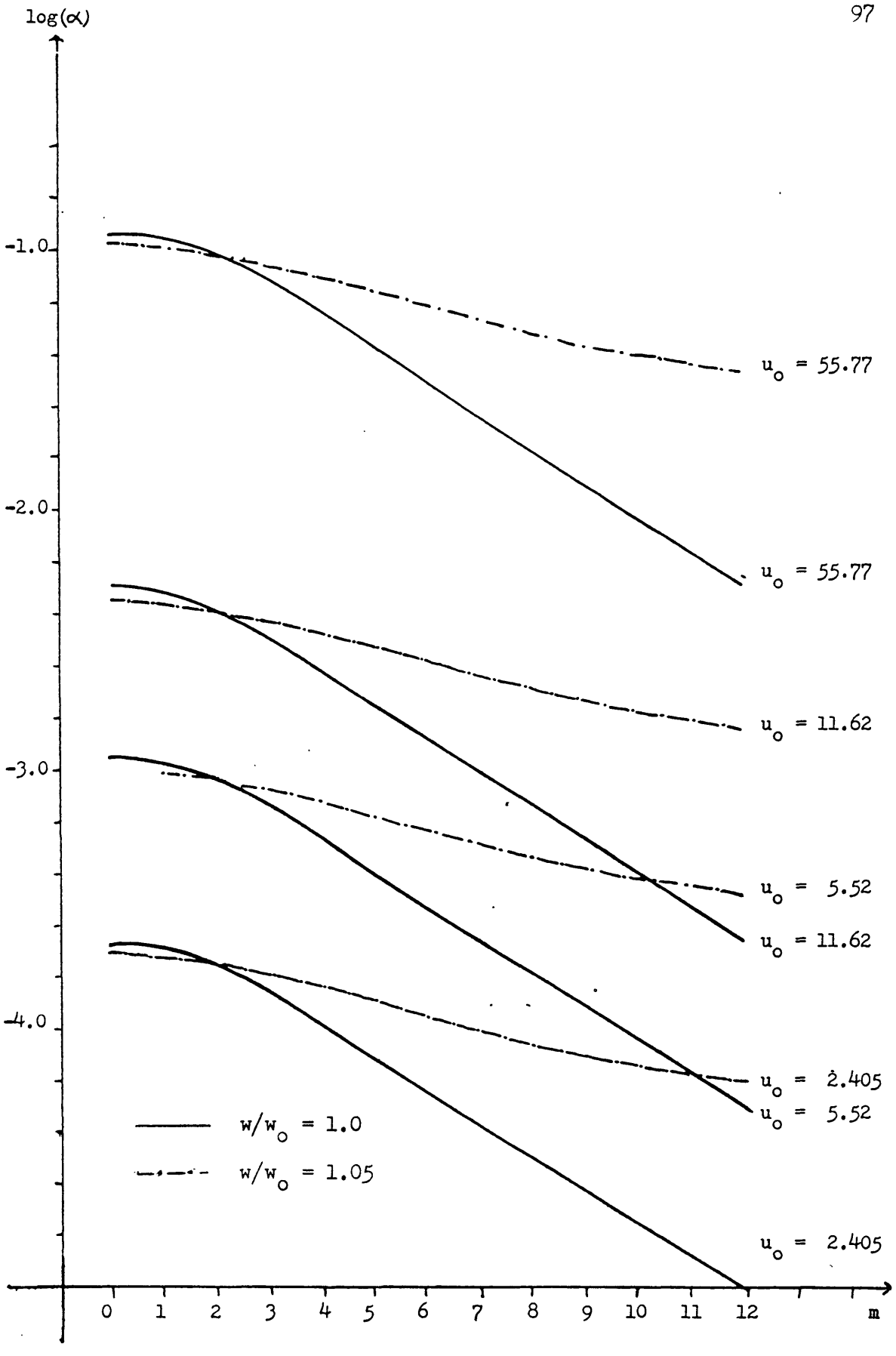

Figure 3.10 Attenuation as a function of the number of cladding pairs m, for various hybrid modes

$n_1 = 2.15$, $n_2 = 1.74$, a = 1mm , $\lambda_o = 1\mu m$

3.5 Absorption and bending losses

So far we have considered the power attenuation which results from the less than unity reflectivity at the interface between the core and the cladding. We now investigate briefly the implications of two other effects, namely the power absorbed by the dielectric cladding and the power lost owing to bends in the guide.

We can calculate the "relative" absorption coefficient α_a numerically using the formula of section 2.6. The results of this calculation for various modes show, perhaps not surprisingly, that α_a/u_o^2 is independent of mode number. Therefore we can compare α_l/u_o^2 with α_a/u_o^2. Figure 3.11 shows α_a/u_o^2 as a function of frequency for various claddings. The variation follows fairly closely that of α_l. This is of course reasonable since the latter describes the leakage loss from the core and the former depends on the proportion of the power in the cladding.

The magnitude of α_a/u_o^2 is of the order of 10^{-9}. This may be compared with $\alpha_l/u_o^2 \sim 5 \times 10^{-5}$. Clearly the absorption loss may be neglected for dielectrics such as magnesium oxide (index 1.74) and zirconium dioxide (index 2.15), which are likely to have absorption coefficients of order one, or less, at a wavelength of 1μm.

A significant disadvantage of hollow index cored optical waveguides is the large increase in loss which occurs for even relatively small axial curvature. This effect has been

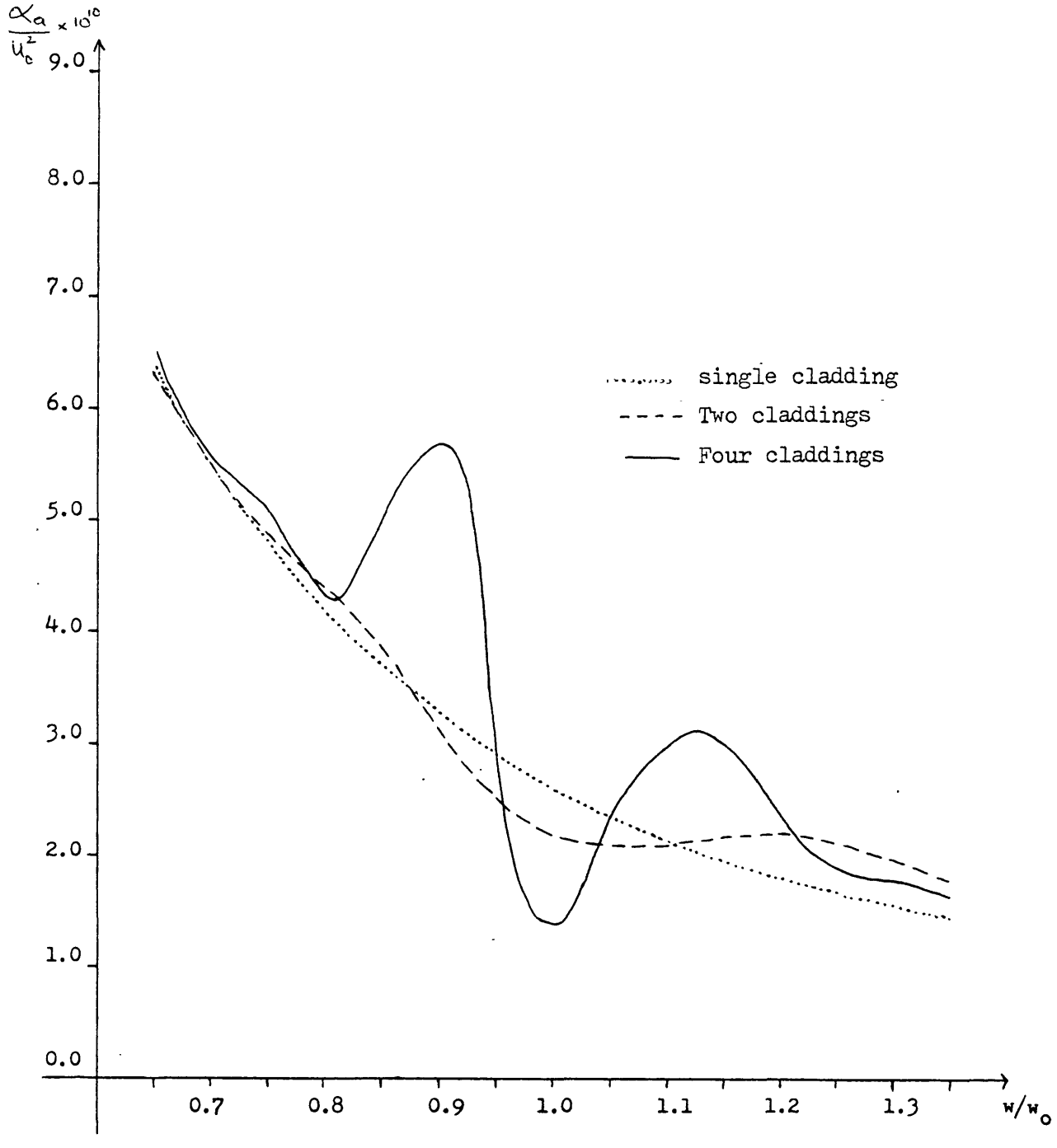

Figure 3.11 Normalised relative absorption coefficient α_a/u_o^2 as a function of normalised frequency w/w_o, for various number of cladding layers

$n_1 = 2.15$, $n_2 = 1.74$, $a = 1mm$, $\lambda_o = 1\mu m$.

analysed by Marcatili et al [50], and more recently by Miyagi et al [55], [62]. In the latter a formula is obtained for the bending loss of a hollow waveguide with given effective small surface impedence and admittance at the boundary between the core and the cladding. This result may be applied directly to the Bragg fibre structure. The derivation of the expression is given in detail in reference [62]. Therefore we will describe only briefly and qualitatively here how it was obtained and then use the result.

The general method is to use toroidal co-ordinates with the curved z-axis along the axis of the bent guide and to calculate the perturbations to the fields and propagation constant of the straight guide as a result of a bend of large radius R. The fields are written as a power series in 1/R, the zeroth order term being equal to the unperturbed value. Maxwell's equations in toroidal co-ordinates are used to express the first and second order perturbations to the field components as functions of the lower order terms. These expressions, Maxwells equations and Green's theorem are then used to obtain the change in the propagation constant. These calculations yield after considerable algebra [62] (in the notation used here) the ratios of the attenuation α_b to the attenuation in a straight guide that is the "relative bending losses"

$$\frac{\alpha_b}{\alpha_1} = 1 - \frac{1}{6}\left(\frac{n_o 2\pi a}{\lambda u_o}\right)^4 \frac{(a)^2}{R}\left(1 - \frac{3\epsilon_1}{\epsilon_o}\frac{\mathrm{Im}(N_M)}{\mathrm{Im}(N_E)}\right) \qquad \text{TE mode}$$

$$\frac{\alpha_b}{\alpha_1} = 1 - \frac{1}{6}\left(\frac{n_o 2\pi a}{\lambda u_o}\right)^4 \frac{(a)^2}{R}\left(1 - \frac{3\epsilon_o}{\epsilon_1}\frac{\mathrm{Im}(N_E)}{\mathrm{Im}(N_M)}\right) \qquad \text{TM mode}$$

$$\frac{\alpha_b}{\alpha_1} = \frac{1+1}{3}\left(\frac{n_o 2\pi a}{\lambda u_o}\right)^4 \frac{(a)^2}{R}\left(1 - \frac{41(1-2)\pm 3\delta_{11}}{u_o^2\ 8}\,\frac{\mathrm{Im}(\epsilon_1 N_M - \epsilon_o N_E)}{\mathrm{Im}(\epsilon_o N_H)}(u_o^2-2)\cos 2\theta\right) \qquad (3.8)$$

hybrid modes

where u_o is the zero of the appropriate Bessel function for the mode and the two signs in the last expression (3.8) refer to HE, EH modes respectivley.

A significant feature of the last expression (3.8) is that the relative loss is independent of the precise nature of the cladding for hybrid modes such that $1 \neq 1$. Therefore for all modes except the TE, TM, HE_{1n} and EH_{1n}, the relative effect of bends is the same for the Bragg fibre as for a singly cladded hollow guide. This is an important result for our purposes. It indicates that although the relative bending loss is not improved, any reduction in loss due to increased number of cladding layers is maintained in the bent guide. This is not the case if for example the loss is reduced by increasing the core radius. The bending loss is directly proportional to the core radius and inversely proportional to the mode number. Thus in general lower order modes and larger, lower loss guides have greater relative bending loss.

Figures 3.12, 3.13, 3.14 show $\epsilon_1 \mathrm{Im}(N_M)/\epsilon_o \mathrm{Im}(N_E)$, $\epsilon_o \mathrm{Im}(N_E)/\epsilon_1 \mathrm{Im}(N_M)$, $\mathrm{Im}(\epsilon_1 N_M - \epsilon_o N_E)/\mathrm{Im}(\epsilon_o N)$ respectivley (that is the cladding dependent factor in the relative bending loss for TE, TM and HE_{1n}, EH_{1n} modes respectively) as a function of frequency for various numbers of cladding layers. The main feature in the case of the first order hybrid modes (figure 3.14) is that for a wide range of wavelengths near the optimum wavelength this function is only weakly dependent on the number of cladding layers and its absolute

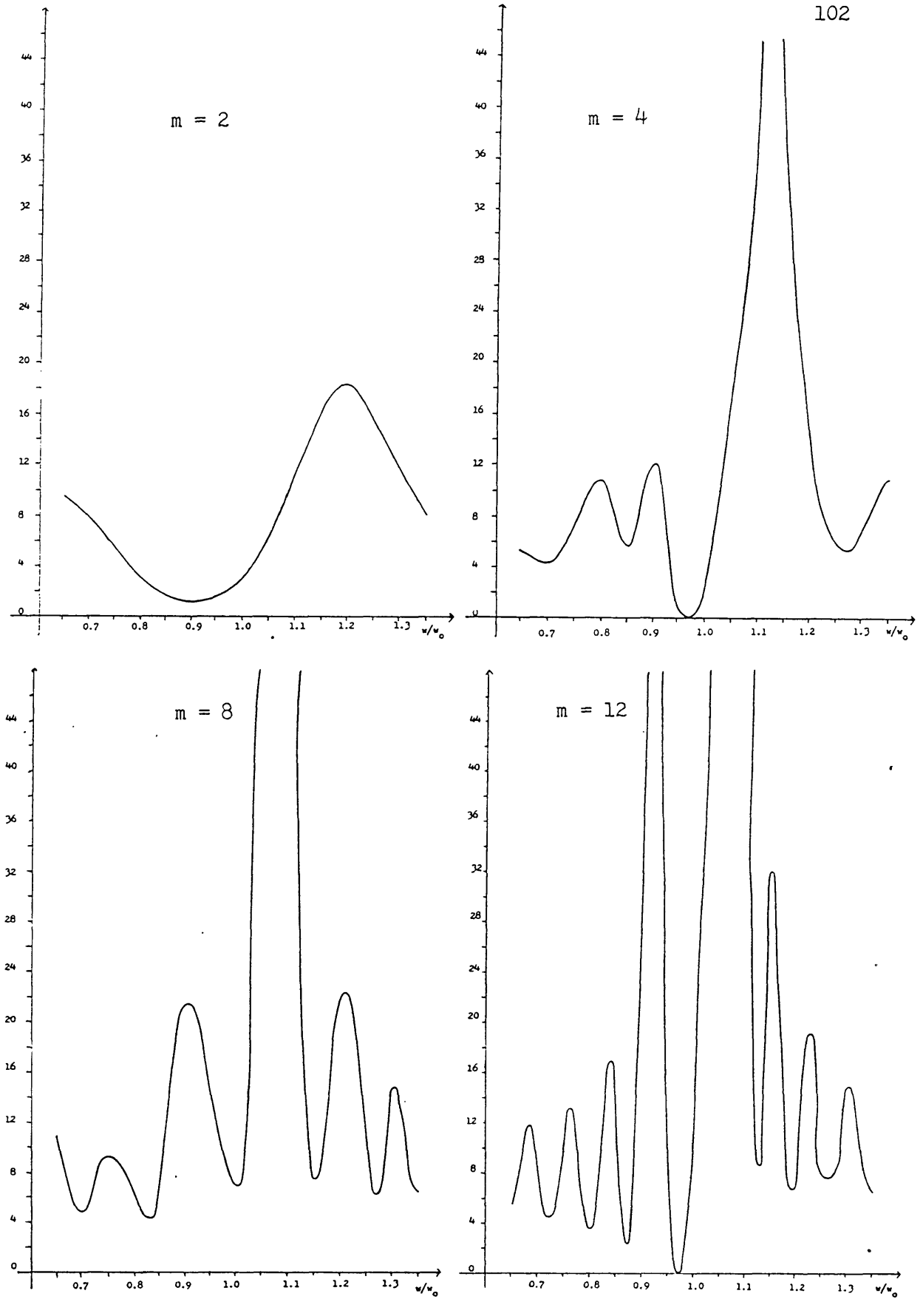

Figure 3.12 Bending loss coefficient for TE modes, $\epsilon_1 \mathrm{Im}(N_M)/\epsilon_o \mathrm{Im}(N_E)$ as a function of normalised frequency w/w_o, for various number of cladding pairs m.

$n_1 = 2.15$, $n_2 = 1.74$, $a = 1$ mm, $\lambda_o = 1\ \mu$m

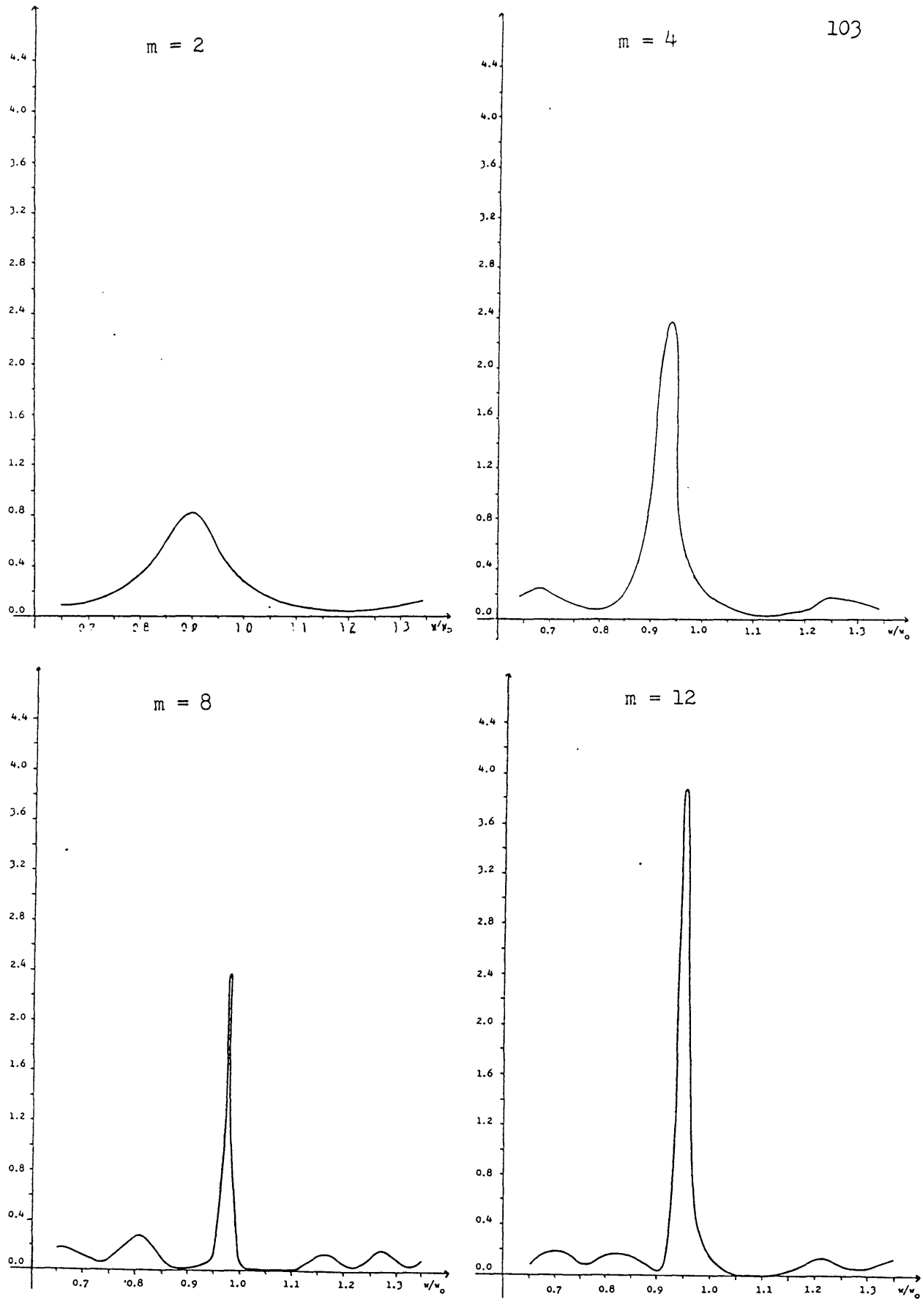

Figure 3.13 Bending loss coefficient for TM modes, $\epsilon_o \mathrm{Im}(N_E)/\epsilon_1 \mathrm{Im}(N_M)$ as a function of normalised frequency w/w_o for various numbers of cladding pairs m

$n_1 = 2.15$, $n_2 = 1.74$, a = 1mm, $\lambda_o = 1\mu m$

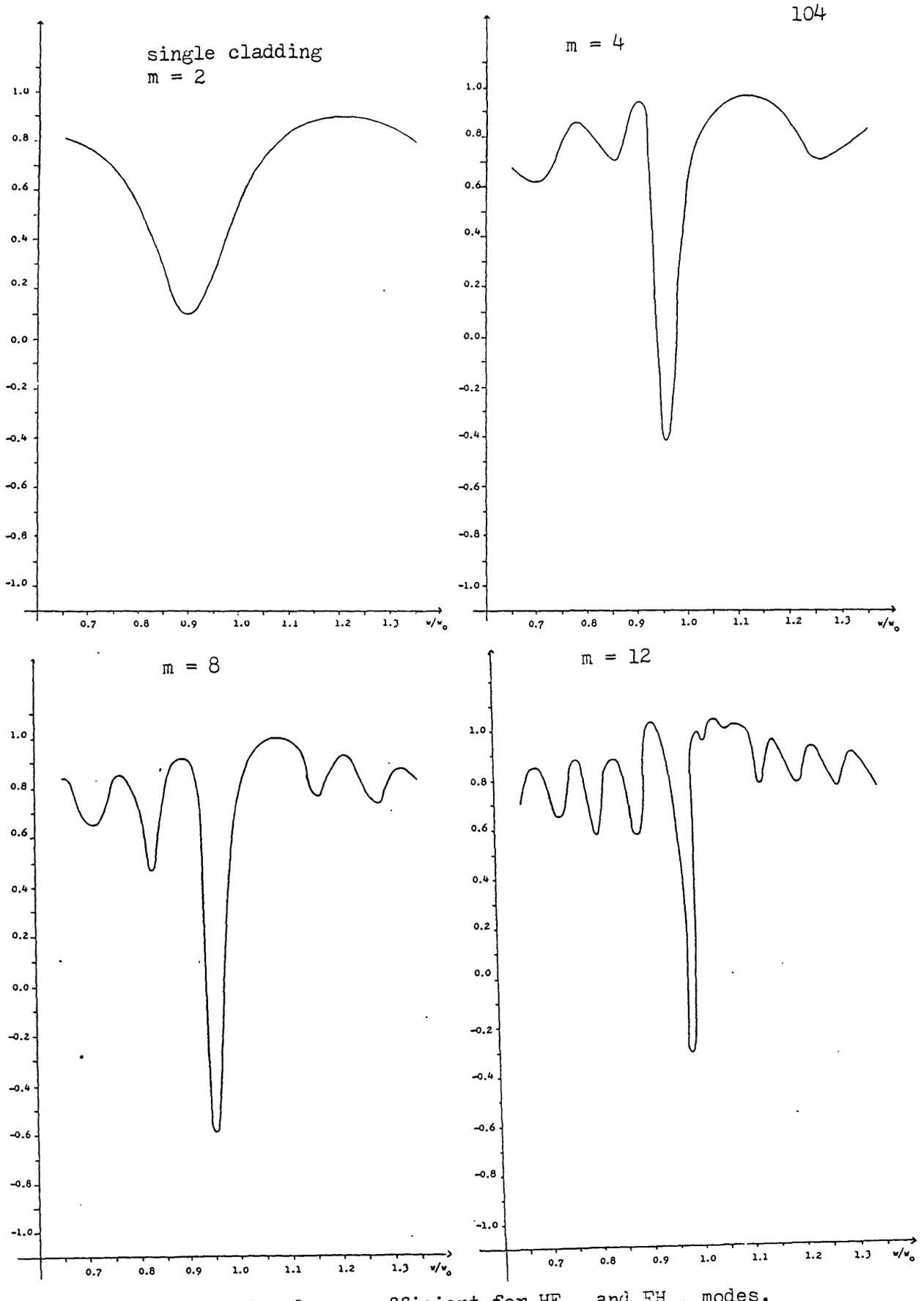

Figure 3.14 Bending loss coefficient for HE_{11} and EH_{11} modes, $Im(\epsilon_1 N_M - \epsilon_o N_E)/Im(\epsilon_o N)$ as a function of normalised frequency w/w_o for various numbers of cladding pairs m

$n_1 = 2.15$, $n_2 = 1.74$, a = 1mm, $\lambda_o = 1\mu m$

value is less than 1 (this may be compared with 0.6443 for these indices for a single cladding). Therefore again the relative bending loss is only slightly altered and the absolute reduction in loss is preserved. For TE and TM modes the additional cladding layers can cause the relative bending loss coefficient to become very large away from the optimal wavelength. However, by comparision with figures 3.3, 3.4 it can be seen that these maxima occur because the absolute attenuation has become very small there. Therefore now the attenuation reduction resulting from additional cladding layers is to a large extent lost at certain wavelengths in the bent guide.

3.6 The Bragg fibre as a multimode waveguide

In the previous sections we have determined the basic characteristics of propagation in the Bragg fibre for various modes and a range of wavelengths. We will now estimate the total power attenuation. This quantity depends of course on the modes and range of wavelengths that are launched.

The wavelength of maximum emission by some object at a temperature of about 2000-2500 °C (radiating it as a black body) is approximately 1μm [63]. In order to determine the temperature from the received radiation we will assume that it is sufficient to detect two wavelengths differing by about 0.1μm near this value [60]. The halfpower bandwidth of the blackbody spectrum near the temperature range of interest is approximately 2μm. Therefore we assume that the variation of power radiated with wavelength may be

neglected within the wavelength interval to be considered. From figure 3.3 we see that although the effect of the multilayers of the Bragg fibre is wavelength dependent, for example for a fibre with 12 cladding pairs there is a significant reduction in loss for wavelengths separated by about 0.1μm about 1μm (although the loss is not reduced throughout this range). In general we may expect to increase this range if we can use indices which lead to a smaller value of g_M (see figure 2.4). Therefore, for simplicity, in the present calculation we will treat the attenuation as being independent of wavelength and equal to the approximate average value in the range of interest, for example for m = 12 we can take $Im(N_H) = 1.0$

The amount of power transmitted also depends on the manner in which the power launched into the guide is distributed amongst the various modes. In the present context it seems reasonable to take the source to be isotropic. In order to estimate the power launched we will use a ray type model. Although this is a very approximate treatment, we are considering the case of a large core guide and so the approximation is relatively good. In addition it is difficult to determine the launching efficiency directly in terms of leaky modes, which are not true modes of the structure and therefore do not each retain a constant amount of power as they propagate through the guide. Mathematically this is manifested by their non-normalisabilty in an infinte space and the subsequent lack of a orthogonality relationship.

Thus we will adopt a perhaps rather simplistic approach here and assume that if the total power radiated into a spherical surface 4π is P_o, the power launched into the mode with angle θ is $P_o d\Omega$, where $d\Omega$ is an element of solid angle. This

requires a formula for the attenuation in terms of a continuous variable $\cos(\theta)$. It is straightforward to extend the expression for the attenuation of the hybrid modes in this way (and since the values of θ corresponding to actual modes are very closely spaced the approximation is likely to be a reasonable one). However TE and TM modes cannot be easily included since this would require the use of a different formula at discrete points. It is difficult to quantify the error resulting from using instead the hybrid mode expression at these points also since, as mentioned above, the mode launching efficiencies are not well defined. If we assume that it is not significant then we obtain simply for the ratio of power remaining in the guide after 1m

$$\frac{P}{P_o} = \int_0^{\theta_o} \exp(-2\alpha_1(\theta))\, 2\pi \sin(\theta)\, d\theta$$

$$\approx 2\pi \int_{\cos(\theta_o)}^{1} \exp\left(-4\frac{(1 - \cos(\theta))}{a\sqrt{n_1^2 - 1}} \mathrm{Im}(N) \right) d(\cos(\theta)) \qquad (3.9)$$

$$\approx \frac{a\sqrt{n_1^2 - 1}}{4\ \mathrm{Im}(N)} \qquad (3.10)$$

The leaky waveguide has no cut-off and so we may set $\theta_o = \pi/2$. However the approximate linearised expression for the attenuation (3.7) used in the integral (3.9) is valid only for θ_o near enough to zero. Therefore we will truncate the integral at the limit of validity of the formula, assuming in effect that all the higher order modes are lossy enough to make no significant

contribution. For this latter approximation to be reasonably accurate it is necessary for the attenuation at θ_o to be large enough, such that $2\alpha_1(\theta_o) = 3$ say. These two constraints together require

$$9a\sqrt{n_1^2 - 1}/\ 2Im(N) << 1$$

so we can assume (3.10) to hold for $Im(N) \gtrsim 0.18$. For smaller values of Im(N) the formula will tend to over-estimate the transmitted power.

From (3.10), the power transmitted is approximately inversely proportional to Im(N). Therefore for example the addition of 9 cladding pairs reduces the loss by one order of magnitude. For a Bragg fibre with 12 cladding pairs, the power remaining after 1m is $10^{-2}\ P_o$. This is a very small fraction but the total power radiated may be large.

We have seen that the absorption loss is negligible for likely materials and so we do not consider this further.

The bending loss of the Bragg fibre is an important consideration, as it is likely to be large. We have seen that the relative increase in attenuation from bending is essentially the same as for a singly clad guide (again considering hybrid modes only). However the absolute value of the attenuation has been reduced and also (as for a singly clad guide), the effect of bending loss is reduced for higher order modes. In order to estimate very approximately the overall effect of bending loss on the power transmitted in a multimode guide we can consider

$$I = 2\pi \int_{\cos(\theta_o)}^{1} d(\cos\theta)\ \exp\left(-4\frac{(1-\cos(\theta))Im(N)}{a\sqrt{n_1^2 - 1}} \left(1 + 1\ \frac{(2\pi a)^4}{\lambda u_o}\ \frac{(a)^2}{R} \right) \right.$$

where we have inserted an approximate form for the bending loss which varies with mode number only simply through u_o^2.

Changing the variable of integration we obtain

$$2\pi a \int_0^{(1-\cos(\theta_o))/a} \exp\left(4\,\mathrm{Im}(N)\left(-x - \frac{1}{12R^2x}\right)\Big/\sqrt{n_1^2-1}\right)dx \qquad (3.11)$$

If we use the same value of θ_o as before, the argument of the exponential at the upper limit of the integral in (3.11) is $3/\mathrm{Im}(N)$. Again we assume that this is large enough for contributions from all larger values to be negligible. Therefore we replace the upper limit by infinity to obtain

$$\frac{1}{R\sqrt{3}}\; K_1\left(\frac{4\mathrm{Im}(N)}{R\sqrt{n_1^2-1}\,\sqrt{3}}\right)$$

where K_1 is a first order modified Bessel function.

Figure 3.15 shows how this varies with bending radius R. The addition of cladding layers leads to a smaller critical bending radius (below which, in effect, no power is transmitted, say). If Im(N) = 0.25 then the power transmitted reduces to half that for a straight guide for a bending radius of $\sim$ 25 cm. This figure, although larger than for a conventional fibre, may not be unacceptably large. However it should be noted that TE and TM modes have been neglected in the calculation.

Thus we have found that the Bragg fibre offers signficant advantages over a singly clad hollow guide in terms of leakage loss and bending loss. The variation of attenuation with wavelength appears to be slow enough for these reductions to be useful. However it is worth noting that the leaky hollow guide may

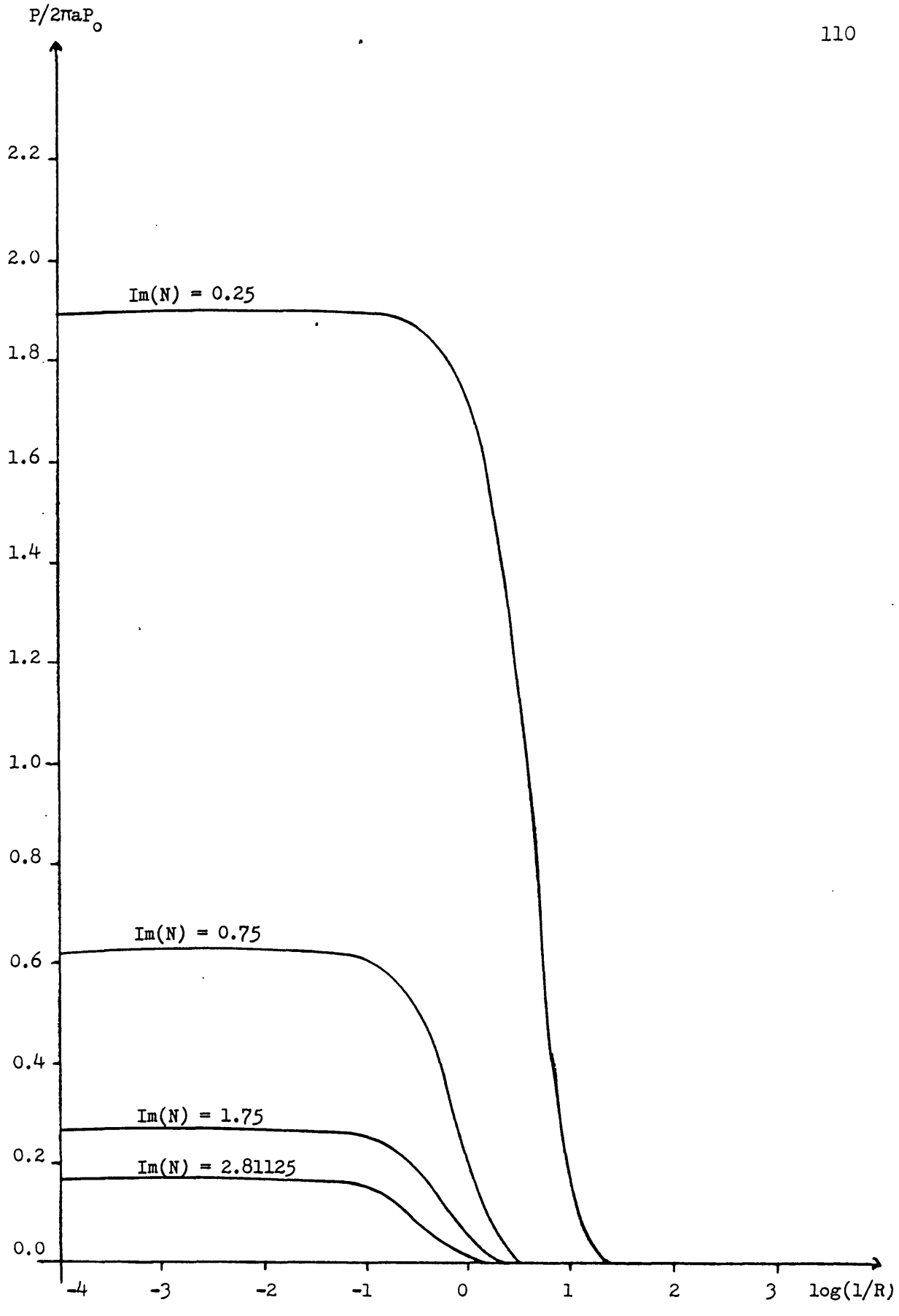

Figure 3.15 Normalised power in guide after propagation through one metre as a function of bend radius R (metres) for various Bragg fibre structures

not, in practise, be the most suitable waveguide for use as part of a high temperature sensor if the absorption losses in a suitable material are small enough for the bulk of the power to be transmitted in it. In this case the difficulty of drawing a rod alone remains and this suggests that the tube waveguide might be a more attractive alternative structure.

CONCLUSIONS FROM CHAPTERS TWO AND THREE

The large-cored hollow Bragg fibre possesses a set of leaky modes, the real parts of the propagation constants and field patterns in the core of which resemble closely those of the modes of a large-cored singly clad fibre. However the mode attenuations in the Bragg fibre are in general significantly different and can be much lower for suitable layer thicknesses and wavelengths.

For the large-cored case considered, the H_z, E_r, E_θ field components (TE-like components) are uncoupled from the E_z, H_r, H_θ field components (TM-like components) in the cladding layers of the Bragg fibre. Therefore the infinite cladding supports Bloch-type modes and a general finite cladding has properties very similar to those of a plane multilayer dielectric mirror.

For operation at some given wavelength, the loss is minimised, to a good approximation, when all the cladding layers, except possibly the first one, are of "quarter-wave" thickness (taking the wavelength in the radial direction, in the material). The optimal thickness of the first layer is also one quarter wavelength when the parameter $g_M = n_2^2\sqrt{n_1^2 - 1}/(n_1^2\sqrt{n_2^2 - 1})$ is less than one. Otherwise the optimal thickness is a function of the number of cladding layers, 2m, and tends to zero as m tends to infinite.

When the wavelength of operation is such that the layer thicknesses are optimised, we can perhaps characterise the multilayer cladding in terms of some equivalent uniform material. Although the Bragg fibre modes are leaky, the field amplitudes decay in the cladding layers. This suggests that the behaviour of

the Bragg fibre will be reproduced by a cladding of a uniform material of refractive index less than one, but very near one, of a finite thickness. In this case the field amplitudes will decay very slowly in the cladding layers. The guide would have a high leakage loss, since the field amplitude would still be significantly large at the further cladding boundary, where it would be surrounded by a necessarily higher index, lossless material, or a lossy material with a possibly lower index. The loss would decrease with increasing cladding thickness, as in the Bragg fibre. The amplitudes of the TE- and TM-like parts of the fields decay at different rates and so the material is in effect birefringent (the form birefringence of planar periodic media is disscussed in reference [31]).

For a radial distance in the claddings of $2m\Lambda$ (assuming that the first layer also is approximately of quarter-wave thickness) the TE and TM like field amplitudes have decayed by $1/g_E^m$ and the minimum of $1/g_M^m$, g_M^m, respectively. Therefore simple calculation gives the effective refractive index of an equivalent uniform cladding in the transverse and radial directions, n_{cE} and n_{cM} respectively, as

$$n_{c\gamma} = \left(1 - \frac{(\ln(g_\gamma))^2}{\pi^2 (1/\sqrt{n_1^2-1} + 1/\sqrt{n_2^2-1})^2} \right)^{1/2} \qquad \gamma = E,M$$

Thus the refractive index is lower (and so the loss is lower) for larger values of $|\ln(gE)|$, $|\ln(gM)|$, as required. When n_1 = 2.15, n_2 = 1.74 this yields n_{cE} = 0.997, n_{cM} = 0.999. In addition, a Bragg fibre cladding of 20 layers is only of the order of 5 wavelengths thick. Therefore the high values of the attenuation compared with conventional high index-cored guides are reasonable.

This analogy with a mode (either leaky or guided) in a uniform material cannot be simply extended to a general wavelength, since now the loss may not be monotonic with increasing number of claddings. The wavelength dependence is similar to that of a multilayer cladding.

The Bragg fibre operating at the optimal wavelength offers an improved performance over the singly cladded hollow guide. All the mode losses are reduced, and so any loss from absorption in the cladding is reduced also. For a core radius of 1mm and a wavelength of 1 μm, and cladding indices 2.15, 1.74, the attenuation of a mode in a Bragg fibre structure with 9 cladding pairs is reduced from the singly cladded case by about a factor of 10. This same reduction occurs for multimode transmission when power is launched uniformly into all modes. The bending loss, which is very large in leaky guides in general, is reduced, although the critical bending radii of the indivdual modes is not significantly altered. The critical bending radius for multimode propagation however, is likely to be reduced with increasing number of layers. The bandwidth of, for example, a Bragg fibre made with about 8-12 cladding pairs of indices, 2.15, 1.74, over which the attenuation is substantially reduced, is 0.05-0.1μm about a wavelength of 1μm. Losses may be large outside this range.

Thus the Bragg fibre is likely to be useful in applications where the singly cladd hollow guide is the main alternative and when only a moderate range of wavelengths need to be transmitted. This is probably the case for transmission of CO_2 laser radiation with a wavelength of 10.6μm, but may not be so for the high temperature tolerant guide considered.

4. PULSE PROPAGATION IN A PERIODIC WAVEGUIDE

4.1 Introduction

Structures which have periodic variations of permittivity are commonly used in optical systems as a means of achieving large and negative group velocity dispersion. For example, the use of grating pairs for compression and shaping of unguided optical signals is well established. This relies on the property of a grating pair that the optical path length and hence the time delay through the system is an increasing function of wavelength. Thus unchirped pulses (a chirped pulse is taken to be a pulse whose phase function is a second or higher order polynomial function of time) may be chirped and temporally shaped by propagation through such a system [6], [64] and previously chirped signals can be compressed for example to generate ultra-short laser pulses. Several methods of chirping the input signal have been considered, such as by propagation through an optical Kerr cell [65] or, more recently, by propagation through an optical fibre [66], [67], [68]. This same dispersive property of the grating pair may be used conversely as an analytical tool for determining the temporal shape and chirp characteristics of very short pulses [69], [70].

The details of the dispersive effect of propagation through a grating pair are generally analysed by assuming each reflected or scattered order (of a monochromatic wave) from a single grating to consist of one plane wave with a well defined propagation constant, which differs from that of the incoming wave by an integer multiple of 2π/pitch of the perturbation [7]. That is,

all the frequencies are assumed to be incident at the Bragg angle, as is justified for thin gratings. The variation with frequency of the angle at which each frequency component is scattered or reflected leads to a variation in path length (in a dispersionless medium) and hence to a frequency dependent time delay.

There has also been interest in the properties of signals reflected from multilayer mirrors and other periodic distributed reflectors. These structures play an important role in various devices, notably Distributed Feedback lasers [71] and Bragg Reflection lasers [72]. There have been several experimental investigations of the pulse chirping caused by a Distributed Feedback laser [73], [74], [75], [76], [77].

A theoretical model of the response of a Bragg Reflection resonator to light pulses has been obtained by numerical integration of the time dependant coupled mode equations [78]. This predicts significant pulse distortion when the width of the input pulse is approximately equal to the transit time through the structure, but little such effect when the pulse width is greater than about ten times this. An experiment to verify these results for a passive waveguiding cavity and a short pulse has yielded qualitative agreement [79].

The coupled mode equations in the spectral domain have been used to analyse the reflected pulse from a quarter-wave dielectric mirror [80]. A numerical integration of these same coupled mode equations for a single periodic structure has been carried out and gives detailed pulse shapes for the cases considered [81].

For optical fibre systems, pulse compression and dispersion cancellation by propagation through a short length of a

periodically perturbed waveguide (the periodicity being in the direction of propagation) have been suggested. This effect is similar to that of a grating pair. However now the thickness of the periodic structure must be considered, so the different frequencies are not all incident at the Bragg condition. The effective dispersion of the medium varies with difference from the Bragg angle and so the frequencies propagate with different time delays. Again the input pulse must be chirped to achieve compression, for example by material dispersion [82] or by non-linearity in the refractive index of the guide [83]. In these cases the periodic structure has been analysed as in reference [80] and [78] respectively. In the former [82] it has been shown that a periodic guide of about 2cm long can equalise the pulse dispersion from propagation through 1km of a conventional single-mode guide when operating at a wavelength of 1.27μm. The latter [83] has shown that, with a germania doped silica fibre of 1m long and with a perturbation of amplitude readily available by the photorefractive effect, a pulse with a peak power of 100W will be compressed by a factor of three.

The use of periodic guides in optical fibre systems has been concerned with insertion of a structure for compression of a broadened pulse. Thus in order to limit the length of the device the pitch of the perturbation has been chosen such that the wavelength of operation occurs near the edge of the reflection band, allowing utilisation of the large values of dispersion available there. In this chapter we will consider instead how we may use the small distortion to the dispersion which occurs when the wavelength of operation is far from the band edge. We will show that this dispersion can be combined with the material and

(unperturbed) waveguide dispersions to create a zero dispersion point at a chosen wavelength. Now we are in effect continuously compensating for the dispersion of the unperturbed guide. It is necessary for the periodic variation to extend through the whole length of the guide. It is not inconceivable that this may be acheived by introducing a controlled high frequency vibration into the fibre production equipment, resulting in a periodic diameter variation of the fibre.

Much work has been done on designing optical waveguides which have a zero of the total dispersion at 1.55μm, the minimum loss wavelength of silica. Particular cases of interest are the triangular index profile core [84], [85], [86] and the quadruply clad guides (these latter guides have a very small dipersion over a broad wavelength range, about 0.35 μm) [87], [88]. It is of course possible to design a step index guide with zero total dispersion at 1.55μm [40]. In general however, rather elaborate refractive index profiles have been favoured, in order to maintain the power confining properties, for example the spot size, of the guides. These modifications may possibly be avoided if a siutable periodic perturbation is imposed along the direction of propagation. However the power attenuation caused by the associated reflection from a periodic structure must be considered.

The next two sections of this chapter, 4.2, 4.3, contain an analysis of the changes to a signal which occur as a result of propagation through a periodic medium of finite length. The general form of the output signal is determined qualitatively and the effective signal velocity and dispersion are obtained in two particular cases of interest.

In the following section, 4.4, and the appendix, approximate analytic formulae are derived for the reflected and transmitted fields by evaluation of the relevant integrals. These resulting pulse shapes after propagation and the implied signal velocity and dispersion, both inside and outside the reflection band are considered in section 4.5. The degree to which some simple definitions for these latter quantities are meaningful in the general case is discussed.

The formulae of these sections differ from analytic expressions previously assumed [80], [82], [83], but agree well with those obtained by numerical calculation [81].

In section 4.6 the particular dispersion characteristics of a longitudinally periodically perturbed waveguide are investigated using the results of the previous sections. The effects of material and waveguide dispersion are now included. It is shown that such a guide does indeed allow a considerable freedom of choice in the wavelength of zero dispersion.

4.2 Phase and Amplitude form of the transmitted and reflected fields

The characteristics of propagation of a monochromatic wave in a periodic medium are well established and can be derived using Coupled Mode theory [31], [35] or, less commonly, a Bloch wave approach [38]. Expressions for the fields at frequencies near that for which the medium is strongly reflecting have been obtained. The configuration is as in figure 4.1. That is, a

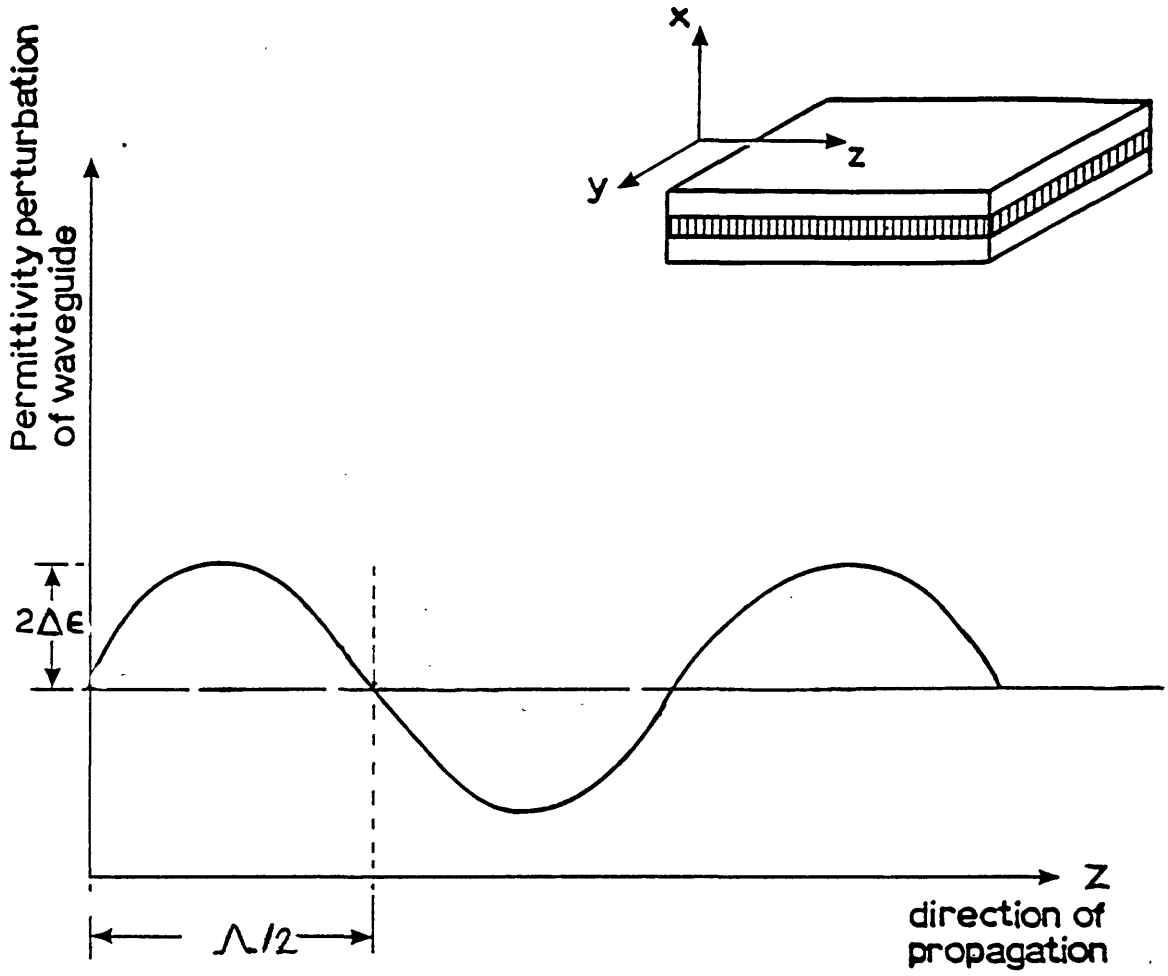

Figure 4.1 Slab waveguide with longitudinal periodic perturbation

planar region, for example a slab dielectric guide, of length L with a periodic perturbation of its permittivity (this may be in all or part of the medium, e.g a grating cut into the cladding surface of a guide) of pitch Λ and amplitude $\Delta\epsilon$. It is assumed that there is an incoming wave ,i.e. a wave with forward phase velocity, at z=0 of the form

$$A \exp(iwt)$$

and that there is no wave travelling into the guide, i.e. no wave with backward phase velocity, at z=L. It has been shown that these boundary conditions are equivalent to requiring continuity of the total electric field and its z-derivative as long as the periodic perturbation is small [89], that is

$$|k| << \beta$$

where k is the coupling coefficient (proportional to $\Delta\epsilon$ [31])

β is the propagation constant of the mode

For the TE mode, the reflected and transmitted fields are given by, respectively [31],

$$E(w,0,t) = A \exp(iwt) \cdot \frac{(-ik^* \sin(sL))}{(s\cos(sL)+iB\sin(sL))} \qquad (4.1)$$

$$E(w,L,t) = A \exp(iwt-igL) \frac{s}{(s\cos(sL)+iB\sin(sL))} \qquad (4.2)$$

where $g = \pi/\Lambda$

$B = \beta - g$

$s^2 = B^2 - |k|^2$

These expressions hold when there is significant coupling only to the backward mode with propagation constant β, and not to any

other modes, in the frequency range of interest.

In general, if

$$E(w,z,t) = A \exp(iwt+if(w,z))\ U(w) \qquad (4.3)$$

for real functions U,f, then for a modulated input at z=0 of the form

$$h(0,t)= \int A(w)\exp(iwt)dw \qquad (4.4)$$

centred at w_o say, the field after propagation through a distance z is given by [40]

$$E(z,t) = \int A(w)\ U(w)\ \exp(iwt + if(w,z))\ dw \qquad (4.5)$$

When U(w) is slowly varying compared to wt+f and $(d^3f/dw^3)/z$ and higher derivatives are small, i.e. when

$$\frac{U'}{U(t + f')} \ll 1 \qquad (4.6)$$

away from the stationary frequency (where t + f' =0)

and

$$\frac{f'''\delta w}{f''} \ll 1$$

where ' denotes differentiation with respect to w

δw is the frequency range for which A(w) is significantly non-zero, i.e. the effective range of integration,

Taylor series expansions of U and f about w_o and use of the method of stationary phase show that the increase in pulse width owing to the dispersive nature of the medium is characterised by the value

$$f''(w_o) \qquad (4.7)$$

This is the standard method for determining the degree of pulse distortion and has been widely applied to both periodic and other dispersive media.

However the field expressions equations (4.1), (4.2) each

represent a summation of two components of two Bloch waves (see later) and thus contain rapidly varying terms besides the exponential term when put in the form of equation (4.3) . For example if we put (4.2) into this form then

$$U(w) = \frac{s}{(s^2 \cos^2(sL) + B^2 \sin^2(sL))}$$

$$f(w) = \arctan (-B \tan(sL) /s) \qquad (4.8)$$

Therefore

$$\frac{U'}{U} = - \frac{BB' |k|^2 \tan(sL) (sL - \tan(sL))}{(1 + (B \tan(sL)/s)^2) s^3}$$

$$f' = \frac{B'(-|k|^2 \tan(sL) + B^2 sL \sec^2(sL))}{(1 + (B \tan(sL)/s)^2) s^3}$$

It is not clear that U is in general more rapidly varying than t+f' for t=f', for example this is not the case when B/|k| is small. Also, if L is very large and w_o lies inside the reflection band,

$$\frac{U'}{U(t + f')} = \frac{BB'|k|^2 L}{(t s^2(1 + (B/s)^2) + B'|k|^2}$$

This is large for large L for $t \approx f'$ so the constraint (4.6) does not hold. Similarly,

$$\frac{f'''}{f''} = sL \frac{((1 + 3t^2) - Bt^2(3 + t^2)/s^2)(1 + O(1/L))}{t (1 + (B/s)^2 t^2)}$$

where $t = \tan(sL)$

and it is clear that this expression is proportional to L for

large L and fixed w. Also it becomes large when $sL = (m + 1/2)\pi$ for integer m. This indicates that the approximation will be invalid for certain frequency intervals. In practise k is often imaginary and so f(w) is identical for (4.1) and (4.2). This implies that, if (4.7) determines the dispersion, the dispersion is identical for the transmitted and reflected pulse.

These considerations suggest that simply considering $f''(w_o)$ may not give an accurate description of the dispersive properties of the medium, especially outside the reflection band, and approximate techniques for evaluating the integral (4.5) must be applied with care.

4.3 Series forms of the reflected and transmitted fields

In order to estimate the shape of the pulses resulting from the field expressions (4.1), (4.2), it is useful to write

$$D = \frac{1}{s\cos(sL) + iB\sin(sL)}$$

$$= 2\,\frac{\exp(-isL)}{(s + B)}\,(1 + G\exp(-2isL) + (G\exp(-2isL))^2 + ...) \qquad (4.9)$$

where $G = (B - s)/(B + s)$

For w outside the reflection band, i.e. for $|B| > |k|$, $\mathrm{sign}(s) = \mathrm{sign}(B)$ (this is clear from physical considerations, since the the properties of the guide must vary continuously from

the case in which there is no periodic perturbation), and so

$$| G \exp(-2isL) | < 1 \qquad (4.10)$$

Inside the reflection band

$$|G \exp(-i2sL)| = |\exp(-2SL)(B + iS)/(B - iS)|$$

where $S = i|s| > 0$ (see figure A4.1 of the appendix for the branch cuts in the w-plane) and so again (4.10) holds. Therefore, except exactly at the band edges (i.e. s=0) the series representation (4.9) is convergent and so is valid. As the band edges are approached, (from any direction), more terms of the series must be retained to give a reasonable approximation to the exact function. As $|k|$ is reduced, that is the amplitude of the periodic perturbation becomes less, more terms must be included in the series if w lies inside the stop band, and less terms need be included if w lies outside the stop band. This indicates that this expansion is most useful when the medium is strongly reflecting and when it is behaving almost as a uniform region.

If the range of integration of (4.5) includes one or more of the band edges, it is convenient to use, in effect, a Laplace Transform A_L of h(t) rather than the Fourier transform of equation (4.4), that is

$$A_L(w-i\Gamma) = 1/2\pi \int_0^{\infty} h(t) \exp(-i(w-i\Gamma)t)\, dt \qquad \Gamma > 0 \qquad (4.11)$$

Since $h(t) = 0$ for $t < 0$,

$$A_L(w-i\Gamma) = A(w-i\Gamma)$$

and so the reflected and transmitted fields, E_r, E_t respectively, are given by

$$E_r(0,t) = \sum_{n=0}^{\infty} \int_{-i\Gamma-\infty}^{-i\Gamma+\infty} \frac{dw\, A(w)\, k^{*} \exp(iwt-2insL)\, p\, (1-G)G^{n-1}}{(B + s)} \qquad (4.12)$$

where $p = G/(G-1)$ if $n = 0$ and $p = 1$ otherwise.

$$E_t(L,t) = \sum_{n=0}^{\infty} \int_{-i\Gamma-\infty}^{-i\Gamma+\infty} dw \exp(iwt-igL-is(2n+1)L)\ A(w)\ (1-G)G^n \qquad (4.13)$$

(extending all functions to the complex plane by their analytic continuations). Now, for large enough Γ, the series representation (4.9) is valid along the whole of the path of integration and additionally the path avoids the branch points of s (which are also at the band edges). The variation of the exponential term increases relative to the rest of the integrand as L increases. The dependence on the length of the medium is as for a uniform medium with dispersive permittivity. In order to estimate the size of the contribution of the terms in (4.12), (4.13), it is useful to consider first their amplitudes for the case

$$A(w) = \delta(w-w_o)$$

(i.e. a monochromatic wave) as a function of the carrier frequency w_o. These are shown in figures 4.2 and 4.3. Clearly the successive terms have decreasing amplitudes. When w_o is inside the stop band , the leading reflected term becomes more dominant as $|kL|$ is increased. When w_o is outside the stop band the amplitudes are a function of $B/|k|$ only and are independent of L. The leading transmitted term dominates as $|k|$ is increased. These conclusions are likely to hold for more general functions A(w) as in practise A(w) is usually sharply peaked at w_o.

Thus it is likely that in general a good approximation to the output fields may be obtained by considering only the first few terms of the series (4.12), (4.13). In particular

(i) w_o outside the reflection band

If $(|k|/B)^2 \ll 4$ then $|G| \ll 1$ (4.14)

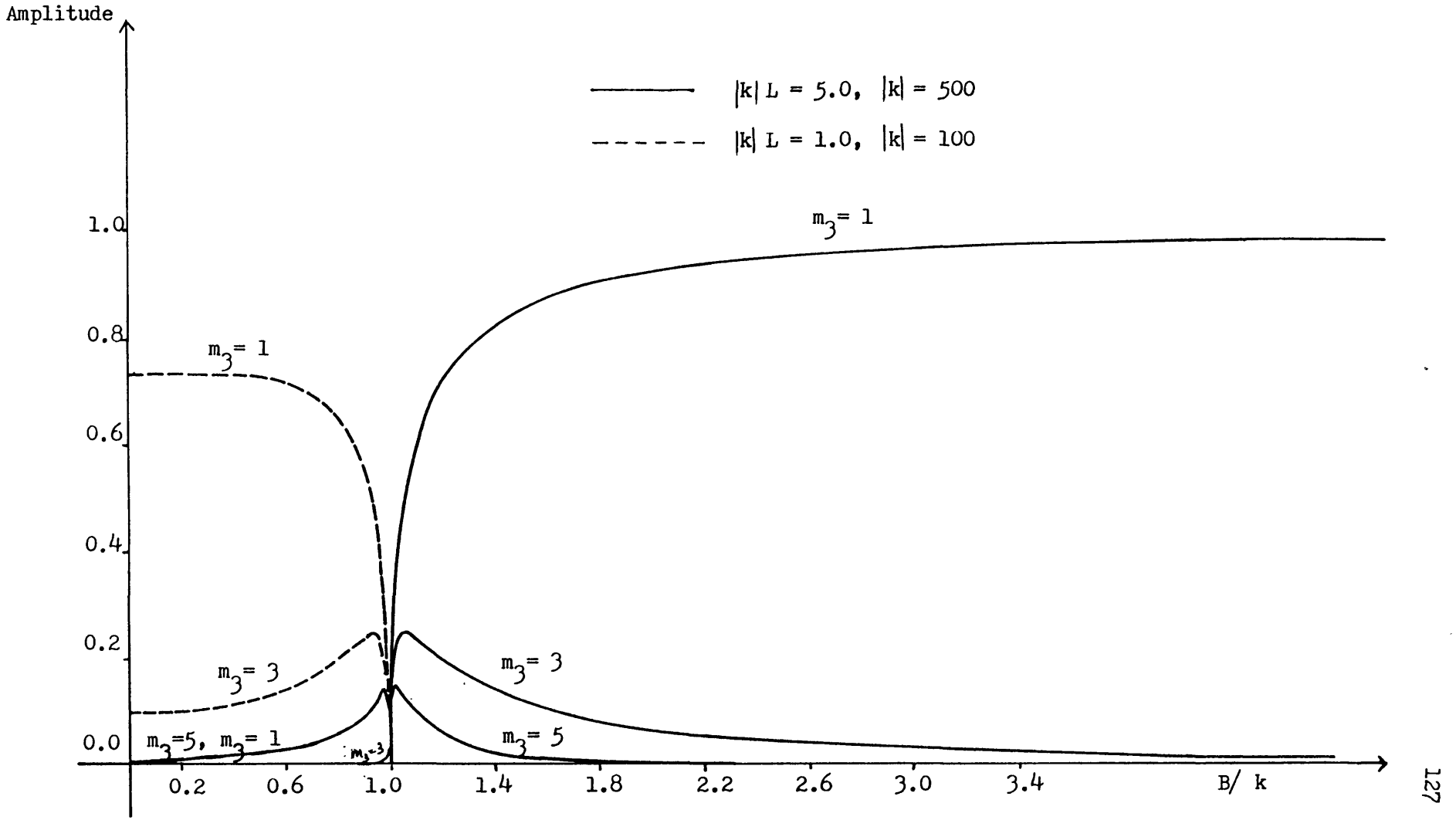

Figure 4.2 Amplitudes of transmitted terms ($m_3 = 2n+1$)
The curves for $m_3 = 5$, $|k|L = 1.0$ and $m_3 = 1$, $|k|L = 5.0$ coincide inside the reflection band.

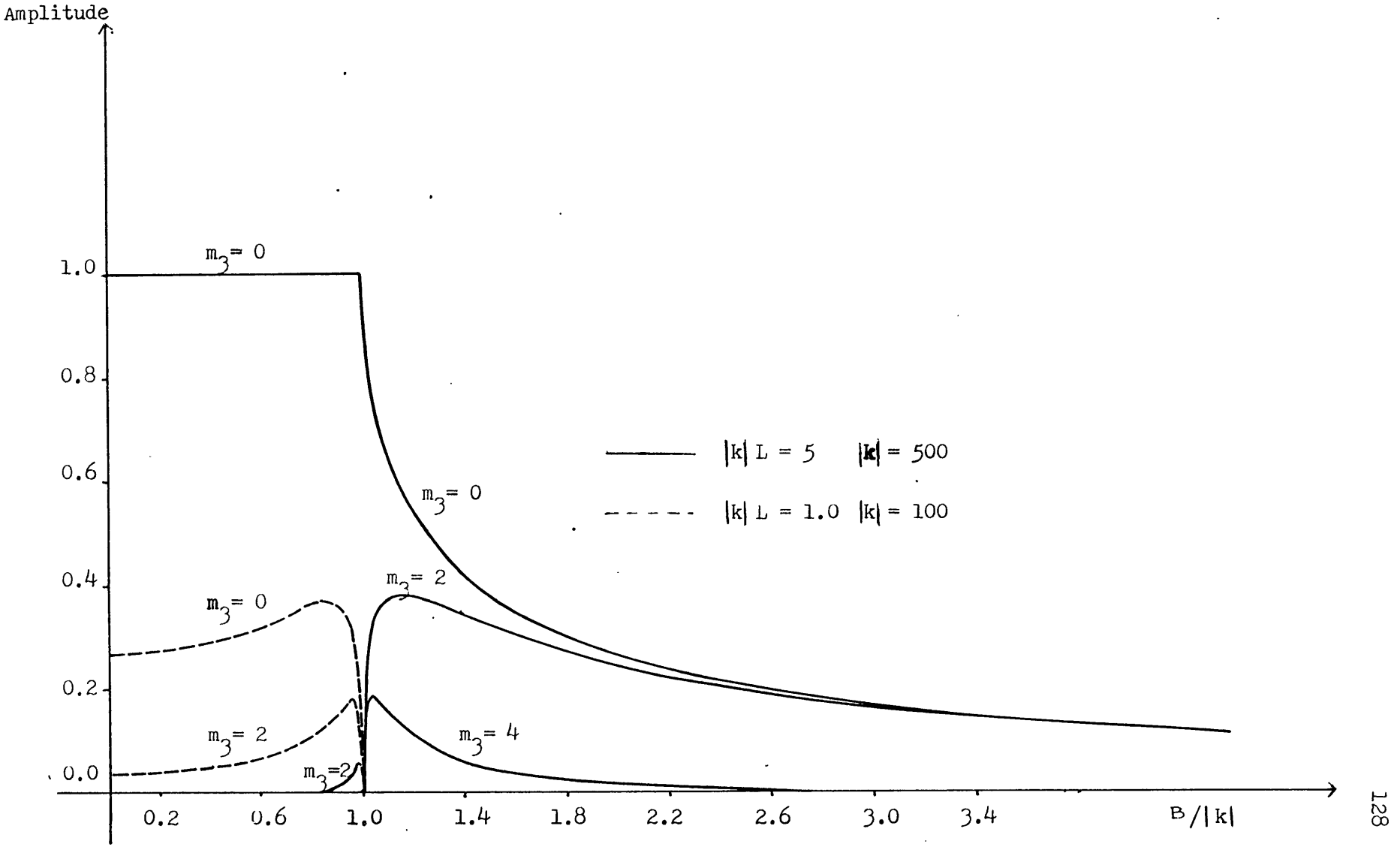

Figure 4.3 Amplitudes of successive reflected terms ($m_3 = 2n$)

and so all the other terms in (4.12), (4.13) are negligible compared with the leading transmitted (n = 0, G^n = 1) term. This latter term has a simple exponential integrand with a real argument for real w and the conventional method of evaluation and use of the second derivative of the phase (4.7) to describe the pulse are justified. Therefore

$$\text{Signal velocity} = v_s = dw/ds = s/(B\,B') \tag{4.15}$$

$$\text{Pulse dispersion} = \frac{d(L/v_s)}{dw} = \frac{(B''B + B'^2 - B'^2B^2/s^2)L}{s}$$

If $|k|L \gg B/|k|$ then the exponential term in each integral with non-zero n is also rapidly varying compared with the rest of the integrand. Then again, as long as A(w) is negligible inside the reflection band, use of (4.7) is valid and so each integral, except the first reflected one, can be taken to represent a pulse travelling with velocity dw/ds through a distance mL (for integer m) with a corresponding dispersion. If the original pulse width is substantially less than the transit time through the structure and the dispersion for this pulse is not too large, there will be little interference between the terms and they will result in a series of output pulses. Then the fields are composed of components each of which has travelled an integer number of round trips through the structure, resembling a conventional non-distributed resonator in a transmission mode.

For example, if a Gaussian pulse has dispersion $m_3 d^2s/dw^2$ per unit length, then from the standard formulae [40] and (4.15), the pulse half width after propagation through a distance L, W(L), is

$$W(L) = W(0)\ \frac{\left(\ 1 + 4\ m_3^{\,2}(|k|L)^2\Delta(B/|k|)\ \right)^{1/2}}{\left(\ (B/|k|)^2 - 1\ \right)^3}$$

where $\beta = nw/c$, and $\Delta(B/|k|)$ is the normalised spectral half width of the pulse.

If $B/|k| = 2$, $\Delta(B/|k|) = 0.25$, $|k|L = 15$, then we can assume that each integral in (4.13) is normally dispersive and also

$$W(0) \approx 0.27Ln/c, \qquad W(L)/W(0) \approx \left(\ 1 + 0.13m_3^{\,2}\ \right)^{1/2}$$

Therefore the first term arrives with a width increase of $\sim 6\%$, and the next contribution is only non-zero after a time interval of about 7 times the half width of the first term, and so does not interfere significantly with it.

(ii) w_o inside the reflection band

Now if $\qquad |k|L\ (1 - (B/|k|)^2)^{1/2} \gtrsim 3$

then all terms except for the leading reflected (n = 0) term may be neglected. The leading reflected term may be written

$$\int_{-i\Gamma\ -\infty}^{-i\Gamma\ +\infty} \frac{dw}{|k|}\ \exp\left(\ i\ \arctan\left(\frac{\sqrt{|k|^2 - B^2}}{B}\right)\right.$$

and, in the approximation that k is constant ($k = k(w_o)$), the signal arrival time t_o and the time dispersion may be obtained in the usual way to give

$$t_o = B'/S$$

$$dt_o/dw = \left(\ B'' + B'^2B\ \right)/s^3 \qquad (4.16)$$

Thus we have determined the dispersion in certain cases for small $|k|/B$ and large $|k|L$. At first sight it is surprising that the dispersion apparently increases as $|k|L$ becomes smaller. However

as |k|L tends to zero, the contribution from frequencies outside the stop band tend to zero. The contribution from frequencies inside the stop band interfere and cancel out. The dispersion may be interpreted as describing this interference. Only the leading transmitted term increases and approaches that for propagation in a uniform medium.

The expressions for the monochromatic fields, equations (4.1), (4.2), and the corresponding equations for the fields with forward and backward phase velocity at some distance z such that $0 < z < L$ [31] can be re-written to emphasise their composition of Bloch wave modes of the periodic structure.The latter become

$$E(z,w)=A(0)\exp(iwt-igz)(s+B)\ \frac{(\exp(isL-isz) + (s-B)\exp(isz-isL))}{\cdot\ 2(s\cos(sL) + iB\sin(sL))}$$

$$E(z,w)=A(0)\exp(iwt+igz)\ k\ \frac{(\exp(isL-isz) + (s-B)\exp(isz-isL))}{2(s\cos(sL) + iB\sin(sL))}$$

Thus the transmitted field, which has forward phase velocity, is the sum of the fundamental component of a Bloch wave with a group velocity +dw/ds and the first harmonic of a Bloch wave with a group velocity -dw/ds . Similarly the reflected field is the sum of two waves with group velocities -dw/ds and +dw/ds. It is well known that the single group velocity of a Bloch wave (its components have propagation constants differing by integer multiples of $2\pi/\lambda$) is equal to the average over one period of the medium of the velocity of the energy flow [31]. However it is clear from above that the propagation of a signal in a finite periodic meduim, which is carried by two Bloch waves, cannot be

described simply in terms of their two group velocities. For instance, from the series representation of the field equations (4.13), all the transmitted components have positive signal velocity, as is necessary physically. The signal velocity and dispersion of the transmitted signal in equation (4.15) are directly related to the slope of the $w-\beta$ curve representing the fundamental component of the forward Bloch wave in the usual way. Equation (4.14) is the condition that the amplitudes of all the other components are negligible. However the propagation characteristics of the reflected pulse described by (4.16) cannot be related so straightforwardly to the $w-\beta$ curve.

It has been shown by Brillouin that, in absorbing dispersive media, the propagation velocity of the signal is not necessarily equal to the group velocity [90], [91]. We have seen that this appears to be the case in periodic media also and we have obtained some of the characteristics of the propagated signal. In order to consider these in more detail we shall apply the general method used by Brillouin, the method of steepest descent [92], to the case of a finite medium with a periodic variation of its refractive index.

4.4 General formulae for the propagated signals

We consider an incoming signal with carrier frequency w_o of the form

$$h(t) = 0 \qquad t < 0$$

$$h(t) = E_o \exp(iw_o t) \qquad t > 0$$

that is, a semi-infinite wave starting at t=0.

The fields resulting from propagation of this signal can be used to obtain simply the output from a rectangular pulse of duration τ by adding the field from h(t) to that from

$$h_1(t) = 0 \qquad t < \tau \qquad (4.17)$$
$$h_1(t) = -E_o \exp(iw_o t) \qquad t > \tau$$

For an input signal h(t), the corresponding "Laplace" transform (4.11) is

$$A(w) = \frac{E_o}{i((w-i\Gamma) - w_o)}$$

and a typical integral appearing in (4.12), (4.13) may be written

$$I = \frac{E_o}{2\pi i} \int_{-i\Gamma - \infty}^{-i\Gamma + \infty} \frac{k^{*\alpha}\, dw \exp(F(w))}{(w - w_o)} \qquad (4.18)$$

where $F(w) = iwt - im_3 sL + m_1 \ln(B - s) - m_2 \ln(B + s)$

for example the first two terms in (4.13) are

$\alpha = 0$ and

$m_3 = 1,\ m_1 = 0,\ m_2 = 0$

$m_3 = 1,\ m_1 = 2,\ m_2 = 2$ etc.

For both clarity and simplicity, in this section and the appendix we will ignore waveguide and material dispersion and consider the dispersive effect of the periodicity alone. Therefore we can write

$$B = (nw/c) - g$$

where n is the (w-independent) average refractive index of the medium and c is the speed of light. Clearly other effects can be included by using the appropriate expression for B. We will also assume that we can set

$$k = k(w_o) = \text{constant}$$

since k is relatively slowly varying with w_o. These restrictions should not effect the results qualitatively and will be removed for a particular case in the next section. Equation (4.18) is in a form which may be evaluated approximately using the method of steepest descent [91], [92]. Details of the calculation are given in the appendix to this chapter. Here and in the following section we will state and discuss the results.

In general the method of steepest descent yields a solution of an integral as a sum of two non-negligible contributions. One, $I_s(t)$, is from the saddle point of the argument of the exponential, and this describes the dispersive effect of the meduim. The other contribution $I_p(t)$, comes from the pole in the integrand at $w = w_o$ and corresponds to the effect of the particular modulation. This form of solution leads to a simple definition for the signal velocity. However it is an approximate method (which improves in accuracy as $|k|L$ increases) and its description of the pulse shape is rather cumbersome. For a periodic medium we find that $I = I_s + I_p$ such that

(i) <u>The saddle point contribution</u>

$$I_s = 0 \qquad \text{for } T < 1 \qquad (4.19)$$

$$I_s = \sum_j \frac{E_o\, k^{*\alpha} \exp(F(w_s{}^j))(1+id_o{}^j)}{i(w_s{}^j - w_o)\sqrt{2\pi K}} \qquad \text{for } T > 1 \qquad (4.20)$$

where $T = tc/(m_3 nL)$ is the normalised time

$$d = m_4/(m_3|k|L)$$

$$m_4 = m_1 + m_2$$

$$e^2 = (\gamma^2/d^2) - 1$$

$$\gamma^2 = T^2 - 1$$

The position ot the saddle point w_s^j and the quantities K, d_o^j are functions of time:

(a) for $0 < \gamma^2 < d^2$

$$j = -$$

$$K^2 = m_4 (-e^2)^{1/2} \frac{n}{c} \frac{d}{|k|} \frac{1}{(1+d^2)} ((-e^2)^{1/2} - T) \qquad (4.21)$$

$$d_o^- = 0$$

$$w_s^- = \frac{c}{n} \left(-\frac{|k|d}{\gamma^2} i (1 + (-e^2)^{1/2}) + g\right)$$

(b) for $\gamma^2 > d^2$

$$j = +,-$$

$$K^2 = 2m_4 e \frac{n}{c} \frac{d}{|k|} \frac{1}{(1+d^2)} \frac{(e^2 + T^2)}{(e + T)} \qquad (4.22)$$

$$w_s^{\pm} = \frac{c}{n} \left(\frac{|k|d}{\gamma^2} (-i \pm e) + g \right)$$

$$d_o^{\pm} = \pm (e - T)^2/(e^2 - T^2)$$

(ii) The pole contribution

$$I_p = 0 \qquad \text{for } T < T_o \qquad (4.23)$$

$$I_p = E_o k \exp(F(w_o)) \qquad \text{for } T > T_o \qquad (4.24)$$

where $T_o > 1$ is a function of the carrier frequency and is defined as follows:

(a) for w_o inside the stop band, $T_o \geq d^2 + 1$ and

$$T_o = d^2 + 1 \qquad \text{for } B_o = 0 \tag{4.25}$$

$T = T_o$ is the solution to

$$B_o T + |k| d \arctan\left(\frac{\sqrt{|k|^2 - B_o^2}}{B_o}\right) = Q^{\pm} \qquad \text{otherwise} \tag{4.46}$$

(b) for wo outside the stop band $T = T_o$ is the solution of

$$B_o = \frac{TQ^{\pm} \pm \sqrt{Q^{\pm 2} - |k|^2 \gamma^2}}{\gamma^2} \tag{4.27}$$

where $B_o = (nw_o/c) - g$

$$Q^{\pm} = |k| d\pi/2 \qquad \gamma^2 < d^2$$

$$Q^{+} = |k| d\,(e + \arctan(1/e)) \qquad \gamma^2 > d^2$$

$$Q^{-} = -|k| d\,(e + \arctan(1/e) - \pi) \qquad \gamma^2 > d^2$$

Clearly T_o tends to unity as $|B_o|$ tends to infinite.

The formulae for I_s and I_p become inaccurate near the lower ends of the ranges for which they are defined but they may be determined there by continuity (see appendix).

From equations (4.19), (4.23), we can interpret the m_3 term in (4.12), (4.13) as the contribution from that part of the field that has travelled at least m_3 rounds trips inside the structure but less than $m_3 + 1$.

4.5 Signal velocity and dispersion

In general, for a uniform dispersive medium, well away from the frequencies of absorption,

$$I_s \ll I_p \qquad (4.28)$$

for all times such that w_s is not too near w_o.

Therefore $t_o = m_3 L\, nT_o/c$, the time when I_p is first non-zero, has been taken as the arrival time of the signal, thus giving the signal velocity. This same quantity has been used to define the signal velocity in absorbing media, when (4.28) may not hold [91].

For a periodic medium, since even a monochromatic wave is not transmitted unperturbed, not only is (4.28) not necessarily true but also the saddle point contribution to the integral does not correspond directly to the distortion of the pulse. For example, greater transmission at frequencies different from w_o will tend to reduce the distortion of the transmitted pulse and the presence of these frequencies is expressed by the saddle point term. Thus in general we cannot use t_o to obtain a signal velocity for each term (even though we have now taken into account the frequency dependence of the whole of each integrand) or dt_o/dw to represent its pulse dispersion, though we may do so in the special cases discussed in previous section.

Figures 4.4 and 4.5 show $m_3 T_o$ as a function of the normalised carrier frequency for the first few values of (m_3, m_4) for $|k|L = 1$ and $|k|L = 5$ (positive B only is shown as the results are symmetric about $B = 0$ in the approximation $|k|$ = constant). An obvious feature of these figures is the near symmetry about $B = |k|$, that is,

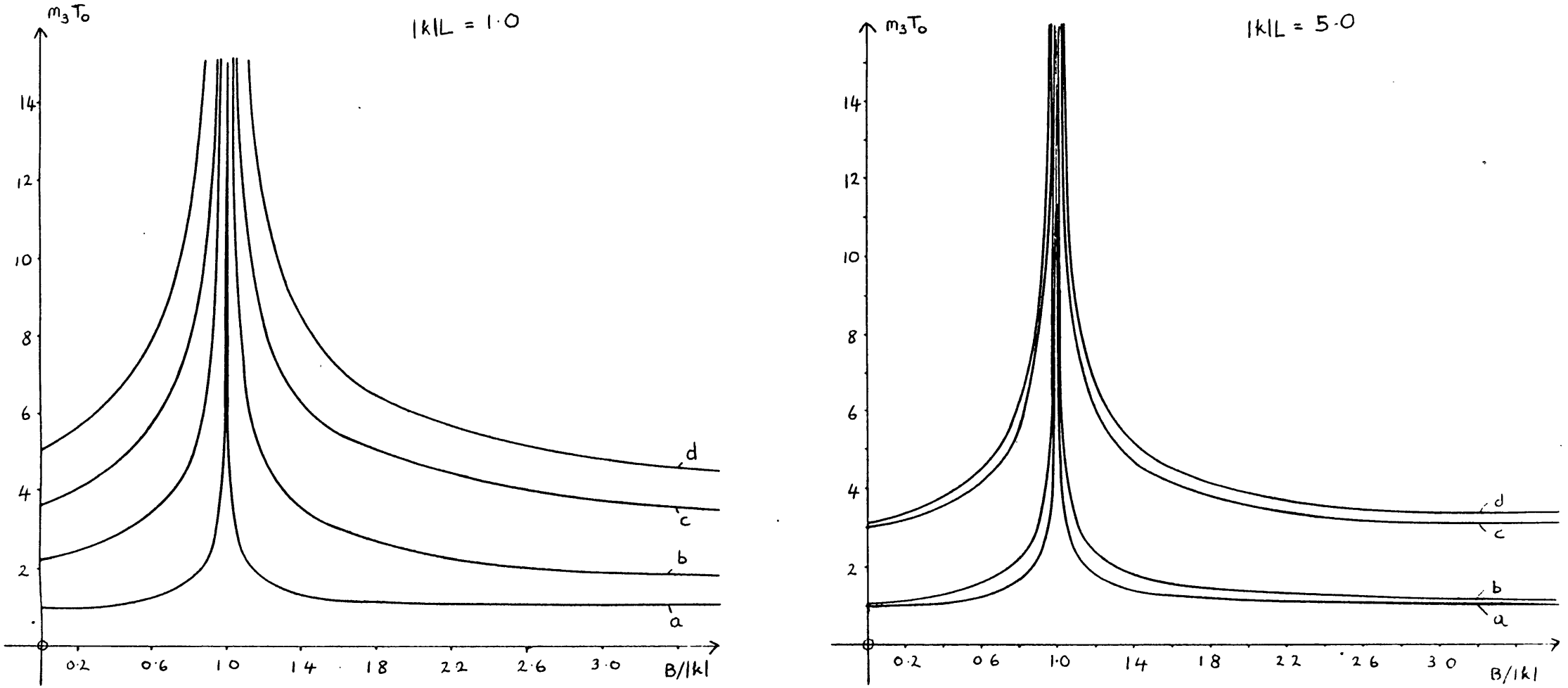

Figure 4.4 Normalised "signal arrival" time m_3T_o as a function of normalised frequency $B/|k|$ for the first few transmitted terms for $|k|L = 1.0$ and $|k|L = 5.0$

a : $m_3 = 1$, $m_4 = 0$ b : $m_3 = 1$, $m_4 = 2$ c : $m_3 = 3$, $m_4 = 2$, d : $m_3 = 3$, $m_4 = 4$

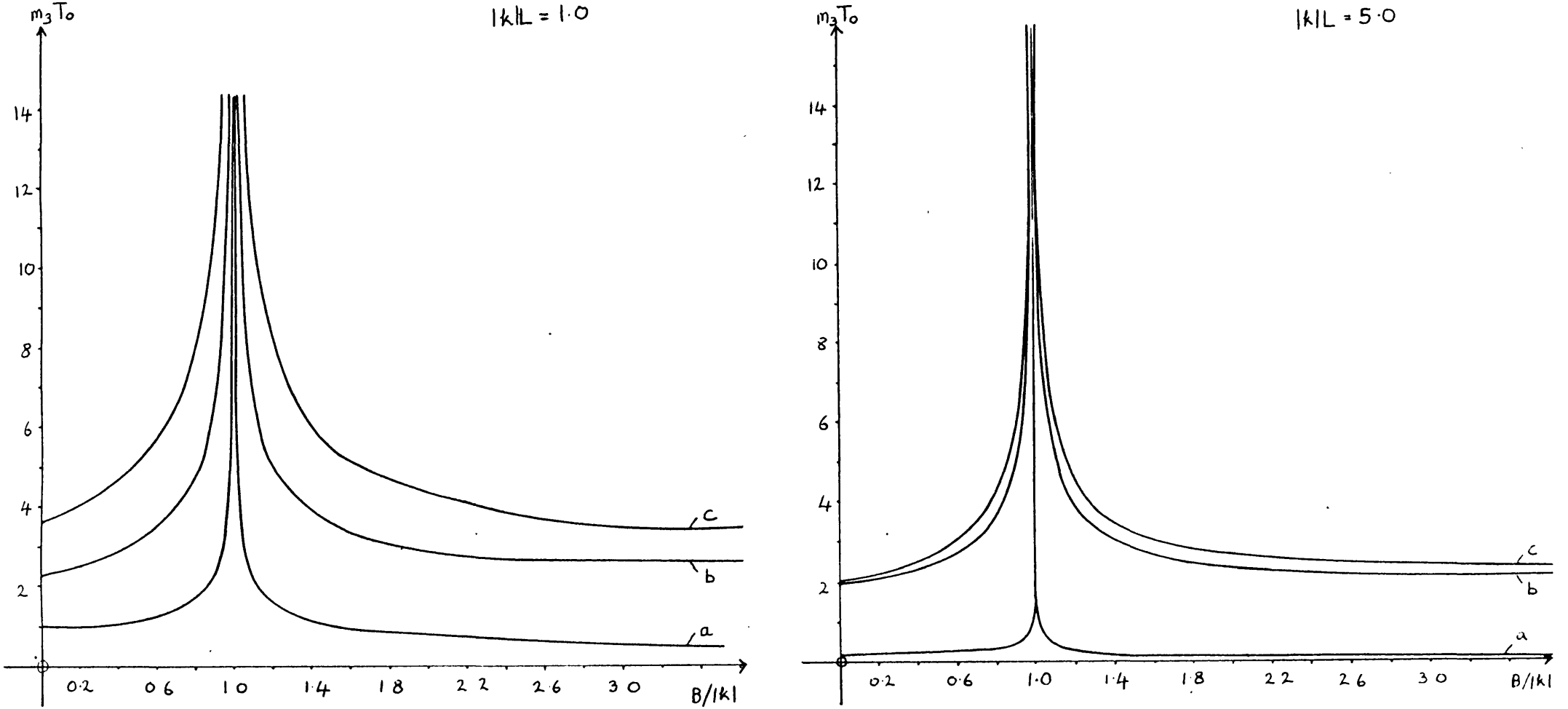

Figure 4.5 Normalised "signal arrival" time m_3T_o as a function of normalised frequency $B/|k|$ for the first few reflected terms for $|k|L = 1.0$ and $|k|L = 5.0$
a : $m_3 = 0$, $m_4 = 1$ b : $m_3 = 2$, $m_4 = 1$, c : $m_3 = 2$, $m_4 = 3$

$$m_3 t_o(B/|k|) = m_3 t_o(|k|/B)$$

From figure 4.4, we see that for small $|k|L$ each integral term is spread out and slowed down by the distributed nature of the structure, since t_o for the two values of m_4 for each m_3 are widely separated. As $|k|L$ is increased, figure 4.5, this effect is reduced and t_o tends to a single value for each value of m_3. In each case a signal velocity may be meaningfully defined if the corresponding pole contribution dominates that of the saddle point.

Figures 4.6 and 4.7 show the transmitted and reflected field amplitudes for $|k|L = 5$ for various values of w_o. The saddle point and pole contribution amplitudes are shown separately and also the amplitude of the sum.These latter results agree well with previous numericial evaluations (which were obtained by calculating 2048 point discrete Fourier transforms) [81] when the effect of a finite pulse width is included (4.17). The agreement improves for the larger value of $|k|L$, as can be seen by comparing figure 4.6 with figure 4.8, which shows the transmitted amplitudes for $|k|L = 1$. From these figures it is clear that the conclusions of section 4.2 concerning special cases are broadly justified, but that in general the signal may be significantly large at times different from the arrival of the pole contribution and that the effect of the periodic medium is to distort considerably the pulse shape. In addition the dispersion may not be negligibly small at the centre of the stop band when the undistorted term itself is very small (figure 4.6(a)).

We may define the dispersion of each term to be (to within a sign, which can be obtained from the signal velocity) $|K|^2$. This then is equal to the usual definition of dipersion when each

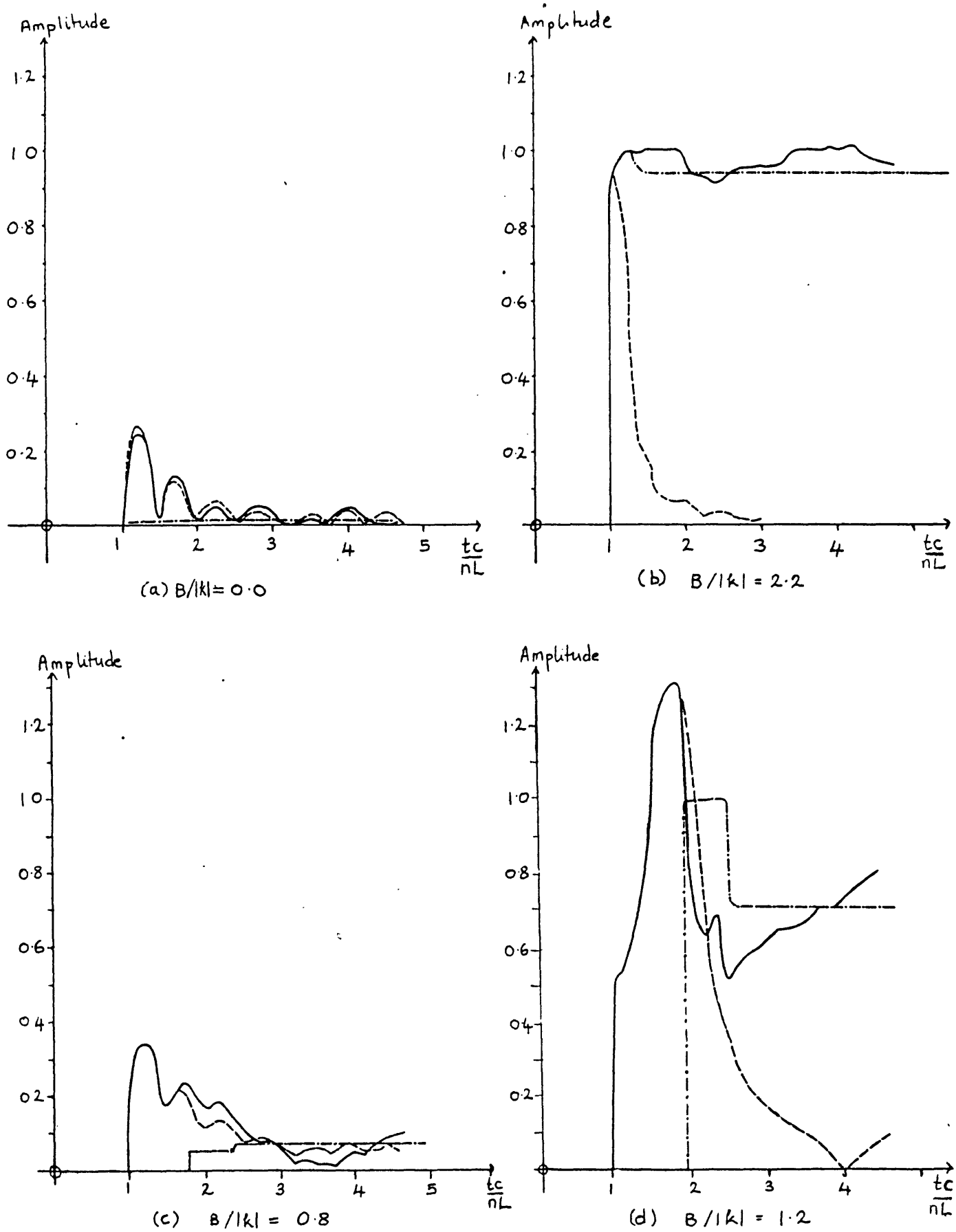

Figure 4.6 Amplitude of transmitted signal as a function of normalised time for $|k|L = 5$

– – – – Saddle point contribution

– · – · – Pole contribution

——— Total

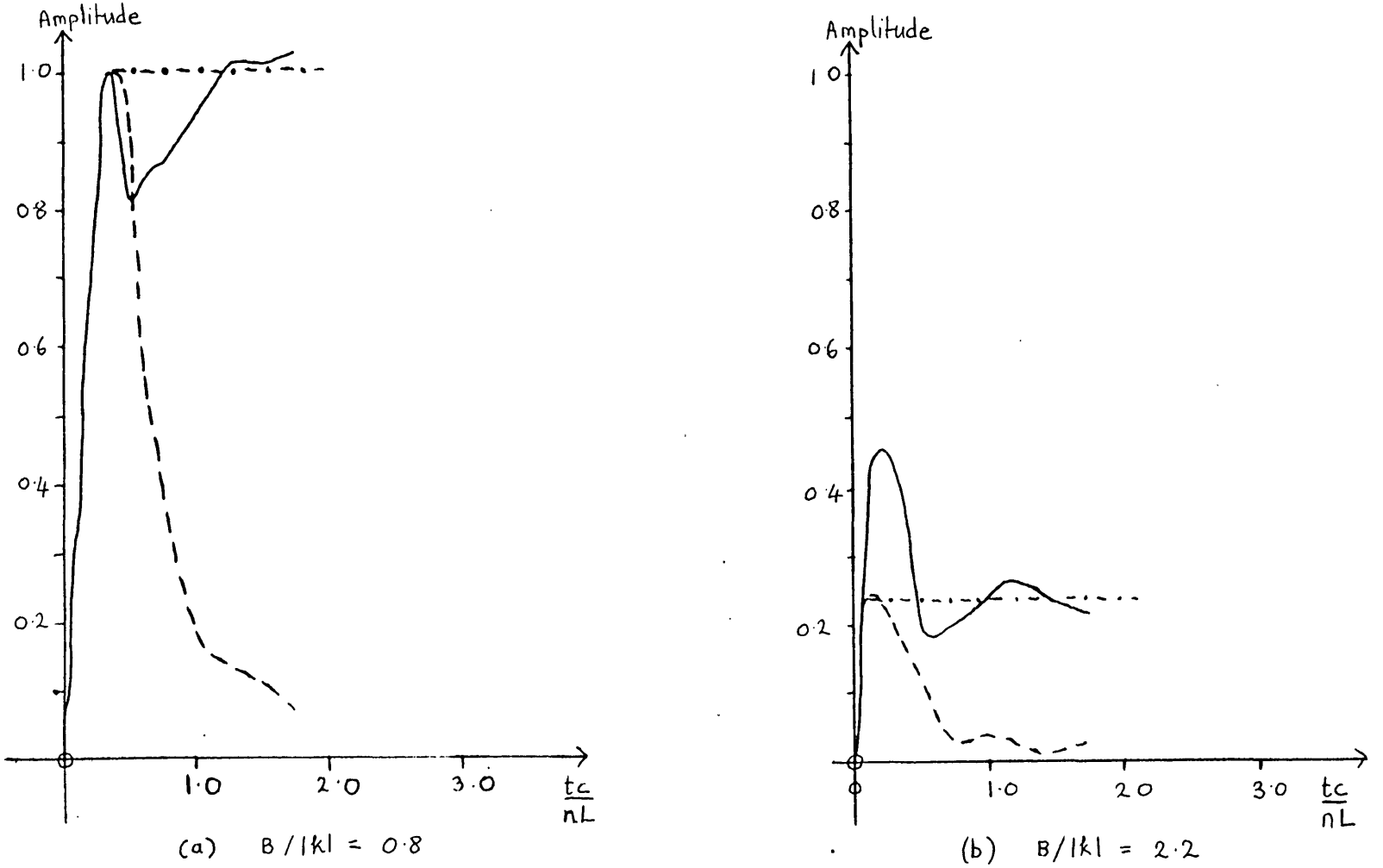

Figure 4.7 Amplitude of reflected signal as a function of normalised time for $|k|L = 5$

– – – – Saddle point contribution; —·—·— Pole contribution; ——— Total amplitude

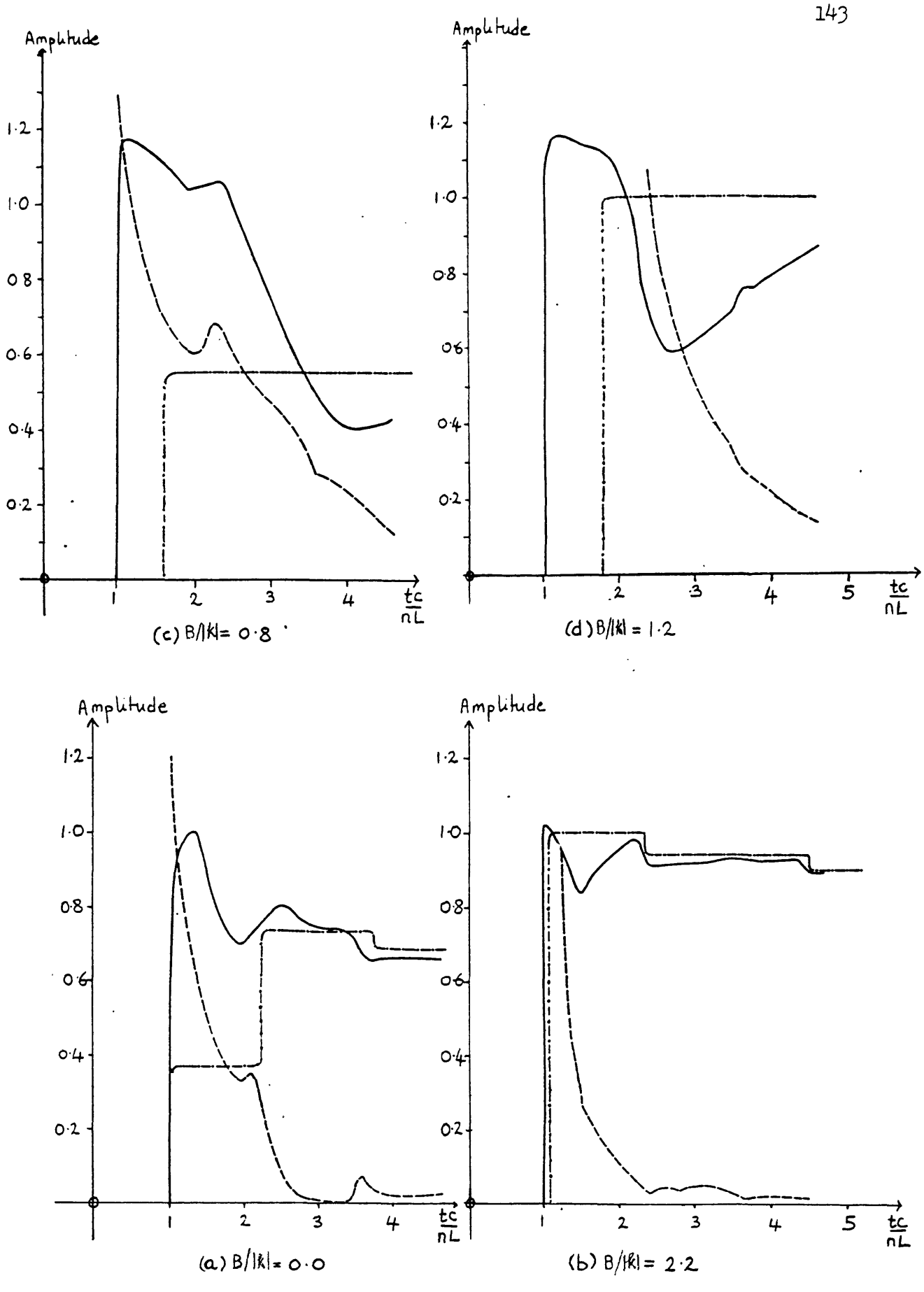

Figure 4.8 Amplitude of transmitted signal as a function of normalised time for $k L = 1$

– – – – Saddle point contribution
– · – · – Pole contribution
——— Total amplitude

integral is normally dispersive, but should be interpreted with care otherwise. Also the dispersion of the total pulse is not in general simply obtained from dispersions of the separate terms. The values of $|K|^2$ are shown in figures 4.9 and 4.10 for $|k|L = 5$. This dispersion is greater for later arriving terms because of their longer effective path length. We have seen already that our expressions do not hold well for $\tau \approx d$, and this is the time at which the pole contribution arrives if $B_o = 0$. Thus the zero value of $|K|$ at this point does not necessarily imply zero dispersion here. From the figures it is clear that the transmitted and reflected pulses have different dispersions in general.

For comparison, the dispersion obtained by using the second derivative of the phase of the total integrand, equations (4.7) and (4.8) is shown in figures 4.9, 4.10 also. This agrees well with the dispersion of the first reflected term inside the stop band since, for $|k|L = 5$, only this term is significantly large and is normally dispersive. The agreement is not so good otherwise. For example we have found that the dispersion has a single sign (on each side) outside the stop band and does not oscillate. In addition the conventional method of evaluation describes the effect of the periodic medium simply as a broadening of the reflected and transmitted pulses and gives no suggestion of the infinite number of smaller following contributions. It is possible that the dispersion obtained by using equations (4.7), (4.8) gives the total dispersion, while our results give approximate values for component terms. However this does not seem to be likely. For example for a carrier frequency outside the stop band, the leading reflected pulse will arrive, with non-zero pulse spreading, before any other contribution is

Figure 4.9 Dispersion term K^2 as a function function of normalised frequency B/ k for the first few transmitted terms. The dotted line shows the dispersion obtained using the phase of the total transmitted field.

k = 500, k = 5

a : $m_3 = 1$, $m_4 = 0$

b : $m_3 = 1$, $m_4 = 2$

c : $m_3 = 3$, $m_4 = 2$

d : $m_3 = 3$, $m_4 = 4$

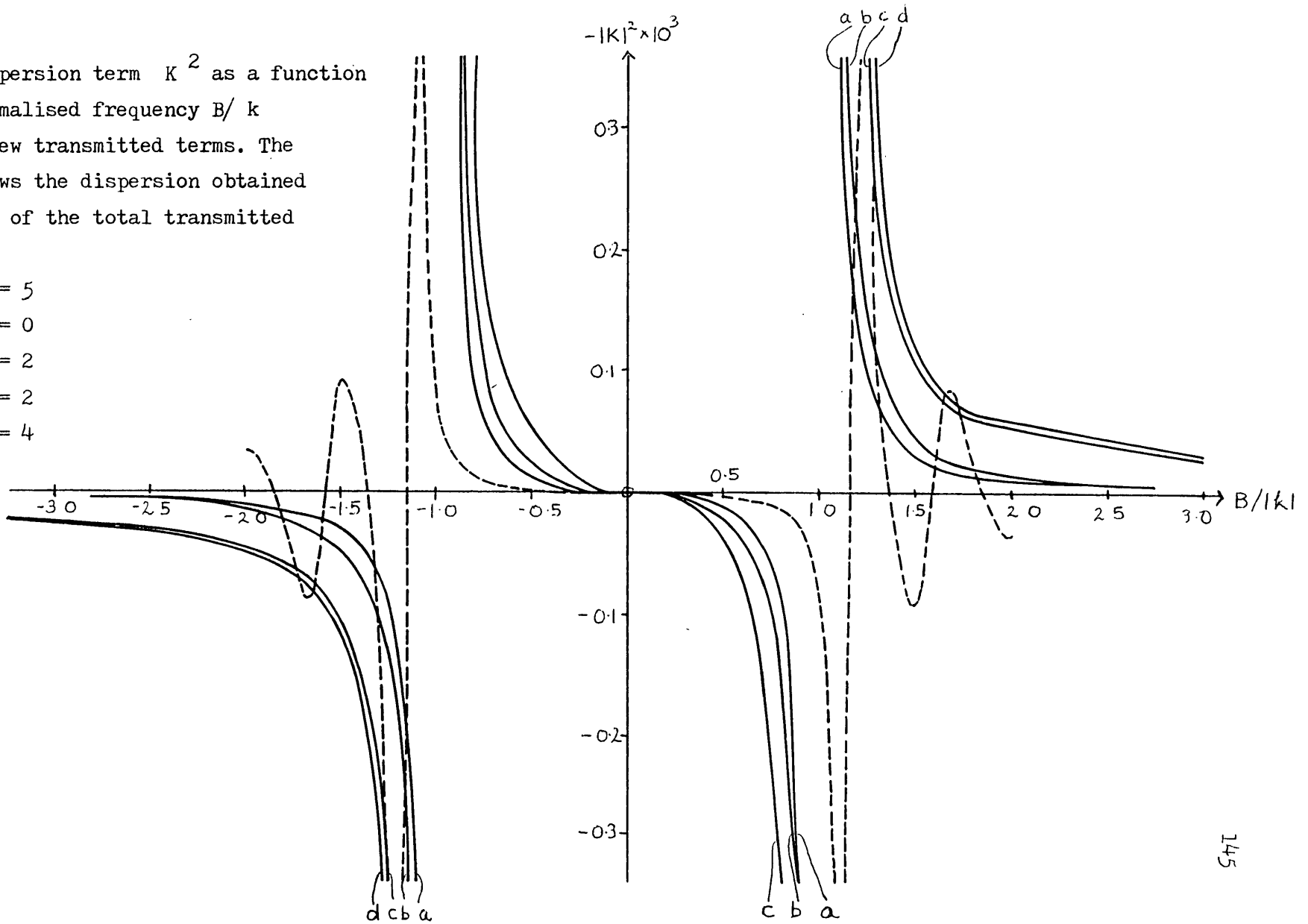

Figure 4.10 Dispersion term $|K|^2$ as a function of normalised frequency $B/|k|$ for the first few reflected terms. The dotted line shows the dispersion obtained by using the phase of the total reflected field.

$|k| = 500$, $|k|L = 5$

a : $m_3 = 0$, $m_4 = 1$

b : $m_3 = 2$, $m_4 = 1$

c : $m_3 = 2$, $m_4 = 3$

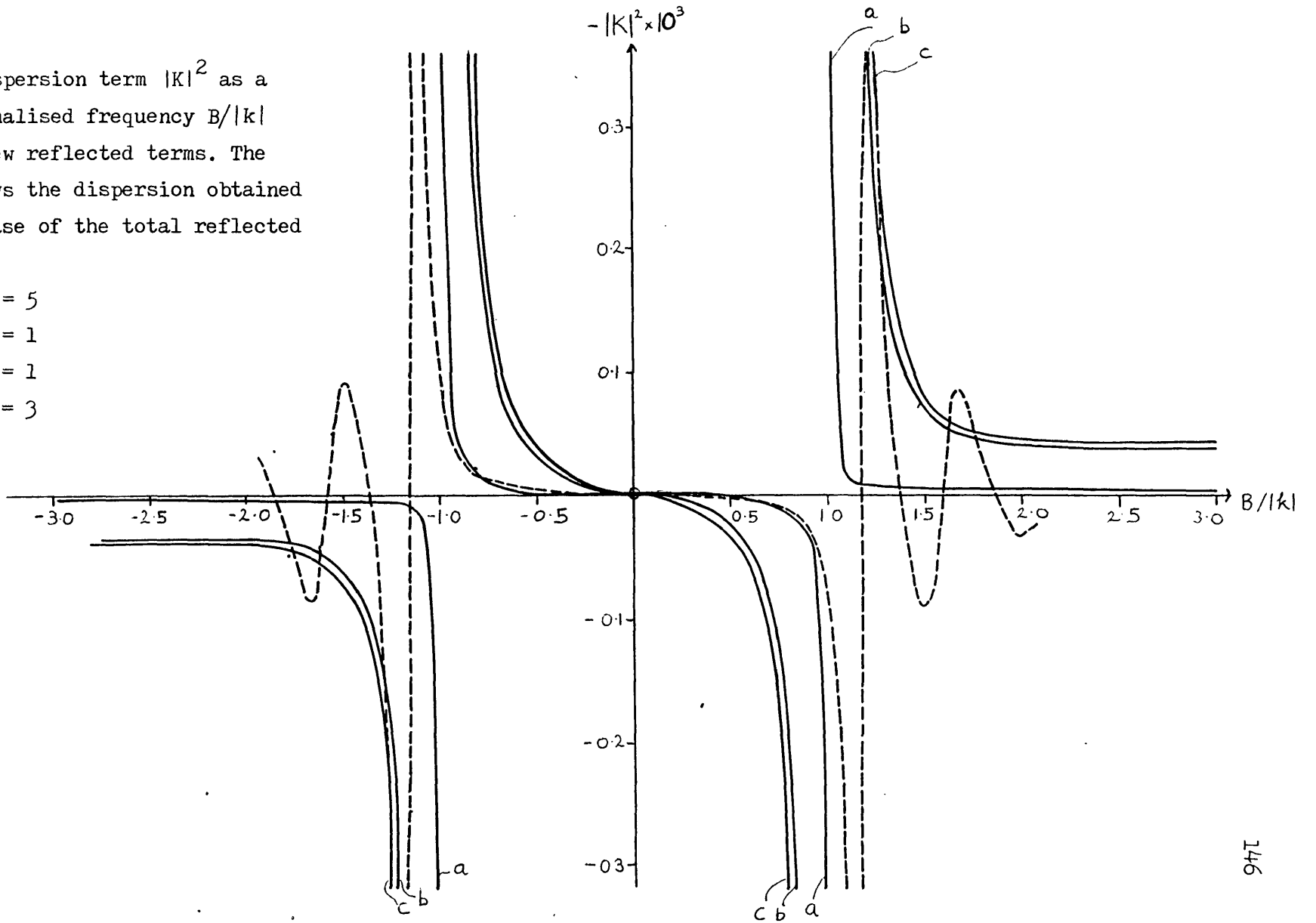

non-zero. The result that these other contributions are zero for times less than twice the transit time is exact. This is not compatible with the existence of frequencies at which the dispersion becomes effectively zero for the total pulse. Similarly, the leading Gaussian transmitted pulse considered in section 4.3(i) will arrive with non-zero dispersion before all other transmitted contributions, at least for $|B|/|k| \geq 2$.

As w_o approaches the band edges, the velocity of the pole contribution tends to zero. This is reasonable since the fields combine to form a standing wave for w_o at the band edges. Each term becomes more dispersed (because of the singularity of d^2s/dw^2) and the magnitude of I_s is comparable with that of I_p. In the limit the pole contribution does not arrive at a finite time and so clearly conservation of energy requires that I_s is non-negligible.

When w_o lies inside the stop band and the reflectivity is large, the main contribution to the reflected field is from terms which have travelled only a short distance inside the structure. Therefore as $|k|L$ increases or w_o tends to the centre of the stop band the dispersion is reduced and becomes essentially independent of the precise length of the structure.

4.6 Periodic perturbation for dispersion control

In this section we will show how a periodic perturbation may be used for the control of the dispersion of a waveguide. We consider a long guide with a small periodic perturbation of its

permittivity. We have seen in the previous sections that the transmission response of such a guide to an input signal with a carrier frequency very far from the band edge consists of a leading pulse of large amplitude, whose dispersion is expressed by d^2s/dw^2, followed by a series of terms of very small amplitude. The reflected field is the sum of a series of very small terms only. The "amplitudes" of these pulses (figures 4.2 and 4.3) are independent of L and ,for all terms except the leading transmitted pulse, decay at least as quickly as

$$|k|/2B \qquad (4.29)$$

Therefore in order to design a periodic guide with a zero of its dipersion at a given wavelength we will assume that only the leading pulse in transmitted and determine the required perturbation. The validity of this can then be checked by calculating the amplitudes of the other reflected and transmitted pulses for this particular guide. We will assume that the dispersion of all these terms is small enough for their amplitudes to be described accurately by equation (4.29). We have seen in the previous section that this is likely to be so as long as

$$|k|L \gg |k/B|$$

or $$|B/k| \gg 1$$

both of which are satisfied in the case considered here. The dispersion of the leading transmitted term may be described using the usual w-β curve for a periodic medium and the qualitative argument for a "dispersionless" frequency at w_d in a periodic waveguide is as shown in figure 4.11

The waveguide and material dispersion play an important part in determining the precise detailed propagation characteristics of a

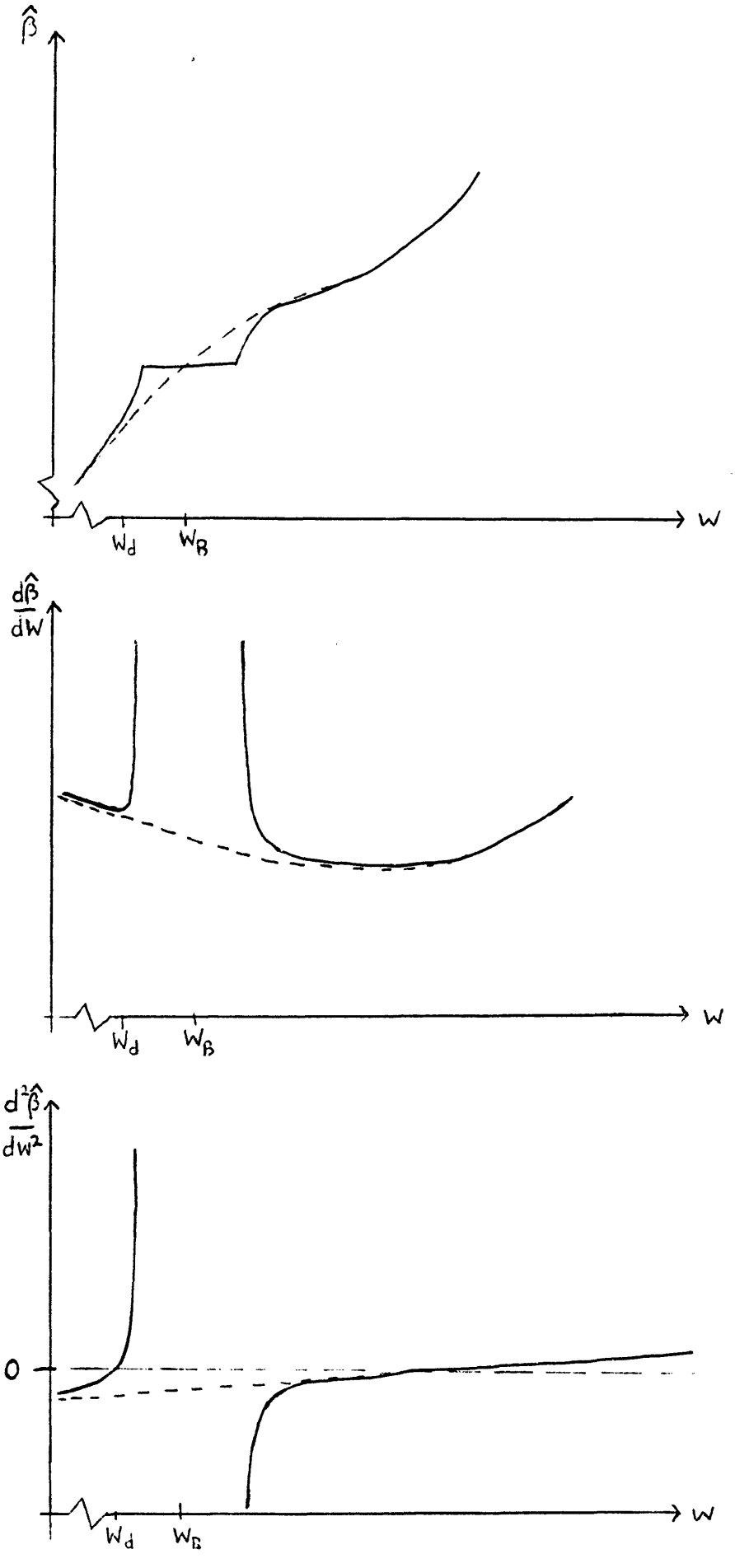

Figure 4.11 Behaviour of the propagation constant $\hat{\beta}$ and its first two derivatives near the Bragg frequency $w_B = \pi c/(\text{effective index}.\Lambda)$

- - - - - - Unperturbed guide, $\hat{\beta} = \beta$
——— Perturbed guide , $\hat{\beta} = \pi/\Lambda + s$

guide and so these effects are now included in the calculation. The refractive index is assumed to have a frequency dependence described by the Sellmeier equation [41] and the expression for the unperturbed propagation constant β is that of the first TE mode in a slab dielectric guide [31].

To a good approximation the pulse width is minimised for $d^2s/dw^2(w_o)=0$,assuming zero spectral width of the source [40]. Now (using again ' to indicate differentiation with respect to w)

$$s'' = (-s'^2 + B\,B'' + B'^2 - |k||k|'' - |k|'^2)/s$$

and so we can vary the pitch or amplitude of the perturbation, or both, in order to make s'' = 0 at some chosen wavelength.

For a given amplitude, the required pitch is given by the solution to the cubic equation

$$B^3B'' - B^2|\tilde{k}|^2 + B|k|(2B'|k|' - B''|k|) + |k|^2(|\tilde{k}|^2 - B'^2) = 0$$

where $|\tilde{k}|^2 = |k||k|'' + |k|'^2$

Since the leading transmitted term propagates with an effective L-independent propagation constant s, the field at z = L resulting from a Gaussian input pulse may be obtained in the usual manner to yield

$$E = \exp(iw_o t - is_o L - igL)\,\frac{AT}{X}\exp\left(-\frac{(t-s_o'L)^2T^2}{|X|^2}\right)\exp\left(is_o''L\frac{(t-s_o'L)^2}{|X|^2}\right)$$

where $s_o = s(w_o)$ and similarly for derivatives

$$X = (T^2 + is_o''L)^{1/2}$$

The guide considered is taken to have a core of silica doped with 13.5% germanium dioxide and a cladding of silica doped with 13.3% boria. The core width is $30/g \sim 5.2\mu m$. Figure 4.12 shows how s' and β' vary as a function of λ for this guide. The unperturbed guide has a zero dipersion point at $1.3\mu m$, near the zero of the

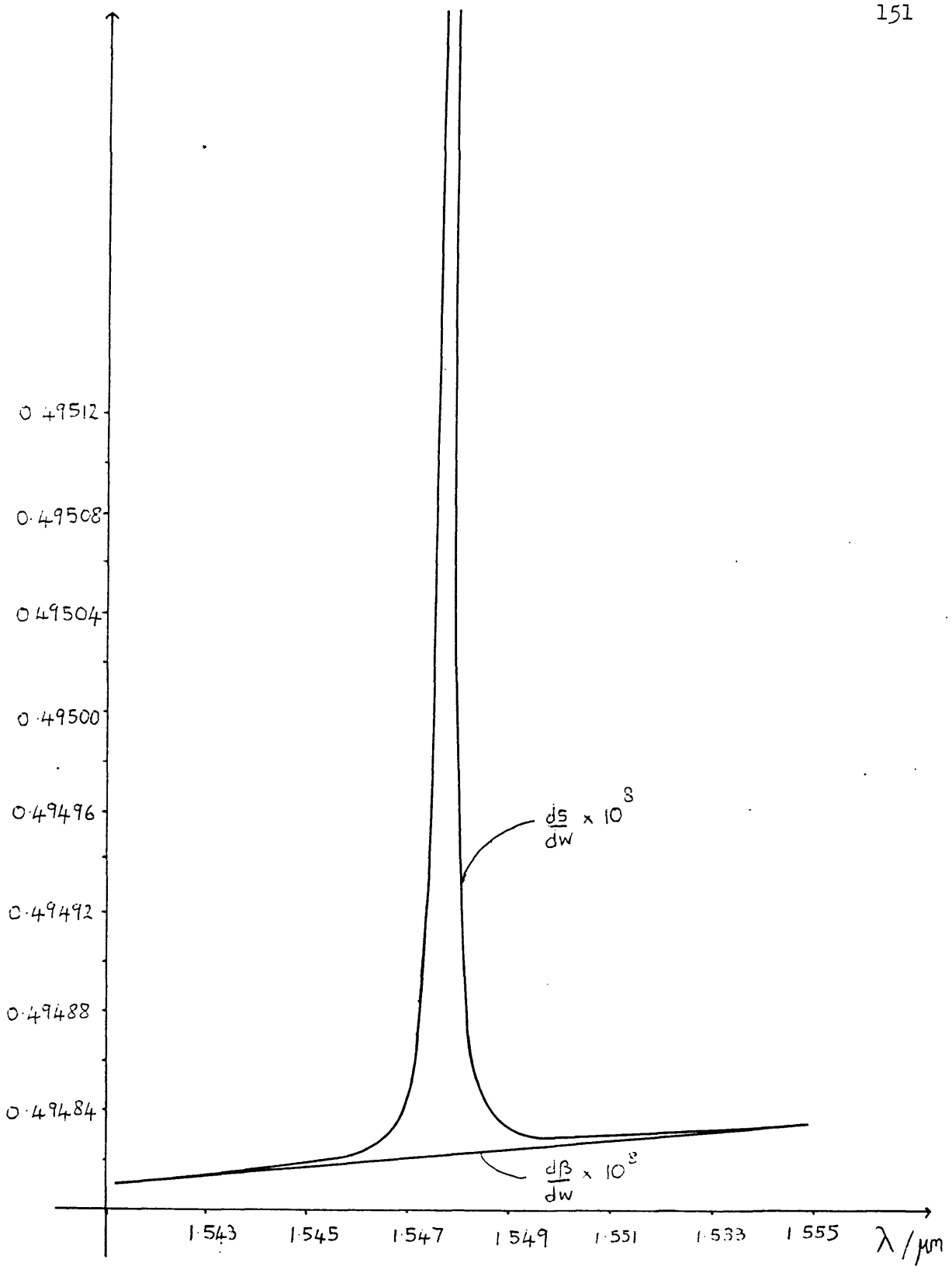

Figure 4.12 Variation of ds/dw and dβ/dw with wavelength λ

material dispersion. It is clear that the effect of the perturbation is to introduce an additional zero dipersion point, since the slope of s' varies from the positive slope of β' for λ far from the band edge to $-\infty$ as λ approaches the band edge (though we have seen in the previous section that d^2s/dw^2 alone does not describe the dispersion near the band edge). The perturbation has been chosen so that the dispersion zero occurs at 1.55μm, the minimum loss wavelength for silica.

Figure 4.13 shows $|k|/|B|$ as a functon of λ for the guide with the perturbation used in figure 4.12. From this we can see that the power loss by reflection $\sim 1.5 \times 10^{-2}$ dB and the noise owing to the subsequent transmitted pulses $\sim 3.0 \times 10^{-5}$ dB, independently of the length of the guide, at $\lambda = 1.55\mu$m. This may be compared with the material loss of silica at this wavelength which is about 0.2dB/km at present. Thus it is possible to make the dispersion at a given point zero and still remain sufficiently far from the stop band (about 100 bandwidths away from the band edge in this case) for the reflective nature of the structure to have a negligible effect on the amount of power transmitted.

Figure 4.14 shows how d^2s/dw^2 varies with λ for various different values for the amplitude of the perturbation. In each case the pitch has been chosen so that the zero of d^2s/dw^2 occurs at 1.55μm (Table 4.1). For comparison, $d^2\beta/dw^2$ is also shown. Clearly, as the perturbation amplitude is increased, the zero dispersion point moves away from the band edge. Since the operating frequency lies below the reflection band and we wish to work at a fixed frequency, the required pitch becomes smaller as the perturbation amplitude is increased.

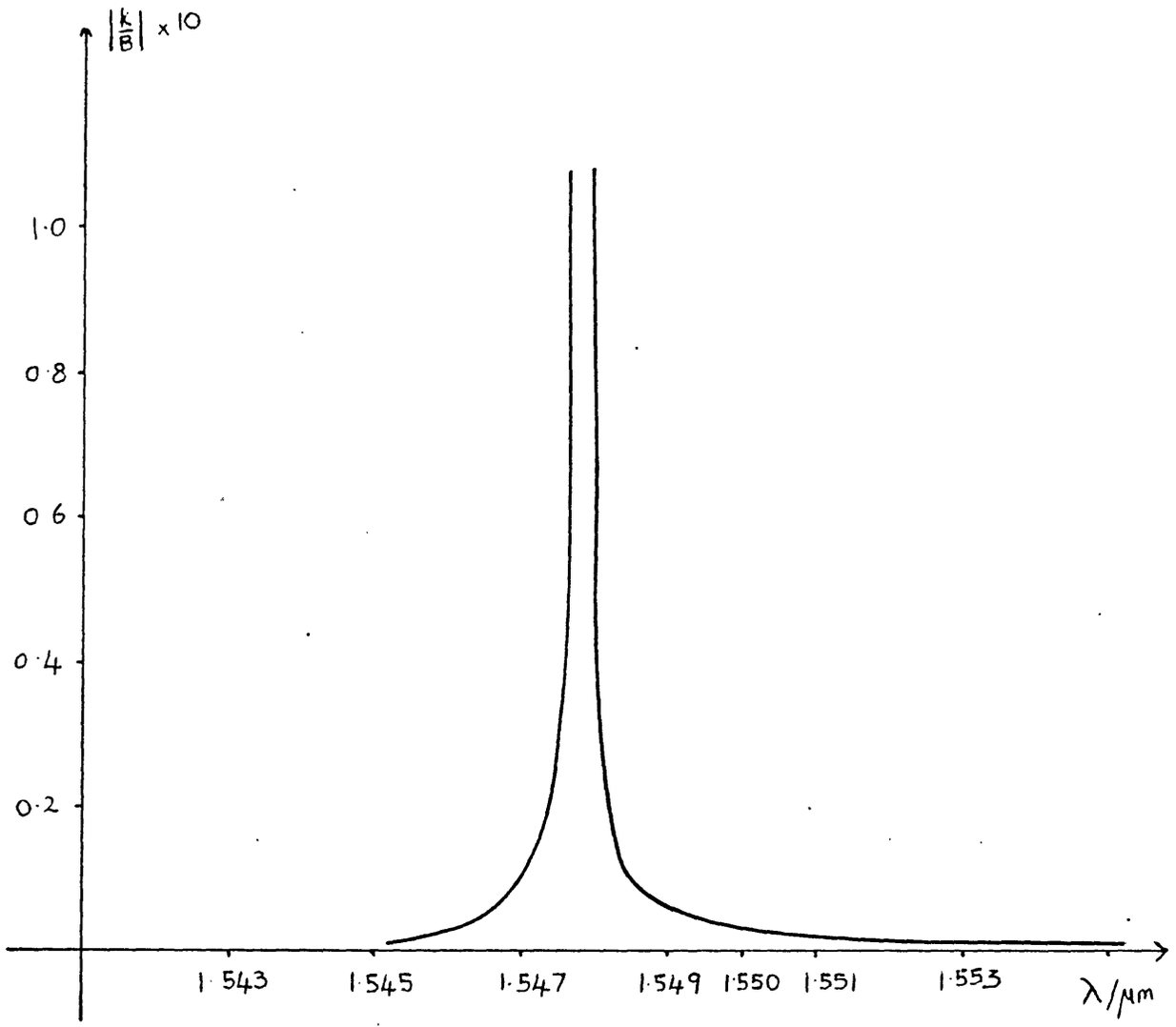

Figure 4.13 Variation of |k|/|B| with wavelength λ

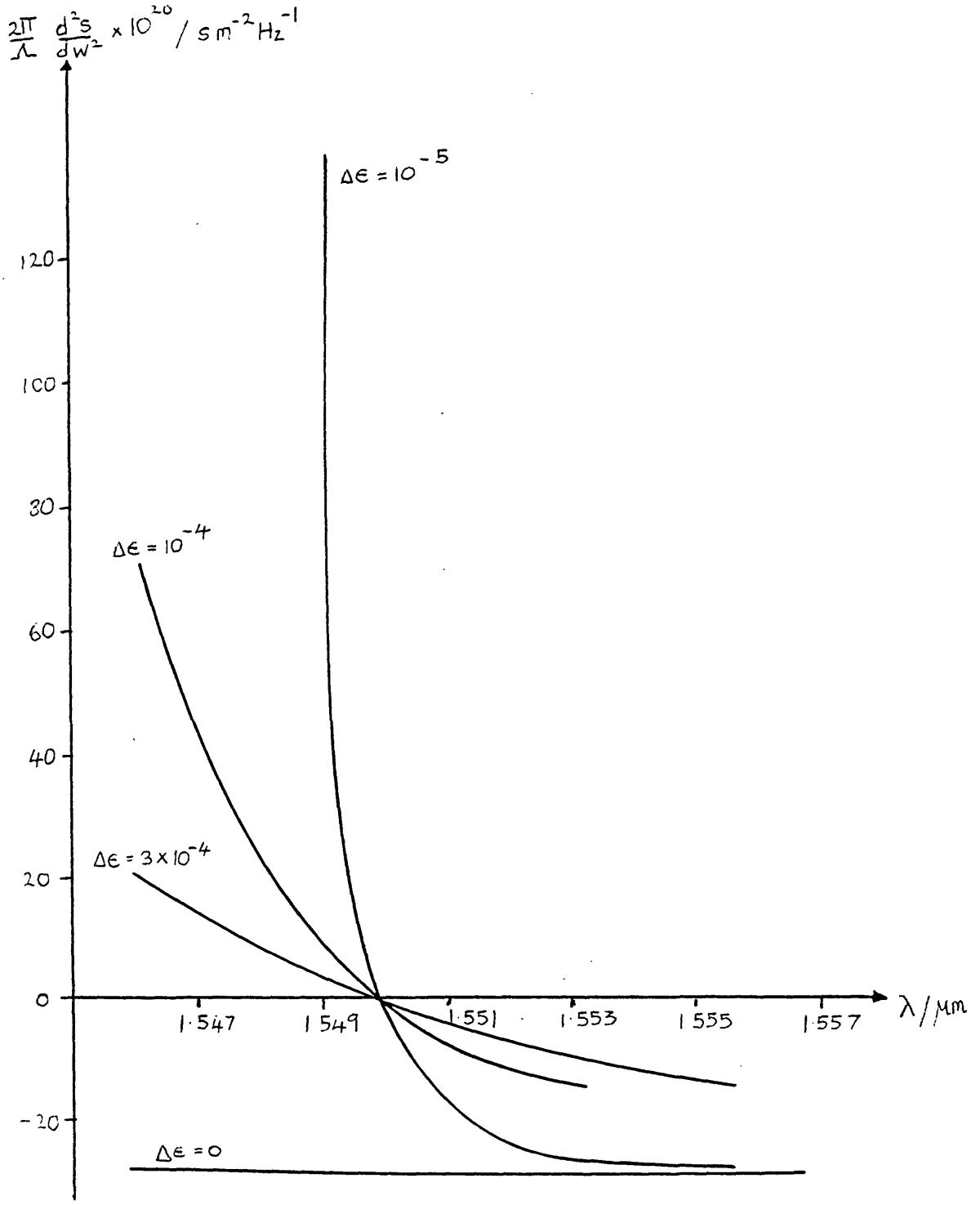

Figure 4.14 Variation of d^2s/dw^2 with wavelength λ for various perturbation amplitudes $\Delta\epsilon$

Table 4.1

$\Delta\epsilon$	grating pitch/μm	dispersion at 1.55 for full width 1 nm	B/|k|	Wavelength tolerance for dispersion < 8 ps/km for full width 1 nm
10^{-5}	0.5296	2.0	-380	0.05 %
10^{-4}	0.5265	0.7	-152	0.18 %
3×10^{-4}	0.5223	0.3	-110	0.40 %
0		17.5		-

It should be noted that if the zero dispersion point is to be introduced in a region of positive dispersion, then the operating point will be at a frequency above the reflection band. In this case the grating may cause coupling to the radiation modes and, if the perturbation is large enough, the resulting radiation losses are likely to be unacceptably high. However when $d^2\beta/dw^2$ is negative, as for lightly doped silica at 1.55μm, this problem does not arise.

A noticeable feature of figure 4.14 is the rapid variation of d^2s/dw^2 with λ compared to that of $d^2\beta/dw^2$. In order to determine the significance of this variation, we consider approximately (Table 1) the effect of the spectral width of the signal at the zero dispersion wavelength. From this we see that the effect of the third derivative on the dispersion is likely to be small (and varies as $(d\lambda)^2$) and that the presence of the perturbation does result in a fairly significant reduction in the dispersion. These values of dispersion may be compared with those of other dispersion shifted waveguides, for example 1.5 ps/(km nm) for a quadruply clad fibre (but this is additionally attained throughout the wavelength range 1.3 to 1.6 μm) [14] and only 0.05 ps/(km nm^2) for a triangular profile fibre [85].

The main consequence of the rapid variation appears to be that it introduces severe constraints on the fabrication tolerances. These are relaxed as the amplitude of the perturbation is increased. However this in turn means that a guide of higher Δn must be used, so that the core size may have to be made smaller in order to keep the guide single-moded, thus reducing the advantages of using a periodic structure.

4.7 Conclusions

The transmitted pulse of a periodically perturbed waveguide may be considered as the sum of terms , the nth one of which is composed of that part of the field which has travelled at least 2n-1 lengths and less than 2n+1 lengths of the guide. These terms all have similar signal velocities and velocity dispersions. Similarly the reflected pulse can be considered to be composed of terms which have travelled at least 2n-2, and less than 2n, lengths of the guide. The successive contributions have decreasing amplitudes and in general may overlap in time and interfere. Relatively simple formulae for these terms may be obtained. The actual signal is the sum of these components and so its shape as a function of time can be determined, but its dispersion cannot be simply directly related to those of these constituent terms.

However, in certain cases, only one term may make a significant contribution and then the dispersion may be straightforwardly obtained. In particular the dispersion of the transmitted pulse for a small perturbation and a carrier frequency well outside the reflection band may be simply expressed. This is similarly true of the dispersion of a reflected pulse subjected to a large perturbation with a carrier frequency near the centre of the reflection band. In both these cases the dispersion is small and varies monotonically as the carrier frequency moves away from the band edge.

For frequencies near the band edge the medium is highly dispersive. The signal velocities of the component terms lose their meaning, as all the terms interfere significantly, but

formally tend to zero here.

Thus it appears that the dispersion characteristics of the periodic medium are strongly influenced by both the distributed nature of the reflection and the finite nature of the device. The dispersion effects are significantly more complicated than those in a typical uniform dispersive dielectric.

However the effect of the periodicity on the dispersion curve is large compared with that of the waveguide and material dispersions. Thus even far away from the reflection band, where all terms except the first transmitted pulse are negligibly small, it can cause the dispersion to change from some relatively large value (for example 15 - 20 ps/(km nm)) to zero. The third order dispersion must be considered here and in fact it is relatively large. It does not nullify the improvement gained by the zero second-order dispersion. A typical value of the dispersion which might be achieved is 2 ps/(km nm^2). However it suggests that the structure may need to be fabricated to great accuracy (less than about 0.1% error in the pitch of the perturbation) if it is to operate as predicted theoretically .

APPENDIX TO CHAPTER 4

We will use the method of steepest descent [91], [92] to evaluate approximately an integral of the form

$$I = E_o \int_{-i\Gamma - \infty}^{-i\Gamma + \infty} \frac{\exp(F(w))}{2\pi i(w-w_o)}\, dw \qquad (A4.1)$$

where $F(w) = iwt - im_3sL + m_1\ln(B-s) - m_2\ln(B+s)$ (A4.2)

and the complex plane has branch cuts as shown in figure A4.1. We use the notation and assumptions described in section 4.3

(i) The integration contour (figure A4.1)

We first note that

if $t < m_3nL/c$ then $Re(F) < 0$ on $\hat{C}'$

where $\hat{C}'$ is a semi-circle at infinity in the lower half w-plane.

Therefore in this case, we can close the contour of integration along $\hat{C}'$ to give, since the integrand is analytic for all $Im(w) < \Gamma$

$I = 0$ for $t < m_3nL/c$

However

if $t > m_3nL/c$ then $Re(F) < 0$ on $\hat{C}$

where $\hat{C}$ is a semi-circle at infinity in $Im(w) > \Gamma$

the integrand has a pole and branch cuts in $Im(w) > \Gamma$. In order to evalulate the integral the path of integration is deformed in accordance with the method of steepest descent to path $\hat{B}$. Thus the integration path starts on $\hat{C}$ at $Im(w) = \Gamma$, then passes along $\hat{C}$

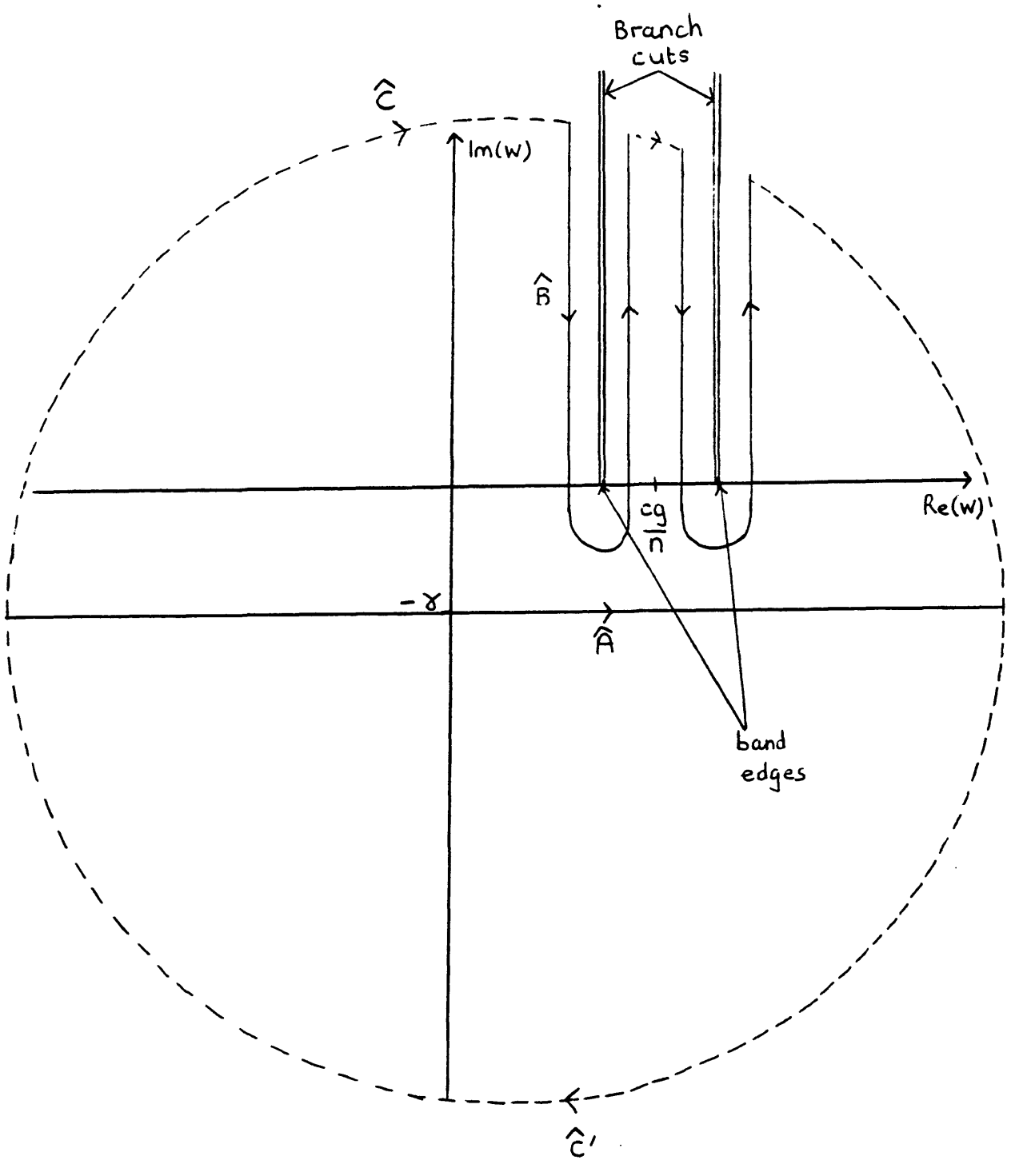

Figure A4.1 w-plane showing branch cuts and integration contours

until this intersects with the lines of steepest descent of F, that is, the contours

$$\mathrm{Im}(F) = \text{constant} \qquad \text{(A4.3)}$$

which pass through the saddle points of F, the points w for which

$$dF/dw = 0 \qquad \text{(A4.4)}$$

From here $\hat{B}$ avoids the branch cuts by passing along these steepest descent lines (see below) and then completes the path to the end point along $\hat{C}$. When a pole of the integrand lies in the region between the original contour $\hat{A}$ and $\hat{B}$, $\hat{B}$ must be further deformed to pass around it.

The integrand vanishes on $\hat{C}$. The steepest descent lines are those along which Re(F) varies most rapidly. Thus by integrating along these lines it may be assumed that the dominant contribution from this part of the integration contour comes from the vicinity of the saddle points (where Re(F) has a local maximum for w varying along one steepest descent line).

(ii) <u>The Saddle Points</u>

From (A4.2), (A4.4) there are two saddle points given by (in the notation of section 4.4)

$$B = |k|d\,(-i \pm Te)/\gamma^2 \qquad \text{(A4.5)}$$

The time dependent variable T appears as a parameter in (A4.5) and so the saddle points and path of integration change with time. The motion of the saddle points is as follows

For $\gamma = 0$ the saddle points are at

$$B = -i\infty \quad , \quad B = i\,d\,|k|(1 - d^2)/2$$

For $0 < \gamma^2 < d^2$ they move towards each other along the line

$$Re(B) = 0$$

meeting at

$$B = -i|k|d/\gamma^2 \quad \text{at time } \gamma = d$$

For $^2 > d^2$ they move apart along the line

$$Im(B) = -i|k|d/\gamma^2$$

and as T tends to infinite they tend to the band edges $B = \pm |k|$. The exception to this type of saddle point motion occurs when $m = 0$. Then the saddle points are on the real axis and outside the stop band always. They start at $\pm\infty$ and tend to the band edges as T tends to infinite.

We will find that the results we obtain do not hold for $\gamma^2 = 0$ and $\gamma^2 = d^2$. At the latter time $F'' = 0$ and so F has a higher order saddle point. The solution for $\gamma^2 = 0$ may be determined as in reference [91]. At other times the solution is valid. In general, at the saddle points,

$$s = |k|d\ (\ -iT \pm e)/\gamma^2 \qquad \text{(A4.6)}$$

$$\frac{d^2F}{dw^2} = \pm \frac{n^2 i m_4}{c^2} \frac{ed^2}{|k|^2} \frac{(\ iT \pm e)^2}{(1 + d^2\ )^2} \qquad \text{(A4.7)}$$

(iii) The lines of steepest descent through the saddle points

The lines of steepest descent through the saddle points are, from (A4.2), (A4.3), the lines defined by

$$w_r t - m_3 aL + m_1 q_1 - m_2 q_2 - K^{\pm} = 0$$

where $w = w_r + iw_i$

$s = a + ib$

q_1 = argument of $(B - s)$

q_2 = argument of (B + s)

and the superscripts +, - on K refer to the two saddle points defined by the +, - signs (the + and - saddle points) respectively in (A4.5).

These steepest descent lines can be re-written

$$\mathrm{Re}(B)T - a + \frac{(m_1 q_1 - m_2 q_2)}{m_3 L} - Q^{\pm} = 0 \qquad \text{(A4.8)}$$

for $Q^{\pm} = (K^{\pm} + gT)/m_3 L$

From B and s at the saddle points (A4.5), (A4.6) and (A4.8), we can solve for $Q^{\pm}$ to obtain

For $\gamma^2 < d^2$

$$Q^{\pm} = |k| d\pi/2 \qquad \text{(A4.9)}$$

For $\gamma^2 > d^2$

$$Q^{+} = |k| d(e + \arctan(1/e)) \qquad \text{(A4.10)}$$

$$Q^{-} = |k| d(-e + \pi - \arctan(1/e))$$

The points at which the steepest descent lines intersect the real axis are obtained by setting $w_i = 0$ in (A4.8). In general these points may occur inside and outside the stop band. It is convenient to consider these cases separately. (Here $Q = Q^{\pm}$)

(a) $B > |k|$

$$B = (TQ \pm \sqrt{Q^2 - \gamma^2 |k|^2})/\gamma^2 \qquad \text{(A4.11)}$$

(b) $-|k| < B < |k|$

B is the solution to the transcendental equation

$$BT + \frac{m_4}{m_3 L} \arctan \left(\sqrt{\frac{|k|^2 - B^2}{B}} \right) = Q \qquad \text{(A4.12)}$$

(c) $B < -|k|$

$$B = \frac{T(Q + M) \pm \sqrt{(Q + M)^2 - \gamma^2|k|^2}}{\gamma^2} \qquad (A4.13)$$

where $M = \pi(m_1 - m_2)/(m_3 L)$

(iv) Gradients of the steepest descent lines in the vicinity of the saddle points.

If $F = F_r + iF_i$ then along the line F_i = constant, (about a saddle point w_s),

$$F_i(w_s+dw_r) = F_i(w_s) + \frac{dF_i}{dw_r}\delta w_r + \frac{d^2F_i}{dw_r^2}\frac{(\delta w_r)^2}{2} + \ldots \qquad (A4.14)$$

$$= F_i(w_s)$$

At a saddle point, $dF_i/dw_r = 0$, and so the gradient at the saddle point along the line of steepest descent is the gradient of the direction in which $d^2F_i/dw_r^2 = 0$ there. Therefore, expressing d^2F_i/dw_r^2 in terms of partial derivatives, the required value of the gradient is

$$d_o = \frac{dw_i}{dw_r} = \frac{-(F_i)w_r w_i \pm \sqrt{((F_i)w_i w_r)^2 - (F_i)w_r w_r\,(F_i)w_i w_i}}{(F_i)w_i w_i} \qquad (A4.15)$$

where $(F_i)xy = \frac{d^2F_i}{dxdy}(w_s)$

This gives the gradients of the two steepest descent lines passing through the saddle point w_s.

For any general analytic function F (where ' denotes differentiation with respect to w)

$$(F_i)w_i w_r = \mathrm{Re}(F'')$$

$$(F_i)w_r w_r = \mathrm{Im}(F'') = -(F_i)w_i w_i$$

Therefore from (A4.7), the two gradients are given by

(a) $\gamma^2 < d^2$

$$d_o = -\,\mathrm{sign}((F_i)w_r w_i \times \infty \qquad \text{(A4.16)}$$

$$d_o = 0$$

(b) $\gamma^2 > d^2$

$$d_o = \mp \frac{(e \pm T)^2}{e^2 - T^2} \qquad \text{at the + saddle point}$$

(A4.17)

$$d_o = \pm \frac{(e \pm T)^2}{e^2 - T^2} \qquad \text{at the - saddle point}$$

(v) Directions of decreasing F_r along steepest descent lines

It is necessary to determine along which of the two lines of steepest descent through each saddle point F_r is decreasing away from the saddle point, since it is this line which must be chosen as part of the integration contour.

At the saddle points,

(a) $\gamma^2 < d^2$

$$\frac{d^2 F_r}{dw_r^2} = F'' \qquad \text{when } d_o = 0$$

(A4.18)

$$\frac{d^2 F_r}{dw_r^2} = -F'' \qquad \text{when } d_o = +\infty$$

The integration path will be deformed to a steepest descent line

with $d_o = 0$ (see below and figure A4.2). From (A4.7), when $\gamma^2 < d^2$,

$$F''(w_s^{\pm}) = \pm \text{ (positive number)}$$

therefore the contour must run along the path through the lower of the two saddle points.

(b) $\gamma^2 > d^2$

$$\frac{d^2F_r}{dw_r^2} = \frac{-2d_o\,|F''|^2}{\mathrm{Im}(F'')} \qquad \text{(A4.19)}$$

and $$\frac{d_o}{\mathrm{Im}(F'')} = \mp \frac{(e-T)^2}{(e^2-T^2)^2} \times \text{positive number}$$

Therefore at both the saddle points the steepest descent line along which F decreases corresponds to the lower sign. From (A4.17) the relevant gradients have opposite signs at the two saddle points.

Using the results of (iii), (iv), (v) and the limiting case of $m_1 = m_2 = 0$ (for which the steepest descent lines have rational equations), the relevant characterstics of the steepest descent lines can be determined. These are shown in figure A4.2 (with arrows pointing in the direction of increasing F_r) together with the resulting path of integration.

(vi) The signal velocity

When the contour $\hat{A}$ is deformed to either of those marked $\hat{A}'$ in figure A4.2, the contribution of a pole lying on the real axis at $B = B_o$ must be included when the points where the new contour

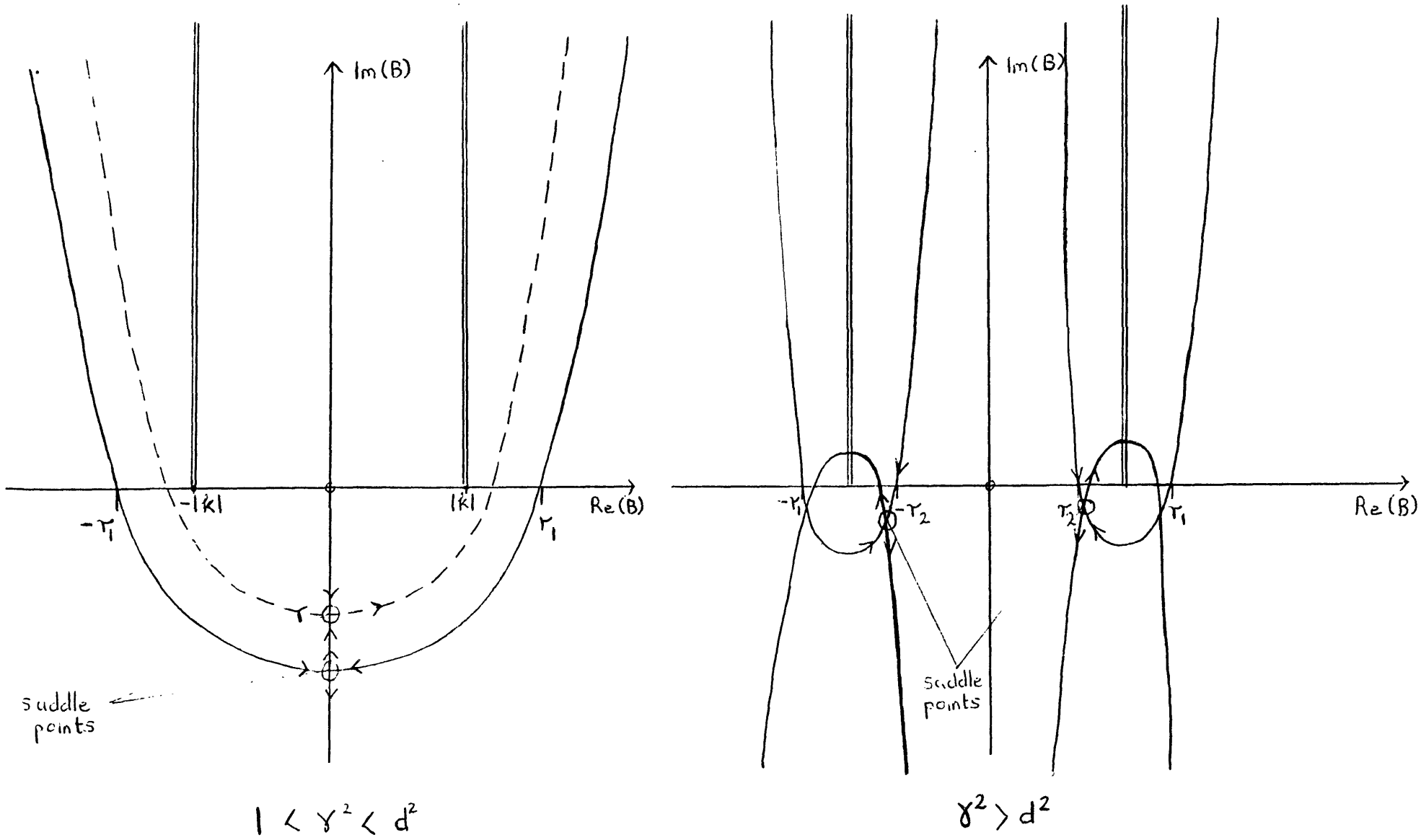

Figure A4.2 Lines of Steepest Descent

intersects the real axis $\pm r_1$, $\pm r_2$ are such that

(a) $|r_1| < |B_o|$ if $B_o > |k|$

(b) $|r_2| > |B_o|$ if $B_o < |k|$

The time at which $|r_1| = |B|$ or $|r_2| = |B|$, whichever is appropriate, may be defined, by analogy with the lossless case [91], as the arrival time of the signal. This leads to the definitions of T_o in equations (4.25), (4.26), (4.27) directly from (A4.11), (A4.12), (A4.13). From this time onwards, the contribution to the integral from the part of the contour encircling the pole must be included. This contribution is obtained very straightforwardly from Cauchy's theorem and is

$$I_p = E_o \exp(F(w_o))$$

(vii) The saddle point contribution

The saddle point contribution, I_s, to the integral is obtained in the usual way by approximating the exponential function to a Gaussian and replacing the integration contour by the tangent to the steepest descent line at the saddle point. The change of path is justified by the assumption that the contributions to both the original and the approximate integral are negligible except near the saddle point, where they coincide.

Thus

$$I_s = E_o \int_{-\infty}^{\infty} \frac{\exp(F(w_s))}{2\pi i} \frac{(1 + id_o)}{(w_s - w_o)} \, dw_r \exp(-K^2(w_{sr}-w_r)^2/2)$$

where $w_s = w_{sr} + iw_{si}$ is the saddle point

$$K^2 = d^2F_r(w_s)/dw_r^2$$

so

$$I_s = \frac{E_o \exp(F(w_s)) (d_o - i)}{(w_s - w_o)\sqrt{2\pi}K}$$

and K, d_o are obtained from (A4.7), (A4.16), (A4.17), (A4.18), (A4.19) to give (4.21), (4.22).

(viii) Limits to the validity of the calculation

The above approximate evaluation of the saddle point contribution ceases to be valid when

(a) $|w - w_o|$ becomes small on the integration contour.

At these times $1/(w - w_o)$ is not slowly varying along the path of integration near the saddle point and so this term cannot be taken as constant for the integration. In order to correct for this, the integration contour may be deformed around the pole as it approaches the pole and so, strictly speaking, this contribution should be added to the integral [91]. This makes I_p continuous.

(b) K tends to zero. At these times the integrand does not become negligible for values of w away from w_s (since the exponential term is not rapidly decreasing for increasing $w - w_s$) and so the change of integration path is not justified. In addition, the approximation of the exponential to a Gaussian form may be invalid if third and higher derivatives of F_r are large enough. From (4.21), (4.22), K becomes small when

$$T \approx 1 \qquad \text{(A4.20)}$$

$$\aleph^2 \approx d^2$$

$$|k|L \text{ is small}$$

In order to determine the range of values of $|k|L$ for which the calculation is valid, we need to calculate

$$\left| \frac{d^2 F_r}{dw_r^2} \frac{(\delta w_r)^2}{2} \right|$$

We will assume that

$$nw_o/c \gg |B|$$

$$dw_r/w_o = 100$$

$$nw_o/c > 400|k| \qquad \text{(in practise } nw_o/c \sim 10^4\ |k|\ )$$

Table A4.1 shows required resulting minimum values for $|k|L$ for various values of T, m_3, m_4

At the times described in (a) and (b) (A4.20), it is most convenient to determine the saddle point contribution graphically by continuity, as illustrated in figure A4.3.

T	m_4 =0	m_4 =1	m_4 =2	m_4 =3
1.1	1.1	3.1	17.0	19.3
2.1	0.2	0.9	1.4	1.9
3.1	0.1	0.5	0.8	1.2
4.1	0.05	0.4	0.6	0.9
5.1	0.02	0.3	0.5	0.7

Table A4.1 Minimum values required for k L for the first few transmitted terms (m_3 = 1 and m_3 = 3 for the corresponding m_4)

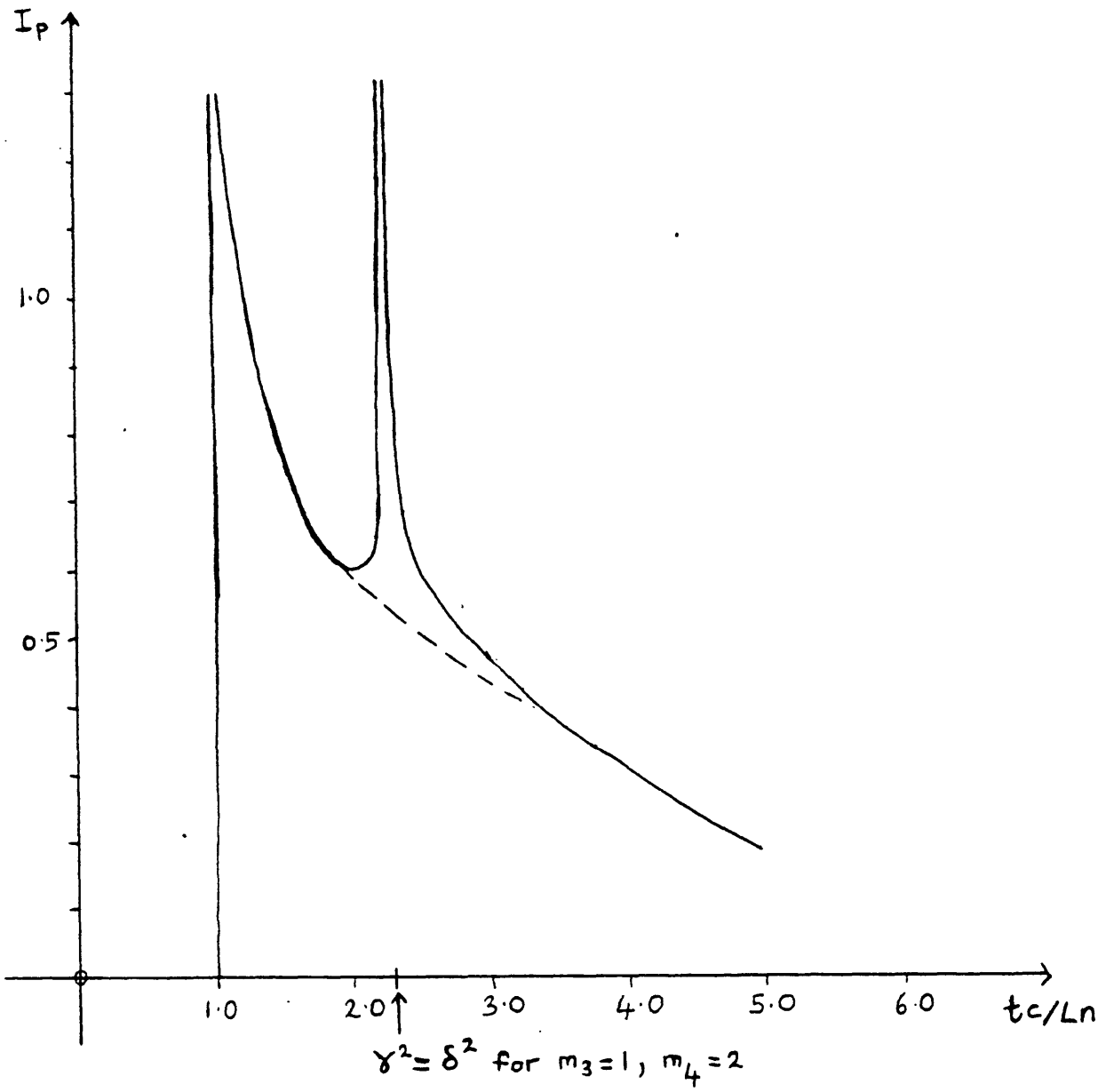

Figure A4.3 Example of how the saddle point contribution may be obtained by continuity at times when the formulae become singular.

——— I_p from formulae

- - - - - - I_p assuming continuity

5. WAVE PROPAGATION IN A DOUBLY PERIODIC GUIDE

5.1 Introduction

A waveguide with more than one periodic perturbation of its refractive index may be described as a multiply periodic guide (figure 5.1). Clearly such a index variation can also be considered as one periodic perturbation of a longer pitch. However, in this case, the amplitudes of the harmonics of the perturbation will not, in general, be decreasing with increasing order, and may affect the propagation at frequencies significantly different from their resonance (maximum reflection) frequencies. This is not so for the perturbation which results from the generally considered small amplitude single periodic variation.

Monochromatic wave propagation in the presence of a single periodic perturbation has been analysed extensively, in particular for unbounded or semi-infinite media [2], [34], [93], [94], [95]. The two methods most commonly employed for this are a Bloch wave expansion and Coupled Mode theory. For infinite media these approaches are very similar and the amplitudes of the coupled waves in the two cases are related directly by Fourier transformation or, for finite truncations, simply by a re-grouping of the modes in the expressions for the fields [96]. In general higher order modes are included in the analysis, but these have only a small effect away from their resonance frequency as long as only one perturbation is considered. Thus the finite set of components which must be retained in the analysis is usually clear from physical considerations. These analyses have led to the well known descriptions of the multiple reflection and

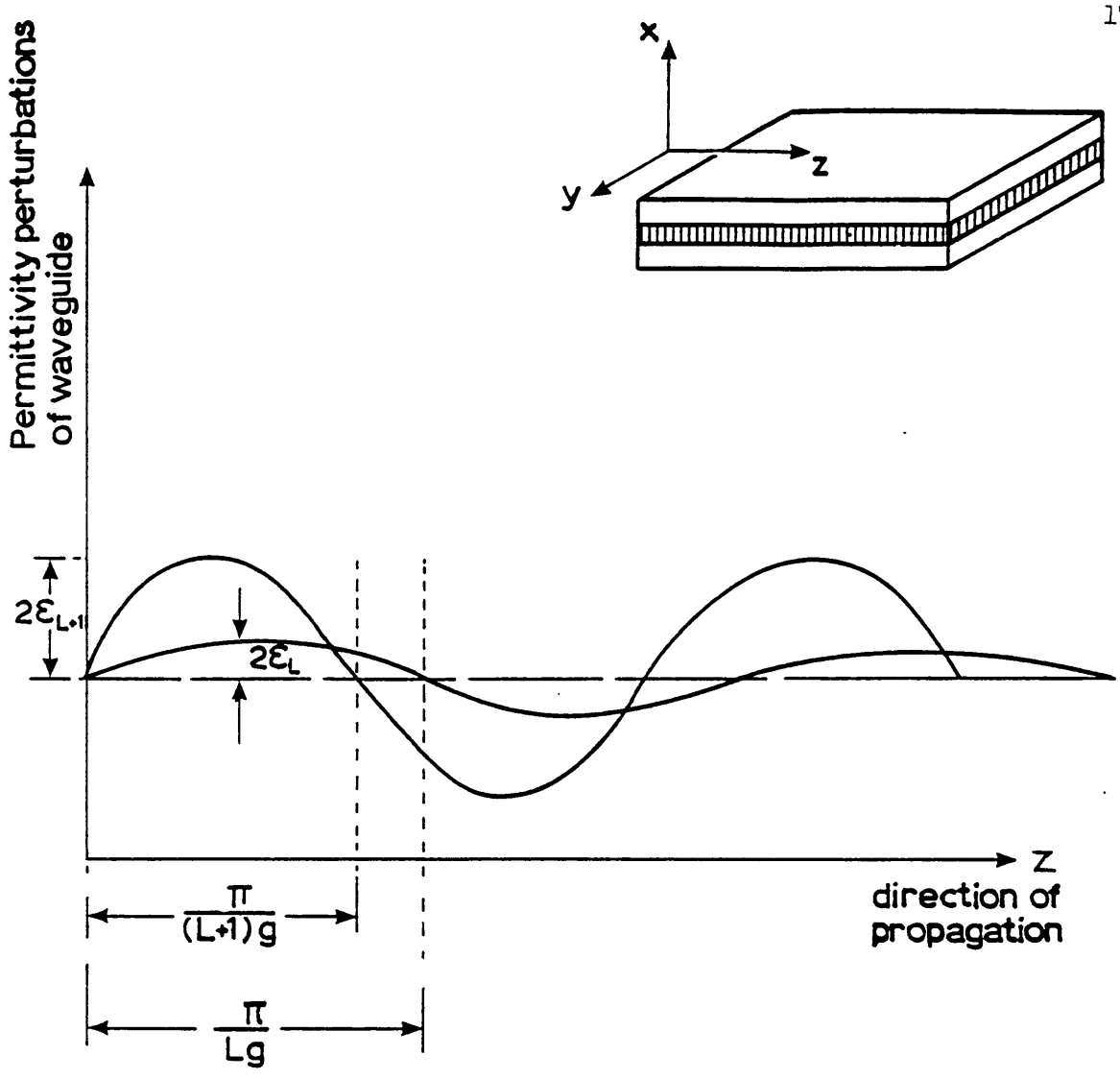

Figure 5.1 Doubly periodic perturbation

transmission bands. It has been shown that there is a weak interaction between the harmonic components which results in "phase-speeding", that is, the occurence of the stop band at a frequency slightly greater than that predicted by the lowest order two-wave approximation [96]. Stronger anomalous interactions have been observed in perfectly conduction gratings, such as Wood's anomalies and the excitation of surface plasmons [97].

A case closer to that of a multiply periodic structure is that of a modulated infinite periodic medium. Such a perturbation has been expressed as the sum of closely spaced harmonics [98] and has been analysed using coupled mode theory. The reflectivity has been obtained from an approximate form of the Riccati equation which is accurate for small perturbations. Only weak inter-harmonic interaction has been considered. It has been shown that for a suitable modulation, the maxima of the side lobes of the reflection band are reduced and the bandwidth of the main lobe is increased.

The multiple harmonics in a periodic waveguide have not been investigated so widely. The Bloch wave approach has been used to analyse unguided and radiation modes in transversely bounded general periodic media [99], [100]. This method has also been used to determine the characteristics of a general periodic dielectric guide [37], again with essentially one perturbation giving rise to the multiple harmonics. In this latter case the (truncated) infinite determinant must first be used to obtain the set of possible transverse dependences (which are coupled together by the periodicity) and then the boundary conditions must be applied to determine the propagation constant. This differs from the case of an infinte medium where the only parameter to be determined is the

propagation constant. Thus the use of the Bloch wave formalism for guided modes requires numerical solution of a complicated transcendental equation.

In contrast, the coupled mode theory for a waveguide is very similar to that for an infinite medium, except that now the unperturbed modes do not relate directly to the Floquet-Bloch case. The only unknown parameter is the propagation constant as the transverse boundary conditions have already been applied to obtain the unperturbed modes. Coupled mode theory has been applied to almost periodic waveguiding structres [101], [102]. These have perturbations which have continuous variations of amplitude or pitch (tapers or chirps respectively) and so cannot be treated as a sum of periodic components.

In this chapter we will use a simple general coupled mode approach in order to determine the characteristics of propagation in a multiply periodic guide in which there is significant interaction between the harmonics.

Previously there has been some interest in multiply periodic waveguides [1] and their analysis using the method of multiple scales [103], [104]. Coupling from one forward guided mode to two backward guided modes via two suitable periodic index variations has been considered. It has been shown that for suitable perturbation amplitudes the three-mode coupling device has, perhaps not surprisingly, lower transmission than a singly periodic two-mode coupling one. However the method of multiple scales [105] requires that more terms must be included as the length of the device is increased, which is a rather undesirable feature.

The singly periodic waveguide has an important use as a narrow

frequency band reflection filter [23]. Because of the interactions which occur in a multiply periodic structure, this device may have potential applications for filtering also. For example, for frequencies in the vicinity of the resonance frequency of a large amplitude perturbation, but outside the stop band, the group velocity is significantly reduced. Thus if another perturbation is imposed with a stop band in this region, it is conceivable that the slow variation of frequency with wavenumber would lead to its having a very narrow frequency bandwidth of reflection. In terms of mode-coupling the bandwidth can be considered to decrease with increasing angle between the two coupled mode dispersion curves (figure 5.2). However the advantage of reducing the group velocity must be balanced against the corresponding increase in reflection.

Using the generalised coupled mode theory described in the following section, 5.2, we determine in this chapter the propagation characteristics for a doubly periodic waveguide. Sections 5.3 and 5.4 are concerned with obtaining the propagation constant and reflection coefficient. Section 5.5 contains a numerical evaluation of these parameters for a suitable guide.

5.2 Generalised Coupled Mode theory

We consider the electric field of the TE mode of a slab waveguide lying in the y-z plane, with propagation in the z-direction. The periodic perturbation is in the z-direction and all quantities are independent of y. The coupled mode equations are derived by

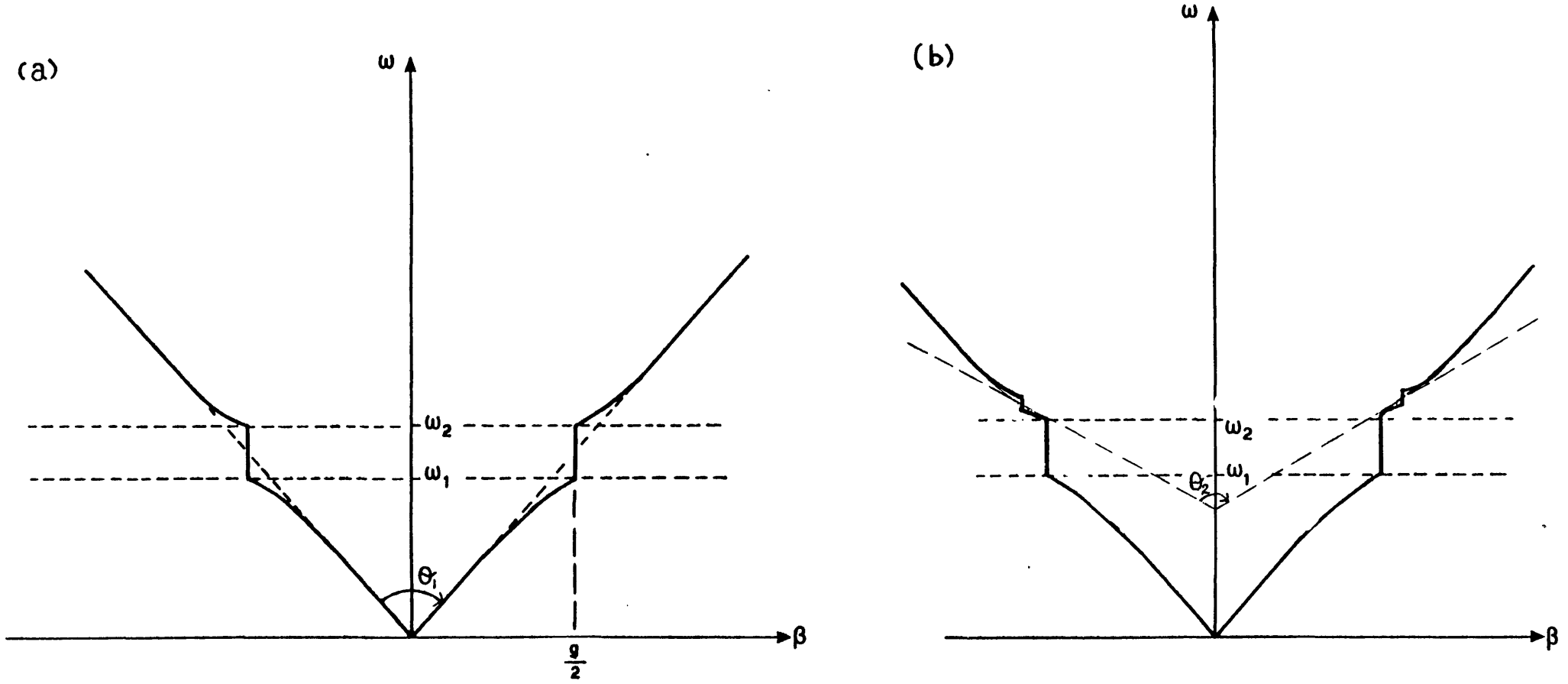

Figure 5.2 Schematic dispersion curves for (a) singly and (b) doubly periodic perturbations, $\theta_2 > \theta_1$

expressing the electric field as a z-dependent superposition of the modes of a uniform guide. That is, if the uniform guide has guided modes $E_m(x)\exp(+i\beta_m z)$ and radiation modes $E(\gamma,x)\exp(+i\beta_\gamma z)$ then the electric field of the perturbed guide is [31], [40]

$$\begin{aligned} E_y &= E\exp(iwt) \\ &= \exp(iwt)\Big[\sum_m \big(A_m^+(z)\exp(-i\beta_m z) + A_m^-(z)\exp(i\beta_m z)\big) E_m(x) \\ &\qquad + \int d\gamma \big(A^+(\gamma,z)\exp(-i\beta_\gamma z) + A^-(\gamma,z)\exp(i\beta_\gamma z)\big) E(\gamma,z)\Big] \end{aligned} \tag{5.1}$$

This infinite sum over all modes is exact and so holds for arbitrarily large perturbations, though any finite approximation must have a limit to its validity. An expression for each mode amplitude is obtained by requiring that E must satisfy the wave equation, that the normal modes satisfy the unperturbed wave equation and by using the orthogonality of the normal modes. This gives, for a perturbation to the permittivity of $\Delta\epsilon$, [31], [40]

$$\Big(\frac{d^2A_n^+}{dz^2} - 2i\beta_n\frac{dA_n^+}{dz} + \exp(2i\beta_n z)\Big(\frac{d^2A_n^-}{dz^2} + 2i\beta_n\frac{dA_n^-}{dz}\Big)\Big) \langle E_n|E_n\rangle +$$

$$w^2\mu \Big(\sum_m + \int d\gamma\Big)\exp(i\beta_n z)\, \langle E_n|\Delta\epsilon|E_m\rangle (A_m^+\exp(-i\beta_m z) + A_m^-\exp(i\beta_m z)) = 0 \tag{5.2}$$

where $\langle E_n|\Delta\epsilon|E_m\rangle = \int E_n(x)\, \Delta\epsilon(x,z)\, E_m(x)dx$

$\langle E_n|E_n\rangle = \langle E_n|\, 1\, |E_n\rangle$

Here and below we use the symbol $\big(\sum_m + \int d\gamma\big)$ to indicate a sum over all guided modes and an integration over all radiation modes. We will also use the suffix m to refer to either a guided or a

radiation mode in this section.

Applying equation (5.2) to each mode in turn yields the set of coupled mode equations. Since the forward and backward propagating modes with the same β_m are not orthogonal, we can define $A_m^+(z)$, $A_m^-(z)$ for each mode to be such that $A_m^+(z)\exp(-i\beta_m z)$ and $A_m^-(z)\exp(i\beta_m z)$ are forward and backward going waves respectively. Then writing

$$A_m^+(z) = \int p_m^+(k)\, \exp(-ikz)\, dk$$
$$A_m^-(z) = \int p_m^-(k)\, \exp(-ikz)\, dk$$

we can assume that

$$p_m^+(k) = 0 \qquad \text{for } k < -\beta_m$$
$$p_m^-(k) = 0 \qquad \text{for } k > \beta_m \tag{5.3}$$

If we take the wave number of the periodicity to be $g = 2\pi/\Lambda$ and write

$$\Delta\epsilon = \sum_{l\neq 0} \epsilon_l(x)\, \exp(-ilgz)$$

then Fourier transforming equation (5.2) gives

$$p_n^+(k) + p_n^-(k + 2\beta_n) = \frac{w^2\mu \left(\sum_m + \int d\gamma\right) \langle E_n|\epsilon_l|E_m\rangle \left\{p_m^+(k+\beta_n-\beta_m-lg) + p_m^-(k+\beta_n+\beta_m-lg)\right\}}{\langle E_n|E_n\rangle k(k+2\beta_n)} \tag{5.4}$$

The right hand side of (5.4) is large when $k \approx 0$ or $k \approx -2\beta_n$. When $k \approx 0$, $p_n^-(k + 2\beta_n) = 0$ from (5.3) and so

$$p_n^+(k) \approx \frac{w^2\mu \left(\sum_m + \int d\gamma\right) \langle E_n|\epsilon_l|E_m\rangle \left\{p_m^+(k+\beta_n-\beta_m-lg) + p_m^-(k+\beta_n+\beta_m-lg)\right\}}{\langle E_n|E_n\rangle k(k+2\beta_n)} \tag{5.5}$$

Similarly when $k \approx -2\beta_n$, $p_n^+(k) = 0$ from (5.3). Writing $k=k'-2\beta_n$,

$$p_n(k') \approx \frac{w^2\mu \quad (\sum_m + \int d\gamma) \quad \langle E_n|\epsilon_1|E_m\rangle\{p_m^+(k'-\beta_n-\beta_m-1g) + p_m^-(k'-\beta_n+\beta_m-1g)\}}{\langle E_n|E_n\rangle k'(k'-2\beta_n)} \tag{5.6}$$

Therefore each Fourier component is large only when the modulus of its argument is small. Thus for example, the only terms which make a significant contribution to the right hand side of (5.4) are those with m and 1 such that

$$k + \beta_m + \beta_n - 1g = 0 \quad \text{or} \quad k + \beta_n - \beta_m - 1g = 0 \tag{5.7}$$

Expressions for these coupled components can in turn be obtained using (5.5) and (5.6) and so on. Equation (5.7) is the familiar phase-matching or resonance condition for coupling between modes by a sinusoidal index variation.

Coupling to several modes, large amplitude perturbations and similar quite complicated problems may be treated by considering the relatively simple simultaneous linear homogeneous equations obtained by retaining only the terms which are large and coupled together from (5.5) and (5.6). A non-trivial solution may be obtained in the usual way by requiring that the determinant of the matrix of coefficients M, say, is zero. In general M is sparse and may be arranged in a banded form, so that a simple iterative expression for its determinant may be derived, for example as in the next section.

Clearly in this form the coupled mode equations are very similar

to the Bloch wave expansion for a periodic guide [37]. However they have the important advantage that they yield an expression for the unknown k (which determines the fundamental propagation constant) directly from det(M) = 0.

5.3 Doubly periodic perturbation

We now apply the results of the previous section to the case of coupling to the backward mode in a single moded guide with two sinusoidal perturbations of the permittivity. The periodicities of the perturbations are taken to be Λ/L, $\Lambda/(L+1)$ for integer L, (so the pitch of the total perturbation is Λ). Therefore

$$\Delta\epsilon = \epsilon_L \exp(-iLgz) + \epsilon_{-L}\exp(iLgz) + \epsilon_{L+1}\exp(-i(L+1)gz) + \epsilon_{-L-1}\exp(i(L+1)gz)$$

When one of the perturbations is large enough, it will affect the propagation significantly even at frequencies rather different from its phase-matching frequency, and in particular at the phase-matching frequency of the other perturbation. At a given frequency w_o, $|2\beta(w_o) - Lg|$ is some fixed value, (where β is the propagation constant of the guided mode) and so if we choose

$$g < |2\beta - Lg| \, (\epsilon_{L+1}/\epsilon_L)^2$$

$$L > \frac{2\beta}{|2\beta - Lg|} (\epsilon_L/\epsilon_{L+1})^2$$

(for $|\epsilon_{L+1}|/|\epsilon_L| \gg 1$ and w_o of the order of a bandwidth from the band edge of the smaller perturbation say) then

$$|\epsilon_L|^2/|2\beta - Lg| \approx |\epsilon_{L+1}|^2/|2\beta - Lg - g| \qquad (5.8)$$

So if we make the two periodicities close enough, then from (5.5),

(5.6) the mode coupling resulting from ϵ_{L+1} is comparable to that resulting from ϵ_L. This in turn implies that components with arguments k+mg and k+2β-Lg+mg for small integers m may be non-negligible. The fact that these components may become significant is generally true when several periodicities are superimposed, thus increasing the pitch of the perturbation.

We will assume that

$$\beta-\beta_\gamma-Lg \;>>\; 2\beta-Lg\;(\epsilon_{L+1}/\epsilon_L)^2$$

for propagation constants β_γ of the radiation modes, so that coupling to the latter is negligible. That is, the perturbation does not cause the waveguide to radiate power in the range of wavelengths of interest here.

From (5.5), (5.6), (5.7), for small integers m,

$$p_1^+(k+mg) = -\frac{(\,C_L\,p_1^-(k+mg+d) + C_{L+1}\,p_1^-(k+mg+d-g)\,)}{(k+mg)(k+mg+2\beta)} \qquad (5.9)$$

$$p_1^-(k+d+mg) = -\frac{(\,C_{-L}\,p_1^+(k+mg) + C_{-L-1}\,p_1^+(k+mg+g)\,)}{(k+d+mg)(k+mg-Lg)} \qquad (5.10)$$

where $d = 2\beta - Lg$

$$C_L = \frac{-w^2\mu}{\langle E_1 \mid E_1\rangle}\langle E_1 \mid \epsilon_L \mid E_1\rangle$$

If we write

$$|\epsilon_L/\epsilon_{L+1}| = \eta << 1$$

then from (5.8)

$$|d|/|d+mg| \sim O(\eta^2)$$

Then for example since

$$O(p_1^+(k)) = O(C_L/(k\;(k+2\beta))),$$

$$p_1^-(k+d-g) = O(\eta^2)\ p_1^+(k-g) + O(\eta)\ p_1^+(k)$$

and so assuming $p_1^-(k-g) \sim 0\ \left(p_1^+(k)\right)$ (this latter assumption is clearly certainly justified physically)

$$p_1^-(k+d-g) \sim O(\eta) p_1^+(k)$$

In this way it is easy to show that a self consistent solution in terms of orders of magnitude is obtained by assuming that $p_1^-(k+d+mg)$, $p_1^+(k+mg)$ are non-increasing for increasing $|m|$ (this then implies they are decreasing) and that if terms of order greater than η^4 are neglected , the only significant terms are

$$p_1^+(k+mg),\quad p_1^-(k+2\beta-Lg-mg) \quad \text{for } m = 0,-1,+1,2 \qquad (5.11)$$

Therefore retaining the terms in (5.11) only and writing

$$D_m = (k+mg)(k+mg+2\beta) \qquad (5.12)$$

$$h_{1,m} = C_1/D_m$$

equations (5.9), (5.10) become

$$M \cdot P = 0 \qquad (5.13)$$

where M is an 8x8 matrix:

$$\begin{bmatrix}
1 & h_{-L-1,-L-2} & 0 & 0 & 0 & 0 & 0 & 0 \\
h_{L+1,-1} & 1 & h_{L,-1} & 0 & 0 & 0 & 0 & 0 \\
0 & h_{-L,-L-1} & 1 & h_{-L-1,-L-1} & 0 & 0 & 0 & 0 \\
0 & 0 & h_{L+1,0} & 1 & h_{L,0} & 0 & 0 & 0 \\
0 & 0 & 0 & h_{-L,-L} & 1 & h_{-L-1,-L} & 0 & 0 \\
0 & 0 & 0 & 0 & h_{L+1,1} & 1 & h_{L,1} & 0 \\
0 & 0 & 0 & 0 & 0 & h_{-L,-L+1} & 1 & h_{-L-1,-L+1} \\
0 & 0 & 0 & 0 & 0 & 0 & h_{L+1,2} & 1
\end{bmatrix}$$

and

$$P = \begin{bmatrix} p_1^-(k + d - 2g) \\ p_1^+(k - g) \\ p_1^-(k + d - g) \\ p_1^+(k) \\ p_1^-(k + d) \\ p_1^+(k + g) \\ p_1^-(k + d + g) \\ p_1^+(k + 2g) \end{bmatrix}$$

Using LU decomposition [106],

$$\det(M) = b_1\, b_2\, b_3\, b_4\, b_5\, b_6\, b_7\, b_8$$

where

$$\begin{aligned} b_1 &= 1 \\ b_{2m} &= 1 - (C_{L+1}\, C_{-L-1})/(b_{2m-1}\, D_{-2+m}\, D_{-L-3+m}) \quad m=1,2,3,4 \\ b_{2m+1} &= 1 - (C_L\, C_{-L})/(b_{2m}\, D_{-2+m}\, D_{-L-2+m}) \quad m=1,2,3 \end{aligned} \tag{5.14}$$

From (5.12) and (5.14), det(M) is a polynomial in k and so

$$\det(M) = 0$$

may be solved quite simply numerically. It is interesting to note that this equation can be written

$$D_2 - |C_{L+1}|^2/(D_{L-1} - |C_L|^2/(...../(D_{-1} - |C_{L+1}|^2/D_{L+2}) = 0$$

and this is very similar to the continued fraction form of the dispersion equation obtained from the Bloch wave method for wave propagation in an infinite periodic medium [93].

Once k is known, (5.13) can be solved for P to within a scalar multiple. This gives

$$\begin{bmatrix} P_1 \\ P_2 \\ P_3 \\ P_5 \\ P_6 \\ P_7 \\ P_8 \end{bmatrix} = p_1^+(k) \begin{bmatrix} -C_L\, C_{-L-1}{}^2/(\, b_1\, b_2\, b_3\, D_{-L-2}\,) \\ C_L\, C_{-L-1}\, /(\, b_2\, b_3\, D_{-1}\,) \\ -C_{L+1}/(\, b_3\, D_{-L-1}) \\ -b_4/(\, C_L\, D_L\,) \\ b_5\, b_4/(\, C_L\, C_{-L-1}\, D_{-L+1}\,) \\ -b_6\, b_5\, b_4/(\, C_L{}^2\, C_{-L-1}\, D_{-L+1}\,) \\ b_7\, b_6\, b_5\, b_4/(\, C_L{}^2\, C_{-L-1}{}^2\, D_2\,) \end{bmatrix} \tag{5.15}$$

For any solution $k+\beta = k_o+\beta$, from (5.9), (5.10), a linearly independent solution is $k+\beta = Ng - (k_o+\beta)$ for integer N. Thus the perturbed guide supports two independent modes. The solution is based on the assumption that $|k| \approx 0$ and so it follows that

$$N = L \tag{5.16}$$

The expressions for the electric field and the reflection coefficient follow exactly as for reflection from a single harmonic perturbation. The results are clearly the intuitive extensions of this latter case. From (5.1), (5.9), (5.16) the electric field in the perturbed guide is

$$\begin{aligned} &E\exp(iwt) = \\ &E_1(x)\exp(iwt)\Big\{ A_o\exp(-i(k_o+\beta)z)\sum_{m=-1}^{2}\big[p_1^+(k_o+mg)\exp(-imgz) + \\ &\qquad p_1^-(k_o+2\beta-mg-Lg)\exp(i(Lg+mg)z)\big] \\ &+ B_o\exp(i(k_o+\beta)z)\sum_{m=-1}^{2}\big[p_1^+(Lg-2\beta-k_o+mg)\exp(-i(Lg+mg)z) + \\ &\qquad p_1^-(-k_o-mg)\exp(imgz)\big]\Big\} \end{aligned}$$

where A_o and B_o are constants determined by the boundary conditions. Identifying the forward and backward propagating parts we can write

$$A_1^+(z) = A_o \exp(-i(k_o+\beta)z) \sum_{m=-1}^{2} p_1^+(k_o+mg)\exp(-imgz)$$
$$+ B_o \exp(-i(Lg-k_o-\beta)z \sum_{m=-1}^{2} p_1^+(Lg-2\beta-k_o+mg)\exp(-imgz)$$

$$A_1^-(z) = B_o \exp(i(k_o+\beta)z) \sum_{m=-1}^{2} p_1^-(-k_o-mg)\exp(-imgz)$$
$$+ A_o \exp(i(Lg-k_o-\beta)z \sum_{m=-1}^{2} p_1^-(-Lg+2\beta+k_o-mg)\exp(imgz)$$

For a perturbation of length D, we take the boundary conditions (for $k << \beta$) as $A_1^+(0) = I$, $A_1^-(D) = 0$.

Then writing

$$Q(k,z) = \sum_{m=-1}^{2} p_1^+(k+mg)\ \exp(-imgz)$$
$$R(k,z) = \sum_{m=-1}^{2} p_1^-(-k-mg)\ \exp(imgz)$$

we have

$$\frac{A_1^-(0)}{A_1^+(0)} = \frac{R(k_o,D)\ R(d-k_o,0) + \exp(-i(2k_o-d)D)\ R(d-k_o,D)\ R(k_o,0)}{R(k_o,D)\ Q(k_o,0) - \exp(-i(2k_o-d)D)\ R(d-k_o,D)\ Q(d-k_o,0)} \qquad (5.17)$$

and this yields the reflection coefficient

$$R = \frac{|\ A_1^-(0)\ |^2}{|\ A_1^+(0)\ |}$$

5.4 Explicit expression for the propagation constant

Before considering the numerical implications of the results of the previous two sections we digress briefly to obtain, for the particular case of coupling to the backward mode only, an explicit solution for k.

By defining

$$q_m(k) = p_m^+(k) + p_m^-(k+2\beta)$$

i.e. expressing each mode

$$A_m^+(z)\exp(-i\beta_m z) + A_m^-(z)\exp(i\beta_m z) = \exp(-i\beta_m z)\int q_m(k)\exp(-ikz)dk$$

we have instead of (5.4),

$$q_n(k) = \frac{w^2\mu}{\langle E_n|E_n\rangle k(k+2\beta_n)} \left(\sum_m + \int d\& \right) \langle E_n|\epsilon_l|E_m\rangle\, q_m(k+\beta_n-\beta_m-lg)$$

and $q_n(k)$ is large for $k \approx 0$, $k \approx -2\beta_n$.

For a single mode guide with perturbations $l = \pm L, \pm(L+1)$ and such that coupling to radiation modes is negligible,

$$q_l(k) = \frac{1}{(k+\beta)^2-\beta^2}\left(C_L q_l(k-Lg) + C_{-L} q_l(k+Lg) + C_{L+1} q_l(k-(L+1)g) - C_{-(L+1)} q_l(k+(L+1)g)\right) \qquad (5.18)$$

Clearly $q_l(k)$ couples only to $q_l(k+mg)$ for integer m as before. Therefore, applying (5.18) to $k=k+mg$ for all integers m leads to a homogeneous set of equations with infinite determinant

$$\Delta(x = k+\beta) = \det(B_{mn})$$

where $B_{mm} = 1$

$B_{m,m+l} = C_{-l}/D_m \quad l=+L, +(L+1)$

$B_{mn} = 0 \quad$ otherwise

This determinant is closely related to Hill's determinant which appears commonly in problems of wave propagation in infinite periodic media [36] and so the condition $\Delta(k+\beta) = 0$ has an explicit solution for k [36]

$$\sin^2\left(\frac{\pi}{g}(k+\beta)\right) = \Delta(0)\,\sin^2\left(\frac{\pi\beta}{g}\right) \qquad (5.19)$$

An alternative form of this equation can be obtained simply by

determining the unknown constant in the derivation of the solution in terms of $\Delta(g/2)$ (appendix). This then gives

$$\cos^2\left(\frac{\pi}{g}(k+\beta)\right) = \Delta(g/2)\cos^2\left(\frac{\pi}{g}\beta\right) \qquad (5.20)$$

The question arises as to whether the exclusion of radiation modes remains justified when (5.18) is applied to k=k+mg for arbitrary integer m. The only terms which make a non-neglgible contribution to Δ are those for which

$$k + mg + \beta \approx \pm\beta$$

Since we have assumed coupling to radiation modes is negligible, the equations represented by these terms are valid. The additional equations are always numerically insignificant (i.e. when evaluated give $O(\eta) = O(\eta)$ for negligible η), so requiring that they are also simultaneously satisfied does not impose a spurious constraint. Thus the infinite determinant has no physical significance and may be considered as resulting from a periodic extension of a finite set of equations. However although the solutions (5.19) (5.20) of $\Delta(k+\beta)=0$ can be obtained to arbitrary accuracy by retaining more terms in the expression for the determinant, the value of k does not become exact because of the exclusion of the radiation modes in the definition of Δ.

$\Delta(0)$ and $\Delta(g/2)$ have to be evaluated by appropriate truncation. When L is large, the truncated form of Δ is necessarily very large. However, Δ is clearly related to det (M) and its extension to include more terms. If $k \approx 0$ then since also $Lg \approx 2\beta$, it follows that $k-Lg \approx -2\beta \approx k - (L+1)g$. Therefore for small

integers m,

$$q_1(k+mg) \approx \frac{1}{(k+mg+\beta)^2-\beta^2} \left(C_L q_1(k+mg-Lg) + C_{L+1} q_1(k+mg-(L+1)g) \right) \tag{5.21}$$

$$q_1(k+mg-Lg) \approx \frac{1}{(k+mg-Lg+\beta)^2-\beta^2} \left(C_{-L} q_1(k+mg) + C_{-L-1} q_1(k+mg+g) \right) \tag{5.22}$$

Clearly equations (5.21) and (5.22) are identical to (5.10), (5.11) by the identifications

$$q_1(k) = p_1^+(k) \qquad k > -\beta$$

$$q_1(k) = p_1^-(k+2\beta) \qquad k < -\beta$$

(this transformation is well defined since either $k \approx 0$ or $k \approx -2\beta$)

Any finite truncation of $\Delta(k+\beta)$ is obtained by using the determinant of the matrix of the set of equations obtained from (5.21), (5.22) by retaining (m s.t. $|k+mg| = 0$) and this is equivalent to the determinant of (5.10) and (5.11) for the same set of m, $\tilde{\Delta}(k+\beta)$ say. Therefore in practice we may take

$$\Delta(k+\beta) = \tilde{\Delta}(k+\beta)$$

Let N be the integer which minimises $|Ng + \beta|$ and write

$$-\delta = Ng + \beta \tag{5.23}$$

Then $\Delta(0) = \Delta(Ng + \delta+\beta) = \Delta(\delta+\beta)$

(since the infinite determinant Δ is periodic with period g)

For small δ/g the appropriate truncation for $\Delta(\delta+\beta)$ is det(M) and so $\Delta(0) = \det(M : k=\delta)$

However for odd integers l, near the phase matching condition $2\beta = Lg$, from (5.23)

$$\delta \approx g/2$$

so $\Delta(\delta+\beta)$ is slowly convergent for large L and may be unstable. Therefore it is now more convenient to define

$$-\delta' = Ng + \beta - g/2$$

again choosing integer N to minimse $|\delta'|$, so that .

$$\Delta(g/2) = \Delta(\beta+\delta'+Ng) = \det(M : k=\delta')$$

and to use equation (5.19).

The frequency range near $2\beta = 1g$ for which k is complex (and so there is locally a significant reflection) can be obtained from

$$\Delta(g/2)\ \cos^2(\pi\beta/g) < 0 \qquad \text{for odd } 1$$

$$\Delta(0)\ \sin^2(\pi\beta/g) < 0 \qquad \text{for even } 1$$

An explicit solution for k cannot be obtained in the manner described in this section for coupling to other guided modes. In these cases the determinant is not in a form which can be related directly to Hill's determinant.

5.5 Numerical results

We now investigate whether a waveguide with two suitable perturbations of very different amplitudes, as described in section 5.1 and figure 5.1, does indeed have a narrower reflection band than the corresponding guide with a single perturbation. The unperturbed slab guide is assumed to be symmetric and single-mode. The cladding index is 1.47, the core index n_1 is 1.50 and the core thickness is 40/Lg. The perturbation amplitudes are $\epsilon_L = 8\times10^{-3} n_1^2$, $\epsilon_{L+1} = 4\times10^{-5} n_1^2$ and the perturbation amplitudes extend over a distance $D = 10^5/(Lg)$. The value of k(w) is calculated using (5.14). P is then evaluated from (5.15) and the reflection coefficient $\mathcal{R}$ from (5.17).

We are concerned here with the effect of the large perturbation, ϵ_L , on the half-power bandwidth of the reflection band of the small perturbation ϵ_{L+1} and how this varies as L/(L+1) tends to unity for fixed Lg (or alternatively as $\epsilon_L/(n_1^2)$ tends to unity). Figures 5.3 and 5.4 show the dispersion curve and group velocity respectively for propagation in a doubly periodic guide for L = 40, 80, 160, 240 and 320. Since Lg is fixed and $\epsilon_{L+1} \ll \epsilon_L$, the curves are independent of L except near $2\beta = (L+1)g$. Figure 5.5 shows how the half-power bandwidth of the reflection peak centred at $2\beta = (L+1)g$ varies with the group velocity near this point (but outside the reflection band). From this it can be seen that the bandwidth does increase with increasing L for $L \lesssim 200$.

When L = 160, that is when the difference in the pitches of the two perturbations 0.6%, the bandwidth is reduced from its value for $\epsilon_{L+1} = 0$ by 11%. The group velocity near $2\beta = 161g$ has been reduced by 13%. This is as we would expect. For coupling to a backward going mode by a single small perturbation, the reflection bandwidth $\sim \delta w \; 2v_g|C_1|/(Lg)$ and it is clear from the figures that for this small value of $\epsilon_{L+1}/\epsilon_L$ the weaker perturbation does not distort the dispersion curve significantly outside its stop band.

However, as the difference between the pitches is reduced further, as for L = 240, 320, the bandwidth increases again. Now the large side bands of the reflection of the strong perturbation overlap with the main reflection band of the small perturbation and the reflections caused by the two perturbations are no longer distinct (figure 5.6). The bandwidth of the reflection from the small perturbation can no longer be meaningfully determined. Thus the bandwidth reduction that can be achieved by this configuration is limited.

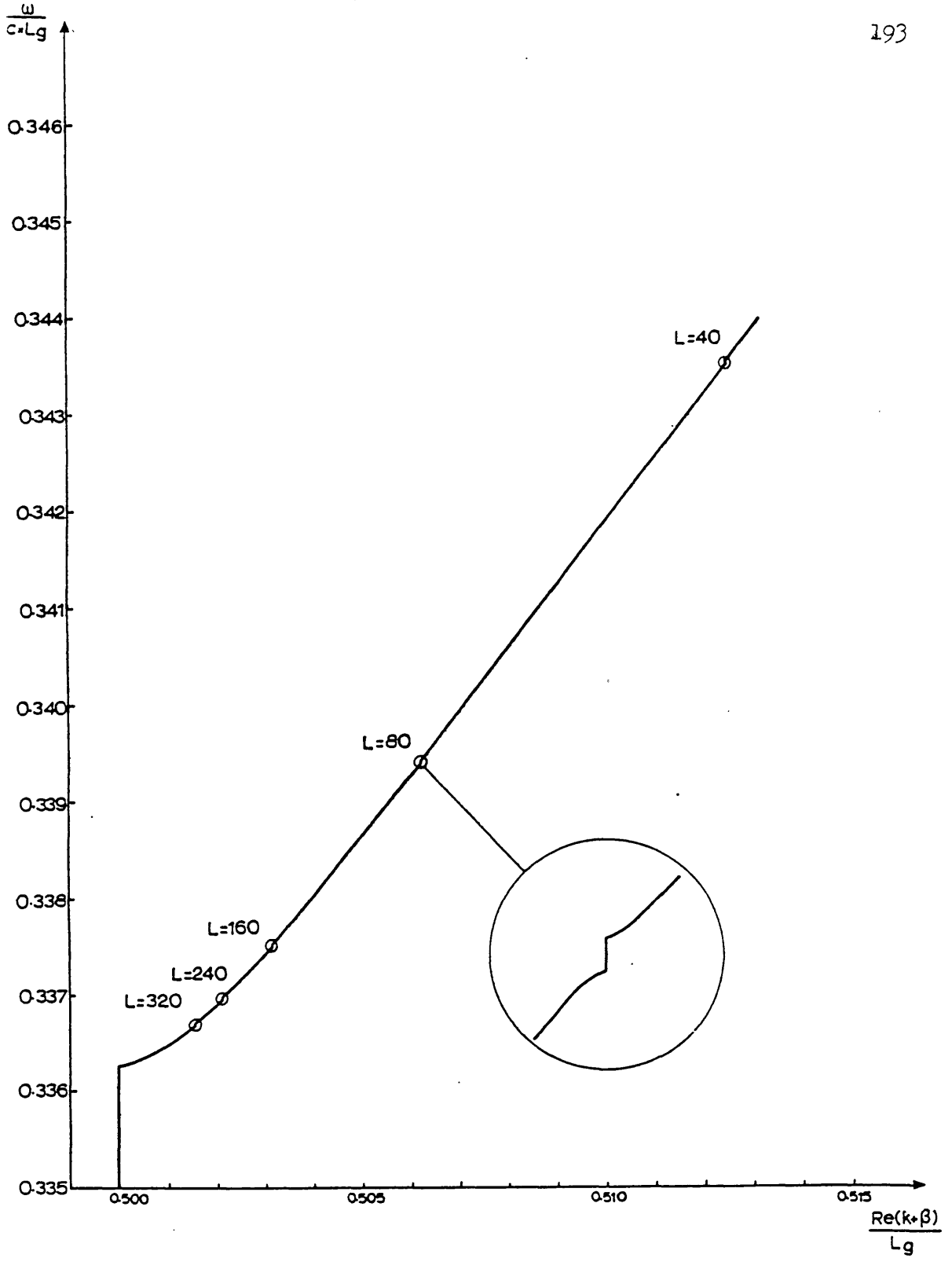

Figure 5.3 Normalised frequency as a function of the normalised real part of the propagation constant for a multiply periodic guide.

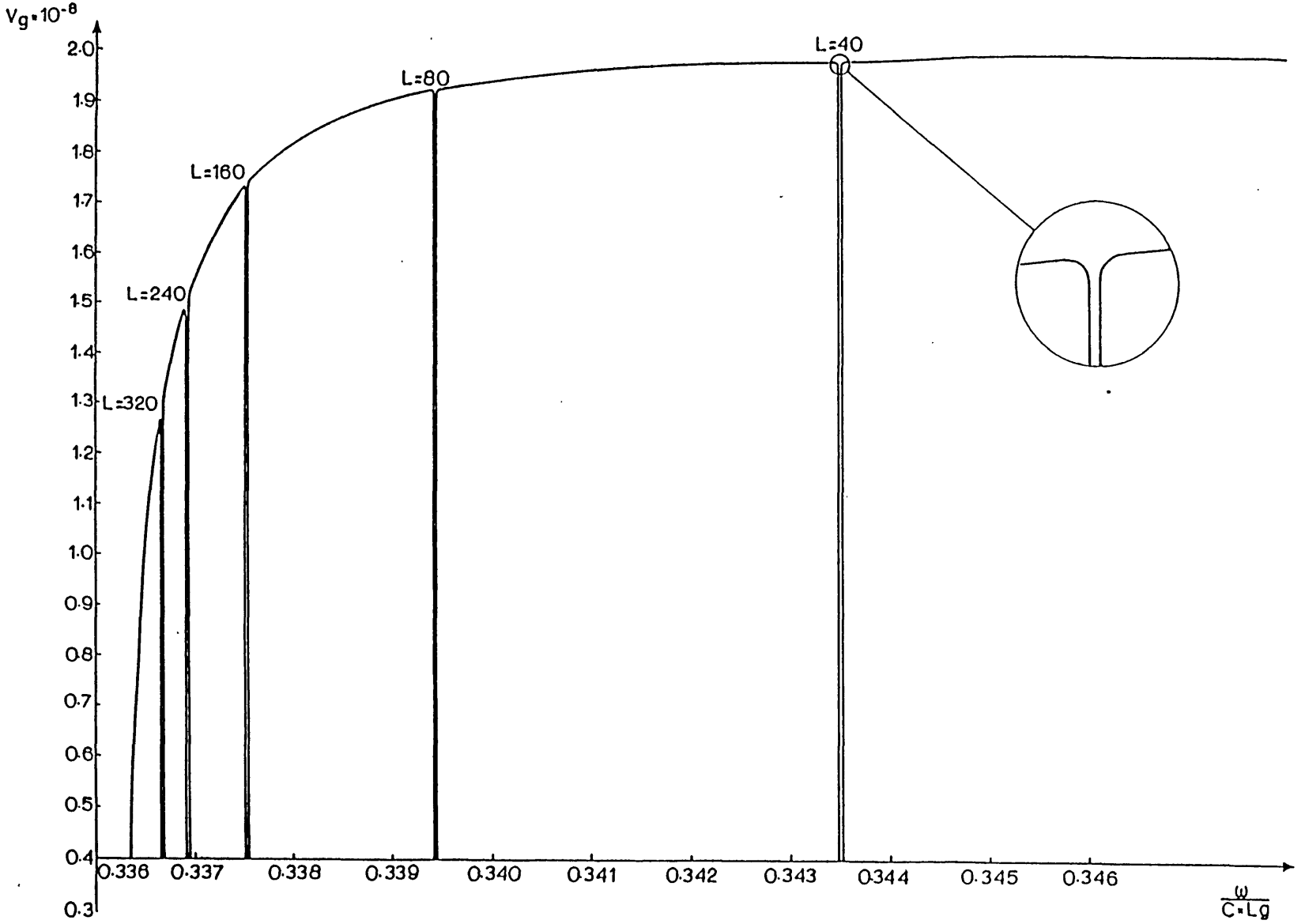

Figure 5.4 Group velocity as a function of frequency in a mutiply periodic guide.

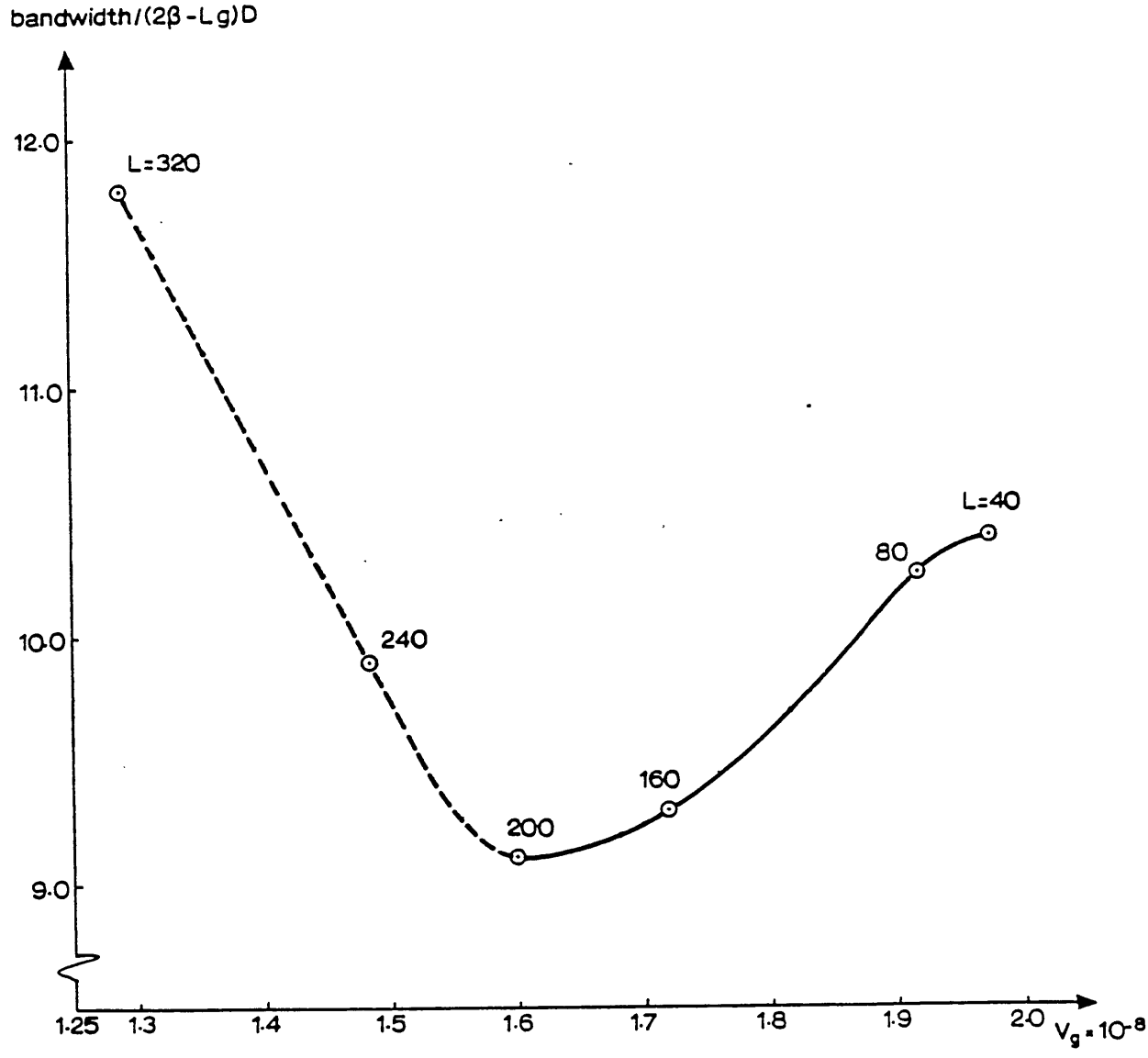

Figure 5.5 Normalised reflection bandwidth of the small pertubation as a function of the group velocity. The group velocity is taken at the reflection frequency, but in the absence of small pertubations.

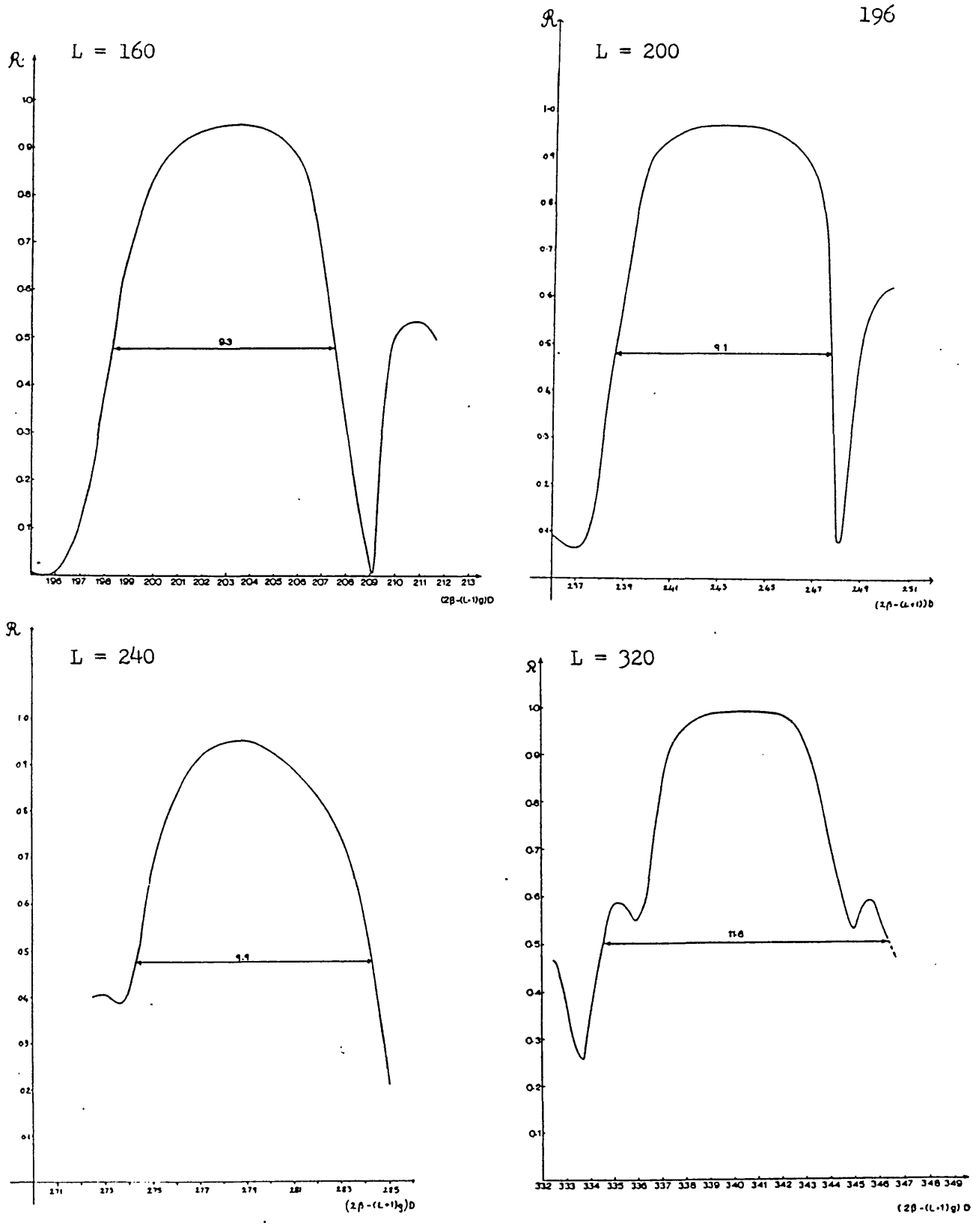

Figure 5.6 Reflectivity near the small amplitude perturbation resonance frequency as a function of normalised frequency for various doubly periodic structures

5.6 Conclusions

We have seen that the signal velocity of a periodic guide may not necessarily be described by its group velocity. However, by definition, the group velocity does determine how the frequency of operation of a mode changes as the propagation constant is varied. By analysing a doubly periodic guide we have found that the characteristics of the reflection phenomena associated with a periodic perturbation are determined essentially by the propagation constant. The centre and edges of the reflection band occur at particular values of β. The frequencies at which these effects occur can vary and may be altered to produce desirable characteristics.

Thus the introduction of a very large amplitude perturbation causes the reflection band of another perturbation to be centred at a different frequency, and occur over a different frequency range, since now the greatly altered propagation characteristic leads to the relevant propagation constants occuring at different frequencies. When the group velocity is very small, as near the band edge of the large amplitude perturbation, the frequency changes very little over the (unchanged) range of β which forms the reflection band of the small perturbation. Thus the bandwidth is indeed reduced. However the obtainable effects are rather small. For example, in order to achieve an 11% reduction in band width it is necessary for the large perturbation amplitude to be approximately 500 times the small one and for the pitches of the two perturbations to differ by only 0.6%. This order of improvement is also likely to represent the maximum possible case. For smaller differences in pitch, the sidelobes of the large

perturbation are significant and overlap with the main reflection band of the small perturbation for smaller differences in pitch, resulting in a broadened composite band.

Therefore again we have found that there are additional effects in a periodic medium which mean that they behave simply as a uniform dispersive dielectric only to a rather limited extent.

APPENDIX TO CHAPTER 5

The derivation of (5.17) is given in reference [36] when the following identifications are made:

$i\mu = 2(k + \beta)/g$

$\Delta_1 = \Delta$

$\theta_o = 2\beta/g$

Also from reference [36], in the same notation, it is clear that

$$\Delta_1(i\mu)\,(\cos(\pi\, i\mu) - \cos(\pi\ \theta_o)) =$$
$$\cos(\pi i\mu) - \cos(\pi\ \theta_o) + 4K \sin^2(\pi\ \theta_o\ /2)\cot(\pi\ \theta_o\ /2)$$

where K is a constant to be determined by setting a value for $i\mu$. The standard method is to set $i\mu=0$, giving (5.17). Setting $i\mu=1$ gives

$$\Delta_1(i\mu)\,(\cos(\pi\, i\mu)-\cos(\pi\ \theta_o)) - \Delta_1(1)\,(-1-\cos(\pi\ \theta_o)) = \cos(\pi i\mu) + 1$$

Therefore $\Delta_1(i\mu) = 0$ implies that

$$\cos(\pi\, i\mu) + 1 = \Delta_1(1)\,(\,1 + \cos(\pi\ \theta_o)\,)$$

i.e. $$\cos^2(\pi\, i\mu/2) = \Delta_1(1)\cos^2(\pi\ \theta_o\ /2)$$

Thus using the identifications above this is equation (5.18)

REFERENCES

1. C. Elachi, " Waves in Active and Passive Periodic Structures: A Review ",
Proc. IEEE vol 64, 1666, Dec 1976

2. T.K Gaylord and M.G. Moharam, " Analysis and Applications of Optical Diffraction Gratings ",
Proc IEEE vol 73, 894, May 1985

3. D.L. Hecht " Spectrum analysis using Acousto-Optic devices "
Opt. Eng., vol 16, 461, Sept/Oct 1977

4. M.C. Hutley, " Diffraction Gratings ",
London Academic Press 1982

5. V.J. Fowler and J. Schlafer, " A Survey of Laser Beam Deflection Techniques ",
Proc. IEEE vol 54, 1437, Oct 1966

6. J. Agonstinelli, G. Harvey, T Stone and C. Gabel,
" Optical Pulse Shaping with a Grating Pair ",
Appl. Opt., vol 18, 2500, July 15 1979

7. E. Treacy, " Optical Pulse Compression with Diffraction Gratings ",
IEEE J. Quantum Electron., vol QE-5, 454, Sept 1969

8. J. Upatnieks, " 360 degrees Hologram Displays for Educational uses ",
J.O.S.A., vol 64, 1396, Oct 1974

9. N.K. Shi and A.L. DeSouza, " Applications of Volume Holograms as Colour-sensitive Spatial Filters ",
J.O.S.A., vol 68, 1415, Oct 1978

10. A. Vander Lugt " Design Relationships for Holographic Memories ",
Appl. Opt., vol 12, 1675, July 1973

11. H. Haus, " Waves and Fields in Optoelectronics ",
Prentice-Hall inc., 1984

12. W.H. Southwell " Coating design using very thin high- and low-index layers ",
Appl. Opt. vol 24, 457, Feb 1985

13. J.E. Midwinter " "Light" Electronics, Myth or Reality ? ",
IEE Proc. J, vol 132, 6, 371, Dec 1985

14. S. E. Miller, " Present thrust of Optical-Fiber Telecommumnications Research - An Individual Perspective "
J. Lightwave Technol., vol LT-2, 488, Aug 1984

15. T. Okoshi, " Recent Progrss in Heterodyne/Coherent Optical-Fiber Communication ",
J. Lightwave Technol., vol LT-2, 341, August 1984

16. G.D Pitt, P. Extance et al, " Optical-Fibre Sensors ",
IEE Proc J, vol 132, 4, 214, August 1985

17. S.D. Smith, An introduction to Optically Bistable Devices and Photonic Logic ",
Proc. IEEE, A313, 195, 1985

18. K.C. Kao and G.A. Hockham, " Dielectric-Fibre Surface Waveguides for Optical Frequencies ",
Proc. IEE, vol 113, 1151, July 1966

19. F.P. Kapron, D.B. Keck and R.D. Mason, "Radiation Losses in Glass Optical Waveguides ",
Appl. Phys. Lett., vol 17, 423, 1970

20. T. Miya, Y. Terunuma, T. Hosaka and T. Miyashita
" Ultimate Low Loss Single-mode Fibre at 1.55μm "
Electronics Letters, vol 15, 106, Feb 1979

21. A. Yariv and M. Nakamura, " Periodic Structures for Integrated Optics ",
IEEE J. Quantum Electron., vol QE-13, 233, April 1977

22. H. Kogelnik and C.V. Shank, " Stimulated Emission in a Periodic Structure ",
Appl. Phys. Lett., vol 18, 152, 1971

23. D.C. Flanders, H. Kogelnik, R.V. Schmidt and C.V. Shank, " Grating Filters for Thin Film Optical waveguides ", Appl. Phys. Lett., vol 24, 194, 1974

24. S. Kim and C.G. Fonstad, " Tunable Narrow-Band Thin-Film Waveguide Grating Filters ", IEEE J. Quantum Electron., vol QE-15, 1405, Dec 1979

25. T.R. Jospeh, " Integrated Optic Spectrum Analyser ", IEE Proc. F, vol 129, 187, June 1982

26. A. Gruss, K.T. Tam and T. Tamir, " Blazed Dielectric Gratings with high Beam-coupling Efficiencies ", Appl. Phy. Lett., vol 36, 523, April 1980

27. P. Yeh and H.F. Taylor, " Contradirectional Frequency-Selective Couplers for Guided-wave Optics ", Appl. Opt., vol 19, 2848, 1980

28. A. Yariv and P. Yeh, " Electromagnetic Propagation in Periodic Stratified Media II. Birefringence, Phase-Matching and X-ray Lasers ", J.O.S.A. vol 67, 438, April 1977

29. W. Ng, H.W. Yen, A. Katzir, I. Samid and A. Yariv, " Room Temperature operation of GaAs Bragg-mirror Laser", Appl. Phys. Lett., vol 29, 684, 15 Nov 1976

30. P. Yeh and A. Yariv, " Bragg Reflection Waveguides ", Opt. Commun., vol 19, 427, 1976

31. A. Yariv and P. Yeh, " Optical waves in Crystals ", Wiley-Interscience, 1984

32. P. Yeh ,A. Yariv and E. Marom, " Theory of Bragg Fibre ", J.O.S.A., vol 68, 1196, sept 1978

33. D. Marcuse, " Theory of Dielectric Optical Waveguides ", Academic Press Inc., 1974

34. L. Brillouin, " Wave Propagation in Periodic Structures ", Dover Publications Inc., 1946

35. H. Kogelnik and C.V. Shank, " Coupled Wave Theory of Distributed-Feedback Lasers ", J. Appl. Phys., vol 43, 2327, 1972

36. E.T. Whittaker and G.N. Watson, "A course in Modern Analysis" Cambrige University Press, 4th ed., 1927

37. S.T. Peng, T. Tamir and H.L. Bertoni, " Theory of Periodic Dielectric Waveguides ", IEEE Trans on Microwave theory and techniques, vol MTT-23, 123, 1975

38. P. Yeh, A. Yariv and C-S Hong, " Electromagnetic Propagation in Periodic Stratified Media I. General Theory ", J.O.S.A. vol 67, 423, 1977

39. R. Collin, " Field Theory of Guided Waves ", McGraw-Hill, 1960

40. D. Marcuse, " Light Transmission Optics ", Van Nostrand Reinhold Company Inc., 2nd ed., 1982

41. J. Gower, "Optical Communication Systems ", Prentice Hall International Inc., 1984

42. M. Born and E. Wolf, " Principles of Optics ", Macmillan, 1964

43. P. Yeh, PhD. Thesis, Caltech, 1977

44. P. Yeh, A. Yariv and A.Y. Cho, " Optical Surface Waves in Periodic Layered Media ", Appl. Phys. Lett., vol 32, 104, 1978

45. A. Hardy, E. Kapron and A. Katzir, "Expression for the Guided TE modes in Periodic Multilayered Waveguides ", J.O.S.A, vol 71, 1283, Oct. 1981

46. A. Y. Cho, A. Yariv and P. Yeh " Observation of Confined Propagation in Bragg Waveguides ", Appl. Phys. Lett. vol 30, 471, 1977

47. T. Hidaka, " Loss-calculation of the Hollow Core Oxide-Glass-cladding Middle-infrared Optical waveguides ", J. Appl. Phys., vol 53, 93, Jan 1982

48. E. Garmire, T. McMahon and M. Bass, " Flexible Infrared Waveguides for High-power Transmission ", IEEE J. Quantum electron, vol QE-16, 23, Jan 1980

49. M.E. Marhic and E. Garmire, "Low-order TE_{oq} operation of a CO_2 Laser for Transmission through Circular Metallic waveguides ", Appl. Phys. Lett., vol 38, 743, May 1981

50. E.A.J. Marcatili and R.A. Schmeltzer, " Hollow Metallic and Dielectric waveguides for Long Distance Optical Transmission and Lasers ", B.S.T.J., vol 43, 1783, July 1964

51. M. Miyagi, A. Hongo and S. Kawakami, " Transmission charactersitics of Dielectric-Coated Metallic Waveguide for Infrared transmission: Slab Waveguide model ", IEEE J. Quantum Electron., vol QE-19, 136, 1983

52. W. Zakowicz, " Low loss Metallic Waveguide for transmission of Optical radiation ", J. Appl. Phys., vol 55, 3421, May 1984

53. M. Miyagi, A. Hongo, Y. Aizawa and S. Kawakami,
" Fabrication of Germanium-coated Nickel Hollow Waveguides for Infrared transmission ",
Appl. Phys. Lett., vol 43, 430, Sept 1983

54. M. Miyagi and S. Kawakami, " Design theory of Dielectric-coated Circular Metallic waveguides for Infrared transmission ",
J. Lightwave Technol. vol LT-2, 116, April 1984

55. M. Miyagi, K. Harada, Y. Aizawa and S. Kawakami,
" Transmission properties of Circular Dielectric-coated Metallic waveguides for Infrared transmission ",
S.P.I.E., vol 484, 117, 1984

56. D. Marcuse, " Radiation losses of the Dominant mode in Round Dielectric Waveguides ",
B.S.T.J., vol 49, 1665, 1970

57. N. Doran and K. Blow, " Cylindrical Bragg fibres: a design and feasibility Study for Optical Communications ",
J. Lightwave Technol., vol LT-1, 588, Dec 1983

58. R.M. Wood, S.K. Sharma and P. Waite ," Laser damage in Optical Materials at 10.6μm ",
GEC Journal of Science and Technology, vol 48, 140, 1982

59. T. Miyashita and T. Manabe, " Infrared Optical Fibres ", IEEE Trans. on Micrwave theory and techniques, vol MTT-30, 1420, Oct 1982

60. R.R. Dils, " High Temperature Optical Fiber Thermometer ", J. Appl. Phys., vol 54, 1198, March 1983

61. R.R. Dils, J. Geist and M.L. Reilly, " Measurement of the Silver Freezing Point with an Optical Fiber Thermometer : Proof of concept ", J. Appl. Phys., vol 59, 1005, 15 Feb 1986

62. M. Miyagi, K. Harada and s. Kawakami, " Wave Propagation and attenuation in the general class of Circular Hollow Waveguides with uniform curvature ", IEEE Trans on Microwave theory and techniques, vol MTT-32 513, May 1984

63. R.C. Weist (Ed) "CRC handbook of Chemistry and Physics ", 62nd Ed., CRC Press Inc, 1981

64. J. Debois, F. Gires and P. Tournois, " A new approach to Picosecond Laser Pulse Analysis, Shaping and Coding ", IEEE J. Quantum Electron., vol QE-9, 213, Feb 1973

65. R.A. Fisher, P.L. Kelly and T.K. Gustafson, "Subpicosecond generation using the Optical Kerr Effect ", Appl. Phys. Lett., vol 14, 140, 15 Feb 1969

66. C.V. Shank, R.L. Fork, R. Yen, R.H. Stolen and W.J. Tomlinson, " Compression of Femtosecond Optical Pulses ", Appl. Phys. Lett., vol 40, 761, 1 May 1982

67. J. P. Heritage, R.N. Thurston, W.J. Tomlinson, A.M. Weiner and R.H. Stolen, " Spectral windowing of Frequency-modulated Optical Pulses in a Grating Compressor ", Appl. Phys. Lett., vol 47, 87, 12 July 1985

68. W.J. Tomlinson, R.H. Stolen and C.V. Shank, " Compression of Optical Pulses chirped by self-phase modulation in Fibres ", J.O.S.A. B, vol 1, 139, April 1984

69. E.B. Treacy, " Compression of Picosecond Light Pulses ", Phys. Lett. vol 28A, 34, Oct 1968

70. E.B. Treacy, " Measurement of Picosecond Pulse Substructure using Compression Techniques ", Appl. Phys. Lett, vol 14, 112, 1969

71. C.V. Shank, J.E. Bjorkholm and H. Kogelnik, "Tunable DFB Dye Laser ", Appl. Phys. Lett., vol 18, 395, 1 May 1971

72. F.K. Reinhart, R.A. Logan and C.V. Shank, " GaAs-AlxGal-xAs Injection Lasers with Distributed Bragg reflectors ", Appl. Phys. Lett., vol 27, 45, 1975

73. Y. Yoshikuni, G. Motosugi, K. Kurumada and T. Ikegami, " Optimum operation of DFB lasers under Chirped Pulse Transmission ", Electronics Letts., vol 21, 476, 23 May 1985

74. Y. Yoshikuni, T. Matsuoka, G. Motosugi and N. Yamaka, " Fine structure in the broadened line of DFB lasers under high speed Direct Modulation ", Appl Phys. Letts., vol 45, 820, 1984

75. L. Bickers and L.D. Westbrook, " Reduction of Laser Chirp in 1.5μm DFB lasers by Modulation Pulse Shaping ", Electronics Letts., vol 21, 103, 1985

76. G.M. Motusugi, Y. Yoshikuni and Y. Itaya, " Spectral characteristics of a DFB Laser under high-speed Direct Modulation ", Electronics Letts., vol 20, 849, 1984

77. N.A. Olsson, H. Temkin and R.A. Logan, " Chirp-free Transmission over 82.5 km of Single-Mode Fibers at 2Gbits/s with Injection Locked DFB Semiconductor Lasers ", J. Lightwave Technol., LT-3, 63, 1 Feb 1985

78. M. Okuda and K. Onaka, " Response of an Optical Resonator with Distributed Bragg Reflectors to Light Pulses ", Japanese J. of Applied Physics, vol 17, 1105, June 1978

79. I.A. Bublichenko, " Investigation of the transmission of Ultrashort Pulses through a Waveguide Resonator with Distributed Bragg mirrors ",
Sov. J. Quantum Electron. vol 11, Feb 1981

80. S. De Silvestri, P. Laporta and O. Svelto, " Analysis of Quarter-wave Dielectric mirror dispersion in Femto-second Dye-laser cavities ",
Optics Letters vol 9, 335, 1984

81. C. Elachi, D.L. Jaggard and C. Yeh, " Transients in a Periodic Slab Waveguide: Coupled Waves approach ",
IEEE Trans on Antennas and Propagation, vol AP-23, May 1975

82. D.K.W. Lam, B.K. Garside and K.O. Hill, " Dispersion cancellation using Optical-Fibre filters ",
Optics Letters, vol 7, 291, June 1982

83. H.G. Winful, " Pulse Compression in Optical Fibre Filters ",
Appl. Phys. Lett., vol 46, 527, 15 March 1985

84. D.M. Cooper. S.P. Craig, B.J. Ainslie and C.R. Day,
" Dispersion shifted Single-mode fibres using Multiple Index Structures ",
British Telecom Technol. J., vol 3, 52, April 1985

85. H-T Shang, T.A. Lenaham, P.F. Glodis and D. Kalish, " Design and Fabrication of Dispersion-shifted Depressed clad Triangular-profile (DDT) single-mode fibre ", Electronics Letts., vol 21, 201, 28 Feb 1985

86. A.D. Pearson, " Optical Transmission in Dispersion-shifted Single mode spliced Fibers and Cables ", IEEE J. Lightwave Technol., LT-2, 346, August 1984

87. L.G. Cohen, W.L. Mammel and S.J. Jang, " Low-loss Quadruply clad Single-Mode light guides with Dispersion below 2psec/km-nm over the 1.28-1.64 wavelength range ", Electronics Letts., vol 18, 1023, 25 Nov 1982

88. P.L. Francois, " Propagation mechanisms in Quadruply-clad fibres: mode coupling, dispersion and pure bend losses ", Electronics Letts., vol 19, 13 Oct 1983

89. A. Yariv and A. Gover, " Equivalence of coupled-mode and Floquet-Bloch formalisms in periodic optical waveguides ", Appl. Phys., Lett., vol 26, 537, 1 May 1975

90. J.A. Stratton, " Electromagnetic theory ", McGraw-Hill 1941

91. L. Brillouin, " Wave propagation and Group velocity ", Academic Press 1960

92. G.F. Carrier, M. Krook and C.E. Pearson, " Functions of a Complex variable ",
McGraw-Hill 1966

93. T. Tamir, H.C. Wang and A.A. Oliner, " Wave propagation in Sinusoidally Stratified Dielectric Media ",
IEEE Trans. on Microwave Theory and Techniques, vol MTT-12, 323, May 1964

94. C. Yeh, K.F. Casey and Z.A. Kaprielian, " Transverse Magnetic wave propagation in Sinusoidally Stratified Dielectric Media ",
IEEE Trans. on Microwave Theory and Techniques, vol MTT-13, 297, May 1964

95. T. Tamir, " Scattering of Electromagnetic waves by a sinusiodally stratified half-space II ",
Canadian Journal of Physics, vol 44, 2461, 1966

96. D.L. Jaggard and C. Elachi, " Floquet and coupled-waves analysis of higher-order Bragg coupling in a periodic medium ",
J.O.S.A., vol 66, 674, July 1976

97. E.A. Nevis and J.E. Harvey, " Angular Grating Anomalies: an apparent violation of the grating equation ",
S.P.I.E., vol 503, 46, 1984

98. D.L. Jaggard and G.T. Warhola, " Characteristics of Modulated Periodic Media: I Passive Structures ",
Radio Science, vol 16, 467, July-Aug 1981

99. K. Roskushima and J. Yamakita, " Analysis of Anisotropic dielectric gratings ",
J.O.S.A., vol 73, 901, July 1983

100. A.A. Spikhal'skii, V.A. Sychugov and A.V. Tishenko,
" Simple method for calculating the optical attenuation coefficient of a Corrugated Waveguide ",
Sov. J. Quantum Electron., vol 13, 592, May 1983

101. H. Kogelnik, " Filter response of nonuniform almost-periodic structures ",
B.S.T.J., vol 55, 109, 1 Jan 1976

102. M. Matsuhara, K.O. Hill and A. Wanatabe, "Optical waveguide filters: synthesis ",
J.O.S.A., vol 65, 804, July 1975

103. O.R. Asfar and A.H. Nayfeh, " Stopbands of the first-order Bragg interaction in a parallel plate waveguide having multiperiodic wall corrugations ",
IEEE Trans. Microwave theory and techniques, vol MTT-28, 1187, 1980

104. K. Yasumoto, " Three-mode coupling in a dielectric slab waveguide with doubly periodic surface corrugations ", J. Appl. Phys., vol 57, 755, 1 Feb 1985

105 A.H. Nayfeh, " Perturbation methods ", Wiley, 1973

106 P.W. Williams, " Numerical Computation ", Nelson, 1972

107. E. Snitzer, " Cylindrical dielectric waveguide modes ", J.O.S.A., vol 51, 491, May 1961

108. M. Miyagi, " Waveguide-loss evaluation in circular hollow waveguides and its ray-optical treatment ", IEEE J. Lightwave technol., vol LT-3, 303, April 1985

109. P. Yeh, " Electromagnetic propagation in birefrigent layered media ", J.O.S.A., vol 69, 742, May 1979

110. C-L. Chen, " Transverse electric fields guided by doubly periodic structures ", J. Appl. Phys, vol 52, 4926, August 1981

111. P. Yeh and S. Sari, " Optical properties of stratified media with exponentially graded refractive index ", Applied Optics, vol 22, 4142, 15 December 1983

112. A.R. Mickelson and D.L. Jaggard, " Electromagnetic wave propagation in almost periodic media ", IEEE Trans. on antennas and propagation, vol AP-27, 34, Jan 1979

113. K. Kiyoshioka and M. Hashimoto, " Coupling of guided light through a periodic multilayer ", Applied Optics, vol 21, 320, 15 January 1982

114. R.R.A. Syms, " Optical directional coupler with a grating overlay ", Applied Optics, vol 24, 717, 1 March 1985

115. D. Marcuse, " Thick dielectric grating on asymmetric slab waveguide ", B.S.T.J., vol 56, 329, March 1977

116. M.G.F. Wilson and S.W. Chan Wong, " Theory of integrated optic diffraction gratings in low Δn waveguides ", Electronics Letters, vol 19, 943, 27 October 1983

117. J. Yamakita and K. Rokushima, " Modal expansion method for dielectric gratings with rectangular grooves ", S.P.I.E., vol 503, 239, 1984

118. G. Evans, " Mode coupling and distributed feedback lasers in periodic fiber waveguides ", IEEE J. Quantum Electron., vol QE-13, 145, April 1977

PART II

6. A STUDY OF THE EFFECTS OF SHORT-RANGE CORRELATION ON THE PERMITTIVITY OF NEMATIC LIQUID CRYSTALS

6.1 Introduction

This chapter is concerned with a theoretical investigation of short-range correlationsin Nematic LiquidCrystals. It is part of a larger study of direct-current field induced behaviour of guest non-linear materials in a host liquid crystal.

Liquid Crystals play an important role in various optical and electro-optical devices. In this context, the attractive property of the liquid crystal is, in many cases, its change in refractive index under the influence of an applied electric field. This change is a result of re-orientation of the anisotropic birefringent molecules of the material. Thus the response times are slow compared to those of electronic effects, and are of the order of milliseconds, but the change in permittivity or refractive index is also very large, since in general the polarisability of the molecules (which are often thin and long) is very different in the directions parallel and perpendicular to the molecular axis. These properties mean that liquid crystals are suited to applications such as displays [1], [2], [3] and slow-speed switches (for example for Local Area Networks).

The anisotropy of the molecules in a typical liquid crystal and the orientational order, which is present at low enough temperatures, mean that in general molecular theories are complicated. Several factors are likely to influence the positions of the molecules, and models of isotropic liquids cannot usually be applied. In addition, the properties are often strongly

temperature dependent. Various models of liquid crystals include the Van der Waals mean field theory [4], the Maier Saupe mean field model and director fluctuation or continuum theory [5].

If a reasonably accurate model is used, it may be hoped that the macroscopic properties such as the dielectric permittivity, the refractive index and the elasticity of a liquid crystal may be predicted from the characteristics of its constituent molecules. This in turn may allow compounds likely to posses some desired property to be suggested. For many applications in optics the refractive index and dielectric permittivity are, of course, of great importance. These quantities may be related to the molecular polarisabilities and permanent dipole moments if these are suitably averaged. Therefore it is useful to consider factors which may effect this average.

The simplest and least ordered type of liquid crystal is the Nematic type. Here there is no long-range translational order (that is, which persists over a distance of a large number of molecules), but there is long-range orientational order below some critical temperature. The average deviation of the axes of the molecules from any given direction is not uniform with direction. It is minimised in some direction which depends on the external or boundary conditions, and this direction is known as the director. A quantity which indicates the degree of ordering with respect to this director has been defined, namely the order parameter S.

The anisotropy of liquid crystal molecules suggests that there is likely to be also some degree of local ordering (for example two neighbouring rod-like shaped molecules seem more likely to lie parallel than perpendicular to each other). It is possible that

this short-range correlation affects the way in which the microscopic and macroscopic dielectric properties, in particular the non-linear optical properties, of a Nematic are related.

In order to determine the dielectric properties of a liquid crystal from its molecular characteristics it is necessary to use a model for the internal field, which effects the equilibrium positions and orientations of the molecules. Several such models have been proposed [6]. However, of the recent models which include the anisotropy of the internal field [7], [8], [9], only that of Bordewijk and de Jeu [10], [11] predicts accurately the observed temperature dependence of the refractive index. From the statistical mechanical expression for the dielectric permittivity [12] it is clear that this latter empirical formula corresponds closely to the assumption that the molecules are totally correlated, that is that they are all oriented at the same (variable) angle to the director.

In this chapter we will investigate the degree to which the dielectric permittivity, $\underline{\epsilon}$, of a nematic liquid crystal is affected by short-range (non-electrostatic) orientational correlation of its molecules, a feature which is ignored in mean field theories. This will be done by first evaluating the term in $\underline{\epsilon}$ which accounts for two-particle interaction using Faber's continuum theory [13], [14] (this theory describes both director fluctuations and short-range correlations), and then inferring from this the effect of local ordering in general.

We will find that, in fact, for a reasonable spatial pair-correlation function, the effect of short-range orientational correlation is rather small and may be neglected. Therefore it is possible to obtain an expression for $\underline{\epsilon}$ from its statistical

mechanical series expansion by assuming that the molecular orientations are uncorrelated. Perhaps surprisingly, the resulting formula yields refractive index values for the liquid crystal p-azoxyanisole (PAA) which agree closely with those predicted by the expression deduced assuming total correlation by Bordewijk and de Jeu [11]. Since the new expression has been derived in a semi-rigorous fashion, this may be seen as a justification for the empirical formula of de Jeu and Bordewijk.

The contents of the remainder of this chapter are follows. In the following section, 6.2, the form of the pair-correlated terms is determined from an expression for $\underset{\sim}{\epsilon}$. This expression relates $\underset{\sim}{\epsilon}$ to the averages of molecular quantities and is a generalisation of the method derived by Bordewijk and de Jeu [10]. In sections 6.3, 6.4 and 6.5 we evaluate the two-particle term and consider the approximations involved in this. The averages appearing in the expression for $\underset{\sim}{\epsilon}$ are calculated by assuming no short-range correlations in section 6.6. In section 6.7 the numerical results for the refractive index of PAA are shown to be close to those obtained from the totally correlated expression of reference [11].

6.2 The Permittivity expression

An expression for the dielectric constant, $\underset{\sim}{\epsilon}$, of an isotropic liquid in terms of averages of the polarisabilities and dipole moments of its molecules (a generalisation of the Kirkwood-Frolich equation) has been derived by Bordewijk [15].

Bordewijk and de Jeu have shown how these averages may be evaluated if a particular internal field factor is assumed [10], [11]. In this section we will use this method, but make no special assumptions about the internal field, and obtain an equation for $\underset{\sim}{\epsilon}$.

From [10], the dielectric constant is given by

$$\frac{\epsilon_o (\epsilon_\gamma - \epsilon_{\infty\gamma})[\epsilon_\gamma + (1 - \epsilon_\gamma) \Omega^{\epsilon}_\gamma]^2 V}{\epsilon_\gamma [\epsilon_\gamma + (\epsilon_{\infty\gamma} - \epsilon_\gamma) \Omega^{\epsilon}_\gamma]} =$$

$$\frac{1}{K_B T} < (\sum_i \underset{\sim}{\mu}^i . \sum_j \underset{\sim}{A}^{ji})_\gamma \; (\sum_{i'} \underset{\sim}{\mu}^{i'} . \sum_{j'} \underset{\sim}{A}^{j'i'})_\gamma >_o \qquad \gamma = \parallel, \perp \qquad (6.1)$$

and the induced moment of the ith dipole due to the external field (that is, for fixed positions and orientations of the molecules) is

$$\underset{\sim}{p}^i = \underset{\sim}{a}^i \sum_j \underset{\sim}{A}^{ji} . \underset{\sim}{\epsilon} [\underset{\sim}{\epsilon} + (\underset{\sim}{I} - \underset{\sim}{\epsilon}) . \underset{\sim}{\Omega}^{\epsilon}]^{-1} . \underset{\sim}{E}$$

$$= \underset{\sim}{a}^i \sum_j \underset{\sim}{A}^{ji} . [\underset{\sim}{\epsilon} + (\underset{\sim}{I} - \underset{\sim}{\epsilon}) . \underset{\sim}{\Omega}^{\epsilon}]^{-1} [\underset{\sim}{\epsilon} + (\underset{\sim}{\epsilon}_\infty - \underset{\sim}{\epsilon}) . \underset{\sim}{\Omega}^{e}] . \underset{\sim}{E}_s \qquad (6.2)$$

The sample is taken to be a sphere of volume V embedded in a dielectric of the same permittivity, the surroundings being treated as a continuous medium. The subscripts $\parallel$ and $\perp$ refer to the directions parallel and perpendicular to the macroscopic director respectively. $\underset{\sim}{\Omega}^{e}$ is a geometrical factor depending on $\epsilon_\parallel / \epsilon_\perp$ and the subscript o indicates that the average is taken for zero external field. $\underset{\sim}{\mu}^i$ is the permanent dipole moment and $\underset{\sim}{a}^i$ the polarisability of the ith molecule. $\underset{\sim}{A}$ is a

3n-dimensional tensor, $\underset{\sim}{A} = (\underset{\sim}{I} + \underset{\sim}{a}.\underset{\sim}{T}')^{-1}$, which accounts for the increase of each dipole due to the effects of the rest of the medium [10] and $\underset{\sim}{A}^{ij}$ is its projection on the product of the i and j subspaces. $\underset{\sim}{E}$ and $\underset{\sim}{E}_s$ are the Maxwell fields in the surrounding dielectric and inside the sample respectively. $\sum_j \underset{\sim}{A}^{ji}$ is obtained by equating the right-hand side of (6.2) to an expression for the polarisation of a dipole in the same sample, but with the permanent moments set to zero, for the same Maxwell field. This is done in [10] using an independently obtained internal field factor. More generally, for given positions and orientations of the molecules, the induced polarisation can be obtained from that of the sphere in vacuo. In this case the external field $\underset{\sim}{E}_o$ for a general Maxwell field inside the sample, $\underset{\sim}{E}_s$, is given by

$$\underset{\sim}{E}_o = (2\underset{\sim}{I} + \underset{\sim}{\epsilon}_\infty) \underset{\sim}{E}_s/3$$

Therefore, if we define

$$\underset{\sim}{A}^i = [\underset{\sim}{I} - \sum_j \underset{\sim}{T}^{ij}.\underset{\sim}{a}^j + \sum_j \underset{\sim}{T}^{ij}.\underset{\sim}{a}^j \sum_k \underset{\sim}{T}^{jk}.\underset{\sim}{a}^k - \ldots.]$$

where Tij is the vacuum dipole propagation tensor, then

$$\underset{\sim}{p}^i = \underset{\sim}{a}^i.\underset{\sim}{A}^i.[2\underset{\sim}{I} + \underset{\sim}{\epsilon}_\infty].\underset{\sim}{E}_s/3 \qquad (6.3)$$

For the case of total correlation of orientation of the molecules, the average value of $\underset{\sim}{p}^i$ is equal to that derived in [11]. However the expression before averaging is different because in the expression (6.3) it has been assumed that the external field $\underset{\sim}{E}_o$ and not the Maxwell field $\underset{\sim}{E}_s$ is uncorrelated with the molecular orientations.

Since (6.3) holds generally for fixed molecules and a given Maxwell field $\underset{\sim}{E}_s$, as in [10] we can equate this expression for

$\underset{\sim}{p}^i$ to that in equation (6.2) to yield an expression for $\sum_j \underset{\sim}{A}^{ji}$

$$\sum_j \underset{\sim}{A}^{ji} = \underset{\sim}{A}^i.(2\underset{\sim}{I} + \underset{\sim}{\epsilon}_\infty).[\ \underset{\sim}{\epsilon} + (\underset{\sim}{I} - \underset{\sim}{\epsilon}).\underset{\sim}{\Omega}^{\epsilon}\ ].[\ \underset{\sim}{\epsilon} + (\underset{\sim}{\epsilon}_\infty - \underset{\sim}{\epsilon}).\underset{\sim}{\Omega}^{\epsilon}\ ]^{-1}/3$$

Therefore from (6.1)

$$\epsilon_o(\epsilon_\gamma - \epsilon_{\infty\gamma})[\ \epsilon_\gamma + (\epsilon_{\infty\gamma} - \epsilon_\gamma)\Omega^e_\gamma\ ]\ V/\epsilon_\gamma\ =$$

$$\frac{1}{9K_BT} < \sum_{ii'} [\underset{\sim}{\mu}^i.\underset{\sim}{A}^i]_\gamma\ [\underset{\sim}{\mu}^{i'}.\underset{\sim}{A}^{i'}]_\gamma >_o\ (2 + \epsilon_{\infty\gamma})^2 \qquad (6.4)$$

This reduces to the Kirkwood-Frolich equation [12] in the isotropic case.

The averages in (6.4) may be calculated in the limiting cases of total orientational correlation and no orientational correlation (this latter calculation is carried out in section 6.6 below), but an exact general evaluation would involve second, third and higher order correlations and would be extremely difficult. In order to estimate the effect of the short-range correlations we consider in the following sections how we may evaluate approximately the two-particle orientational averages.

6.3 The Pair Correlation term in the Permittivity

In this section we will consider the terms on the right-hand side of equation (6.4) which contain only orientational correlation of two particles. These terms can be expressed in a simple form by making certain assumptions and may then be evaluated using Faber's

continuum theory.

Since there is no long-range translational ordering in the Nematic phase, we will ignore third and higher order positional correlation and express all positional averages in terms of the spatial pair-correlation function $g_2(\underset{\sim}{R}, \underset{\sim}{n}^i, \underset{\sim}{n}^j)$, where $\underset{\sim}{R}$ is the intermolecular separation and $\underset{\sim}{n}^i$ is the director at the position of the ith molecule. For each position of the jth molecule we take for its orientation the average value given the position and orientation of the ith molecule. Thus we assume

$$g_2 = g_2(\underset{\sim}{R}, \underset{\sim}{n}^i, \underset{\sim}{n}^j(\underset{\sim}{R}, \underset{\sim}{n}^i)) = g(\underset{\sim}{R}, \underset{\sim}{n}^i)$$

Using this we will replace the moment of the jth molecule by its average value over all positions. Finally we average over the positions and orientations of the ith molecule. We will assume also that, with respect to axes fixed in the ith molecule, g is independent of the orientation of molecule i [16]. The first orientationally correlated term is:

$$\overline{\langle \underset{\sim}{\mu}^i \cdot \underset{\sim}{e}\, \underset{\sim}{\mu}^i \cdot \underset{\sim}{T}^{ij} \cdot \underset{\sim}{a}^j \cdot \underset{\sim}{e} \rangle} = \overline{-\underset{\sim}{e} \cdot \frac{1}{4\pi\epsilon_o V}} \left\langle \int_{V_1+V_2} g(\underset{\sim}{R}, \underset{\sim}{n}^i)\, \underset{\sim}{\mu}^i\, \underset{\sim}{\mu}^i \cdot \frac{(\underset{\sim}{I} - 3\underset{\sim}{\hat{R}}\underset{\sim}{\hat{R}})}{R^3} \cdot \underset{\sim}{a}^j\, d^3\underset{\sim}{R} \right\rangle \cdot \underset{\sim}{e} \qquad (6.5)$$

(since $\underset{\sim}{\mu}^i$ is independent of $\underset{\sim}{R}$ for given $\underset{\sim}{n}^i$) where $R = |\underset{\sim}{R}|$, $\hat{R} = \underset{\sim}{R}/R$, the symbols $\overline{\ }$ and $\langle\ \rangle$ denote a positional and orientational average respectively and $\underset{\sim}{e}$ is the unit vector in the direction of the applied field ($\parallel$ or $\perp$). The integration is performed over volumes V_1, V_2 as shown in figure 6.1, where the radius R_2 is large enough for short-range correlations to be neglected in V_2. Then for a spherical sample the integral over V_2 vanishes.

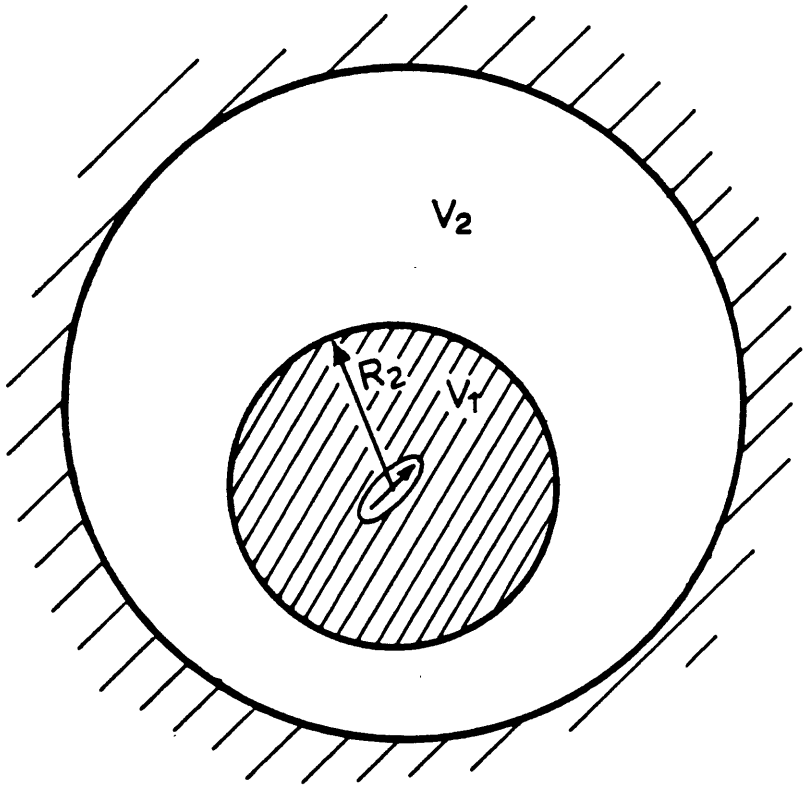

Figure 6.1 Integration volumes V_1 and V_2

We will use axes fixed in the ith molecule, with one axis parallel to the molecular long axis (i-axes). Then $g = g(\underset{\sim}{R})$ and we assume further that g is independent of the azimuthal angle ϕ_R. As in continuum theory [13], [14], we take the correlations to be isotropic. Therefore in equation (6.5) only $\hat{\underset{\sim}{R}}\,\hat{\underset{\sim}{R}}$ has any ϕ_R dependence and when this tensor is expressed in i-axes the contributions from its off-diagonal elements vanish because of the ϕ_R integration. Therefore by rotation of uniaxial tensors the average on the right-hand side of (6.5) is

$$\underset{\sim}{H} = -\int_{V_1} \frac{g(\underset{\sim}{R})}{R^3} < [\mu_\perp^2(1-3R_\perp^2)\underset{\sim}{I} + \Delta(\underset{\sim}{\mu}^2.(\underset{\sim}{I}-3\underset{\sim}{\mathcal{R}}^2))\,\underset{\sim}{n}^i\underset{\sim}{n}^i].[a_\perp\underset{\sim}{I} + \Delta a\underset{\sim}{n}^j\underset{\sim}{n}^j] > d^3\underset{\sim}{R} \qquad (6.6)$$

where $\underset{\sim}{a}$, $\underset{\sim}{\mu}\underset{\sim}{\mu} = \underset{\sim}{\mu}^2$ and $\hat{\underset{\sim}{R}}\hat{\underset{\sim}{R}} = \underset{\sim}{\mathcal{R}}^2$ are referred to axes fixed in the molecule (The molecule is assumed to be rotating about its long axis so we treat $\underset{\sim}{\mu}\underset{\sim}{\mu}$ as a uniaxial tensor), $\Delta a = a_\parallel - a_\perp$ and similarly for $\Delta(\underset{\sim}{\mu}^2.(\underset{\sim}{I} - 3\underset{\sim}{\mathcal{R}}^2))$.

From (6.6) the only term in H which depends on short-range correlation is

$$\underset{\sim}{J} = \Delta a\,(\mu_\parallel^2 + \mu_\perp^2/2)\int_{V_1} d^3\underset{\sim}{R}\,\frac{g(\underset{\sim}{R})}{R^3}(1 - 3R_\parallel^2) < \underset{\sim}{n}^i\underset{\sim}{n}^i.\underset{\sim}{n}^j\underset{\sim}{n}^j > \qquad (6.7)$$

In the next section we will use continuum theory to evaluate this integral.

6.4 Evaluation using Fluctuation Theory

In Faber's continuum theory [13], orientation dependent averages may be expressed (in the Random Phase Approximation (R.P.A.)) in terms of the sum of the director fluctuations X defined in [14] and, if the orientations of two molecules are involved, a factor $\alpha(R)$ indicating the lack of correlation at separation R:

$$\alpha(R) = \frac{2}{q_c} \int_0^{q_c} \left(1 - \frac{\sin(qR)}{qR} \right) dq$$

where the minimum wavelength of the fluctuations is $2\pi/q_c$.

The parallel and perpendicular components of $\underset{\sim}{J}$ may be evaluated using [13]

$$U = \langle \cos(\theta^i)\cos(\theta^{ij})\cos(\theta^j) \rangle$$

$$= 4S/9 + 1/9 - 2Q/9 + (4/9\alpha)\, dQ/dX$$

and

$$\langle \sin(\theta^i)\cos(\phi^i)\cos(\theta^{ij})\sin(\theta^j)\cos(\phi^j) \rangle$$

$$= U/2 - V/4 + 1/12 - S/3 + 2\mathrm{Re}(C)/3$$

respectivley,

where θ^i, ϕ^i, are the polar angles of $\underset{\sim}{n}^i$ w.r.t to the fixed frame

θ^{ij} is the angle between $\underset{\sim}{n}^i$ and $\underset{\sim}{n}^j$

$Q = \langle 3\cos^2(\theta^{ij}) - 1 \rangle/2$

$V = \langle \cos^2(\theta^i)\, \cos^2(\theta^j) \rangle$

$C = 4\pi \langle Y_{22}(\theta^i, \phi^i)\, Y_{22}^*(\theta^j, \phi^j) \rangle/5$

$Y_{22}(\theta, \phi)$ is a normalised spherical harmonic

U, Q, V, C can all be obtained from differential equations in X.

In figure 6.2 we show

$$J_{\parallel} = \int_{V_1} \frac{g(\underset{\sim}{R})}{R^3} \left(1 - 3\hat{R}_{\parallel}^2 \right) U(R)\, d^3\underset{\sim}{R}$$

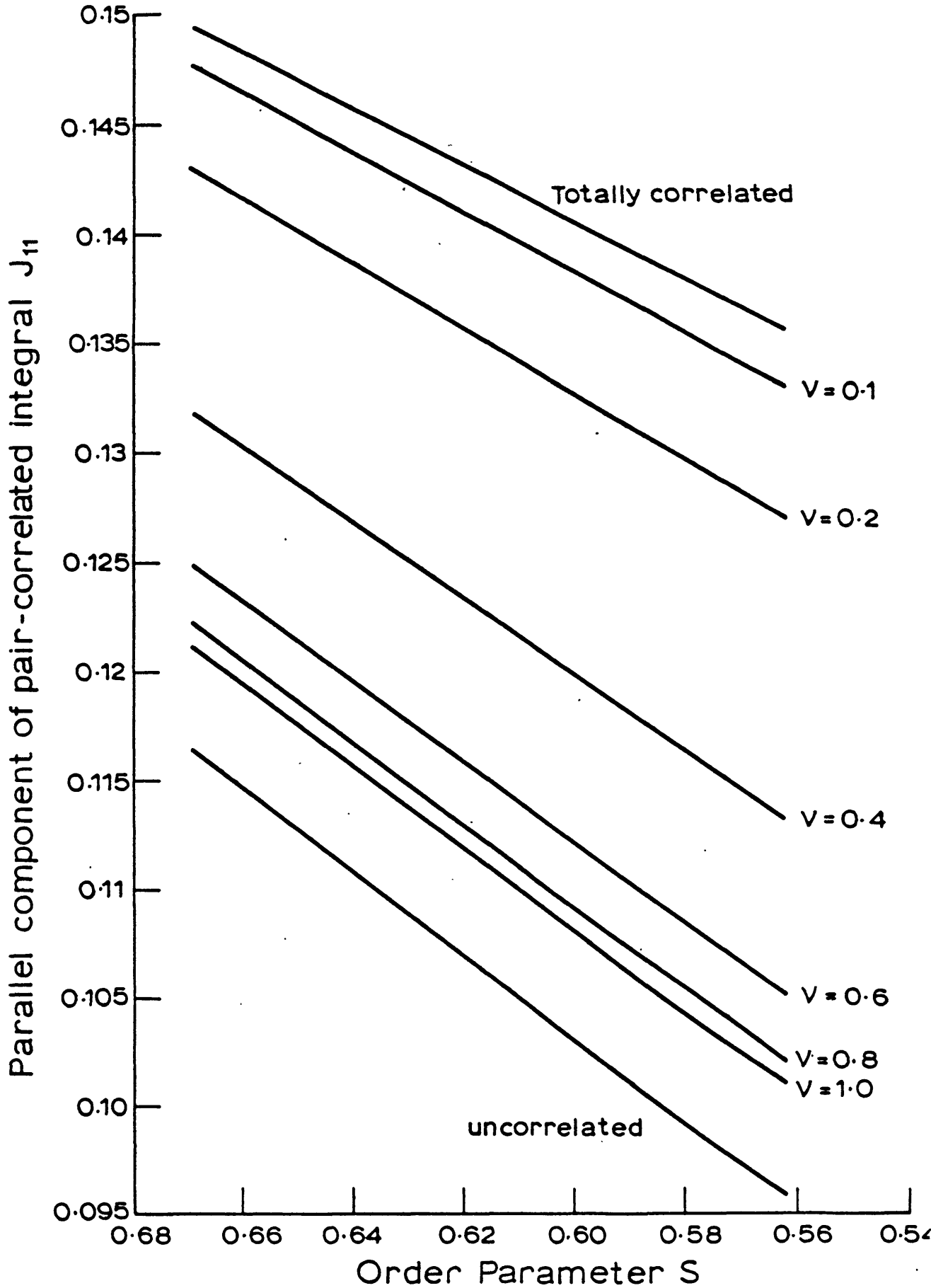

Figure 6.2 Variation with S of pair correlated integral assuming isotropic correlations, $J_{11}.(b_l/b_t) = 2.4$. Curves are shown for $b_t = v.2\pi/q_c$ for various v and for the totally correlated and uncorrelated cases

as a function of the order parameter S, limiting our consideration to high values of S, for which the R.P.A. should be valid. We have taken

$$g(R) = \begin{cases} 0 & \text{if } \underset{\sim}{R} \in E \\ 1 & \text{if } \underset{\sim}{R} \notin E \end{cases} \qquad (6.8)$$

where E is the set of points in a spheroid with the long molecular axis as its major axis. The ratio of the major to minor axis b_l/b_t is 2.4, and we have assumed this to be independent of temperature. The error introduced by this approximation is likely to be small as we are considering a small temperature range and additionally there is short-range correlation of anisotropic molecules even in the isotropic phase [16].

Changing b_l/b_t to, for example, 1.8 appears to make mo qualitative difference to $J_{\|}$, which is not surprising in view of the isotropy of α.

Clearly the shortest wavelength fluctuation must be at least as long as b_t and so $b_t = v2\pi/q_c$ for some $v < 1$. Faber has suggested that for a nematic composed of hard spheres with packing fraction 0.4, $v \sim 0.64$ [13]. By the same reasoning, for hard spheriods with packing fraction p,

$$q_c b_t \approx 1.1 \left[\frac{36\pi p}{b_l/b_t} \right]^{1/3}$$

Since there is long-range orientational order we would expect $p > 0.4$, but $b_l/b_t > 1$ also and so $q_c b_t$ is likely to be only weakly temperature dependent for small values of b_l/b_t. Therefore we would expect $v \approx 0.55 - 0.6$.

For the purpose of comparison, we have shown in figure 6.2 $J_{\|}$ for several values of v and also for no correlation and total correlation. The totally correlated case appears to be a good

approximation only when the shortest fluctuation wavelength is significantly longer than ($\sim$ 5-10 times) b_t, that is, when there is very little disorder at lengths of 2-3 molecular widths. Clearly for $v \sim 0.6$ the S dependence of $J_{||}$ is closer to that for no short-range correlation.

The obvious limitation of the above considerations is the neglect of the anisotropy of the correlations. We discuss this briefly in the next section.

6.5 Anisotropy of the correlations

In reality, because the bend elastic constant K_3 is larger than the splay elastic constant K_1, the orientational correlation between two molecules is likely to be larger when $\underset{\sim}{R}$ is parallel to the director than when it is perpendicular to it. We can include this anisotropy into the R.P.A. averages of correlated terms if the degree of uncorrelation a depends on the direction as well as the magnitude of $\underset{\sim}{R}$.

In the appendix an approximate analytical expression is derived for $\alpha(\underset{\sim}{R})$. For PAA for S = 0.669, 0.562, using data from references [6] and [7], we find that the anisotropy of α is less than $\pm$ 20 % and is only weakly temperature dependent, figure 6.3. (This may help to justify the assumed temperature independence of b_1/b_t). We can try to quantify the effect of this small anisotropy by calculating the pair-correlation dependent term in equation (6.5) with an isotropic excluded volume (for isotropic correlations this integral vanishes).Now $\hat{\underset{\sim}{R}}\,\hat{\underset{\sim}{R}}$ cannot be replaced

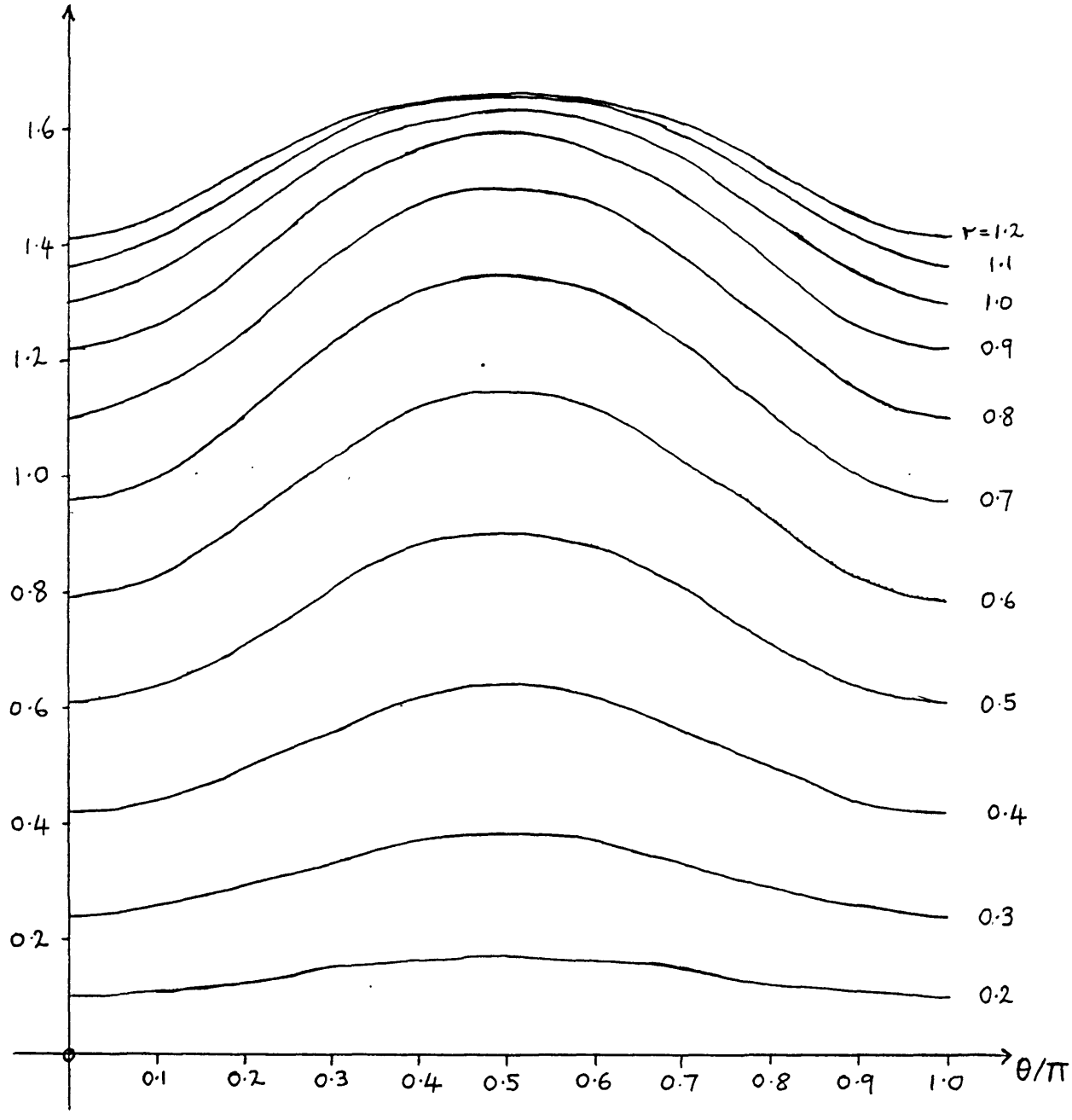

Figure 6.3 Anisotropy of pair correlation factor $\alpha(\underline{R})$ as a function of θ, the angle between $\underline{R}$ and the director, for various values of $|\underline{R}| = r.2\pi/q_c$.

$T = 378^{\circ}K$, $\dot{S} = 0.669$

by a diagonal molecular tensor since the correlations are not independent of the azimuthal angle in the molecular axes. For example the parallel component is given by

$$L_{\parallel} = \int_{R>v2\pi/q_c} d^3\underset{\sim}{R} \; \frac{(3\cos^2(\theta) - 1)}{R^3} \frac{(3V - U)}{2}$$

In table 6.1 we give some values of $L_{\parallel}$ for PAA, for various S. Clearly the integral is nearly two orders of magnitude smaller than $J_{\parallel}$. We conclude that the anisotropy of the hard core is much more important than that of the correlations.

In order to express the anisotropy of the correlations relative to molecular axes it is necessary to consider the change locally of the elastic constants resulting from the disorder. Thus the correlations between fluctuations must be described and so the random phase approximation should be abandoned. This can be avoided by simply using the anisotropic expression for $\alpha(\underset{\sim}{R})$ in the expressions for $\langle \underset{\sim}{n}^i \underset{\sim}{n}^i . \underset{\sim}{n}^j \underset{\sim}{n}^j \rangle$ in (6.7) The effect of this on $J_{\parallel}$ is shown in figure 6.4. However the physical interpretation of the integral is now not clear. Since we have found that the anisotropy of the correlations is small, we shall assume that the isotropic case is a good approximation to the correct value.

6.6 Expression for the Permittivity neglecting correlations

We now consider how we may obtain an expression for $\underset{\sim}{\epsilon}$. Using the approximations described in section 6.3, the average in (6.4) can be evaluated in the limiting cases of no short-range correlation

T/K \ V / S	0.6	0.8
378	0.669	0.237×10^{-2}	0.203×10^{-2}
383	0.646	0.221×10^{-2}	0.193×10^{-2}
388	0.620	0.210×10^{-2}	0.187×10^{-2}
393	0.597	0.190×10^{-2}	0.173×10^{-2}
398	0.562	0.170×10^{-2}	0.160×10^{-2}

Table 6.1 Values of the integral L for PAA for $b_t = b_\ell = v \frac{2\pi}{q_c}$

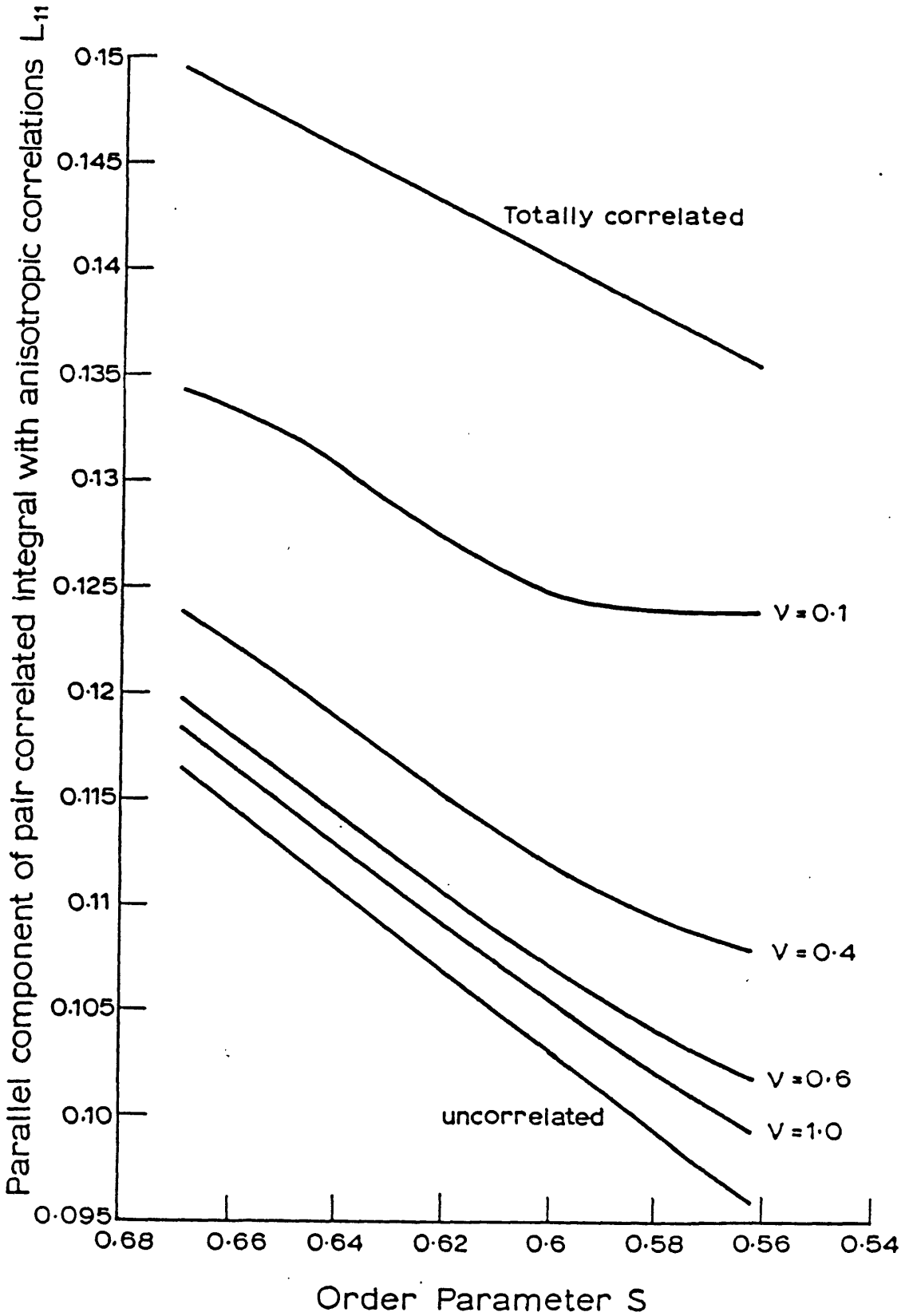

Figure 6.4 Variation of the pair correlated integral assuming anisotropic correlations, $\hat{J}_{\parallel}$, with S, for PAA. Curves are shown for $b_t = v2\pi/q_c$ for various v and for the totally correlated and uncorrelated cases.

and total orientational correlation. The latter leads to a formula similar to that derived by Bordewijk and de Jeu [10] (see section (6.2)). However, from figure 6.2, the uncorrelated value of $J_{||}$ is ~ 9 % less than its value when $b_t = 0.6 \times 2\pi/q_c$, while the totally correlated value is $\sim$ 19 % larger than this value. Therefore if we assume that these results hold qualitatively for higher order correlations too, we would expect the uncorrelated case to lead to a better approximation to e. The term containing $\underset{\sim}{J}$ is likely to contribute ~ 25 % of the value of $\underset{\sim}{I}$, which suggests ~ 3 % error from the neglect of local order.

In the absence of short-range order we have

$$\langle \overline{\underset{\sim}{\mu}^i \underset{\sim}{\mu}^i . \underset{\sim}{T}^{ij} . \underset{\sim}{a}^j . \underset{\sim}{T}^{jk} \ldots . \underset{\sim}{a}^r} \rangle_o =$$

$$. \langle \overline{\underset{\sim}{\mu}^i \underset{\sim}{\mu}^i . \underset{\sim}{T}^{ij}} \rangle_o . \langle \overline{\underset{\sim}{a}^j . \underset{\sim}{T}^{jk}} \rangle_o . \langle \overline{\underset{\sim}{a}^k . \underset{\sim}{T}^{kl}} \rangle_o \ldots\ldots . \langle \overline{\underset{\sim}{a}^r} \rangle$$

and for a large number of molecules N, such that

$$N^p + O(N^{p-1}) \sim N^p$$

since $\langle \overline{\underset{\sim}{a}^j . \underset{\sim}{T}^{jk}} \rangle$, $\langle \overline{\underset{\sim}{a}^j} \rangle$ are independent of j, k, we have

$$\sum_i \sum_{i'} \langle \overline{\underset{\sim}{\mu}^i . \underset{\sim}{A}^i . \underset{\sim}{e} \; \underset{\sim}{\mu}^{i'} . \underset{\sim}{A}^{i'} . \underset{\sim}{e}} \rangle_o \approx$$

$$\sum_i \sum_{i'} \langle \overline{(\underset{\sim}{\mu}^i - N\underset{\sim}{\mu}^i . \underset{\sim}{T}^{ij} . (\underset{\sim}{I} + \langle \underset{\sim}{a}^j . \underset{\sim}{T}^{jk} \rangle)^{-1} . \langle \underset{\sim}{a}^k \rangle) . \underset{\sim}{e}} \; x$$

$$\overline{(\underset{\sim}{\mu}^{i'} - N\underset{\sim}{\mu}^{i'} . \underset{\sim}{T}^{i'j'} . (\underset{\sim}{I} + \langle \underset{\sim}{a}^{j'} . \underset{\sim}{T}^{j'k'} \rangle)^{-1} . \langle \underset{\sim}{a}^{k'} \rangle) . \underset{\sim}{e}} \rangle \qquad (6.9)$$

Writing $\underset{\sim}{D}^i = N\underset{\sim}{\mu}^i . (\underset{\sim}{T}^{ij} . \langle \underset{\sim}{a}^j \rangle - \langle \underset{\sim}{a}^j . \underset{\sim}{T}^{jk} \rangle)$, since $\langle \overline{\underset{\sim}{a}^j \underset{\sim}{T}^{jk}} \rangle$ is diagonal, (6.9) becomes

$$\sum_i \sum_{i'} \langle \overline{\underset{\sim}{\mu}^i \cdot \underset{\sim}{A}^i \cdot \underset{\sim}{e}\ \underset{\sim}{\mu}^{i'} \cdot \underset{\sim}{A}^{i'} \cdot \underset{\sim}{e}} \rangle_o =$$

$$\sum_i \sum_{i'} \langle \overline{(\underset{\sim}{\mu}^i - \underset{\sim}{D}^i) \cdot \underset{\sim}{e}\ (\underset{\sim}{\mu}^{i'} - \underset{\sim}{D}^{i'}) \cdot \underset{\sim}{e}} \rangle_o \underset{\sim}{e} (\underset{\sim}{I} + \langle \overline{\underset{\sim}{a}^j \underset{\sim}{T}^{jk}} \rangle)^{-2} \cdot \underset{\sim}{e}$$

$\langle \overline{\underset{\sim}{a}^j \cdot \underset{\sim}{T}^{jk}} \rangle$ can be evaluated as in section 6.3, but more simply as now all correlations are neglected, to give

$$\langle \overline{\underset{\sim}{a}^j \cdot \underset{\sim}{T}^{jk}} \rangle = [\ a_\perp U_\perp \underset{\sim}{I} + (a_\parallel U_\parallel - a_\perp U_\perp) \langle \underset{\sim}{n}^j \underset{\sim}{n}^j \rangle\ ] / (V \epsilon_o) \qquad (6.10)$$

where

$$\underset{\sim}{U} = - \frac{1}{4\pi} \int_{V_1} d^3 \underset{\sim}{R}\ \frac{g(\underset{\sim}{R})}{R^3} (\underset{\sim}{I} - 3 \underset{\sim}{R}^2)$$

For g as in (6.8), $\underset{\sim}{U} = - \underset{\sim}{\Omega} + \underset{\sim}{I}/3$, where $\underset{\sim}{\Omega}$ is the depolarising tensor of the ellipsoid E. Similarly,

$$\langle \overline{(\underset{\sim}{\mu}^i - \underset{\sim}{D}^i) \cdot \underset{\sim}{e}\ (\underset{\sim}{\mu}^i - \underset{\sim}{D}^i) \cdot \underset{\sim}{e}} \rangle_o = \underset{\sim}{e} \cdot (M_\perp^2 \underset{\sim}{I} + (M_\parallel^2 - M_\perp^2) \langle \underset{\sim}{n}\ \underset{\sim}{n} \rangle) \cdot \underset{\sim}{e}$$

where

$$M_\perp^2 = \mu_\perp^2\ \underset{\sim}{e} \cdot (\underset{\sim}{I} + N \Delta U a_\parallel \langle \underset{\sim}{n}\ \underset{\sim}{n} \rangle / V)^2 \cdot e$$

$$M_\parallel^2 = \mu_\parallel^2\ \underset{\sim}{e} \cdot (\underset{\sim}{I} - N \Delta U a_\perp (\underset{\sim}{I} - \langle \underset{\sim}{n}\ \underset{\sim}{n} \rangle) / V)^2 \cdot e$$

Thus if as usual we write

$$g_k = 1 + \sum_{i \neq i'} \frac{\langle (\underset{\sim}{\mu}^i - \underset{\sim}{D}^i) \cdot \underset{\sim}{e}\ (\underset{\sim}{\mu}^{i'} - \underset{\sim}{D}^{i'}) \cdot \underset{\sim}{e} \rangle}{\langle (\underset{\sim}{\mu}^i - \underset{\sim}{D}^i) \cdot \underset{\sim}{e}\ (\underset{\sim}{\mu}^i - \underset{\sim}{D}^i) \cdot \underset{\sim}{e} \rangle}$$

then from (6.4),

$$\frac{\epsilon_o (\epsilon_\gamma - \epsilon_{\infty\gamma}) [\ \epsilon_\gamma + (\epsilon_{\infty\gamma} - \epsilon_\gamma) \Omega_\gamma^\epsilon\ ]\ V}{\epsilon_\gamma\ (2 + \epsilon_{\infty\gamma})^2} =$$

$$\frac{N\ g_{k\gamma}}{9\ K_B T} \frac{\underset{\sim}{e} \cdot (M_\perp^2 \underset{\sim}{I} + (M_\parallel^2 - M_\perp^2) \langle \underset{\sim}{n}\ \underset{\sim}{n} \rangle) \cdot \underset{\sim}{e}}{\underset{\sim}{e} \cdot (\underset{\sim}{I} + N \langle \overline{\underset{\sim}{a}^i \cdot \underset{\sim}{T}^{ij}} \rangle)^2 \cdot \underset{\sim}{e}} \qquad \gamma = \parallel, \perp$$

Hence in addition to the long-range orientational order effects, there is an effective contribution to the dipole moment as a result of the anisotropy of the molecules, ΔU, even when short-range order is neglected.

As usual we can derive $\underset{\sim}{a}$ from the extrapolated high frequency permittivity $\underset{\sim}{\epsilon}_\infty$. From (6.3), summing terms as in (6.9),

$$\epsilon_o\,(\underset{\sim}{\epsilon}_\infty - I) = (N/V)[\,\underset{\sim}{I} + (N/V)\overline{\langle \underset{\sim}{a}^i . \underset{\sim}{T}^{ij} \rangle}\,]^{-1} . \langle \underset{\sim}{a}^j \rangle \qquad (6.11)$$

and $\overline{\langle \underset{\sim}{a}^i . \underset{\sim}{T}^{ij} \rangle}$ is given by (6.10).

6.7 Comparison with Experimental Data

In general, verification of expressions for $\underset{\sim}{\epsilon}$ is difficult because of the uncertainty in the values of the various molecular parameters, for example $\underset{\sim}{a}$, $\underset{\sim}{\mu}$. For polar molecules it is further complicated by the lack of a model for the degree of permanent dipole anti-parallel ordering; an alternative expression for $\underset{\sim}{\epsilon}$ just provides another possible value for g_k. For the refractive index (and the permittivity of non-polar molecules) this latter problem does not arise and so we will compare the theory with the experimental data for this case.

From (6.11) and (6.10), for $g(\underset{\sim}{R})$ as in (6.8),

$$\epsilon_{\infty\gamma} = 1 + \frac{(N/V\epsilon_o)\,[\,\bar{a} + \Delta a(\,\langle \underset{\sim}{n}\,\underset{\sim}{n} \rangle_\gamma - 1/3\,)\,]}{1 - (N/V\epsilon_o)\,[\,\overline{a\Omega} + \Delta(\underset{\sim}{a}\underset{\sim}{\Omega})\,(\,\langle \underset{\sim}{n}\,\underset{\sim}{n} \rangle_\gamma - 1/3\,)\,]} \qquad (6.12)$$

where $\gamma = \parallel, \perp$

$$\overline{a} = a_{\parallel}/3 + 2a_{\perp}/3$$

$$\overline{a\Omega} = a_{\parallel}\Omega_{\parallel}/3 + 2a_{\perp}\Omega_{\perp}/3$$

$$\Delta(\underset{\sim}{a}\underset{\sim}{\Omega}) = a_{\parallel}\Omega_{\parallel} - a_{\perp}\Omega_{\perp}$$

Equation (6.12) is rather similar to the expression derived by Palffy-Muhoray and Balzarini [8], [18]. However they assumed that the polarisation $\underset{\sim}{P}$ and the local field $\underset{\sim}{F}$ satisfy

$$\langle\underset{\sim}{P}\rangle = \langle\underset{\sim}{a}.\underset{\sim}{F}\rangle = \langle\underset{\sim}{a}\rangle.\langle\underset{\sim}{F}\rangle$$

while we have found that the second inequality does not hold for anisotropic molecules.

We have calculated values for the components of the refractive index $n_{\parallel}$, $n_{\perp}$ for PAA from (6.12) (with $n_{\gamma}^2 = \epsilon_{\infty\gamma}$) and from the totally correlated case as in [11], i.e. from

$$n_{\gamma}^2 = 1 + (N/V\epsilon_o)\left[\frac{a_{\parallel}}{3(1 - (N/V\epsilon_o)a_{\parallel}\Omega_{\parallel})} + \frac{2a_{\perp}}{3(1 - (N/V\epsilon_o)a_{\perp}\Omega_{\perp})}\right.$$

$$\left. + \left(\frac{a_{\parallel}}{(1 - (N/V\epsilon_o)a_{\parallel}\Omega_{\parallel})} - \frac{a_{\perp}}{(1 - (N/V\epsilon_o)a_{\perp}\Omega_{\perp})}\right)(\langle\underset{\sim}{n}\,\underset{\sim}{n}\rangle - 1/3)\right] \qquad (6.13)$$

We have used values from [11] for a, b_l and b_t. Since (6.12) and (6.13) are identical for S = 1 we have used the value of a calculated from the solid state refractive indices. The values of b_l and b_t are those generated from the crystallographic data. S and the density ρ are from references [6] and [19] respectively. Figure 6.5 shows the percentage deviation of the calculated value of $n_{\gamma}^2 - 1$ ($\gamma = \parallel, \perp$) from the measured value [20] as a function of

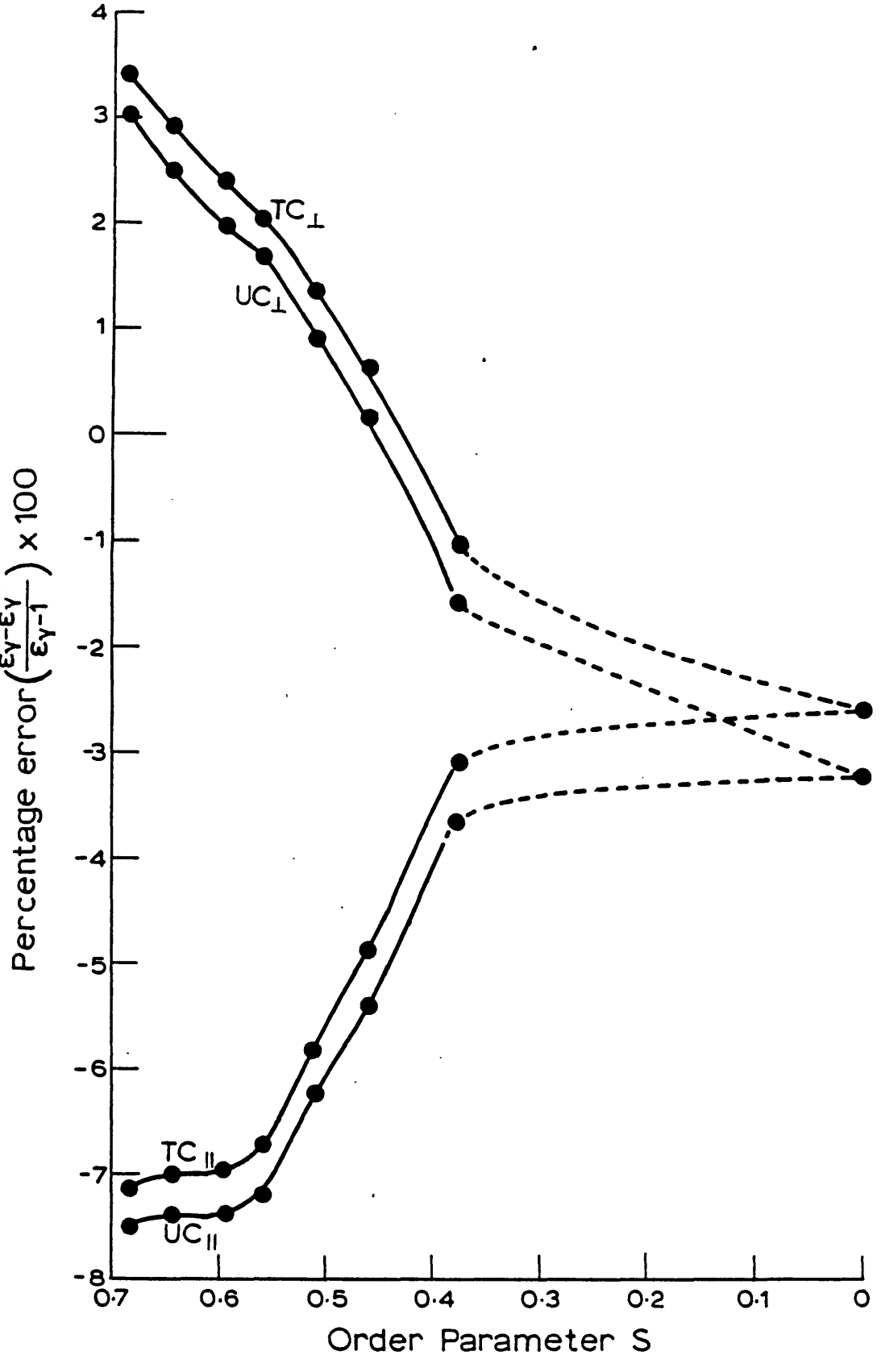

Figure 6.5 Graph showing percentage difference of calculated $\epsilon_\gamma^{(\alpha)} - 1$ ($\gamma = ||, \perp$) from the measured value $\epsilon_\gamma - 1$ as a function of S for PAA. The curves $TC_{||}$, $TC_\perp$ show the results using the totally correlated formula and $UC_{||}$, $UC_\perp$ show the results using the uncorrelated formula.

S. The two sets of curves correspond to equations (6.12) and (6.13).

From figure 6.5 it is clear that both sets of curves deviate from the measured value in a very similar way, which suggest a common error. The deviation is consistent with errors in the values of $\bar{a}$, Δa and indeed, for example, $\bar{n}^2/\rho$ is different for the nematic phase and solid phase data. This effect appears to dominate any which might result from the neglect or otherwise of the short-range correlation. There is no indication that (6.12) is a better approximation than (6.13). However, if the treatment of the correlation were the only error, we would expect the measured value to lie between the two calculated ones. Since this is not the case it is difficult to determine the degree of correlation suggested by the data.

Equation (6.13) was derived in order to satisfy the conditions

$$\Delta n^2/\rho \sim S \quad , \quad (\bar{n}^2 - 1)/\rho \sim \text{constant}$$

obtained from the experimental data. Since the values of $n_{\parallel}$, $n_{\perp}$ calculated from (6.12) and (6.13) are very similar it follows that (6.12) too has these properties to a good approximation. Therefore it seems that the observed temperature dependence of the refractive indices may be obtained without any assumption about the degree of correlation, as long as the dependence of $g(\underline{R})$ on the orientation of the molecules is properly accounted for. The close agreement between the totally correlated and uncorrelated cases may be seen as a justification for the empirical equation (6.13). However, the different S dependences may be significant to the calculation of the static permittivity.

Thus, in conclusion, we have investigated the effect of short-range orientational correlation on the term in the

expression for $\underset{\sim}{\epsilon}$ which describes two-particle interaction and we have found that it is likely to be small. Therefore we have averaged over molecular orientations by neglecting the effects of local ordering. Hence we have obtained a relationship between $\underset{\sim}{\epsilon}$, the molecular parameters $\underset{\sim}{a}$, $\underset{\sim}{\mu}$, $\underset{\sim}{\Omega}$ and the order parameter S. This equation both describes an anisotropic internal field and predicts, to a good approximation, the temperature dependence of the refractive index data. Theoretical considerations suggest that it should be an improvement on the previous expressions for $\underset{\sim}{\epsilon}$. However, because of the difficulty in extracting molecular parameters from the experimental data, we have not yet been able to determine whether this is in fact the case.

APPENDIX TO CHAPTER 6

A method for predicting the degree of short-range correlation using continuum theory has been given in reference [13]. However the calculation has been simplified by considering isotropically averaged correlations. In this appendix we will remove this simplification and determine approximately the anisotropy of the correlations. We use the notation of reference [13].

For a single fluctuation $\psi = \psi_o \cos(\underset{\sim}{q}.\underset{\sim}{R})$, the difference between the twists at $\underset{\sim}{R}_i$ and $\underset{\sim}{R}_j$ is [13]

$$\Delta\psi = \psi_j - \psi_i = -2\,\psi_o \sin(\,\underset{\sim}{q}.(\underset{\sim}{R}_j+\underset{\sim}{R}_i)/2\,)\sin(\,\underset{\sim}{q}.(\underset{\sim}{R}_j-\underset{\sim}{R}_i)/2\,)$$

Averaging over $\underset{\sim}{R}_i + \underset{\sim}{R}_j$ for fixed $\underset{\sim}{R}_i - \underset{\sim}{R}_j$ gives

$$(\Delta\psi)^2 = 2\psi_o^{\,2}\,(\,1 - \cos(\underset{\sim}{q}.(\underset{\sim}{R}_j - \underset{\sim}{R}_i))\,)/3$$

Taking a thermal average, using the average of $\psi_o^{\,2}$,

$$\langle (\Delta\psi)_\gamma^{\,2} \rangle = \frac{2K_BT}{Vq^2}\,\frac{(\,1 - \cos(\,\underset{\sim}{q}.(\underset{\sim}{R}_j - \underset{\sim}{R}_i)\,)}{(\,K_\gamma \sin^2(\theta) + K_3 \cos^2(\theta)\,)}$$

where γ =1,2 for a splay/bend, twist/bend mode respectively, and

$\underset{\sim}{q}$ = (qsin(θ)cos(ϕ), qsin(θ)sin(ϕ), qcos(θ))

Summing all the modes, retaining an isotropic cut-off for the fluctuation wavelengths, $2\pi/q_c$, and using the definitions of X,K

$$\sum_{\gamma=1}^{2} \langle (\Delta\psi_\gamma)^2 \rangle = \frac{V}{(2\pi)^3} \sum_{\gamma=1}^{2} \int \frac{2K_BT}{Vq^2}\,\frac{K\,(\,1 - \cos(qR\cos(\theta_{qR}))\,)}{K_\gamma \sin^2(\theta) + K_3\cos^2(\theta)}\; d^3\underset{\sim}{q}$$

$$= X\,[\,2 - \frac{K}{4\pi q_c} \sum_{\gamma=1}^{2} \int \frac{\cos(qR\cos(\theta_{qR}))\,\sin(\theta)}{K_\gamma \sin^2(\theta) + K_3\cos^2(\theta)}\; d\theta d\phi dq\,]$$

where θ_{qR} is the angle between $\underset{\sim}{q}$ and $\underset{\sim}{R}$

Thus we define $\alpha(\underset{\sim}{R})$ analogously to $\alpha(R)$ by

$$\alpha(\underset{\sim}{R}) = 2 - \frac{K}{4\pi q_c^{\gamma-1}} \sum^{2} \int \frac{\cos(qR\cos(\theta_{qR}))\sin(\theta)\, d\theta d\phi dq}{K_\gamma \sin^2(\theta) + K_3 \cos^2(\theta)}$$

The integral appearing in this expression, M, cannot be evaluated straightforwardly. However the $\underset{\sim}{R}$ dependence is contained in the term $\cos(qR\cos(\theta_{qR}))$ and the denominator is just a "weighting" factor indicating the fluctuation amplitude for each $\underset{\sim}{q}$. Therefore we substitute

$$D_2 = 1/K_\gamma + (1/K_3 - 1/K_\gamma)\,[(1 + \overline{K}_\gamma)\cos^2(\theta) - \overline{K}_\gamma \cos^4(\theta)]$$

for

$$D_1 = 1/(\, K_\gamma \sin^2(\theta) + K_3 \cos^2(\theta)\,)$$

and assume that the anisotropy with respect to $\underset{\sim}{R}$ will not be significantly altered. The two expressions are equal for $\cos(\theta) = 0$ and $\cos(\theta) = 1$. $\overline{K}_\gamma$ is obtained by a least squares estimate fit of D_1 to D_2 for $\theta = 0$ to π. This yields

$$\overline{K}_\gamma = 128\,[1/16 - 3/8L - 3/2L^2 - 1/L^3 + (1/L + 2/L^2 + 1/L^3)/(\sqrt{L+1})\,]/3$$

where

$$L = (K_3 - K_\gamma)/K_\gamma$$

With this substitution and by taking the polar axis parallel to $\underset{\sim}{R}$ we can write for M

$$M \approx \int \cos(qR\cos(\theta_{qR}))\sin(\theta_{qR})\, D_2(\theta)\, d\theta_{qR} d\phi_{qR} dq$$

Since $\cos(\theta) = \cos(\theta_{qR})\cos(\theta_R) + \sin(\theta_{qR})\sin(\theta_R)\cos(\phi_{qR} - \phi_R)$

where $\underset{\sim}{R} = (R,\ \theta_R,\ \phi_R)$ with respect to the fixed z (extraordinary) axis, the expression can be integrated to yield

$$\alpha(\underset{\sim}{R}) \approx 2 - K\sum_{\gamma=1}^{2} \left[\frac{Q_1(q_cR)}{K_\gamma} + \frac{1}{2}\left(\frac{1}{K_3} - \frac{1}{K_\gamma}\right)\left[P_{1\gamma}(\cos^2(\theta_R))Q_1(q_cR) + \right.\right.$$

$$\left.\left. P_{2\gamma}(\cos^2(\theta_R))Q_2(q_cR)+P_{3\gamma}(\cos^2(\theta_R))Q_3(q_cR)+P_{4\gamma}(\cos^2(\theta_R))Q_4(q_cR) \right]\right]$$

where

$$Q_1(q_cR) = \int (\sin(q_cRx)/q_cRx)dx$$

$$Q_2(q_cR) = \cos(q_cR)/(q_c^2R^2)$$

$$Q_3(q_cR) = \sin(q_cR)/(q_c^3R^3)$$

$$Q_4(q_cR) = [\cos(q_cR) - \sin(q_cR)/(q_cR)]/(q_c^4R^4)$$

$$P_{1\gamma}(\cos^2(\theta_R)) = 1 + K_\gamma/4 + (-1 + K_\gamma/2)\cos^2(\theta_R) - 3K_\gamma\cos^4(\theta_R)/4$$

$$P_{2\gamma}(\cos^2(\theta_R)) = 1 + K_\gamma/4 - 3(1 + K_\gamma/2)\cos^2(\theta_R) + 5K_\gamma\cos^4(\theta_R)/4$$

$$P_{3\gamma}(\cos^2(\theta_R)) =-1 -7K_\gamma/4 + (3 +33K_\gamma/2)\cos^2(\theta_R)- 75K_\gamma\cos^4(\theta_R)/4$$

$$P_{4\gamma}(\cos^2(\theta_R)) = -6K_\gamma[3/4 + 15\cos^2(\theta_R)/2 + 35\cos^4(\theta_R)/4]$$

REFERENCES

1. B. Needham, " Practical limits on addressing twisted nematic displays ", in
"Liquid Crystals: Their Physics, Chemistry and Applications"
The Royal Society of London, 1983

2. T.J. Scheffer, " Guest-host devices using anisotropic dyes ", in
"Liquid Crystals: Their Physics, Chemistry and Applications"
The Royal Society of London, 1983

3. D.W. Berreman, " Numerical modelling of twisted nematic devices ", in
"Liquid Crystals: Their Physics, Chemistry and Applications"
The Royal Society of London, 1983

4. M.A. Cotter, " The van der Waals theory of nematic liquids ", in
"Liquid Crystals: Their Physics, Chemistry and Applications"
The Royal Society of London, 1983

5. T.E. Faber, " Theories of nematic order ", in
"Liquid Crystals: Their Physics, Chemistry and Applications"
The Royal Society of London, 1983

6. W.H. de Jeu, " Physical Properties of Liquid Crystalline Materials " Chaps 4 and 5
Gordon and Breach, 1980

7. D.M.F. Edwards and P.A. Madden, " A molecular theory of the dielectric permittivity of a nematic liquid crystal ", Molecular Physics, vol 48, 471, 1983

8. P. Palffy-Muhoray and D.A. Balzarini, " The Clausius-Mosotti relation for anisotropic molecular fluids ", Can. J. Phys., vol 59, 375, 1981

9. U. Serge, " Cavity and reaction fields in anisotropic dielectrics ", Mol. Cryst. Liq. Cryst., vol 90, 239, 1983

10. P. Bordewijk and W.H. de Jeu, " Calculation of dipole correlation factors in liquid crystals with use of a semiempirical expression for the internal field ", J. Chem. Phys., vol 68, 116, 1978

11. W.H. de Jeu and P. Bordewijk, " Physical studies of nematic azoxybenzenes. II. Refractive indices and the internal field ", J. Chem. Phys., vol 68, 109, 1978

12. C.J.F. Bottcher and P. Bordewijk, " Theory of electric polarization ", Elsevier, 2nd ed., vol I, 1973 and vol II, 1978

13. T.E. Faber, " A continuum theory of disorder in nematic liquid crystals. II. Intermolecular correlations ", Proc. R. Soc. Lond. A, vol 353, 261, 1977

14. T.E. Faber, " A continuum theory of disorder in nematic liquid crystals. I ",
Proc. R. Soc. Lond. A, vol 353, 247, 1977

15. P. Bordewijk, " Extension of the Kirkwood-Frohlich theory of the static dielectric permittivity to anisotropic liquids ",
Physica, vol 75, 146, 1974

16. J.G. Kirkwood, " On the theory of dielectric polarisation ",
J. Chem. Phys., vol 4, 592, 1936

17. M. Kelker and R. Hatz, " Handbook of Liquid Crystals ",
Verlag Chemie, Weinheim, 1979

18. P. Palffy-Muhoray, D.A. Balzarini and D.A. Dunmur, " Local field anisotropy in nematic liquid crystals ",
Mol. Cryst. Liq. Cryst., vol 110, 315, 1984

19. W. Maier and A. Saupe, " A simple molecular statistical theory of the nematic liquid crystalline phase ",
Z. Naturforsch, vol A 15, 287, 1960

20. P. Chatlain and M. Germain,
C.R. Acad. Sci., 259, 1964

PAPERS WRITTEN ON THE MATERIAL CONTAINED IN THIS THESIS

1. S.L. Arambepola and J.R. Cozens

   HE_{11}-mode propagation in the cylindrical hollow Bragg fibre

   IEE Proceedings, Vol. 132, Pt. J, 207, August 1985.

2. S.L. Arambepola and K.D. Leaver

   A study of the effects of short-range correlations on the permittivity of Nematic Liquid Crystals

   Molecular Crystals and Liquid Crystals, Vol. 133, 313, 1986.

3. S.L. Arambepola and J.R. Cozens

   Wave propagation in a doubly periodic dielectric guide

   IEE Proceedings, Vol. 133, Pt. J, 332, October 1986.

4. S.L. Arambepola and J.R. Cozens

   Pulse propagation in a periodic waveguide

   Submitted to Journal of the Optical Society of America, B.